Experimental investigation of polymeric nanoparticles for enhanced drug delivery processes in cancer chemotherapy treatments

Georgia Englezou

A thesis submitted in partial fulfilment of the requirements for the degree of Doctor of Philosophy

The University of Sheffield
Faculty of Engineering
Department of Chemical and Biological Engineering

May 2024

Declaration of authenticity

This thesis presents research conducted at the Department of Chemical and Biological Engineering at The University of Sheffield, for the award of a Doctor of Philosophy degree. All work included in this thesis is my own original work, except where explicitly stated in the document with the correct citation. No part of this work has previously been submitted for any degree, diploma, or other qualification at any other institution.

Peer reviewed publications

Englezou G, Kortsen K, Pacheco AAC, et al. 2-Methyltetrahydrofuran (2- MeTHF) as a versatile green solvent for the synthesis of amphiphilic copolymers via ROP, FRP, and RAFT tandem polymerizations. *J Polym Sci.* 2020;58:1571–1581. https://doi.org/10.1002/pol.20200183

Phan H, Kortsen K, **Englezou G**, et al. Functional initiators for the ring-opening polymerization of polyesters and polycarbonates: An overview. *J Polym Sci.* 2020;58: 1911–1923. https://doi.org/10.1002/pol.20200313

Preprint papers

Hart A, Lu X, **Englezou G**, Wheatcroft L, Patel C, Stallard JC, Booth SG, Stothard C, Fleck N, Ebbens SJ, Inkson BJ, Cussen SA, Cumming DJ, Nedoma AJ. Role of Binder Molecular Weight on the Rheology and Microstructure of Cathode Slurries for Lithium-Ion Batteries. Available at *SSRN*:
https://ssrn.com/abstract=4524048 or http://dx.doi.org/10.2139/ssrn.4524048

Conference proceedings

Englezou G, Kortsen K, Pacheco AAC, Howdle SM, Nedoma AJ, Taresco V. Novel greener strategies for polymer chemistry; 2-Methyltetrahydrofuran green solvent. In *Macro group UK Young Researchers Meeting – YRM2020* (Oral presentation)

Englezou G, Kortsen K, Pacheco AAC, Howdle SM, Nedoma AJ, Taresco V. Novel greener strategies for polymer synthesis; 2-Methyltetrahydrofuran as a green solvent. In Polymer synthesis and reaction engineering. In *2020 AIChE Annual meeting* (Oral presentation)

Englezou G, Krumins E, Lentz JC, Taresco V, Nedoma AJ. Thermodynamic formulation of polymeric micelles for cancer chemotherapy. In *2022 IOP Physical aspects of polymer science (PAPS)* (Poster presentation)

Acknowledgments

Firstly, I would like to thank my primary supervisor, Dr Alisyn Nedoma, for giving me the opportunity to do a PhD at the University of Sheffield and allowing me to direct my research in the area of my personal interest. I would also like to thank my secondary supervisors, Dr Rachel Smith and Dr Vincenzo Taresco, for all your help and for welcoming me into your research groups. The support and advice, from all of you, throughout my studies have been very valuable and I am very grateful for all our insightful discussions. I am deeply thankful to the Department of Chemical and Biological Engineering for providing the resources, the environment and the funding needed for my research.

I would like to express my biggest thanks to the Nedoma research group, the Particle Technology group and the Howdle group for all their support, the interesting collaborations and the times we have shared together. My deepest gratitude goes to Dr Kate Pitt, for being very supportive in every step of the way and for all the advice, guidance and help she has generously provided throughout all my studies and time in Sheffield. Special thanks are going to Ana and Kris for supporting me and being patient with me during our collaboration for our research paper and to Dr Robert Cavanagh for performing the cytotoxicity experiments. Also, to Eduards and Chris for their valuable help and guidance in performing the synthesis procedures in this thesis and to Carlos for introducing me to DLS. My gratitude goes to Laurie for all his help and support with the SEM measurements, to Calum for all our research discussions and to Andy for all our drug delivery and Nile red discussions.

I am deeply grateful to all my amazing friends. To Victoria and Suruthi for always listening, supporting, and lifting my spirits up. To Jed, Chirag and Guo for always allowing me to rant in times of stress and pressure. My heartfelt thanks are going to all my amazing and loving friends for being always there for me and supporting me even when we are miles away. Rafaelia thank you for always being there, encouraging me, providing the best possible advice all these years, and for making a small and cute copy of you. Zacharias and Andreas thank you for always finding a way to make me relax, unwind and laugh. Maria, Chrystalleni and Antonis thank you for being my Sheffield family, keeping me strong, and cheering me up even when we are scattered across the globe. My most sincere gratitude goes to my partner, David, thank you for being my rock, always guiding me and reassuring me in tough times.

Last but definitely not least, I would like to express my most sincere and deepest gratitude and love to my family. My sisters, Eliana and Maria, my parents, Antonis and Loukia and my dearest niece Loukia and loving nephew Isaias. I cannot even express how grateful I am to have you all in my life. Thank you for always being there for me since the start of time! For believing in me, lifting me up, supporting me, listening to me, advising me, being patient with me and reminding what is truly important in life!

Abstract

In 2022, nearly 20 million new cancer cases were reported globally, with cancer-related deaths amounting to 9.7 million, making cancer one of the leading causes of death worldwide. Approximately 25% of cancer patients undergo chemotherapy, with the number of patients requiring chemotherapy expected to increase in the future. Chemotherapy costs account for the largest share in health system budgets and chemo patients experience a vast range of unpleasant side effects and diminished life quality. All these emphasise the requirement for development of novel techniques aiming for the enhanced drug delivery of anticancer drugs on the cancer site with minimal side effects to patients and high treatment efficiency with limited drug waste.

The development of antineoplastic drug delivery systems (DDS) formed by the self-assembly of biodegradable and biocompatible amphiphilic block copolymers was a major research focus in recent years. Although these polymers are intended for pharmaceutical applications, their synthesis is performed in solvents that are highly harmful and toxic. The focus of this work was employing 2-MeTHF as a bio-based polymerisation solvent for the synthesis of amphiphilic block copolymers aimed for chemotherapy DDSs. The results advocate the application of 2-MeTHF as an effective and sustainable multi-polymerisation solvent for the synthesis of various copolymers with varying chemistry, architecture and biodegradability.

The self-assembly mechanism of block copolymer into nanoparticles has been extensively investigated in this work by employing multiple formulation techniques, including the widely used nanoprecipitation process. The development of thermodynamically-driven formulation techniques, which are scarce in the literature, was performed to offer a greater understanding of the nanoparticle formulation. The exact position where the micellisation initiates during the solvent exchange process, is indicated within 20-30vol% of aqueous solvent composition. The formulation of polymeric micelles close to a thermodynamic balance was successful. In addition, nanoprecipitation was proven to be a highly robust, reproducible and easy process for formulation of polymeric nanoparticles with highly desirable size and narrow size distributions.

An improved long-term storage stability of the polymeric DDSs is experienced when the nanoparticle formulations are freeze-dried. However, freeze-drying is a very intensive process requiring the use of cryoprotectants to preserve the materials integrity. In this work, the first ever systematic study of PEGs used for cryopreservation of PEG-PLA nanoparticles was performed with an emphasis on the freezing step of the process. The results show that PEGs are highly successful in preserving the PEG-PLA formulation properties with reconstitution times less than 10 min. Lower molecular weight PEGs appear as more efficient cryoprotectants.

To assess the capabilities of polymeric nanoparticles based on PEG-PLA to form an effective DDSs for cancer chemotherapy, the encapsulation of the hydrophobic Nile Red as a model anticancer drug was performed. The challenges faced with separation of the unencapsulated drug from the drug-loaded nanoparticle suspension were addressed with the employment of diethyl ether as a Nile Red extraction solvent. The encapsulation of Nile Red within the PEG-PLA nanoparticles was highly successful. The final formulation sizes and PDI were in the ideal DDS range and experienced higher encapsulation efficiency compared to data in the literature.

Contents

List of figures

List of tables

Nomenclature

Symbol	Definition	Units
b	Statistical segment length	Å
C_∞	Characteristic ratio	-
D_τ	Translational diffusion coefficient - rate of Brownian motion	m^2/s
$Đ_M$	Molecular weight dispersity	-
F	Total energy of micelle	J
f_A	Volume fraction of block A in copolymer	-
f_B	Volume fraction of block B in copolymer	-
F_d	Deformation energy	J
F_m	Entropy of mixing	J
F_M	Total free energy of micellar phase	J
F_{mix}	Free energy of mixing	J
$\vec{h}$	End-to-end distance	Å
h_{rms}	Root-mean-square end-to-end distance	Å
k_B	Boltzmann constant	J/K
l	Characteristic segment length	Å
l_b	Average length of chemical bonds	Å
L_c	Contour length	Å
L_B	Length of hydrophobic block	Å
L_p	Persistence length	Å
m_A	Ratio between molecular volume of block A and solvent	-
M_A	Molecular weight of block A	Da
m_B	Ratio between molecular volume of block B and solvent	-
M_B	Molecular weight of block B	Da
M_n	Number average molecular weight	Da
n	Number of chemical bonds in one monomer	-
N	Number of repeating segment in polymer	-
p	Aggregation number	-
R	Universal gas constant	J/mol·K
R_A	Micelle corona thickness	m
R_B	Micelle core radius	m

R_g	Radius of gyration	nm
R_H	Hydrodynamic radius	m
R_t	Radius of spherical micelle	m
S_m	Translational entropy of micelle gas	J
T	Temperature	K
T_b	Boiling point	K
T_g	Glass transition temperature	K
T_m	Melting temperature	K
ΔG_{mix}	Gibbs free energy of mixing	J
ΔH_{mix}	Enthalpy term of mixing	J
ΔS_{mix}	Entropy term of mixing	J

Greek letter	Definition	Units
α	Kuhn segment length	Å
α_0	Contact area of hydrophilic block	$Å^2$
γ	Interfacial tension	dyn/cm
γ_{BS}	Interfacial tension between solvent and block B	dyn/cm
ε	Dielectric constant	$C^2/N \cdot m^2$
ζ	Zeta potential	V
η	Dynamic viscosity	Pa·s
μ	Electrophoretic mobility	$cm^3/V \cdot s$
ρ	Density	kg/m^3
υ	Molecular volume	$Å^3$
υ_B	Molecular volume of hydrophobic block	$Å^3$
φ	Volume fraction	-
χ	Flory-Huggins interaction parameter	-
χ_{AS}	Block A and solvent Flory-Huggins interaction parameter	-
χ_{BS}	Block B and solvent Flory-Huggins interaction parameter	-
Ω	Total number of monomers	-

Abbreviation	Definition
^{1}H NMR	^{1}H Nuclear magnetic resonance spectroscopy
2-MeTHF	2-methyltetrahydrofuran
AIBN	Azobisisobutyronitrile
AMPs	Antimicrobial peptides
API	Active pharmaceutical ingredient
Ar	Argon
ATRP	Atom transfer radical polymerisation
BCP(s)	Block copolymer(s)
$CDCl_3$	Deuterated chloroform
cmc	Critical micelle concentration
CPAB	4-cyano-4-(phenylcarbonothioylthio) pentanoic acid
CPDB	2-cyano-2-propyl dithiobenzoates
cpp	Critical packing parameter
CPT	Camptothecin
CRP	Controlled radical polymerisation
CTA	Chain-transfer agent
DBU	1,8-diazabicyclo[5.4.0]undec-7-ene
DCM	Dichloromethane
DDS(s)	Drug delivery system(s)
DLS	Dynamic light scattering
DMSO	Dimethyl sulfoxide
DP_n	Degree of polymerisation
DRI	Differential refractometer
EE%	Encapsulation efficiency
eROP	Enzymatic ring opening polymerisation
FREP	Free radical emulsion polymerisation
FRP	Free radical polymerisation
GDMA	Glycerol dimethacrylate
GPC	Gel permeation chromatography
HCl	Hydrochloric acid
HEA	Hydroxyethyl acrylate

HEMA	2-hydroxyethyl methacrylate
HPLC	High-performance liquid chromatography
IARC	International agency for research on cancer
LA	Lactide (3,6-Dimethyl-1,4-dioxan-2,5-dione)
LC%	Drug loading capacity
MDR	Multidrug resistance
mPEG	Poly(ethylene) glycol methyl ether
MSSEP	Monomer-starved semibatch emulsion polymerisation
Mw	Molecular weight
NaCl	Sodium chloride
NC(s)	Nanocapsule(s)
NMP	Nitroxide-mediated polymerisation
NP(s)	Nanoparticle(s)
NR	Nile red
PCL	Poly(caprolactone)
PDI	Polydispersity index
PDLLA	Poly(DL-lactide)
PEG	Poly(ethylene) glycol
PEGMA	Poly(ethylene) glycol methacrylate
PGA	Poly(glycolide)
P-gp	P-glycoprotein plasma membrane
PLA	Poly(lactide)
PLGA	Poly(lactic-co-glycolic) acid
PMMA	Poly(methyl methacrylate)
PSD	Particle size distribution
Ptxl	Paclitaxel
RAFT	Reversible addition-fragmentation chain-transfer polymerisation
REACH	Registration, evaluation, authorisation and restriction of chemicals
RES	Reticuloendothelial system
RI	Refractive index
ROP	Ring opening polymerisation
rpm	Revolutions per minute

RT	Room temperature
SAXS	Small-angle X-ray scattering
SE	Standard error
SEC	Size exclusion chromatography
SEM	Scanning electron microscopy
Sn(Oct)2	Tin(II) 2-ethylhexanoate
TBD	Triazabicyclodecene
tBSC	Serinol-based cyclic carbonate
TEM	Transmission electron microscopy
THF	Tetrahydrofuran
TMC	Trimethylene carbonate
UV-vis	Ultraviolet-visible
WHO	World health organisation
wrt	With respect to
ε-CL	ε-Caprolactone

1. Introduction

1.1. Background

On average, in the UK every year there are around 376,000 new reported cases of cancer, with approximately 100,000 of these cases undergoing chemotherapy treatment (Cancer Research UK, 2020). Currently, chemotherapy treatment accounts for a tenth of the whole central NHS budget, estimated at approximately £1.4 billion per year, making it the single biggest spend (NHS, 2016). Therefore, reducing the costs associated with chemotherapy alone, can have a significant impact on the financial costs required for maintaining the NHS.

Chemotherapy treatment has a number of drawbacks. The anticancer drugs are cytotoxic and they are not selective for cancer cells, meaning that a lot of the normal and healthy cells are also damaged (Azarova *et al.*, 2007). The disruption of the operation of the healthy cells and tissue leads to a number of undesirable side effects experienced by cancer patients. Many patients, in addition to the various and unpleasant complications, experience a decrease in the quality of life during their chemotherapy treatment.

There are a number of problems related to the application of chemotherapy drugs. Most anticancer agents are highly hydrophobic and insoluble in water. This affects the biodistribution of the drug in the human body. A high retention time of the drug in the circulation system is desirable to increase the possibility of reaching the cancerous site. This would also lead to an increase in the concentration of available drug and its prolonged exposure on the tumour. Another issue of chemotherapy treatments is the anticancer drug resistance exerted from the tumour site, which introduces further barriers on the penetration and accumulation of the chemotherapeutics on the cancerous tissue (Park *et al.*, 2008).

The costs and setbacks associated with chemotherapy treatment can be significantly minimised by addressing the optimisation of the drug formulations used in chemotherapy. By implementing a more effective antineoplastic drug delivery system (DDS), the drug concentration wasted through immune system rejection and the frequency of the chemotherapy sessions required for treatment could be reduced, overall minimising the costs associated with chemotherapy treatment.

An ideal DDS for chemotherapy treatment applications would encapsulate the anticancer drug within an enclosed structure forming a protective layer from chemical and environmental changes, and providing a masking effect to avoid recognition from the immune response system (Lipinski, 2000). The most important physical properties of a highly efficient DDS include biodegradability, biocompatibility, thermal stability and increase of aqueous solubility of the antineoplastic drug (Gatti *et al.*, 2018).

Polymeric micellar structures constructed from amphiphilic block copolymers comprised from a hydrophobic core and a hydrophilic corona are the ideal structures for encapsulation of chemotherapy drugs. The residence time of the drug in the circulation system is increased due to the hydrophilic corona, which increases drastically the effective aqueous solubility of the drug (Savjani, Gajjar and Savjani, 2012). The drug release profile is more controlled when incorporated inside a polymeric nanoparticle structure enabling a slow and sustained release of the drug over time, a highly desirable characteristic for chemotherapy DDS (Iaccarino *et al.*, 2019).

Polymeric nanoparticles represent a promising approach to enhance the efficacy of chemotherapy while minimising side effects. By enclosing anticancer drugs within these nanoparticles, the drugs are protected from premature release and can circulate in the bloodstream with reduced exposure to healthy cells and tissues (Xiao *et al.*, 2022a; Yousefi Rizi, Shin and Rizi, 2022). This encapsulation allows for targeted release of the drug primarily within the tumour environment, where factors such as the slightly acidic pH, specific enzymes, and higher levels of certain biomolecules trigger the nanoparticles to release their contents (Katayama, Sonoda and Maeda, 2001; Lee, Na and Bae, 2003; Rapoport, 2007). Additionally, these nanoparticles can be functionalised with ligands that bind specifically to receptors on cancer cells, enhancing their uptake (Oerlemans *et al.*, 2010). By concentrating the drug at the tumour site and minimizing its presence in healthy tissues, polymeric nanoparticles significantly reduce the side effects experienced by patients undergoing chemotherapy treatment.

Even though polymeric nanoparticles are a very promising structure for the drug delivery of anticancer agents, there are only very few such systems available. At the moment of writing, there are no commercially available polymeric micelles for cancer chemotherapy. Although, there are a few micelle-based formulations currently either in the pre-clinical phase or in

clinical trials. A possible reason behind the delay of a commercially available polymeric micellar structure for chemotherapy treatments is potential issues encountered with the long-term stability and storage of the nanodrugs (De Jaeghere *et al.*, 1999; Abdelwahed *et al.*, 2006).

The poor stability of the polymeric nanoparticles in aqueous mediums is caused by their physical instabilities, such as particle aggregation, and their chemical instabilities, based on polymer hydrolysis (Abdelwahed *et al.*, 2006). These instabilities can be addressed by water removal from the system. The most common method used for water removal, when high storage stability is required, is freeze-drying (Franks, 1998). This is a very intensive process giving rise to considerable of stresses in the suspension. Polymeric nanoparticles are considered fragile suspensions and without caution they could be damaged through this process (De Jaeghere *et al.*, 1999). Mechanical stresses and pressures could make the nanoparticles unstable. Excipients called cryoprotectants and lyoprotectants are commonly used to avoid this and preserving the properties of the polymeric material during the freezing step and the drying step of the freeze-drying process, respectively (Trenkenschuh and Friess, 2021).

1.2. Research aims and objectives

1.2.1. Research aim

The aim of the experimental research performed in this thesis is to examine in depth and perform the different stages required to produce an enhanced drug delivery system intended for cancer chemotherapy treatment. These stages would include the synthesis of biodegradable and biocompatible block copolymers, their successful self-assembly into polymeric nanoparticles, the improvement of their stability for long-term storage and the high encapsulation efficiency of a chemotherapy drug within the structure of the produced polymeric nanoparticles.

1.2.2. Research objectives

1. Create a large library of biodegradable and biocompatible block copolymers with varying chemical and physical properties, through the employment of various polymerisation techniques, using green synthesis pathways.

2. Investigate in depth the self-assembly of polymeric nanoparticles by varying the formulation technique, the polymer properties and the processing conditions applied, to examine their ability to act as enhanced DDS for cancer treatment.
3. Examine freeze-drying as a method for increasing the stability of polymeric nanoparticles for long-term storage with the incorporation of cryoprotectants to preserve the structure and integrity of the yielded nanoparticle suspensions.
4. Evaluate the ability of the constructed polymeric nanoparticles to form an enhanced DDS for anticancer drugs by encapsulating a model hydrophobic drug at various processing conditions and testing their drug loading capabilities.

1.3. Thesis structure

Chapter 2 of this thesis comprises from a comprehensive review and analysis of existing literature around the application of polymeric nanoparticles made from amphiphilic block copolymers for cancer chemotherapy. The main problems associated with chemotherapy treatment and the rationale behind their cause is discussed. This knowledge is used leading to a better understanding of the ideal characteristics that an effective DDS should have to mitigate the problems rising during the anticancer drug applications. Important theories, terms and phenomena associated with the physics and chemistry of the block copolymers are discussed. A greater emphasis was given in two particular areas of the literature, the current state of the art synthesis processes that are followed for the production of block copolymers utilised for pharmaceutical applications, and the nanoparticle formulation routes commonly employed for the self-assembly of block copolymers. The research gaps in the existing literature are identified leading to the aim and objectives of this thesis presented in section 1.2.

The experimental methodologies and procedures followed to perform the research presented in this thesis are summarised in Chapter 3. A detailed account of all the materials used for all experimental investigations are included. Also, all the characterisation techniques and analysis performed to study the final product are provided.

In Chapter 4, the research work completed and published in collaboration with Prof Steve Howdle's group at the University of Nottingham is presented. The use of 2-Methyltetrahydrofuran (2-MeTHF), a green, bio-based solvent, for synthesising amphiphilic

block copolymers through various polymerisation techniques is discussed. The study aims to investigate the ability of 2-MeTHF in reducing the environmental impact while maintaining effective synthesis of block copolymers. The ability of 2-MeTHF to facilitate complex polymerisation processes in a greener and more sustainable manner is tested to evaluate its potential in replacing harmful petrochemical solvents commonly used in the industry.

Chapter 5 presents the research performed to deepen the understanding of amphiphilic diblock copolymers self-assembly into polymeric nanoparticles through various formulation techniques and parameter adjustments. The impacts of the two blocks length and polymer molecular weight on nanoparticle properties are studied. Techniques such as conventional nanoprecipitation and two thermodynamically-driven processes are evaluated to identify the optimal process for creating an ideal DDS. The study assesses the influence of formulation parameters such as solvent and anti-solvent addition rates and copolymer concentration. The outcomes are compared to determine the most effective methodology for amphiphilic diblock copolymer nanoparticle formulation.

The limitations faced by block copolymers in commercial use due to their poor long-term stability in aqueous mediums are addressed in Chapter 6 through the application of the freeze-drying process. A systematic study is performed to examine the use of various cryoprotectants during freeze-drying, with a particular focus on the freezing step. The results obtained from the six different cryoprotectants employed are compared. The effectiveness of the different cryoprotectants to control and reduce the mechanical stresses experienced from ice crystal formation during freeze-drying and preserve the polymeric nanoparticle structure, size and functionality is evaluated.

In Chapter 7, the encapsulation abilities of diblock copolymers are investigated. The self-assembly of diblock copolymers with the aim of encapsulating a model drug within the hydrophobic core of the polymeric nanoparticles is performed. Nile Red is employed as a model drug mimicking the effects and interactions that would be experienced by a chemotherapy drug. The challenges faced after encapsulation for the separation of the unloaded drug from the drug-loaded nanoparticle suspension are addressed by the employment and comparison of three different Nile Red extraction solvents. The encapsulation efficiency and the drug loading capacity of the constructed drug-loaded polymeric nanoparticles is evaluated to assess their ability to form an effective DDS for cancer chemotherapy applications.

Finally, in Chapter 8 the overall conclusions from the research investigations performed in this thesis are summarised alongside some recommendations for future work.

2. Literature Review

2.1. Cancer Chemotherapy

According to the International Agency for Research on Cancer, in 2020 approximately 19.3 million people were diagnosed with cancer worldwide (Globocan, 2020). In England, as part of their cancer treatment, 28.5% of all the patients diagnosed with cancer have palliative or curative chemotherapy treatment (NCRAS and CRUK, 2017). Chemotherapy can also be used as a therapeutic treatment for other serious diseases, such as immune system disorders and bone marrow diseases. Chemotherapy is a drug treatment that targets and destroys the fast-growing cells in the human body with the use of strong chemicals (NHS, 2020a). Cancer cells multiply and grow at a much faster pace than most cells in the human body. That is the reason behind the common and effective use of chemotherapy as a treatment method of different types of cancer. However, there is the risk of many side effects that the patients might experience. The unwanted implications are associated with the drugs usually used during chemotherapy treatments and their delivery methods.

2.2. Chemotherapy drugs implications

2.2.1. Patient health problems

The side effects caused by the chemotherapy drugs are very common across different patients and they can be significant in some cases. There is a variety of chemotherapy drugs available and they are used for different types of cancer treatments leading to a number of side effects, either short-term or long-term, depending on each situation (Miller *et al.*, 2016). Chemotherapy is connected to many side effects because it is not specific to cancer cells only. The chemotherapy drugs are cytotoxic for both cancerous and normal cells. Therefore, other normal and healthy human body cells are also affected by the implementation of chemotherapy drugs. Especially fast-growing healthy cells are more likely to be attacked and damaged by chemotherapy.

The most common healthy cells that are targeted from chemotherapy drugs are the hair follicles, the mouth and digestive tract cells, the blood-producing cells in bone marrow, and the cells of the reproductive system (American Cancer Society, 2020). The destructive effect that the chemotherapy drugs have to these healthy cells leads to many unpleasant side effects for the chemotherapy patients. The damage of the digestive track cells leads to side effects such as

nausea, vomiting, appetite changes and constipation. The disruption on the normal operation of the blood-forming cells in the bone marrow results in complications in the production of red blood cells, white blood cells (leukocytes) and platelets. Low levels of red blood cells, which are the cells that carry oxygen around the human body, can cause anaemia accompanied by tiredness, fatigue, pale complexion etc. A reduction in the number of white blood cells, which are part of the immune system, can cause higher risks of chemotherapy patients getting seriously ill from infections. Decreasing the amount of platelets in the blood, which are the cells that stop severe bleeding after injuries, leads to easier bruising and bleeding of patients (NHS, 2020b). In addition to these severe side effects, many patients experience repeated treatments and diminished quality of life during their chemotherapy treatment.

To minimise the side effects and therapeutic efficiency issues associated with chemotherapy treatment and improve the overall experience and quality of life of cancer patients, a better understanding of the origin of those issues is required.

2.2.2. Problem origin

The two most common administration techniques for cancer chemotherapy drugs are through chemotherapy infusions, where the drug is injected directly into a vein (intravenously), and through oral administration, where the drug is provided in the form of a capsule or pill (Macmillan Cancer Support, 2018). Across all administration methods, the main aim is to have a long circulation time of the administered chemotherapy drug in the circulation system of the cancer patient. Long retention of the chemotherapy drug in the circulation system is required to increase the possibility of reaching the target site and increasing the concentration and contact time of the drug with the cancerous cells (Park *et al.*, 2008).

The biggest challenge with most cancer chemotherapy drugs is that they are highly hydrophobic and have low aqueous solubility (Lipinski, 2000; Lipinski *et al.*, 2001). The oral bioavailability of a drug is depended on a number of elements, including the aqueous solubility of the drug, the drug intestinal permeability and the rate of dissolution of the drug. Poor solubility in water and low intestinal permeability are the predominant factors limiting the presence of the administered drug in the circulation system (Savjani, Gajjar and Savjani, 2012). Other administration methods, such as parenteral preparations, also require high aqueous solubility for enhanced bioavailability of the drug (Edward and Li, 2008). To achieve the

desirad pharmacological response, a high concentration of the chemotherapy drug in systematic circulation is required and this is dependent on the solubility of the drug. Therefore, drugs with poor aqueous solubility will usually require higher administration dosages to attain the therapeutic plasma concentration (Vemula, Lagishetty and Lingala, 2010). Although, in the case of chemotherapy drugs, the cytotoxicity of the drug makes the increased dosage option non beneficial. Another problem that may arise in the case of intravenous injections of chemotherapy drugs is the embolization of blood vessels. The highly insoluble nature of the chemotherapy drugs could lead to their aggregation within the blood vessels causing a blockage accompanied by local toxicity due to the increased drug concentration in the area of accumulation (Park *et al.*, 2008). Therefore, a drug delivery method that will increase the aqueous solubility and intestinal permeability of the chemotherapy drug is required to overcome these problems and ensure a high drug bioavailability and retention time in the circulation system.

Another challenge that chemotherapy drugs face in their delivery to the cancerous site is the drug resistance of the tumour cells. The surrounding tissue of cancer tissue, in contrast with healthy tissue, experiences high hydrostatic pressure. This causes interstitial convective flow from the tumour site outwards developing a resistance to the drug by pushing it away and making it difficult to reach the target area (Park *et al.*, 2008). Moreover, even in the case that the chemotherapy drug effectively entered the tumour interstitium, its anticancer activity may be restricted when the cancer cells have developed multidrug resistance (MDR) (Brigger, Dubernet and Couvreur, 2002). MDR is when cells can repel drugs from the cancerous area due to the overexpression of P-glycoprotein (P-gp) plasma membrane (Fu, 2013).

All these issues associated with the implementation of anticancer drugs are the cause of limited chemotherapeutic efficiency. These problems can be addressed and resolved with the use of an effective, safe and reliable drug delivery system (DDS) that would aim to deliver the anticancer drug on the cancerous site with a minimal disruption to the healthy cells and tissue.

2.3. Drug performance improvement

2.3.1. Ideal drug delivery system characteristics

After analysing the main chemotherapeutic problems in the previous section, the properties that the ideal drug delivery system (DDS) should have to improve the anticancer drug applications are determined and summarised in this section.

First of all, the most important characteristic that the ideal drug delivery system should necessarily have is biocompatibility and biodegradability (Agostini *et al.*, 2017; Capasso Palmiero *et al.*, 2018). The materials used for the DDS have to be safe and compatible with the human tissue and should not be harmful or toxic to the living cells. Also, the delivery device should be able to degrade naturally in the human body leading to its exit through natural excretory pathways (Vasey *et al.*, 2019).

One of the main aims of a drug delivery system should be the maximisation of the drug retention time in the human body. The presence of the drug in the bloodstream of the patient for a long period of time is of great importance (Park *et al.*, 2008). Therefore, an ideal drug delivery system should enhance the circulation time of the chemotherapy drug in the vascular system, allowing for improved efficacy. To achieve this, the DDS is required to increase the aqueous solubility of the commonly insoluble and hydrophobic anticancer drugs (Savjani, Gajjar and Savjani, 2012). Moreover, the DDS should be responsible for avoiding the recognition and removal of the anticancer drug from the reticuloendothelial system (RES) (Lepeltier, Bourgaux and Couvreur, 2014).

Another important characteristic of the ideal DDS is high thermodynamic and chemical stability (Ferrari *et al.*, 2013; Iqbal and Ahmad, 2018). The method of delivery of the chemotherapy drug has to be strong, robust and reliable. Therefore, the DDS should have a tolerance in relatively mild thermal and chemical fluctuations to avoid its decomposition before the cancer target site or the desired retention (circulation) time is reached.

Finally, an important parameter is that the ideal drug delivery system should be cost effective. The cost should reflect the benefits that the DDS is providing into the delivery of the anticancer drug in the human body, but should also be kept in a reasonable range to ensure the widespread and commercial application of the drug delivery system in the future.

2.3.2. Polymeric nanostructures

The drawbacks and high costs associated with chemotherapy can be addressed and reduced by an effective DDS. Polymeric nanoparticles are particularly promising materials for serving as safe and robust DDSs for cancer chemotherapy drugs. A wide variety of polymeric nanoparticles with diverse properties and functionalities have been explored in the literature, each offering unique benefits for drug delivery. Here, the most commonly researched polymeric nanoparticles for DDS applications in cancer chemotherapy are presented and discussed. A schematic representation of these polymeric nanostructures is shown in Figure 2.1.

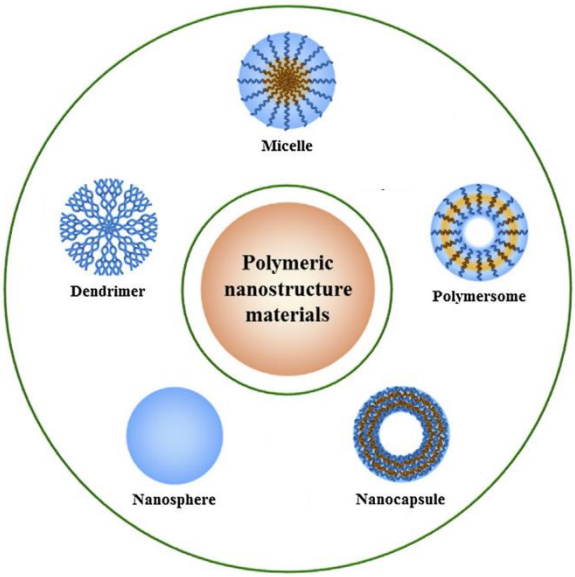

Figure 2.1: Schematic representation of the most commonly employed polymeric nanostructures in cancer chemotherapy drug delivery research. Taken and modified from Tang *et al.* (2016).

Polymeric micelles: These self-assembled structures are formed by amphiphilic block copolymers and are among the most extensively researched polymeric nanoparticles in the literature for drug delivery applications in cancer chemotherapy. This research focuses on polymeric micelles due to their highly desirable characteristics for effective drug delivery. Further details on their structure and properties are provided in section 2.3.3 of this literature review.

Polymersomes: These are vesicle-like nanostructures formed by the self-assembly of amphiphilic block copolymers in aqueous environments, creating a hollow core enclosed by a bilayer membrane. Their structure resembles liposomes but offers enhanced stability, tunable size, and greater control over membrane thickness due to the synthetic flexibility of polymers (Scheerstra *et al.*, 2022). In cancer chemotherapy, polymersomes are used as drug delivery vehicles to encapsulate both hydrophobic and hydrophilic drugs within the bilayer or core of the vesicle, respectively. This versatility allows for controlled and sustained drug release, while surface modifications can be added for targeted delivery to cancer cells, improving therapeutic efficacy and reducing side effects (Guan, Rizzello and Battaglia, 2015; Thambi, Park and Lee, 2015).

Nanospheres: These are solid, spherical nanoparticles typically composed of biodegradable polymers that encapsulate drugs within their matrix. Unlike hollow structures like polymersomes, nanospheres provide a dense core, making them highly effective for protecting encapsulated drugs from degradation and enabling controlled, sustained release (Tang *et al.*, 2016). In cancer chemotherapy, nanospheres can deliver hydrophobic or hydrophilic drugs, which are either dispersed within the polymer matrix or adsorbed onto the surface. Surface modifications, such as the addition of targeting ligands, allow for selective accumulation in cancerous tissues, enhancing treatment efficacy while minimizing side effects on healthy cells (Xiao *et al.*, 2022b; Elumalai, Srinivasan and Shanmugam, 2024).

Nanocapsules: These are core-shell nanoparticles where the drug is confined within a liquid or semi-solid core surrounded by a polymeric shell. This unique structure enables nanocapsules to effectively protect encapsulated drugs from premature degradation while allowing for controlled drug release (Bhardwaj and Jangde, 2023). In cancer chemotherapy, nanocapsules are used to deliver hydrophobic drugs within the core, while the polymer shell can be functionalized with targeting ligands for selective delivery to tumour cells. This design enhances drug stability, reduces side effects, and improves therapeutic efficacy by concentrating the drug at the cancer site, ultimately minimising adverse effects on healthy tissues (Deng *et al.*, 2020; Yousefi Rizi, Shin and Rizi, 2022).

Dendrimers: These are highly branched, tree-like macromolecules characterised by a central core, branching units, and terminal functional groups. Their precise structure and multi-functionality provide unique properties, such as highly controllable size and predictable release

profile, making them ideal for drug delivery applications (Kesharwani and Iyer, 2014). In cancer chemotherapy, dendrimers serve as nanocarriers that encapsulate chemotherapeutic agents, enhancing their solubility and stability while facilitating controlled release. Functionalisation of dendrimer surfaces with targeting ligands allows for selective delivery to cancer cells by active targeting, minimising toxicity effects and improving therapeutic efficacy (Ambekar, Choudhary and Kandasubramanian, 2020; Crintea *et al.*, 2023).

Polymeric liposomes: These are nanoscale vesicles with a lipid bilayer structure that incorporates polymers to enhance stability and control over drug release. A schematic representation of the different types of this polymeric nanoparticles is presented in Figure 2.2. Similar to traditional liposomes, they have an aqueous core for encapsulating hydrophilic drugs, while hydrophobic drugs can be embedded within the bilayer. The addition of polymers, however, provides increased structural integrity, prolonged circulation time, and the ability to fine-tune release rates, making them particularly useful in cancer chemotherapy (Cao, Dong and Chen, 2022; Sriwidodo *et al.*, 2022). Similarly to previous polymeric nanostructures, polymeric liposomes can be functionalised with targeting ligands for selective delivery to tumour cells for enhanced therapeutic efficacy.

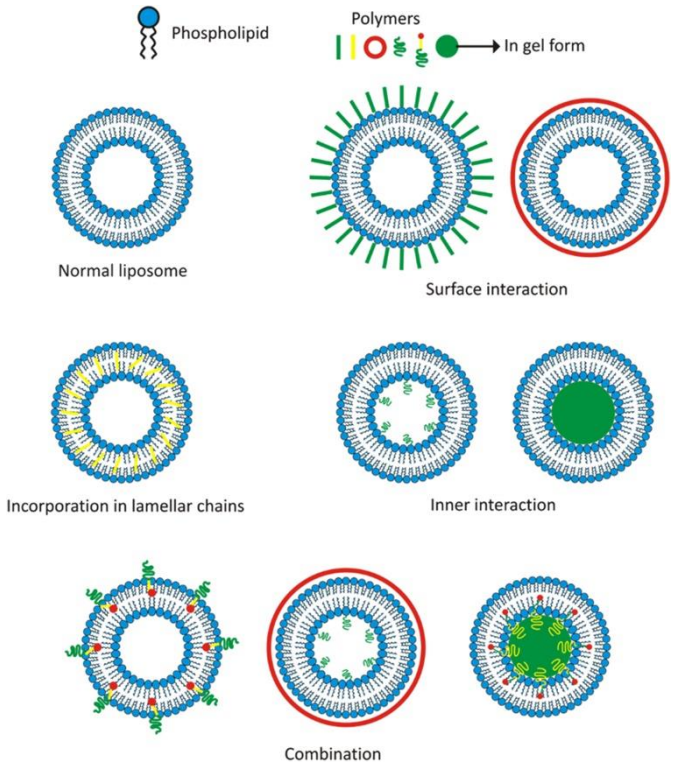

Figure 2.2: Schematic representation of the various types of polymeric liposomes that can be formed through different liposome-polymer interactions. Taken from Sriwidodo et al. (2022).

2.3.3. Polymeric micelles

Polymeric micelles are structures in the nano-scale formulated by the self-assembly of amphiphilic block copolymers when present in aqueous (polar) environments (Yadav *et al.*, 2019). Figure 2.3 shows schematically the generation of these type of polymeric nanoparticles. As seen from the diagram micelles are nanoparticles with a hydrophobic core and a hydrophilic corona and their size ranges from 10-100 nm (Park *et al.*, 2008).

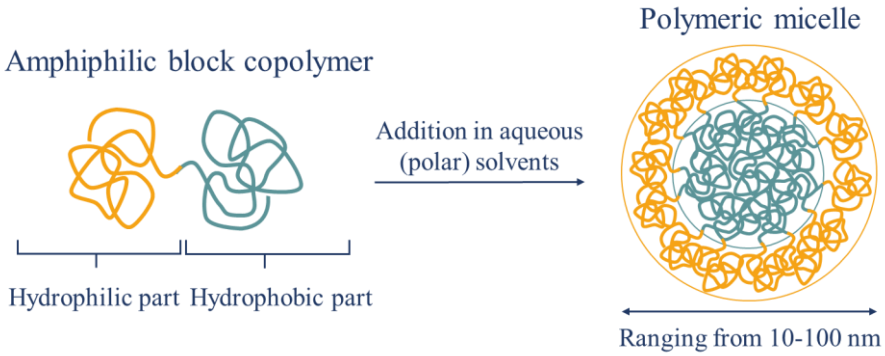

Figure 2.3: Schematic representation of the self-assembly of amphiphilic block copolymers into polymeric micelles when added in aqueous (polar) environments.

These particulate systems have gained a lot of attention in recent years due to their inherently good characteristics. It has been reported that they have high stability and tailorability (Tong and Cheng, 2008; Yin *et al.*, 2014). They are non-toxic, biodegradable and biocompatible, depending on the amphiphilic block copolymers forming the micelles, these are extremely important parameters for pharmaceutical and biomedical applications (Agostini *et al.*, 2017).

Therefore, polymeric micelles, constructed from biodegradable and biocompatible amphiphilic block copolymers (BCPs), containing a hydrophobic core and a hydrophilic shell are a promising DDS for chemotherapy drug encapsulation. The drug bioavailability and residence time in the circulation system is increased due to the hydrophilic shell, which increases the effective aqueous solubility of the drug. Moreover, anticancer drug encapsulation in polymeric micelles provides a masking effect to avoid recognition and removal from the reticuloendothelial system (RES) (Park et al., 2008).

The polymerisation reactions and synthesis methodology applied in literature to prepare the polymeric materials, which meet all the above requirements and lead to the construction of polymeric micelles and nanoparticles for pharmaceutical applications, are included in section 2.5 of this chapter. More details about the characteristics, the self-assembling behaviour and the different techniques followed in the literature to formulate the amphiphilic block copolymers into polymeric nanoparticles are incorporated in section 2.8 of this literature review.

2.4. Polymers for biomedical applications

2.4.1. Aliphatic polyesters

The use of aliphatic polyesters in biological and pharmaceutical applications has been in the centre of focus for a few decades. They have been explored for a range of biological applications including bone and tissue scaffolds, sutures and pharmaceutical encapsulation for drug and vaccine delivery systems (Oh, 2011; Hege and Schiller, 2014; Lepeltier, Bourgaux and Couvreur, 2014; Zhu *et al.*, 2016; Agostini *et al.*, 2018). The most important and researched aliphatic polyesters are the poly(lactide)s (PDLLA), poly(caprolactone)s (PCL), and poly(glycolide)s (PGA) and their copolymers, which have gained a lot of attention for biomedical applications (Seyednejad *et al.*, 2011; Brannigan and Dove, 2017). One of the benefits of these materials is that they can be produced through biological feedstocks, thus constituting them as environmentally friendly alternatives to petrochemical polymers.

These aliphatic polyesters have all the desirable characteristics mentioned earlier in this literature review that the ideal drug delivery system requires. They are biocompatible and hydrolytically degraded which allows the removal of their breakdown metabolites through natural excretory pathways in the human body. Moreover, they are mechanically strong, they can be sourced from abundant biological feedstocks, and can be produced via multiple synthesis pathways (Englezou *et al.*, 2020). All these properties of PLA, PCL and PLGA qualify them as extremely desirable materials for pharmaceutical applications.

2.4.2. Polymer classification

The simultaneous polymerisation of more than one type of monomers results in the formation of copolymers. The classification of the final material depends on the organisation of the different monomer types on the copolymer backbone. When the organisation of the monomer

species is completed randomly, then the resultant material is a random copolymer. When the monomer types are alternating across the polymer chain, then the final result is an alternating copolymer. If the repeating units form blocks of different molecular weights, then the polymer is termed a block copolymer. A grafted copolymer is formed when blocks of any monomer species branch from multiple points of the copolymer backbone. In the case that the blocks of any repeating unit all branch from the same point of the copolymer backbone, then the final material is a star copolymer. A schematic representation of the different copolymer structures mentioned is shown in Figure 2.4 for when two different types of repeating units are present.

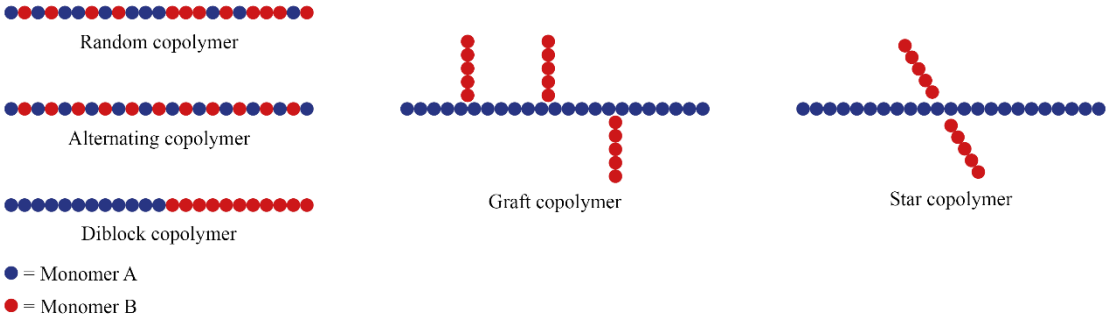

Figure 2.4: Schematic illustration of the different copolymer architectures that can be obtained from two different monomer species.

2.5. Polymer synthesis

2.5.1. Polymerisation reactions

Polymerisation reaction is the process of chemically combining relatively smaller molecules, called monomers, together to form larger chain or network molecules, called polymers. The combined monomers might be the same compound repeating in the polymer or they might be two or more different compounds, depending on the functionality of the final polymer product. When the repeating unit is the same monomer compound, then the final product is a homopolymer. When the final polymer contains more than one monomer compound this is called a copolymer (Young and Lovell, 2011).

There are many different types of polymerisation reactions and their reaction mechanisms vary from one another. The main classification used for the polymerisation reaction mechanism is step-growth and chain-growth polymerisation.

Step-growth polymerisation

This is also known as condensation polymerisation as defined by Paul J. Flory (1953). During the chain growth of the polymer a small molecule, usually water, is formed, hence the name condensation polymerisation. This type of polymerisation reaction proceeds in a step-wise manner. A pair of reactants (any size) combine at each step to form a longer molecule. The polymer molecule size and molecular weight increase at a slow rate and large polymer chains are obtained only at high conversions of monomer (Subramanian, 2015). One chain is created from two monomer molecules that combine to form a dimer. Then, it moves from dimer to trimer, to tetramer and so on until a high molecular weight molecule is finally formed (Figure 2.5). The reaction can proceed between any length size species present in the reaction system (Odian, 2004). For example, a dimer can combine with a monomer, dimer, trimer, tetramer etc to form a higher molecular weight compound.

Chain-growth polymerisation

This is also known as addition polymerisation as defined by Paul J. Flory (1953). No by-products are formed during the propagation of the polymer chain. A chain initiator is introduced into the reaction system to form the primary reactive centre such as a free radical, cation or anion to initiate the growth of the chain. Propagation of the polymer chain occurs with the successive addition of a number of monomers to the reactive centre. Polymer growth happens only by the reaction between monomer molecules and the reactive centre (Odian, 2004). The reactive centre is regenerated after every monomer addition (Figure 2.5). The rate of propagation happens at a faster pace than step polymerisation, forming high molecular weight molecules from the initial stages of the reaction (at lower conversions of monomer). Finally, the polymer chain growth stops with a termination reaction that deactivates the reactive centre (Figure 2.5) (Subramanian, 2015).

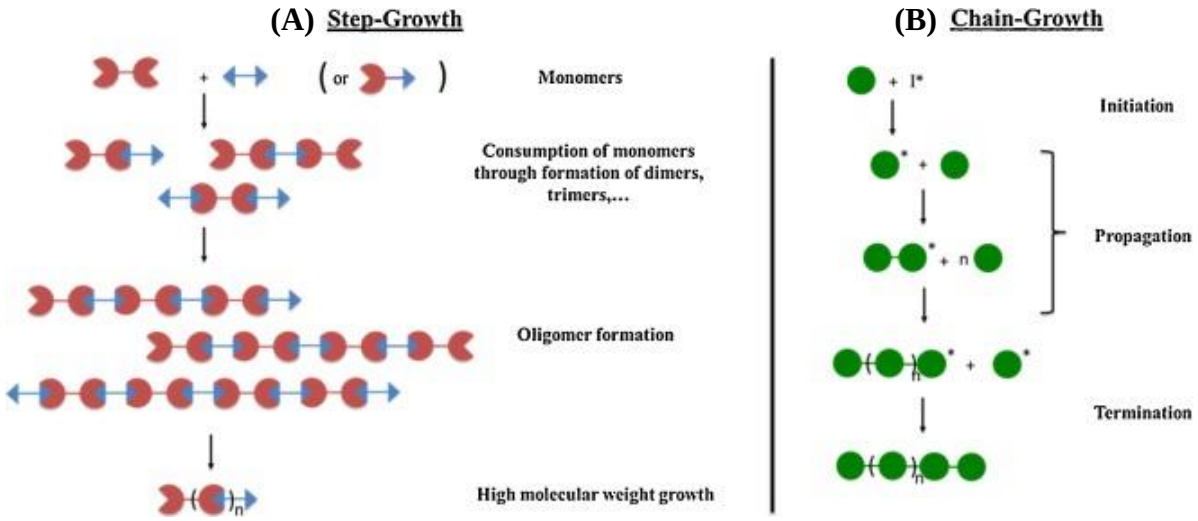

Figure 2.5: Schematic representation of the two main polymerisation mechanisms (A) Step-growth polymerisation and (B) Chain-growth polymerisation. Taken from Bossion et al. (2019).

Both step-growth and chain-growth polymerisations are valuable techniques for producing biodegradable and biocompatible block copolymers suitable for DDS. Step-growth polymerisation, commonly used to synthesise polymers like poly(lactic acid) (PLA), poly(glycolic acid) (PGA), and poly(lactic-co-glycolic acid) (PLGA), allows for precise control over polymer structure, enabling tailored hydrophilic-hydrophobic balances and degradation rates essential for sustained drug release (Balla *et al.*, 2021; Xu *et al.*, 2023). Chain-growth polymerisation, particularly through ring-opening polymerization (ROP), facilitates the creation of block copolymers such as poly(ε-caprolactone)-*block*-poly(ethylene glycol) (PCL-PEG) and poly(lactic acid)-*block*-poly(ethylene glycol) (PLA-PEG), which are ideal for forming nanoparticles or micelles that improve drug solubility and circulation time. Controlled polymerisation techniques in chain-growth methods also allow for fine-tuning of molecular weight and composition, enhancing DDS properties like drug release profile and biocompatibility (Matyjaszewski and Spanswick, 2005; Parkatzidis *et al.*, 2020). Together, these polymerisation methods enable the design of DDS with customisable degradation rates, amphiphilic characteristics, and compatibility with physiological environments.

The polymerisation reactions most commonly reported in the literature for the production of poly(lactide), poly(ε-caprolactone), poly(glycolide), and their copolymers, which are the focus of this research, are introduced and described below.

Ring Opening Polymerisation (ROP)

Ring Opening Polymerisation (ROP) is a type of chain-growth polymerisation. In this form of polymerisation, the monomer is a cyclic compound undergoing a ring breakage (opening of the cyclic structure) to form a linear polymer chain by successive addition of the, initially, cyclic monomers. The end of the growing polymer chain contains the reactive centre, which reacts with the cyclic monomers, breaks one bond to open up their structure and adds the monomer in the chain to form a longer polymer. The reactive centre is regenerated in the last added monomer and it can be anionic, cationic or radical (Young and Lovell, 2011). The most common monomers undergoing ROPs are cyclic esters (lactones), amides (lactams), ethers, acetals and siloxanes.

This is the primary polymerisation reaction and the first step to the procedures applied to produce aliphatic polyesters PLA, PCL and PLGA for biological applications.

Free Radical Polymerisation (FRP)

Free Radical Polymerisation (FRP) is a type of chain-growth polymerisation. This means that the three basic reactions taking place during FRPs are initiation, propagation and termination. The initiation reactions involve the constant formation of free radicals. These are the primary active centres that would enable the polymer chain growth. During propagation, the free radicals formed are facilitating the successive addition of monomer molecules to construct a larger polymer chain. Finally, during the termination stage a bimolecular reaction takes place between two reactive radical centres of two growing polymer chains converting them simultaneously to stable molecules. The two reactive radical centres are deactivated ending the chain growth for both growing polymers (Bailey *et al.*, 1984). The polymers produced from FRP are usually highly atactic and branched (Subramanian, 2015).

The conventional FRP process has a few limitations in the final polymer product functionality and properties. The slow initiation and inevitable termination associated with FRP results in poor control over the macromolecular structure during the polymerisation reaction. This leads to low control over the degree of polymerisation and the polydispersity of the final polymer product. Moreover, FRP has a restricted control on the chain architecture, chain composition and the end functionality of the final polymeric materials (Matyjaszewski, 1998). These limitations were address by the development of controlled radical polymerisations (CRP).

Controlled Radical Polymerisation (CRP)

Controlled Radical Polymerisations (CRP) are relatively new reaction techniques developed towards the end of the 1990s and start of 2000s. Before CRPs the production of polymers with an end-chain functionalisation were produced by the use of functional initiators or the use of a functional transfer agents. Although, there was no control over the final molecular weight of the synthesised polymers. With the use of CRP processes, the synthesis of end-chain functionalised polymers with controlled final molecular weights and low molecular weight distributions became easily accessible (Chen, Zhong and Johnson, 2016). Furthermore, CRPs enable the construction of more complicated macromolecular structures, such as block copolymers with controlled chain structures (Beija, Charreyre and Martinho, 2011). The ability to form polymeric materials with a great control over their final macromolecular structure enables the tuning of their final chemistry and properties, leading to their use in a number of different applications.

Some of the most commonly used CRPs include Nitroxide-mediated polymerisation (NMP) (Nicolas *et al.*, 2013), Atom transfer radical polymerisation (ATRP) (Siegwart, Oh and Matyjaszewski, 2012) and Reversible addition-fragmentation chain-transfer polymerisation (RAFT) (Barner-Kowollik, 2008).

Atom Transfer Radical Polymerisation (ATRP)

Atom Transfer Radical Polymerisation (ATRP) is a commonly used CRP. ATRP can take place in many different reaction conditions and various polymerisation solvents including water at room temperature. By varying the reaction conditions, the reaction kinetics can be altered to provide enhanced control over the polymerisation process. The final molecular weight, the molecular weight distribution and the end-functionality of the final polymer product can be regulated effectively with the use of ATRP. It can handle a variety of functional groups and it has been employed in a number of occasions to synthesize polymers intended for biomedical applications (Siegwart, Oh and Matyjaszewski, 2012).

The main advantages of ATRP when compared with other CRP processes is that it is a catalytic reaction (metal catalyst), it is compatible with a large number of initiators (including macroinitiators) and it can polymerise a number of monomer species. Moreover, it can be used for the simple substitution of the end-chain halogens by more functional groups using techniques such as electrophilic and nucleophilic displacement (Matyjaszewski, 1998).

Reversible Addition-Fragmentation chain-transfer polymerisation (RAFT)

Reversible Addition-Fragmentation chain-transfer (RAFT) polymerisation is a type of living and controlled radical polymerisation technique. It is the most commonly used polymerisation for the preparation of polymer material intended for biomedical applications after the ring opening polymerisation. RAFT polymerisation is a form of reversible-deactivation radical polymerisation. It utilizes a chain-transfer agent (CTA), typically a thiocarbonylthio compound referred to as a RAFT agent, to control the resulting molecular weight and polydispersity of polymers during the free-radical polymerisation processes (Ana A.C. Pacheco *et al.*, 2021). Therefore, RAFT provides polymers with low molecular weight dispersities and highly controlled molecular weights. The application of this type of polymerisation technique results in polymers with higher architecture complexity, such as brush, grafted and star copolymers (Le Hellaye *et al.*, 2008; Zhu *et al.*, 2016).

A lot of the times the combination of one or more of the discussed polymerisation reactions is incorporated in the polymer synthesis of poly(lactide)s, poly(caprolactone)s and poly(glycolide)s with the aim to develop material with enhanced and flexible properties and complex architectures to enhance their potential as an ideal polymeric material for biomedical applications (Capasso Palmiero *et al.*, 2018; Guo *et al.*, 2018).

2.5.2. Synthesis methodology of aliphatic polyesters

In this section the current state of the art in the synthesis procedures followed to produce the aliphatic polyesters of poly(lactide) (PLA) and poly(ε-caprolactone) (PCL) is analysed. The different methodologies applied to construct these polymers are critically analysed to find the optimal polymerisation conditions (temperatures, catalysts, time duration, etc) and apply them later in this research project to form the polymer library required for this investigation as part of the first objective of this thesis.

A summary of the synthesis papers available in the literature and the detailed methodology applied to construct block copolymers based on the aliphatic polyesters of PLA and PCL is presented in Table 2.1.

Table 2.1: Summary of PLA, PLGA and PCL synthesis papers in literature

Reference	Polymer	Method	Solvent	Main aim	Synthesis process	Main outcomes
Tunable PLGA-Based Nanoparticles Synthesized Through Free-Radical Polymerization - (Ferrari *et al.*, 2013)	HEMA-PLGA	ROP FRP	Bulk DCM	Qualitative degradation study for different compositions of PLGA nanoparticle suspensions.	• The desired amounts of $Sn(Oct)_2$ (catalyst), HEMA (initiator), lactide and glycolide (monomers) were all added after preparation into a glass vial under magnetic stirring and heated at 130 ºC. • After 90 min the reaction was stopped by refrigerating the reaction products at 4 ºC. • The HEMA-PLGA macromonomers were further polymerised to grafted materials through MSSEP (type of FRP) under a nitrogen stream and by heating at 80 ºC, which finally formed the desired nanoparticle colloidal suspensions.	• The two step synthetic procedure has successfully produced small NPs (40-200 nm) with low PSD (~0.1). • Full degradation of the material was achieved within 5 to 8 days at 50 ºC. • The degradation study has proven that the degradation time of the macromonomer can be tuned by its properties, such as chain composition and length.
Synthesis of Methacrylate-Terminated Block Copolymers with Reduced Transesterification by Controlled Ring-Opening Polymerization - (Ruiz-Cantu *et al.*, 2019)	HEMA-PCL/-PLA/-PTMC	ROP	DCM	Controlled ROP synthesis of end-group functional diblock and triblock copolymers by minimising transesterification reactions.	• The desired amounts of cyclic monomer (LA, CL or TMC) and initiator (HEMA or HEMA-PCL) were added in a stirred vial and closed with a rubber septum. 10 ml of anhydrous DCM was added and left at room temperature for 5-10 min to dissolve the mixture. TBD catalyst (based on monomer) was added to start the ROP. • The reaction was terminated by catalyst deactivation through acidic solution addition after the selected timeframe based on reagents ratios. Polymers were	• First successful HEMA-initiated ROP of LA, CL and TMC with TBD as catalyst. • Final diblock and triblock copolymers were synthesised with controlled Mw, low PDI and a monomethacrylate architecture. • By controlling the HEMA:TBD ratio and the reaction time the unwanted transesterification reactions were minimised for all the selected polyesters.

					purified through multiple precipitation steps and dried in a vacuum oven.	
Synthesis and Degradation Study of Cationic Polycaprolactone-Based Nanoparticles for Biomedical and Industrial Applications - (Agostini *et al.*, 2017)	HEMA-PCL	ROP FRP	Bulk DCM	Synthesis and degradation of positively charged HEMA-PCL nanoparticles prepared through ROP combined with free radical emulsion polymerisation (FREP).	• ε-caprolactone (monomer) was added in a stirred flask and heated up to 130 ºC to melt. The desired amounts of HEMA (initiator) and $Sn(Oct)_2$ (catalyst) were then added to start the ROP. • After 2.5 hours the reaction was stopped and the material was stored at 4 ºC. • The HEMA-PCL macromonomer was used in an acylation reaction with succinic anhydride and then a condensation reaction with choline chloride to positively charge the macromonomer, which was purified and stored in DCM at 4 ºC. • Finally, the cationic NPs were formed through FREP of the cationic macromonomers under a nitrogen stream and heating at 80 ºC.	• Cationic HEMA-PCL nanoparticles of different PCL lengths are successfully produced through a four step procedure. Namely ROP, acylation, condensation reaction and FREP. • From the degradation study it was concluded that the chain length is the main parameter affecting the degradation behaviour of the NPs. • The degradation time of the NPs can be tuned from the number of monomer units depending on the desired application.
Simultaneous Reversible Addition Fragmentation Chain Transfer and Ring-Opening Polymerization - (Le Hellaye *et al.*, 2008)	PHEMA-PCL	ROP-RAFT	Toluene	Combing ROP and RAFT in a simultaneous 'one-step' for the synthesis of grafted HEMA-PCL.	• CPDB (RAFT agent), AIBN (radical initiator), HEMA (ROP initiator), ε-CL (ROP monomer), $Sn(Oct)_2$ (ROP catalyst) and Toluene (solvent) were prepared and added in a stirred flask under nitrogen atmosphere at 100 ºC for 150 min. • Reaction was terminated by cooling down and exposing to air.	• Grafted copolymer HEMA-PCL was synthesised in a 'one-step' process combining RAFT and ROP for the first time. • This was verified by NMR and SEC analyses and consequent hydrolysis of PCL blocks.

					• Grafted HEMA-PCL was recovered and purified through a two-step precipitation process in pentane followed by methanol. • Final polymer product was dried at room temperature under vacuum for 24 hours.	• The resultant grafted copolymers are monodispersed with a narrow molar mass distribution.
Versatile, Highly Controlled Synthesis of Hybrid (Meth)acrylate-Polyester-Carbonates and their Exploitation in Tandem Post-Polymerization-Functionalization - (Pearce *et al.*, 2019)	HEMA-PLA(-tBSC) PEGMA-PLA(-tBSC) GDMA-PLA HEA-PLA(-tBSC)	ROP RAFT	DCM THF	Controlled synthesis of various LA and tBSC (cyclic carbonate monomer) polymers through (bis)(meth)acrylate initiated ROP with the use of DBU as organocatalyst.	• The predetermined amount of cyclic monomers (LA and/or tBSC) and initiator (HEMA, PEGMA, HEA or GDMA) were added in a stirred vial capped with a rubber septum. Anhydrous DCM was added to fully dissolve mixture at RT for 5-10 min. DBU catalyst (1.5mol% wrt monomer) was added to start the ROP. • The reaction was terminated by catalyst deactivation through addition into cold hexane after 15 min. Polymer was purified through multiple precipitation steps and dried in a vacuum oven. • The macromonomers were functionalised through RAFT reactions in THF in the presence of AIBN (radical initiator) and RAFT agent at 70 ºC for 8 h. • Finally, polymeric nanoparticles were prepared through nanoprecipitation.	• The ROP of LA and tBSC with a number of labile ester (bis)(meth)acrylate initiators was successful and controlled with the use of DBU as the organocatalyst. • Short homo- and copolymers were synthesised with good control over their final composition and properties. • Random and block amphiphilic copolymers were synthesised successfully through the tandem ROP-RAFT reaction with low dispersities in Mw. • DBU was proven to be suitable and versatile as a selective and mild ROP catalyst.
Strategies from nature: polycaprolactone-based mimetic antimicrobial	PCL-NH_2	ROP	Toluene THF	Design of novel biocompatible antibacterial agents based	• The first step for the synthesis of PCL-K_n is the synthesis of PCL-NH_2. ε-CL and toluene were added in a stirred flask at 110 ºC under nitrogen stream. *N*-Boc-	• The use of PCL-based diblock copolymers prepared through ROP to mimic AMPs was successful.

peptide block copolymers with low cytotoxicity and excellent antibacterial efficiency - (Zhou, He and Zhou, 2019)				on diblock copolymers of PCL-K_n (polylysine) mimicking the action mechanism and structure of natural antimicrobial peptides (AMPs).	ethanolamine and $Sn(Oct)_2$ were then added to start the ROP. • Reaction was terminated by cooling to room temperature after 48 hours. • The solution was treated with three precipitation steps in excess methanol and filtration. • Finally, it was mixed with excess HCl to remove the amino protection group (Boc) and dried under vacuum. • The lysine monomer was synthesised, polymerised through ROP in THF and reacted with PCL-NH_2 to from the final PCL-K_n product.	• Through haemolysis and cytotoxicity tests it was proven that PCL-K_n have enhanced biocompatibility compared to conventional methods. • They have comparable bactericidal mechanism with AMPs, rapid (within 30 min) bactericidal action and avoided the drug resistance of both *S. aureus* and *E. coli* bacteria.
Polylactide-Based Nanoparticles with Tailor-Made Functionalization - (Beer *et al.*, 2015)	HEMA-PLA	ROP	p-xylene Toluene	Prove the versatility of emulsification/ solvent evaporation process for the formulation of PLA-based NPs with covalently bonded carboxyl groups and fluorescent dye.	• In a magnetically stirred flask lactide and p-xylene were added at 130 ºC under nitrogen stream. HEMA and $Sn(Oct)_2$ were injected to start the ROP reaction. • Cooling of the mixture after 4 h terminated the reaction and the material was recovered through precipitation, multiple dissolve-wash steps and drying in a vacuum oven at 80 ºC for 2 h. • The covalent bonding of carboxyl groups and fluorescent dye was performed through FRP in toluene under Ar stream at 40 ºC overnight. Same procedure with before was followed for recovery and purification of the material.	• Successfully covalently bonded fluorescent dye molecules for particle tracking and carboxyl groups located on particle surface aimed for targeted delivery. • NPs were formed using two different methods; pre-functionalisation followed by NP formation and the simultaneous process. • NP results were similar for the two processes and the functionalised ones showed increased stability in NaCl.

Paclitaxel-Initiated, Controlled Polymerization of Lactide for the Formulation of Polymeric Nanoparticulate Delivery Vehicles - (Tong and Cheng, 2008)	Ptxl-PLA PEG-PLGA	ROP	THF	Prepare paclitaxel conjugates with PLA (Ptxl-PLA) through ROP to form nano-conjugates (NCs) for cancer chemotherapy	• The predetermined amounts of Ptxl and BDI-Mg catalyst were added in a stirred vial with anhydrous THF. LA dissolved in THF was added dropwise into the former vial to initiate the ROP carried out at room temperature for a few hours. • The reaction mixture was precipitated in ethyl ether after full LA consumption to recover the Ptxl-PLA conjugate. • PEGylated nanoconjugates were formulated through co-precipitation of Ptxl-PLA with PEG-PLGA.	• Demonstrated a new method for nanoconjugate preparation using a drug-initiated ROP of LA. • The NCs experienced high drug loadings, narrow PSDs and an improved release profile by minimising the drug burst release issues. • Zn has proven to control the LA ROP better than Mg with targeted Mws and low Đ.
Anticancer camptothecin-*N*-poly(lactic acid) nanoconjugates with facile hydrolysable linker - (Yin *et al.*, 2014)	CPT-*N*-PLA PEG-PLA	ROP	THF	Perform the conjugation of camptothecin (CPT) to the terminal carboxylate group of PLA through a hydrolysable amino ester linker via a controlled ROP.	• BDI-Zn catalyst and CPT-*N*-OH (drug initiator) were weighted and added in a stirred vial to dissolve in anhydrous THF. LA was also weighted and added in a vial to dissolve in THF. The latter solution was added to the former to initiate the ROP reaction. • After full consumption of LA, the reaction mixture was quenched into ice cold methanol, centrifuged and dried in a vacuum oven. • The CPT-*N*-PLA nanoconjugates (NCs) were formed through co-precipitation with mPEG-PLA copolymer.	• The conjugation of CPT and PLA through a hydrolysable amino ester linker was successful. • The CPT-*N*-PLA NCs were able to self-assemble with sizes smaller than 100 nm. • Compared to previous CPT-PLA NCs they have accelerated and improved release kinetics. • The NCs exhibit higher *in vivo* efficiency and minimise systemic toxicity.
Role of Self-Assembly Conditions and	PEG-PLA	ROP	DCM	Complete a systematic study of the	• The desired amount of mPEG (2000 or 5000) initiator and DL-LA were weighted and added in a stirred capped vial.	• The nature of the organic and aqueous solvent, their ratios during

Amphiphilic Balance on Nanoparticle Formation of PEG-PDLLA Copolymers in Aqueous Environments - (Phan *et al.*, 2019)				different parameters that influence the formation of PEG-PLA nanoparticles, based on the NP size and stability.	Anhydrous DCM was added to fully dissolve the mixture. DBU catalyst (3%w/w wrt LA) was added to start the ROP at room temperature. • Reaction mixture was quenched dropwise in cold hexane after 15 min. • Polymer was purified and collected via multiple precipitation steps (hexane and diethyl ether) and vacuum oven drying. • The different BCPs produced were formulated into NPs though varying the different processing conditions of the solvent displacement method.	nanoprecipitation and the hydrophobic and hydrophilic composition of the BCPs were investigated to assess their influence on the size and stability of the NPs. • It was observed that BPCs NPs with small hydrophilic block% have higher stability. • A methodological process to achieve NPs with desired properties was performed.
Amphiphilic tri- and tetra-block co-polymers combining versatile functionality with facile assembly into cytocompatible nanoparticles - (Vasey *et al.*, 2019)	PEG-PLA-tBSC HEMA-PLA-tBSC	ROP RAFT	DCM THF	Construct a library of mixed-polyester-polycarbonate polymers with different characteristics desirable in biomedical and therapeutical applications.	• The PEGylated initiator, lactide and tBSC were added in a magnetically stirred vial and capped with rubber septum. Dry DCM was added to fully dissolve the mixture. The catalyst (DBU) was added (1.5-3%mol/mol wrt total monomers) to initiate the ROP at room temperature. • The catalyst was deactivated through precipitation in cold hexane (or diethyl ether in the case of HEMA) to stop the reaction after 15 min. • The polymer was purified after multiple precipitation steps and vacuum drying.	• DBU was employed as a selective and mild catalyst for the controlled ROP of different PEGylated initiators. • The polymers were produced through an easy and accessible method, required minimal purification steps, were successfully functionalised with drug molecules and labels and their cytocompatibility was proven on a model cell-line.

There are a variety of catalysts (metal-based or metal-free) able to catalyse an ROP process (Table 2.1), in solution or bulk (Shoda *et al.*, 2016). Among the commercially available catalyst, the organocatalyst DBU and the enzyme Lipase are able to catalyse the ring opening of various cyclic monomers in mild and controlled conditions (Kumar and Gross, 2000; Pratt *et al.*, 2006). Due to their different chemical affinity it is fundamental to combine the two catalysts for the production of mixed lactone-lactide copolymers. However, the reaction timeframe in which they act is completely different (minutes for DBU and hours for the biocatalyst) and difficulties can be encountered as well as side reactions may occur (Huang *et al.*, 2019).

As seen from Table 2.1, the most commonly used solvents for polymerisation processes are petrochemical solvents such as toluene, dichloromethane (DCM) and tetrahydrofuran (THF). The rationale behind their wide usage is owned to their great dissolving properties and their relatively lower cost. Although, these solvents are harmful to the environment (Byrne *et al.*, 2016) and hazardous to human health according to the International Agency for Research on Cancer (IARC) evaluations by the World Health Organisation (IARC Monographs, 2016, 2019). Moreover, toluene is a highly flammable substance. Therefore, the use of these chemical solvents poses environmental and health risks. The fundamental principles of green chemistry promote the use of 'greener' and safer chemicals to replace harmful substances. This proposition has been codified by European Union (EU) legislation and the Registration, Evaluation, Authorisation and Restriction of Chemicals (REACH) has applied restrictions on the use of these petrochemical solvents (European Commission *et al.*, 2017).

Economic pressure drives the use of 'greener' solvents that are sourced through biological and renewable feedstocks to replace petrochemical solvents in polymerisation processes (Machado *et al.*, 2018; d'Almeida Gameiro *et al.*, 2020; Vergaelen *et al.*, 2020). 2-Methyltetrahydrofuran (2-MeTHF) has been proposed as a suitable bio-sourced substitute to petrochemical solvents.

2-MeTHF is a neoteric volatile cyclic ether produced from the chemo-catalytic treatment of biomass (Pace *et al.*, 2012; Pellis *et al.*, 2019). It has been utilised in various laboratory-scale chemical processes (Aycock, 2007), including the ROP of terpene-initiated LA (O'Brien *et al.*, 2020), and it has been characterised for biological applications (Antonucci *et al.*, 2011).

Table 2.2 contains information about selected solvent properties of 2-MeTHF in comparison with DCM and THF polymerisation solvents. The cost of 2-MeTHF, at laboratory scale, is

comparable to that of DCM and THF and is expected to be reduced with scale-up production. The Hildebrand solubility parameter of 2-MeTHF is reported to be 16.9 $MPa^{1/2}$ (Aycock, 2007). Therefore, 2-MeTHF is expected to be a good solvent for ROP with a solvent power close to DCM and THF, which have Hildebrand solubility parameters of 20.2 and 18.6 $MPa^{1/2}$ respectively. Moreover, the boiling point of 2-MeTHF is higher than the conventional petrochemical solvents, allowing reactions to take place at higher temperatures. This enables its use as a solvent for thermally initiated radical reactions under ambient pressure. These physical properties of 2-MeTHF suggest that it could be used as an effective solvent for various reactions. Testing the ability of 2-MeTHF to perform as the polymerisation solvent for multiple synthesis procedures is the aim of the experimental work completed and presented later in this thesis (Chapter 4).

Table 2.2: Comparison of selected solvent properties taken from (Englezou *et al.*, 2020).

Solvent	Cost (£/L)[a]	$d_{Hildebrand}$ ($MPa^{1/2}$)	T_b (°C)[a]
2-MeTHF	51.5	16.9[b]	80.2
DCM	25.4	20.2[c]	39.8
THF	37.9-81.0	18.6[c]	65.0

[a]All costs and boiling points tabulated for laboratory scale materials sourced from Sigma-Aldrich website; [b]Value obtained from Aycock (2007); [c]Values obtained from Physical Properties of Polymers Handbook, 2nd ed., J. E. Mark (Mark, 2007).

In some cases, papers in the literature researching on the synthesis of block copolymers based on aliphatic polyesters emphasise on studying the degradability and the solution behaviour of the constructed polymeric materials. Since these materials are usually aimed for biomedical and pharmaceutical applications, their degradability and decomposition profile should be investigated and analysed.

The effect of polymer characteristics, such as the composition and the chain length, as well as the processing conditions on the degradation behaviour of HEMA-PLGA polymers was investigated by Ferrari *et al.* (2013). The first step of this investigation was the synthesis of controlled length and composition polymers based on lactide and glycolide with the use of a ROP reaction initiated by HEMA. HEMA-L_xG_yA macromonomers were successfully constructed and utilised in a second step using a free radical polymerisation to form small nanoparticles of grafted polymers. More specifically, PLGA nanoparticles with a controlled size and low polydispersity index (PDI) were formulated by emulsion polymerisation of the

prepared HEMA-L_xG_yA macromonomers under starved conditions. Moreover, the stability and the degradability of the PLGA nanoparticles produced was examined with a qualitative degradation study with the aim to extract a relationship between the degradation time and the polymer material characteristics. The change of nanoparticle sizes over time of different lactide and glycolide composition nanoparticle suspensions was monitored with the use of Dynamic light scattering (DLS) until the full extinction of nanoparticles. The pH of the nanoparticle suspension was also monitored during the degradation study to examine the release of acidic species related to the degradation of the HEMA-PLGA nanoparticles to lactic acid, glycolic acid and poly(methacrylic) acid (see Figure 2.6(A)). In Figure 2.6(B) is observed that the nanoparticle size the first days was constant, followed by an increase in size in the following days till the full disappearance of the nanoparticles. The nanoparticle size increase is justified since during their degradation they release hydrophobic oligomers in solution, which increases their hydrophilicity and affinity towards water. Therefore, this leads to the swelling of the nanoparticles, followed by finally their dissolution and extinction. Finally, from Figure 2.6(B) one can see that the degradation time increases in the following order, poly(HEMA-g-GA_4), poly(HEMA-g-L_2G_2A), poly(HEMA-g-L_3G_1A) and poly(HEMA-g-LA_4). This is due to more hydrophobic materials requiring a longer degradation time (LA is more hydrophobic than GA) and is also observed when the polymer hydrophobic length is higher, leading to a higher degradation time. Therefore, the degradability of the polymer and nanoparticles can be tuned by controlling the hydrophobic/hydrophilic lengths and the monomer types of the polymer (Ferrari *et al.*, 2013).

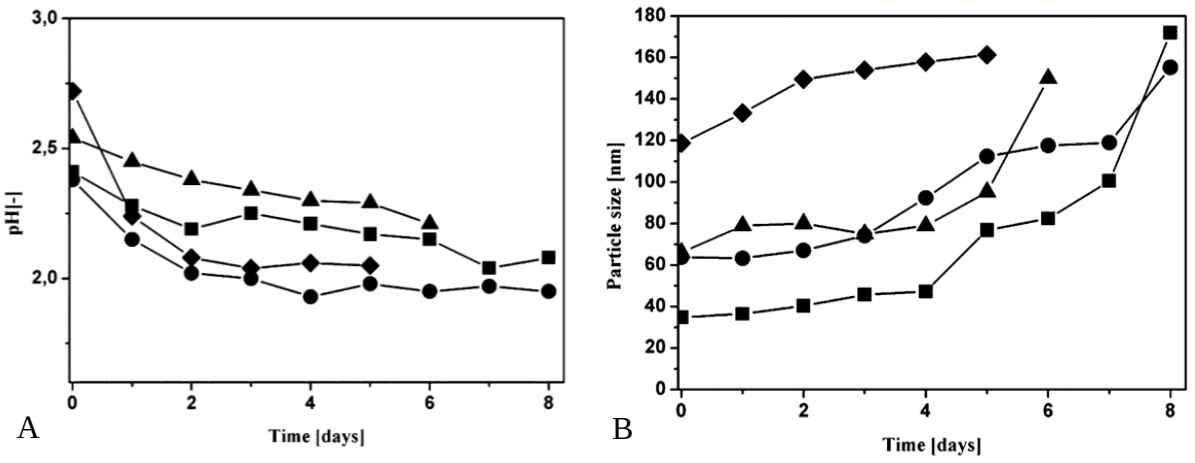

Figure 2.6: pH (A) and particle size (B) versus time during the nanoparticle degradation study for poly(HEMA-g-LA4) (■), poly(HEMA-g-L3G1A) (●), poly(HEMA-g-L2G2A) (▲) and poly(HEMA-g-GA4) (♦). Diagram from (Ferrari et al., 2013).

The use of triazabicyclodecene (TBD) as a catalyst for the ROP of HEMA-initiated polymers has been investigated by Ruiz-Cantu *et al.* (2019). The final macromolecule structure produced based on various feed compositions is examined and the optimal reaction conditions and HEMA:TBD ratio are established for minimisation of the competing transesterification reactions and leading to polymerisation control. TBD has a higher catalytic activity than other organic catalysts because it activates both the monomer and the initiator during a polymerisation process (Kamber *et al.*, 2007). The aim of this paper was to develop a high selectivity synthesis pathway for polymerisation when employing functional initiators, such as HEMA, by accommodating for the retention of their end-group functionality. The ROP of three different monomers; lactide (LA), ε-caprolactone (CL) and trimethylene carbonate (TMC) was performed. The synthesis of polymers with only one methacrylate terminus, low molecular weights, high conversion of monomer and controlled polydispersity was successful for all the monomers and their combinations forming mixed block copolymers. The results of this synthetic route have shown the ability of TBD to be applied as an active and selective catalyst for the controlled ROP of HEMA-initiated polymers, in contrast to the uncontrolled polymerisation reaction that was suggested by Capasso Palmiero *et al.* (2018) due to a series of competing side reactions. Ruiz-Cantu *et al.* (2019) demonstrated that the polymerisation control and the minimisation of the unwanted side reactions is achieved when the polymerisation kinetics of the monomer are fast. This is accomplished in this investigation by controlling the reaction time and the HEMA:TBD reaction ratio.

Positively charged HEMA-PCL polymeric nanoparticles were constructed via a four-step reaction procedure by Agostini *et al.* (2017). The use of positively charged polymers has a number of industrial and biomedical applications, such as flocculants in wastewater treatment (Lee, Robinson and Chong, 2014; Gumfekar *et al.*, 2017), oral delivery of drugs in biological systems (Jain *et al.*, 2012; Schulz, Gauthier and Leroux, 2015) and delivery of genetic material inside cells (Han *et al.*, 2014; Ramamoorth and Narvekar, 2015). The formulation of biodegradable and biocompatible cationic HEMA-PCL nanoparticles is based on a four-step synthesis pathway. Initially, the synthesis of ester-based macromonomers is performed through the HEMA-initiated ROP of ε-caprolactone (CL) leading to HEMA-PCL block copolymers. The second step involves the acylation reaction of the resulted HEMA-PCL macromonomers with succinic anhydride followed by the condensation of the acylation product with choline chloride to produce the cationic macromonomer. The final step is the free radical emulsion

polymerisation (FREP) of the positively charged macromonomer to form the cationic-based nanoparticles. The nanoparticles were produced by applying two different FREP approaches; the batch emulsion polymerisation (BEP) and the monomer-starved semi-batch emulsion polymerisation (MSSEP). The influence of the reaction conditions on the final product properties was investigated and it was concluded that at MSSEP the nanoparticle sizes were smaller, although the PDI is higher than at BEP. Moreover, the tunability of the constructed nanoparticles in terms of degradation time was studied. The degradation study was carried out in two different mediums and conditions. Namely the degradation kinetics in an aqueous cell medium at 37 ºC and in deionized water at 90 ºC were investigated. The results obtained from the degradation study of the final nanoparticles are in agreement with the conclusions drawn by Ferrari *et al.* (2013), including that the degradation rate of the polymers is controlled by the length of the hydrophobic block and its hydrophobic nature. The longer the length of the hydrophobic block the longer the degradation time and the higher temperature of the medium the higher the degradation rate.

In the case of Ruiz-Cantu *et al.* (2019) the ROP was achieved under mild reaction conditions (room temperature and atmosphere) by combining the use of DCM as a solvent and the active catalyst TBD. In contrast to other papers that have used a bulk polymerisation condition with tin octoate as the catalyst, where a significantly higher reaction temperature (>130 ºC) is required for both the activation of the catalyst and to fully melt the initiator and monomer to enhance their mixing for the reaction to be possible. In the latter case, a critically higher reaction time is also required for the ROP completion, thus leading to an extremely higher energy requirement for the ROP reaction to be performed under bulk conditions and with tin octoate as the catalyst.

In summary, the findings from the polymer synthesis area analysis show that there is a robust and generally reproducible synthesis technique for cyclic polyesters, such as PLA and PCL. The knowledge gathered from the literature papers analysed in this area will be applied when the synthesis of the BCPs in this investigation is performed. Most importantly, the research gap in this area is identified, which is the requirement to use a green polymerisation solvent for the synthesis of these polymers and the avoidance of harmful and toxic DCM, THF and Toluene, since the material is intended as a drug delivery system for cancer chemotherapy.

2.6. Polymer physics background

Polymers in solutions or in melt would take the conformation of a random coil. The polymer backbone (i.e. the polymer main chain) randomly adopts all possible configurations in three dimensions following the random walk model, where the covalently bonded monomer subunits of the polymer are aligned randomly in space (Rubin, 1965; Haber, Ruiz and Wirtz, 2000). A schematic depiction of a polymer random walk and a random coil configuration is presented in Figure 2.7.

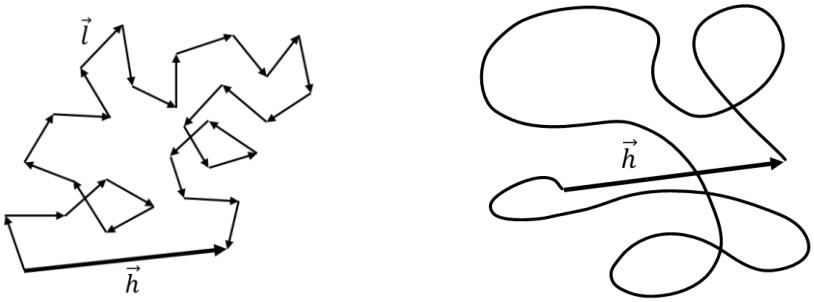

Figure 2.7: Schematic diagram on the left of a polymer random walk depicted with the monomer subunits oriented randomly in space. The average chemical bond length in the polymer backbone is symbolised with $\vec{l}$. On the right is a simplified depiction of a random polymer coil. The end-to-end distance ($\vec{h}$) of the polymer is shown in the diagrams.

End-to-end distance ($\vec{h}$) is the distance between the two chain ends for a coiled polymer. The number of repeating monomer units in a polymer chain is defined as the Polymerisation Index or the Degree of Polymerisation and is symbolised by DP_n or N. The length of a single monomer subunit of a polymer chain is estimated by the statistical segment length (b). The root-mean-square end-to-end distance (h_{rms}) of a polymer chain of N repeating units of b length is given by Equation 2.1.

Equation 2.1: Root-mean-square end-to-end distance

$$h_{rms} = \sqrt{\langle \vec{h}^2 \rangle} = \sqrt{C_\infty n}\, l_b = \sqrt{N}\, b$$

h_{rms} Root-mean-square end-to-end distance

$\vec{h}$ End-to-end distance

C_∞ Characteristic ratio

n Number of chemical bonds in one repeating unit (monomer)

l_b Average length of the chemical bonds in the monomer

N Number of repeating segments in the polymer

b Statistical segment length

The characteristic ratio (C_∞) is a characteristic property of the polymer and is related to the rigidity and flexibility of the polymer chain. Its value is dependent on the angle of the polymer backbone bonds and the walk model followed by the polymer (i.e. freely joint, free rotation or hindered rotation bonds) (Paul J. Flory, 1953).

Another property of the polymer chain that is important is the Kuhn length developed by Hans Kuhn (Kuhn, 1950; Kuhn, Försterling and Waldeck, 2009). This is a theoretical approach applied for real polymer molecules, where they are regarded as a number *N* Kuhn segments of *a* Kuhn segment length. Scientists are often using the Kuhn length interchangeably with the statistical segment length *b*. In worm-like (i.e. semiflexible) polymer chains, the Kuhn length is twice the value of the persistence length ($\mathfrak{a} = 2L_p$), which is described as the distance in which the chemical bond orientation persists and is measure of the stiffness of the polymer chain (Zhang *et al.*, 2019; Gerrits, Hammink and Kouwer, 2021). The Kuhn length can be estimated using Equation 2.2.

Equation 2.2: Kuhn length

$$\mathfrak{a} = \frac{\langle h^2 \rangle}{L_C}$$

$\mathfrak{a}$ Kuhn length

$\langle h^2 \rangle$ Mean-square end-to-end distance

L_C Contour length

Contour length (L_C) is the length of the fully extended polymer chain and it can be calculated by Equation 2.3.

Equation 2.3: Contour length

$$L_C = \varepsilon n l_b = N\alpha$$

L_C Contour length

ε Geometric factor < 1

n Number of chemical bonds

l_b Average length of the chemical bonds

N Number of repeating segments in the polymer

α Kuhn length

When describing the structure and dimensions of macromolecules in polymer physics an essential property that has to be defined is the radius of gyration (R_g) of the polymer chain. The radius of gyration is a measure of the average distance of each of the monomer units in the polymer chain from the centre of mass of the polymer coil (Fixman, 1962). Under theta conditions (i.e. polymer follows the random walk model) the radius of gyration can be estimated using Equation 2.4.

Equation 2.4: Radius of gyration

$$R_g{}^2 = \frac{\langle h^2 \rangle}{6} = \frac{Nb^2}{6}$$

R_g Radius of gyration

$\langle h^2 \rangle$ Mean-square end-to-end distance

N Number of repeating segments in the polymer

b Statistical segment length

The radius of gyration is extremely important because it can be established through experimental techniques, such as light scattering (static and dynamic) and small angle neutron- and X-ray scattering, and therefore the rest of the polymer physical properties can be derived by applying the polymer physics theory (Kratky and Laggner, 2003; Ochbaum and Bitton, 2018).

2.7. Block copolymers in solution

When amphiphilic block copolymers are in solution with a block selective solvent they self-assemble into micelles, which are nanoparticle structures in suspension with the solvent. This is a significantly valuable property of amphiphilic block copolymers with numerous applications. In this case, the focus of this work is on exploiting this ability of block copolymers to form drug delivery systems that can solubilise insoluble substances, such as the chemotherapy drugs, in aqueous media.

The critical micelle concentration (cmc) is defined as the concentration above which the amphiphilic block copolymer chains associate with each other to form micelles in solution. At this concentration, amphiphilic block copolymers begin to self-assemble. Above this concentration any additional block copolymers chains in the solution will enter the micellar phase (Kozlov *et al.*, 2000; Liu, Liu and Chu, 2000; Topel *et al.*, 2013; Baccile and Poirier, 2023). Below the cmc, the copolymer chains remain as individual, unassociated molecules that interact freely with the solvent and there are no micelle structures present. This is represented schematically in Figure 2.8. The micellar phase represents an equilibrium state, and the system is considered to be at thermodynamic equilibrium. Therefore, the presence of micelles in solution does not preclude some individual block copolymer chains from remaining free in the surrounding solution. There is a constant exchange of individual chains between the micelles and the solution, with this dynamic balance influenced by factors such as temperature, pH, polymer concentration, and solvent conditions (Leibler, Orland and Wheeler, 1983; Munch and Gast, 1988).

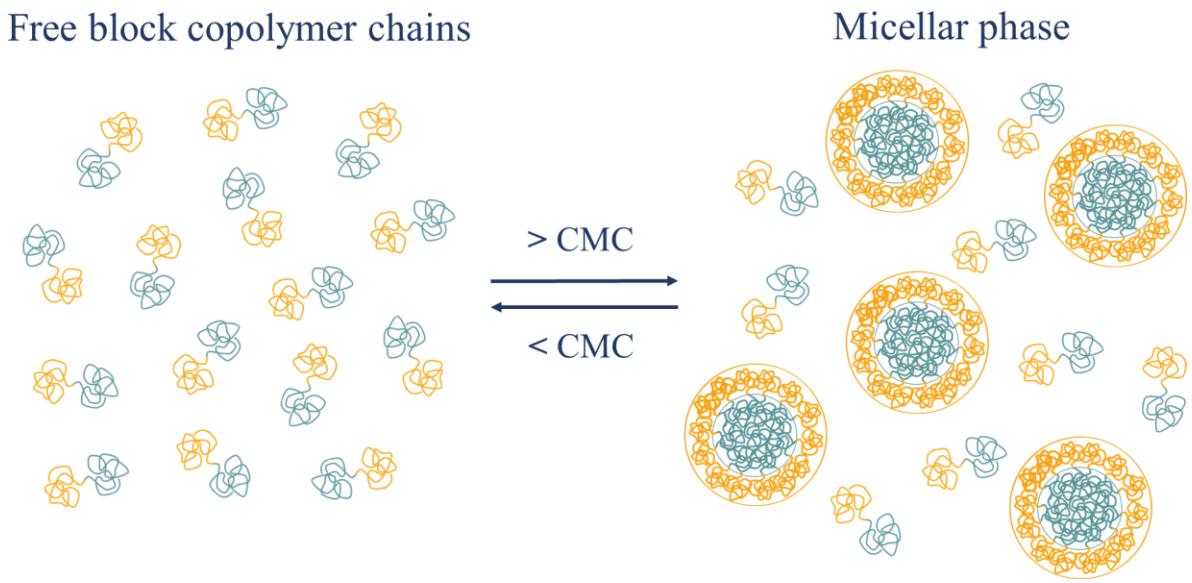

Figure 2.8: Schematic representation of amphiphilic block copolymers in solution. Below the cmc, the block copolymers chains interact freely with the solvent, while above the cmc, they assemble into polymeric micelles. The micellar phase displays a dynamic balance between polymeric micelles and individual free block copolymer chains.

2.7.1. Flory Huggins solution theory

Flory-Huggins solution theory is a simplified lattice model, which can be used to describe the thermodynamic state of a polymer solution. It is an expression based on the Gibbs free energy thermodynamic equation (see Equation 2.5) applied for the mixing of a polymer with a solvent.

Equation 2.5: Gibbs free energy

$$\Delta G_{mix} = \Delta H_{mix} - T\Delta S_{mix}$$

ΔG_{mix} Gibbs free energy of mixing

ΔH_{mix} Enthalpy term of the mixing process

T Absolute temperature

ΔS_{mix} Entropy term of the mixing process

The Flory-Huggins theory can be applied to estimate the solubility of a polymer in a solvent by taking into consideration a limited set of system parameters. Namely, one would require the Flory-Huggins interaction parameter between the polymer and the solvent, the composition of the polymer solution and the chain length of the polymer molecule to define the mixing energy

between polymer and solvent (Paul J. Flory, 1941; Maurice L. Huggins, 1941). The Flory-Huggins expression for a polymer-solvent system is given in Equation 2.6.

Equation 2.6: Flory-Huggins theory for polymer-solvent systems

$$\frac{\Delta G_{mix}}{RT} = n_1 \ln \varphi_1 + n_2 \ln \varphi_2 + n_1 \varphi_2 \chi_{12}$$

ΔG_{mix} Gibbs free energy of polymer-solvent mixing

R Universal gas constant

T Absolute temperature

n_1 Number of moles of component 1 (solvent)

n_2 Number of moles of component 2 (polymer)

φ_1 Volume fraction of component 1 (solvent)

φ_2 Volume fraction of component 2 (polymer)

χ_{12} Flory-Huggins interaction parameter between solvent and polymer

The Flory-Huggins interaction parameter is a quantitative measure of the interaction degree between the two components (solvent-polymer) in the system. It considers the energy of interspersing the component molecules on a lattice (Tambasco, Lipson and Higgins, 2006; Nistane *et al.*, 2022). When the interaction parameter is lower, then the solvent and polymer interactions are favourable leading to higher mixing of the two components. Therefore, low χ parameter means the polymer is soluble in the solvent (Lindvig, Michelsen and Kontogeorgis, 2002).

2.7.2. Self-assembly of block copolymers

It was mentioned at the beginning of section 2.7 that when the block copolymers are in solution above a specified concentration, defined as the critical micelle concentration, they tend to self-assemble into micellar structures in suspension with the solvent. The micellar structures formed by the block copolymers vary in size and geometry depending on the polymer and solvent properties and interactions (Yamada, 2014).

Critical packing parameter

The critical packing parameter (*cpp*) of the copolymer chain was introduced and applied to determine the morphology and geometry that the amphiphilic molecules will acquire when in solution above the critical micelle concentration (Nagarajan, 2002). Some of the properties of the polymer-solvent system that can affect the *cpp* include the polymer composition and concentration, the solvent quality, water content in the solution and the presence of surfactants and additives (Li *et al.*, 2020). The critical packing parameter can be calculated using Equation 2.7.

Equation 2.7: Critical packing parameter of the copolymer chains

$$cpp = \frac{v_B}{a_0 L_B}$$

cpp Critical packing parameter

v_B Volume of the hydrophobic block

a_0 Contact area of the hydrophilic block

L_B Length of the hydrophobic block

When *cpp* < 1/3, it was observed that the block copolymers were forming spherical micelles. When 1/3 < *cpp* < 1/2, the block copolymers would compose cylindrical micelles. If the packing parameter ranges from 1/2 < *cpp* < 1, then the block copolymers would organise into vesicles. Finally, when *cpp* = 1, the block copolymers construct planar bilayers or lamellae and when *cpp* > 1, they assemble into inverted spherical micelles (Yamada, 2014; Kuperkar *et al.*, 2022). The different geometries that are adopted from block copolymers in solutions based on their critical packing factor are demonstrated in Figure 2.9.

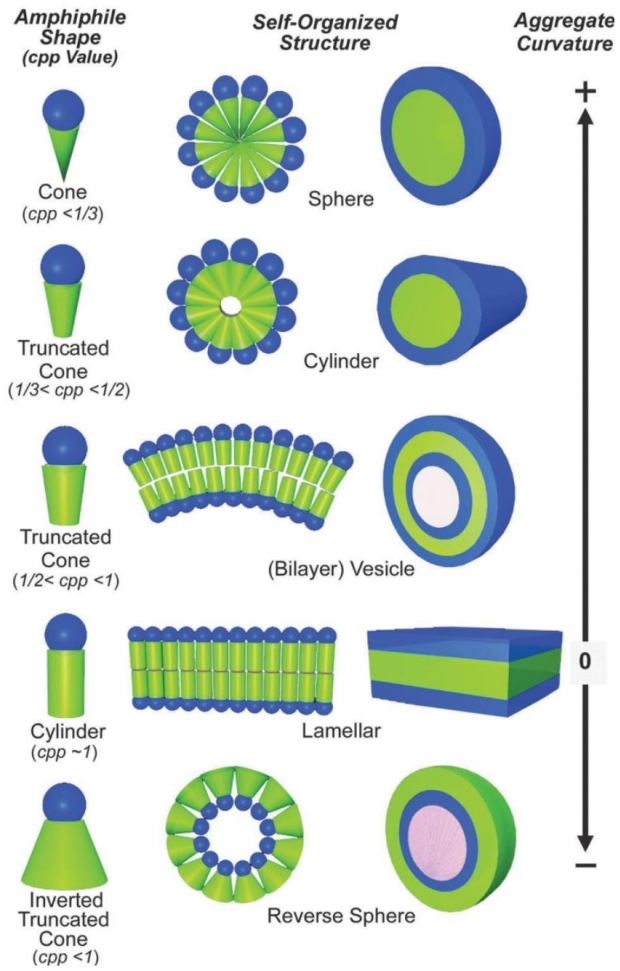

Figure 2.9: Schematic diagram representing the self-assembly of block copolymers in solutions. This is separated in the different morphologies that can be adopted by the block copolymers, which are determined by the critical packing parameter (*cpp*) of the copolymer. Diagram taken from Ramanathan *et al.* (2013).

2.7.3. Spherical micellisation theoretical models

From all the structures that the block copolymers can construct when they are in solutions above the critical micelle concentration, the one that received the most interest in the literature is the spherical polymeric micelles. A number of theoretical micellisation studies based on spherical polymeric micelles have been developed over the years. In this section, the theoretical models of spherical micelles that have drawn more attention in the literature are presented in detail.

Leibler, Orland and Wheeler (1983) micellisation theory

Leibler, Orland and Wheeler (1983) presented a simple mean field model for micelle formation by calculating the total free energy of the micellar phase (Leibler, Orland and Wheeler, 1983). The theory is considering a simple system, a solution of A-B diblock copolymers in melts of A homopolymer. A schematic diagram of one single micelle, as presented in their theory, is shown in Figure 2.10.

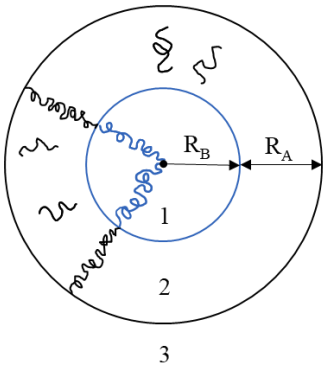

Figure 2.10: Schematic diagram of a single micelle, reproduced from Leibler, Orland and Wheeler (1983). Region 1 is the core of the micelle with diameter R_B and is comprised only by monomers B. Region 2 is the shell or corona of the micelle with a thickness of R_A and is comprised only by monomers A. The corona contains both monomers A from the A-B diblock copolymer and the homopolymer A melt. Region 3 is the area surrounding the micelles and it contains the homopolymer A melt and free A-B diblock copolymer in a homogeneous mixture.

Their theoretical model was based on a number of assumptions. These are listed below:

1. A symmetric system is considered for simplicity, where the number of repeating units of block A and B of the diblock copolymer is the same ($N_A = N_B = N/2$).
2. The A homopolymer has a smaller number of repeating units than the A block of the diblock copolymer ($N_h < N_A$).
3. A p amount of copolymer chains form one spherical micelle of radius R_t ($R_t = R_A + R_B$). Only spherical micelles are considered in this model.
4. The interface between the core and the corona of the micelle is treated as an interface between two incompatible homopolymers.
5. The A and B blocks of the copolymers forming the micelles have an average end-to-end distance of about R_A and R_B respectively. Their deformation is related to their unperturbed dimensions ($[N/2]^{1/2}a$).

6. The free energy expressions are based on a reference state in which chain A and B are separated and therefore there are no A-B interactions ($\chi_{AB} = 0$).
7. The entropic effect due to localisation of the A-B connections was disregarded in the model.
8. The small compressibility of the polymeric liquid is ignored to derive simple relations to estimate micelle dimensions.
9. The polydispersity of the micelles dimensions has been neglected in the total free energy of the micellar phase expression. All micelles are considered as identical, including the same amount *p* of copolymer chains.

Initially, Leibler, Orland and Wheeler (1983) presented a model to estimate the free energy of formation of a single micelle similar to the model suggested by de Gennes for copolymers in solvents (see Equation 2.8).

Equation 2.8: Free energy of a single micelle

$$F = 4\pi {R_B}^2 \gamma + F_d + F_m$$

F Total free energy of a single micelle

R_B Micelle core radius

γ Interfacial tension

F_d Energy of deformation of copolymer chains

F_m Entropy of mixing A chains of the copolymer and homopolymer in micelle corona

The first term of Equation 2.8 is representing the interfacial energy of the region between the core and the corona of the micelle and it can be calculated with the help of Equation 2.9 derived by Helfand and Tagami (1971). This expression of the interfacial tension was derived for an interface between two incompatible pure homopolymers (see Assumption 4). Although, it can be successfully applied in this case, since it was proven that the presence of solvent (or homopolymer) molecules will only have a very small effect in the total free energy of the micelle (Munch and Gast, 1988).

Equation 2.9: Interfacial tension

$$\gamma = (k_b T/a^2)(\chi/6)^{1/2}$$

γ Interfacial tension

k_b Boltzmann constant

T Temperature

a Kuhn segment length

χ Flory-Huggins interaction parameter

Then, the total free energy of the micellar phase (see Equation 2.10) is calculated taking into consideration that the system's entropy reduces significantly with the association of A-B copolymer chains in micelles. Therefore, a fraction of the copolymer chains has to remain free in the homopolymer matrix and not participate in the formation of micelles. This is to ensure that the system is under dynamic equilibrium.

Equation 2.10: Free energy of the micellar phase

$$F_M = \left({}^{\Omega\varphi\zeta}/_{pN}\right) F + F_{mix} - TS_m$$

F_M Total free energy of the micellar phase

Ω Total number of monomers A and B in the system

φ Concentration of copolymer monomers

ζ Average fraction of copolymer chains aggregating in micelles

p Number of copolymer chains in one micelle

N Polymerisation Index

F Total free energy of a single micelle

F_{mix} Free energy of mixing copolymers and homopolymers outside the micelles

S_m Translational entropy of the gas of micelles

Once the total free energy of the micellar phase (F_M) is calculated using Equation 2.10, is compared with the free energy of the homogeneous mixture of homopolymers and copolymers. The phase that has the lowest free energy dominates in the system.

Leibler, Orland and Wheeler (1983) have discovered that the existence and stability of the micellar phase instead of a homogeneous phase is dependent on a balance between the micelles

internal energy and the mixing entropy of micelles, free A-B copolymer chains and the A homopolymer melt. Consequently, the equilibrium properties of the micellar phase, such as the micelle dimensions, the fraction of A-B copolymer chains forming micelles and the average number of free copolymer chains is regulated by this balance. The results prove that the system thermodynamics may promote a micellar phase instead of a homogeneous phase even in cases of low copolymer concentrations and low degree of incompatibility. Finally, they have concluded that when the degree of incompatibility (χN) increases, the cmc decreases and more copolymer chains aggregate to form micelles, to reduce the interaction energy of the system. In these cases, the copolymer chains in the micelles would be stretched and therefore the micelles would be bigger in size.

Munch and Gast (1988) micellisation theory

The micellisation theory presented by Much and Gast (1988) is based on the theory developed by Leibler, Orland and Wheeler (1983) to describe the micelle formation of diblock copolymers in solutions. The scope of their study was to construct a model that could represent micellisation of block copolymers with much smaller solvent-incompatible blocks and in solution of smaller solvent molecules compared to previous models (Leibler, Orland and Wheeler, 1983). A schematic diagram of one single micelle, as presented in their theory, is shown in Figure 2.11.

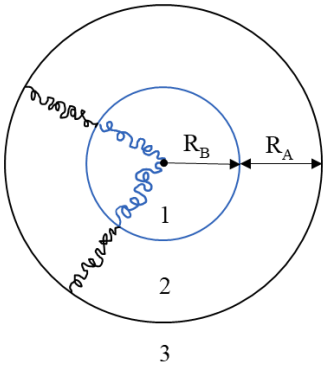

Figure 2.11: Schematic diagram of a single micelle, reproduced from Munch and Cast (1988). Region 1 is the core of the micelle with diameter R_B and is comprised only by monomers B. Region 2 is the shell or corona of the micelle with a thickness of R_A and it contains the A blocks of the copolymer chains and solvent molecules S. Region 3 is the area surrounding the micelles and it contains the solvent molecules S and free A-B diblock copolymer in a homogeneous mixture.

The interactions between the solvent compatible block of the copolymer A and the solvent S are considered to be athermal for simplicity ($\chi_{AS} = 0$). Therefore, the product $\chi_{BS}N_B$ describes the overall effective interaction per copolymer chain with the solvent and reflects the degree of incompatibility of the system.

Munch and Gast (1988) have studied the effects of the degree of incompatibility of the system, the solvent molecule size and the copolymer block lengths on the micellisation process. The numerical results show that the critical micelle concentration and the number of *p* copolymer chains per micelle are lower when the incompatibility between the insoluble B block and the solvent increases ($\chi_{BS}N_B$ increases). More specifically, the cmc and number of *p* chains reduce when the relative length of the insoluble block increases, when the solvent S molecule size increases and when the solubility of the less soluble group in the solvent decreases (χ_{BS} increases).

Another outcome of their investigation is that the micelle radius increases as the solubility of the insoluble block reduces, which is in agreement with what was observed before (Leibler, Orland and Wheeler, 1983), although the amount of *p* copolymer chains per micelle reduces. This phenomenon is explained with the help of Figure 2.12, which is showing the phase transition from a homogeneous mixture of free copolymer and solvent to a micellar phase. The osmotic pressure of each molecule should be the same in the two phases, since these are in equilibrium. The A chains in the corona extend and compress to satisfy this condition. When the $\chi_{BS}N_B$ is small, the cmc is high and phase I in Figure 2.12 would be concentrated. Consequently, the A chains in the corona in phase II would form a concentrated map by compressing. When $\chi_{BS}N_B$ is large, the cmc is low and phase I would be less concentrated, then the A chains in the corona would extend past the random coil configuration to dilute phase II. Therefore, increasing the degree of incompatibility $\chi_{BS}N_B$ causes swelling of the micelle corona and increases the overall micelle radius.

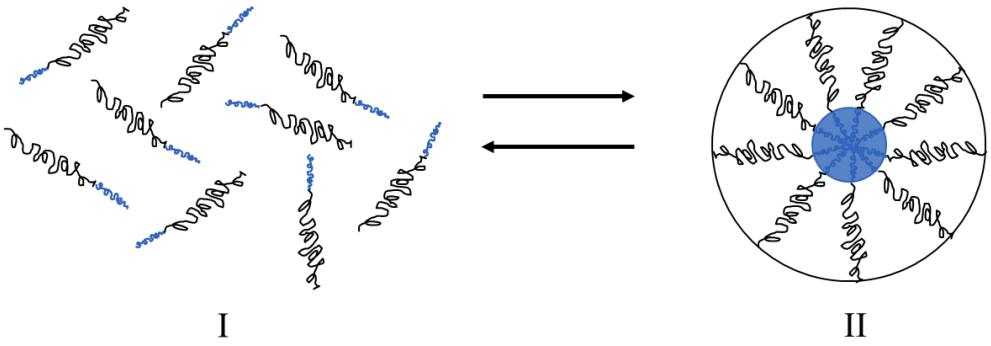

Figure 2.12: Schematic diagram of the phase transition from diblock copolymer chains in solution with solvent S (I) and micellar formation (II), reproduced from Munch and Cast (1988). The degree of incompatibility $\chi_{BS}N_B$ determines the thickness of the corona R_A and the overall micelle radius R.

Munch and Gast (1988) have also tested the effectiveness of the model and established its credibility limits using simple asymptotic results. It was concluded that the application of a monodisperse micelle size model is limited when the solvent molecule size is very small (monomeric solvent) and the aggregation number p is large. The micelle properties are not influenced by the concentration of the free copolymer chains, when the aggregation number is very small, and therefore they can be calculated from the single micelle expression. The cmc in this region can be estimated with a simple expression. Finally, a simple lamellar micellisation model is presented briefly and it is determined that, at a given degree of incompatibility ($\chi_{BS}N_B$), a lamellae geometry surpasses a spherical micelle structure when the A and B block lengths are equal and the solvent size is large relative to the polymer.

Nagarajan and Ganesh (1989) micellisation theory

A thermodynamic model to predict the self-assembly behaviour of AB diblock copolymers in selective solvents S has been developed by Nagarajan and Ganesh (1989) based on the micellisation theory of low molecular weight surfactants established by the same authors in earlier years (Nagarajan and Ruckenstein, 1979; Nagarajan and Ruckenstein, 1983; Nagarajan, 1986). This block copolymer micellisation theory has taken into consideration the effects of the solvent compatible block of the copolymer in the micellisation behaviour, in contrast to earlier studies (Leibler, Orland and Wheeler, 1983; Munch and Gast, 1988). A schematic diagram of the system investigated in this theory is shown in Figure 2.13. This model can be applied to estimate the micelle size distribution, the critical micelle concentration, the average aggregation number and the micelle sizing parameters.

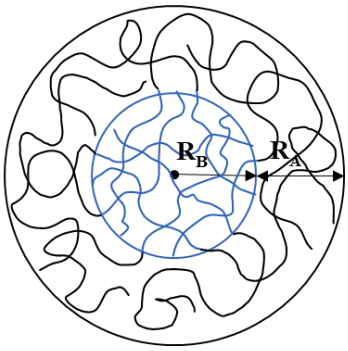

Figure 2.13: Schematic diagram of a single spherical micelle, reproduced from Nagarajan and Ganesh (1989). The core of the micelle with diameter R_B is completely segregated and is comprised only by monomers B of the copolymer. The shell or corona of the micelle with a thickness of R_A contains the solvent compatible A block of the copolymer chains and solvent molecules S.

The solvent and copolymer system is regarded as a multicomponent solution of three distinct chemical components; the solvent molecules, the singly dispersed copolymer chains and micelles of all possible aggregation numbers (p). The equilibrium size distribution of micelles in the system is established by minimisation of the free energy of this multicomponent system and the equivalence of the chemical potential of the singly dispersed block copolymer molecule with the chemical potential per molecule of micelles of any size (p). The expression for the equilibrium size distribution of micelles is given in Equation 2.11.

Equation 2.11: Equilibrium micelle size distribution

$$\varphi_p = \varphi_I^p exp(p-1) exp - \left(\frac{\mu_p^0 - p\mu_I^0}{k_b T}\right)$$

φ_p Volume fraction of micelles of aggregation number p

φ_I^p Volume fraction of singly dispersed copolymer molecules

p Aggregation number

μ_p^0 Standard chemical potential of micelles of size p

μ_I^0 Standard chemical potential of singly dispersed copolymer molecules

k_b Boltzmann constant

T Temperature

The average properties of the micellar phase and the micelle size distribution are determined from the difference in the free energy of a copolymer chain when in the singly dispersed phase and when in the micellised phase. This free energy of micellisation expression accounts for all

the physicochemical transitions that a copolymer chain encounters while moving from the singly dispersed phase to a micellar phase. Namely the expression incorporates the influence of the changes in the states of dilution and deformation of block A, the changes in the states of dilution and deformation of block B, the localisation entropy of the blocks of the copolymer in the micelles and the micelle core-corona interface formation contribution. The free energy of micellisation per molecule can be estimated using Equation 2.12.

Equation 2.12: Free energy of micellisation per molecule

$$\left(\frac{\mu_p^0}{p} - \mu_I^0\right) = \Delta\mu_p^0 = \left(\Delta\mu_p^0\right)_{A,dil} + \left(\Delta\mu_p^0\right)_{A,def} + \left(\Delta\mu_p^0\right)_{B,dil} + \left(\Delta\mu_p^0\right)_{B,def} + \left(\Delta\mu_p^0\right)_{loc} + \left(\Delta\mu_p^0\right)_{int}$$

μ_p^0 Standard chemical potential of micelles of size p

p Aggregation number

μ_I^0 Standard chemical potential of singly dispersed copolymer molecules

$\Delta\mu_p^0$ Free energy of micellisation per molecule

Nagarajan and Ganesh (1989) employed five different solvent-copolymer systems with a broad range of properties to analyse the effect of the solvent-copolymer characteristics on the micellar phase properties. It was observed that when the solvent S represents a very good solvent for the solvent compatible A block of the copolymer, the influence of this block's characteristics dominates the micellisation behaviour.

Finally, Nagarajan and Ganesh (1989) established general (not system specific) scaling equations that relate the micelle sizing parameters (core radius-R_B, corona thickness-R_A and aggregation number-p) to the molecular characteristics of the solvent and the block copolymer, including the interaction nature of the solvent and the A block of the micelle corona. The scaling relations generated are given in Equation 2.13 for the micelle core radius R_B, in Equation 2.14 for the micelle corona thickness R_A and in Equation 2.15 for the aggregation number p.

Equation 2.13: Scaling relation for the micelle core radius

$$R_B = \frac{\left[3m_B^2(\gamma_{BS}l^2/k_bT) + m_B^{3/2} + m_A^{1/2}m_B(R_B/R_A)\right]^{1/3}}{\left[1 + m_B^{-1/3} + (m_B/m_A)(R_A/R_B)^2\right]^{1/3}} l$$

R_B Micelle core radius

R_A Micelle corona thickness

m_B Ratio between the molecular volume of block B and solvent S

m_A Ratio between the molecular volume of block A and solvent S

γ_{BS} Interfacial tension between solvent S and B block of the copolymer

l Characteristic segment length

k_b Boltzmann constant

T Temperature

Equation 2.14: Scaling relation for the micelle corona dimensionless thickness

$$\frac{R_A}{R_B} = 0.867\left[\frac{1}{2} + \frac{m_A m_B^2}{(m_A + m_B)^3} - \chi_{AS}\right]^{1/5} m_A^{6/7} m_B^{-8/11}$$

R_A Micelle corona thickness

R_B Micelle core radius

m_A Ratio between the molecular volume of block A and solvent S

m_B Ratio between the molecular volume of block B and solvent S

χ_{AS} Flory Huggins interaction parameter between the block A and solvent S

Equation 2.15: Scaling relation for the aggregation number of the equilibrium micelle

$$p = \frac{\left[4\pi m_B(\gamma_{BS}l^2/k_bT) + (4\pi/3)m_B^{1/2} + (4\pi/3)m_A^{1/2}(R_B/R_A)\right]}{\left[1 + m_B^{-1/3} + (m_B/m_A)(R_A/R_B)^2\right]}$$

p Aggregation number

R_A Micelle corona thickness

R_B Micelle core radius

m_A Ratio between the molecular volume of block A and solvent S

m_B Ratio between the molecular volume of block B and solvent S

γ_{BS} Interfacial tension between solvent S and B block of the copolymer

l Characteristic segment length

k_b Boltzmann constant

T Temperature

In summary, different theoretical models have been constructed over the years to estimate the micellar core radius, thickness of micellar shell and other important physical parameters of a polymeric micelle. The model developed by Nagarajan and Ganesh (1989) has an increased level of complexity compared to previous models, approaching this way closer to the experimental results that would be expected for a system with an amphiphilic diblock copolymer in a selective solvent. These models were studied and analysed in depth to understand the underlying principles taking place during the self-assembly procedures of diblock copolymers and leading to the construction of spherical micelles in solutions.

2.8. Nanoparticle formulation techniques

The formulation of nanoparticles from polymeric materials is of great importance. Polymeric nanoparticles have applications across various industries and fields due to their desirable characteristics, such as nanoscale size, tailorability, and stability. The literature describes several methods for self-assembling or organising polymeric materials into nanoparticles. The numerous available techniques provide researchers with a range of options to create different types of polymeric nanoparticles with specific properties and functionalities for the targeted application. Some of the methods that are most commonly applied are presented in Table 2.3.

Table 2.3: Different techniques available in literature for nanoparticle formulation

Method name	**Procedure**
Nanoprecipitation or Solvent displacement	Involves the precipitation of a produced polymer (or other material) from an organic solvent (dissolved phase) into an aqueous solvent (NP phase) in the presence or not of a surfactant (Bansal *et al.*, 2015; Kakde *et al.*, 2016; Phan *et al.*, 2019).
Thin film hydration	In thin-film hydration, lipid components are initially dissolved in an appropriate solvent and subsequently dried to form a thin film using a rotary evaporator. This film is then hydrated in an aqueous buffer above its phase-transition temperature (Chu *et al.*, 2016; Ho *et al.*, 2020).
Emulsion polymerisation	Emulsion polymerisation begins with the emulsification of hydrophobic polymers in an aqueous environment using amphipathic emulsifiers, followed by the initiation of free radicals using either oil or water soluble initiators (Ferrari *et al.*, 2013; Colombo *et al.*, 2014; Agostini *et al.*, 2018).
Salting out method	Salting out is a purification method that relies on the decreased solubility of certain molecules in a solution with a very high ionic strength. This technique is often employed to precipitate large biomolecules such as DNA or proteins (Gumfekar *et al.*, 2017).
Solvent evaporation	The solvent evaporation technique is a versatile approach for particle formation, accommodating a range of drugs and macromolecules. The parameters of the emulsion formed during the initial step of particle formation are essential factors influencing particle size, morphology and drug loading (Beer *et al.*, 2015; Ho *et al.*, 2020).

The selection of a formulation method for nanoparticle synthesis is critical and must be carefully tailored to the desired nanostructure type, as each method provides unique characteristics that impact nanoparticle morphology, size, and drug loading efficiency. For instance, techniques such as nanoprecipitation are ideal for forming polymeric micelles with hydrophobic cores for drug encapsulation (Capretto *et al.*, 2011; Salvage *et al.*, 2015), while emulsion-based methods are more suited for generating core-shell nanocapsules (Zambrano-Zaragoza *et al.*, 2011; Zhou *et al.*, 2023). Additional factors influencing the choice of method include the physicochemical properties of the drug (such as hydrophobicity and stability), polymer compatibility, required particle size and uniformity, and release profile. The removal

of residual solvents, scalability, and preservation of drug bioactivity are also crucial considerations to ensure the formulation efficacy and biocompatibility for therapeutic applications (Tang *et al.*, 2016; Bhardwaj and Jangde, 2023). Selecting the appropriate method is therefore an important and careful process, balancing the specific structural needs of the nanoparticle type with operational and practical constraints.

A combination of the particle formation methods included in Table 2.3 was also observed in literature to formulate nanoparticle of the desired characteristics. The combination of miniemulsion and solvent evaporation was performed in Beer *et al.* (2015) for the formulation of HEMA-PLA functionalised nanoparticles. Also, the use of multiple formulation techniques was established in cases where the encapsulation of multiple of drugs within one polymeric nanoparticle was desirable (Ho *et al.*, 2020).

From all the techniques presented in Table 2.3 the method that has received the most attention and has been applied the most in the literature is the nanoprecipitation or solvent displacement method. The reasoning behind the widespread implementation of this technique is the ease and straight-forwardness of execution and the fact that is a very fast process compared to others like the thin film hydration, emulsion polymerisation and the solvent evaporation (Lepeltier, Bourgaux and Couvreur, 2014; Almoustafa, Alshawsh and Chik, 2017). Moreover, its ability to formulate controlled nanoscale particles has been documented in multiple papers (Ruiz-Cantu *et al.*, 2019; Vasey *et al.*, 2019). In addition, by changing the different nanoprecipitation parameters (such as solvent/antisolvent qualities, solvent-to-antisolvent ratio, temperature etc) the final nanoparticle properties can be tuned (Phan *et al.*, 2019).

The most important advantage of the nanoprecipitation technique is its potential ability to be a scalable process in the future. This makes the nanoprecipitation procedure a lot more promising since the current state of formulation of polymeric nanoparticles is only carried out at a lab scale with only a very few commercial formulations in the market (Almoustafa, Alshawsh and Chik, 2017). Therefore, if a self-assembling methodology is developed and is applicable for a scale-up process, then the promotion of novel polymeric nanoparticles enhancing the therapeutic effects of poorly soluble drugs is going to move to the next level with the costs of production decreasing and the availability issues reduced.

All the techniques in Table 2.3 are kinetic processes. Meaning that the driving forces of the procedures are based on the kinetics and not the thermodynamics of the system. These kinetic formulation techniques could result in the production of polymeric micelles that are kinetically trapped (otherwise known as kinetically frozen) (Almoustafa, Alshawsh and Chik, 2017). This phenomenon has been documented and discussed in the literature based on observations emerged from results obtained when the nanoprecipitation technique was applied (Letchford and Burt, 2007). The term kinetically trapped is used when the kinetics and dynamics of the self-assembly processes are so fast that the system does not have enough time to conform into a structure that is under thermodynamic equilibrium. This leads to the formation of a kinetically trapped micellar structure, where there is no distinct interface between the two blocks of the polymer (hydrophilic and hydrophobic blocks) since some of the polymer hydrophilic chains could be kinetically trapped inside the nanoparticle core (hydrophobic region) (Zhu, 2013).

A polymeric structure at thermodynamic equilibrium could be extremely beneficial for the stability of the system and the improved retention of the encapsulated drug when in the blood circulation system. This is not quite evident in the literature, which leaves a clear gap for the implementation of the traditional nanoprecipitation process and a thermodynamically-driven procedure with slower kinetics in this research project. Their comparison will finally be used to assess which system would be considered more ideal as a drug delivery system for cancer chemotherapy, a kinetically trapped one or a system at thermodynamic equilibrium.

2.9. Summary

The key points and findings of the extensive literature review performed for this thesis and presented in this chapter are summarised in this section. Cancer chemotherapy is an extremely significant sector of the health organisation worldwide, holding the biggest economic budget contribution in the whole NHS. There are a number of implications related with the application of chemotherapy, with the most important being the multiple side effects experienced by chemotherapy patients. The reason behind all these implications is the nature of the chemotherapy drugs. These are cytotoxic, non-polar, highly hydrophobic compounds, with low aqueous solubilities. An ideal DDS that can encapsulate the hydrophobic drugs is required to limit the side effects experienced by patients and to reduce the costs related to cancer chemotherapy. Polymeric nanoparticles are highly used materials with promising applications as DDS of anticancer drugs. The type of polymeric nanoparticles that have gained the most

attention in literature are the polymeric micelles. These are core-shell structures formed from self-assembly of amphiphilic block copolymers when present in aqueous environments are concentrations above the cmc. It was proven that they are capable of encapsulating tumour therapeutics with their nanoparticle core. The most widely used materials for constructing the polymeric micelles are based on polymers of poly(ethylene glycol), poly(lactide), poly(ε-caprolactone), poly(glycolide) and their copolymers. A number of polymerisation techniques can be applied for the successful synthesis of these type of materials, with the most applied reactions being ROP, FRP, ATRP, RAFT polymerisations and their combinations. Usually these reactions are taking place in a petrochemical solvent, such as DCM, THF, toluene and xylene. It is well known that these solvents are highly toxic and harmful for the environment, animals and humans. Also, these are being used for the synthesis of materials that are intended for biomedical applications. Therefore, it is of great importance to replace these with safer and 'greener' alternatives. On another note, the investigation of the self-assembling behaviour of block copolymers into nanoparticles is required to form a greater understanding about the influence of different formulations techniques, polymer molecular structures, processing parameters and surrounding environment conditions on the final formulated product and its properties. This can be achieved by performing experimental procedures that are developed based on the understanding and application of different micellisation theories established and refined over the years by numerous authors.

3. Materials and methods

The research methodology and experimental procedures performed in this thesis are presented in this chapter. All the materials used in this thesis with information on their grade, purity and supplier are given in section 3.1. The methodology followed for the block copolymer syntheses, the self-assembly techniques, the cryoprotectant systematic study and the model drug encapsulation experiments performed in this thesis are presented in sections 3.2, 3.3, 3.4 and 3.5 respectively. Finally, the characterisation techniques implemented to analyse and monitor the properties of the constructed materials are demonstrated in section 3.6.

3.1. Materials

All the chemical reagents and solvents used are commercially available and were purchased from Merck (Darmstadt, Germany), Sigma Aldrich (St. Louis, MO, USA) or Fisher Scientific (Loughborough, UK) and used as received unless otherwise stated. The distilled water used throughout this thesis was purified using Stuart Distinction D4000 water still (Bibby Scientific Ltd, Cole-Parmer UK supplier). The lipase, Novozym 435 (*Candida Antarctica* lipase B immobilized on acrylic resin), that was utilised for the enzymatic ring opening polymerisation (eROP) of ε-CL in Chapter 4, was kindly donated by Novozymes A/S, Denmark. Table 3.1 shows alphabetically all the chemical reagents and solvents used in this thesis, their purchasing company and information on their grade/purity.

Table 3.1: Purchasing company and grade/purity of all chemicals used in this thesis.

Material	Company	Grade/Purity
2-MeTHF	Sigma-Aldrich	99%
Acetone	Sigma-Aldrich	99%
Acetonitrile	Fisher Scientific	HPLC Gradient grade
AIBN	Sigma-Aldrich	98%
Chloroform-d	Fisher Scientific	99.8% D
CPAB	Sigma-Aldrich	N/A
DBU	Sigma-Aldrich	98%
Diethyl Ether	Sigma-Aldrich	99%
DMSO	Sigma-Aldrich	ACS reagent, ≥99.9%
Ethyl acetate	Sigma-Aldrich	≥99.5%
Glycerol	Sigma-Aldrich	99%
HEMA	Sigma-Aldrich	≥99%
Lactide	Sigma-Aldrich	99%
Methanol	Sigma-Aldrich	99.8%
$mPEG_{2000}$	Sigma-Aldrich	N/A
$mPEG_{5000}$	Sigma-Aldrich	N/A
n-Heptane	Sigma-Aldrich	Anhydrous, 99%
n-Hexane	Sigma-Aldrich	99%
Nile Red	Sigma-Aldrich	N/A
Novozym 435	Novozymes A/S	N/A
PEG1000	Sigma-Aldrich	BioUltra
PEG6000	Sigma-Aldrich	BioUltra
PEG10000	Sigma-Aldrich	BioUltra
PEG35000	Sigma-Aldrich	BioUltra
PEGMA	Sigma-Aldrich	N/A
THF	Fisher Scientific	99.5%
ε-Caprolactone	Sigma-Aldrich	97%

3.2. BCP synthesis experimental methodology

3.2.1. Selection of polymerisation components

The rationale behind the selection of the different chemical reagents and the solvent used in Chapter 4 and Chapter 5 of this thesis for the synthesis of a block copolymer (BCP) library of

biodegradable and biocompatible materials intended for biomedical and pharmaceutical applications are presented here.

Solvent - 2-MeTHF: As already mentioned in section 2.5.2, 2-methyltetrahyfrofuran (2-MeTHF) is a neoteric volatile cyclic ether sourced from biomass, which is a renewable feedstock (Huber, Iborra and Corma, 2006; Corma Canos, Iborra and Velty, 2007). Relevant to its use in pharmaceutical manufacturing, it has been characterised for biological applications with negative genotoxicity and mutagenicity (Antonucci *et al.*, 2011). Furthermore, its solvent properties, reported in Table 2.2, suggest that 2-MeTHF is a promising green-polymerisation solvent when compared to the conventional polymerisation solvents. 2-MeTHF has previously been employed as the polymerisation solvent for the ring opening polymerisation (ROP) of terpene-initiated lactide (LA), proving its suitability as a solvent for sustainable ROP processes (O'Brien *et al.*, 2020). In Chapter 4 the aim was to assess its ability to act as a multi-polymerisation solvent for the synthesis of biocompatible and biodegradable BCPs for medical applications.

Monomers – Lactide (LA) and ε-Caprolactone (ε-CL): Both monomers are hydrophobic compounds and can undergo ROP to form biodegradable and biocompatible aliphatic polyesters. The selection of these specific monomers enabled us to assess 2-MeTHF as a polymerisation solvent for both metal-free and enzymatic ROP in Chapter 4. Lactide was selected because it is the benchmark for biopolymers and has been shown to polymerise efficiently in the presence of 1,8-Diazabicyclo[5.4.0]undec-7-ene (DBU), which is the metal-free catalyst chosen in this investigation (Lohmeijer *et al.*, 2006). Previous studies demonstrated that ε-CL can be polymerized via enzymatic ROP catalysed by Novozym 435 (Kumar and Gross, 2000; Kumar *et al.*, 2000). For Chapter 5, the synthesis of LA-based diblock copolymers only was preferred to emphasise on the effect of BCP properties, such as hydrophilic-to-hydrophobic ratio, hydrophobic and hydrophilic block lengths and overall polymer molecular weight, on the self-assembly behavior of these polymeric materials.

Catalysts – DBU and Novozym 435: The organocatalyst, 1,8-diazabicyclo[5.4.0]undec-7-ene (DBU), and the enzyme, *Candida antarctica* lipase B (CALB) also known as Novozym 435 (lipase), were employed in Chapter 4 for the synthesis of PLA and PCL respectively. Both catalysts are metal-free to eliminate the risk of residual salts remaining in the final pharmaceutical product, as most conventional metal catalysts are toxic to human health

(Jaishankar *et al.*, 2014; Egorova and Ananikov, 2017; Engwa *et al.*, 2019). The activity of these catalyst is reduced compared to conventional metal catalysts (Pratt *et al.*, 2006; Pearce *et al.*, 2019); however, they can catalyse the ROP of a variety of cyclic monomers at low temperatures offering greater control over the polymerization process (Kumar and Gross, 2000; Kumar *et al.*, 2000; Lohmeijer *et al.*, 2006). The DBU catalyst can perform the fast ROP of lactide (Vasey *et al.*, 2019; O'Brien *et al.*, 2020), but exhibits limited activity for the ROP of lactones, including ε-caprolactone (Lohmeijer *et al.*, 2006). The opposite is true for lipase, which has a low activity for the ROP of LA in contrast to its reactivity and chemical affinity for ε-CL, which has been documented in the literature (Peeters *et al.*, 2005; Castano *et al.*, 2014; Bao *et al.*, 2020). For the ROPs initiated by labile-esters (HEMA and PEGMA) the use of the mild catalyst DBU prevents transesterification and dimerisation side-reactions that are encountered in the presence of active and bifunctional ROP catalysts, including lipase and triazabicyclodecene (TBD) (Takwa *et al.*, 2008; Xiao *et al.*, 2009; Pearce *et al.*, 2019; Ruiz-Cantu *et al.*, 2019).

Initiators – mPEG$_{2000}$, mPEG$_{5000}$, HEMA and PEGMA: Methyl-polyethylene glycol 2000 Da (mPEG$_{2000}$), methyl-polyethylene glycol 5000 Da (mPEG$_{5000}$), polyethylene glycol methacrylate 300 Da (PEGMA) and 2-hydroxyethyl methacrylate (HEMA) have been selected as the initiators of the polymerisation process. All these are hydrophilic compounds and initiate effectively the hydrophobic monomers of LA and ε-CL, constructing amphiphilic block copolymers. The rationale for their selection is their high biocompatibility, which has been previously documented due to their repeated use in initiating polymers for pharmaceutical and medical applications (Albertsson and Varma, 2003; Xie *et al.*, 2009; Xu *et al.*, 2009; Ferrari *et al.*, 2013; Kakde *et al.*, 2016). The use of initiators bearing functional groups, such as methacrylates, which introduce an end-chain reactive double bond to the final polymer product, lead to the generation of versatile biodegradable copolymers with hybrid architectures (Pearce *et al.*, 2019). The resultant copolymers can be further investigated in a second polymerisation step, such as FRP and RAFT (Vasey *et al.*, 2019). In the case of HEMA and PEGMA the end-chain double bond opens up in radical polymerisations to connect individual linear polymers leading to products with hybrid structures. All the materials produced using the two mPEG initiators have a linear configuration (Chapter 5), whereas the block copolymers produced from the labile-ester PEGMA and HEMA initiated ROPs have grafted polymer architectures. Although, both architectures enable the amphiphilic block copolymers to self-assemble into nanoparticles in aqueous environments as documented in Chapter 4.

RAFT agent and radical initiator – CPAB and AIBN: RAFT polymerisation is a radical process with a controlled reaction mechanism. In this type of polymerisations, a RAFT agent is present to control the kinetics of the radical polymerisation. In the RAFT polymerisation reactions performed in Chapter 4, 4-cyano-4-(phenylcarbonothioylthio) pentanoic acid (CPAB) was used as the RAFT agent. CPAB gives a high degree of control over the molecular weight and the polydispersity of the final polymeric product during radical polymerisation and it is suitable for the polymerisation of methacrylate monomers (Moad, Rizzardo and Thang, 2012; Ana A. C. Pacheco *et al.*, 2021). Azobisisobutyronitrile (AIBN) has been employed as the radical initiator for both the RAFT and FRP polymerisations. AIBN is a commonly used radical initiator because it provides good control over the molecular weights and low polydispersity index (PDI) for the final polymer products (Chu and Lin, 2003; Nita *et al.*, 2011; Zhong *et al.*, 2017). This radical initiator thermally decomposes in solution releasing free radicals to initiate the radical polymerisation (Krstina *et al.*, 1993; Moad, Rizzardo and Thang, 2012). The reaction temperature applied for the radical polymerisations in Chapter 4 is 65^{o}C, at which the decomposition rate of AIBN generates the radical flux required for the radical polymerisations (Ana A. C. Pacheco *et al.*, 2021).

3.2.2. Synthesis procedures

The synthesis of multiple amphiphilic block copolymers, with a hydrophilic poly(ethylene) glycol (PEG)-based block and a hydrophobic PLA- or PCL-based block, was performed in Chapters 4 and 5 of this thesis. Details of the specific block copolymer libraries produced and the detailed synthesis procedures followed in each case are included in the relevant chapters.

As already mentioned in the literature review in Chapter 2, there is a consistent and vigorous synthesis procedure that is commonly followed by researchers for the construction of block copolymers. This general procedure of polymerisation reaction techniques was followed for the production of the amphiphilic BCPs, both in Chapter 4 and Chapter 5 of this thesis.

The general synthesis process followed, involved the measurement and addition of the desired amounts of monomer, initiator and polymerisation solvent in a glass vial under constant stirring at the required reaction temperature. In the case of radical polymerisations, this process was completed under inert gas conditions. After the full dissolution of the materials, the insertion

of the pre-determined amount of catalyst was performed to start the polymerisation reaction. After the required reaction time has passed, the polymerisation reaction was terminated via precipitation of the reaction mixture in a non-solvent for the polymer. In some cases, this step is applied at reduced temperatures to accelerate the sedimentation process of the material. Multiple precipitation steps were followed to purify the final polymer product, which subsequently was fully dried followed by its analysis through the different characterisation techniques in section 3.6.1.

3.3. BCP self-assembly investigation methodology

All the block copolymers produced in this thesis are able to self-assemble into polymeric nanoparticles (NPs) in selective solvents due to their amphiphilic nature. The synthesised BCPs consist of a hydrophobic block (PLA or PCL) and a PEG-based hydrophilic block. Therefore, when a selective solvent, such as an aqueous solvent, is introduced in the system, the block copolymers self-assemble into particulates. The driving force of this polymer chain organisation is the unfavourable molecular interaction of the hydrophobic BCP block with the aqueous solvent. Thus, the polymer chains are physically arranged in solution to construct nanoparticles with a hydrophobic core surrounded by a hydrophilic corona, which is in contact with the aqueous solvent.

As already discussed in the literature review in Chapter 2, this is a highly desirable property of the amphiphilic block copolymers, since it can be applied for the formulation of polymeric nanoparticles that can act as drug delivery devices of highly hydrophobic drugs to cancerous target areas in the human body.

3.3.1. Process parameters under investigation

The organisation of the BCPs into these advantageous nanostructures has been achieved using a variety of formulation processes before as seen in section 2.8 of the literature review. The formulation technique that has gathered the most attention in literature is the nanoprecipitation, or otherwise known as solvent displacement, technique. The wide application of this method is based on its processing characteristic, such as the simplicity, speediness and scalability, when compared to other nanoformulation techniques. The nanoprecipitation process was employed to self-assemble the amphiphilic block copolymers produced in this thesis.

The driving force applied during the nanoprecipitation technique for the self-assembly of the BCPs, in terms of BCP concentration in solution, was investigated in Chapter 5. In the same chapter, the self-assembly process speed and the rate of addition of the BCP solution into the anti-solvent (water in this case) was also examined. As mentioned before, the effect of the amphiphilic BCP properties on their nanoparticle (NP) arrangement was also studied by varying the hydrophobic block length, the hydrophilic block length, the polymer total molecular weight and the hydrophobic-to-hydrophilic ratio of the same material (mPEG-PLA diblock copolymer). The main goal of these experiments was to gain a deeper understanding of the self-assembly mechanism of amphiphilic block copolymers.

3.3.2. Self-assembly procedures

The general experimental procedure applied in this thesis for the self-assembly of the synthesised amphiphilic block copolymers into NPs involves the preparation of a good solvent and an anti-solvent solution and their mixing to induce the particulate formulation. The BCP is fully dissolved in a good solvent for both blocks. The good solvent used for the dissolution of both blocks is the organic solvent, acetonitrile. A pre-determined amount of a selective solvent for one of the polymer blocks is also prepared in another container. The selective solvent used throughout this thesis in distilled water (purified as mentioned in section 3.1). The goal is to form NP suspensions through solvent exchange between the organic good solvent (acetonitrile) and the aqueous block selective medium (distilled water). During the NP formulation process, the BCP is transitioning from a fully dissolved (free, open and expanded polymer chains) phase to an ordered and structured phase, where nanoparticles are suspended evenly in distilled water. The contents of the two containers (solvent and anti-solvent) were mixed to commence the process of solvent exchange and the phase transition of the BCPs from fully dissolved to NPs in suspension.

The mixing process was performed by adopting various methods. In the regular nanoprecipitation process, the polymer solution in acetonitrile was added dropwise, either by hand or with the help of a syringe pump (Standard Infuse/Withdraw PHD ULTRA™ Syringe Pump, Harvard Apparatus, Massachusetts, USA), into the distilled water container under constant stirring. The rate of addition of the polymer-acetonitrile solution in water was varied to investigate its effect on the final NP suspension. The other process employed in Chapter 5

was the slow addition of the desired amount of distilled water into the container of the dissolved polymer in acetonitrile, again under constant stirring. This method was utilised with the aim to slow down the fast process kinetics of the nanoprecipitation technique and study the effect of this on the final NP properties. For all the acetonitrile-water mixing procedures followed, the experiments were completed in a fume cupboard, since the final step of all the formulation processes was the removal of the volatile acetonitrile solvent by evaporation to complete the solvent exchange process.

Further information and the specific experimental details applied for the BCP self-assembly experiments (polymer material, process conditions, process duration etc) are included in each of the relevant chapters.

3.4. Cryoprotectants systematic study methodology

Polymeric nanoparticles are promising vehicles for delivering hydrophobic chemotherapy drugs to cancer sites, but their commercial use is limited due to inadequate long-term stability in aqueous solutions. This leads to the research avenue of enhancing their stability for extended storage. The poor stability of polymeric nanoparticles in aqueous mediums originates from both physical (aggregation, fusion) and chemical (hydrolysis, drug reactivity, drug leakage) instabilities, which can be mitigated by removing water through freeze-drying. This process removes the solution water by sublimation under low pressure in three steps: freezing, primary drying (ice crystal removal), and secondary drying (removal of residual water), but it can stress fragile suspensions like polymeric nanoparticles. This could lead to the potential disruption of their stability and size due to mechanical stresses from ice crystal formation. Excipients known as cryoprotectants and lyoprotectants can be added to nanoparticle suspensions before freeze-drying to prevent the disorganization of the formulation, to enhance the stability during the process and to improve the material physical stability during storage.

The main aim of Chapter 6 was to investigate the impact of the freezing step of the freeze-drying process on mPEG-PLA nanoparticle suspensions and minimisation of mechanical stresses from ice crystal formation. To achieve this a number of common cryoprotectants, including different molecular weight PEGs, were employed to perform a systematic study of their shielding behaviour on the BCP nanoparticles. The cryoprotectants were assessed on

whether they are able to preserve the nanoparticle sizes and structures through control of the ice crystal formation during the freezing step.

3.4.1. Selection of cryoprotectants

The three different types of cryoprotectants employed in the systematic study performed in Chapter 6 are PEG, DMSO and glycerol. These cryoprotectants were used to examine their control and minimisation of the ice crystal formation, which leads to the disruption on BCP NPs, occurring during the freezing step of the freeze-drying process. The reasoning behind the selection of the different cryoprotectants chosen in this study is presented here.

PEG of different molecular weights:

Poly(ethylene) glycol is regularly used as a cryoprotectant in various nanoparticle and biological systems. Moreover, it is well known in the literature that the effect of PEG is very important during the freezing process, since it is very efficient at limiting and controlling the ice crystal formation of water within the sample (Mi, Wood and Thoma, 2004; Mohammady, Mohammadi and Yousefi, 2020; Jang *et al.*, 2022). However, there are only very limited cases that it has been used as a cryoprotectant for polymeric nanoparticles (Almalik *et al.*, 2017; Umerska *et al.*, 2018). Therefore, there is limited information in the literature about its behaviour and efficiency to act as a cryoprotectant of polymeric nanoformulations. Additionally, the effect of the PEG chain length on the PEG-PLA pharmaceutical product properties during the freezing stage has never been systematically reported before in the literature, leaving a clear research gap for this experimental investigation to address.

DMSO:

In addition to PEG, other cryoprotectants that are commonly used to preserve the properties of biological and pharmaceutical systems are dimethyl sulfoxide (DMSO) and glycerol. DMSO is the most applied excipient utilised for the protection of living cells (Patel, Park and Jeong, 2023). The wide usage of DMSO is due to its cell-penetrating ability. It can penetrate into the cell by diffusion, protecting it from ice crystal formation during cryopreservation. Ultimately it replaces the intracellular water and stabilises the biological system (Bhattacharya, 2018). As a solvent, it is miscible with a wide range of organic and non-organic solvents, including water, and it dissolves polar and non-polar materials due to its polar aprotic solvent nature. DMSO is

a cost-effective solvent with minor cytotoxicity at high concentrations and high freezing temperature (~16-19 ºC) making it a very popular cryoprotective agent.

Glycerol:

Glycerol is an odourless and colourless liquid and the most frequent polyol (sugar alcohol) employed for cryopreservation (Storey and Storey, 1991). It is a material with high viscosity forming hydrogen bonds with water molecules. Both properties are very important to achieve a successful cryoprotection, since they restrain the ice crystal formation of water and reduce the sample osmotic pressure differences during the cooling processes (Keros *et al.*, 2005; Bhattacharya, 2018). Glycerol is less toxic than other commonly used cryoprotectants at high concentrations (Zhang *et al.*, 2022). Moreover, it is a permeating cryoprotectant and highly water soluble even at low temperatures, like DMSO (Jang *et al.*, 2022). These are properties that allow the excipients to penetrate easily through biological membranes and shield the biomedical products from the mechanical and osmotic stresses of freezing (Whaley *et al.*, 2021).

3.4.2. Experimental procedure

In the investigation carried out in Chapter 6, four different molecular weight variants of PEG (1000, 6000, 10000, and 35000 Da), along with the conventional cryoprotectants DMSO and glycerol were employed. The aim was to examine how the length of the PEG chains influences the properties of the mPEG-PLA nanoparticle suspensions after freezing and in the final freeze-dried product.

Briefly, the procedure followed to assess the ability of the selected materials to act as successful cryoprotectants starts with the preparation of mPEG-PLA nanoparticles by nanoprecipitation, following the general procedure discussed in section 3.3.2. Then, the mixing of the produced NP suspension with solutions of the cryoprotectants chosen, is completed. The freezing and thawing of the NP-cryoprotectant suspension formed is performed to simulate the freezing step of the freeze-drying process. The effect of the freeze-thaw process on the properties of the suspension is monitored with the help of Dynamic light scattering (DLS). Later, the freeze-drying process is completed in the Telstar LyoQuest freeze-drier (Azbil Telstar, S.L.U., Barcelona, Spain) and the surface and structure of the final dried material is observed under SEM. Finally, the re-dispersal of the recovered freeze-dried material in distilled water (purified

as mentioned in section 3.1) is performed to estimate the reconstitution time and the final re-dispersed NP size via DLS.

Further information on the experimental procedure details and the process conditions applied for the investigation of the effectiveness of the chosen cryoprotectants in shielding and protecting the nanoparticle suspension characteristics, are presented in Chapter 6.

3.5. Model drug encapsulation methodology

The amphiphilic block copolymer nanoparticles produced in this thesis are envisaged for use in the biomedical sector, as drug delivery systems (DDS) for highly hydrophobic cancer chemotherapy drugs. Thus, it is a requirement that these materials are capable of encapsulating the hydrophobic drugs inside their hydrophobic core and surrounding them with their hydrophilic corona to constitute an efficient drug delivery vehicle. Therefore, the evaluation of the ability of these BCP nanoparticles to encapsulate highly hydrophobic molecules is essential.

The main aim of Chapter 7 was assessing the capacity of the mPEG-PLA nanoparticles constructed via nanoprecipitation to encapsulate a hydrophobic compound, which is acting as a model drug imitating the properties and interactions of chemotherapy drugs. The effect of the block copolymer final concentration in NP suspension on the encapsulation process of the model drug was investigated. The encapsulation of the model drug was quantified through the measurement of the encapsulation efficiency (EE%) and the drug loading capacity (LC%) of each of the drug loaded nanoparticle formulations constructed.

3.5.1. Encapsulation procedure

For the encapsulation of the model drug, the same procedure carried out for the self-assembly of the amphiphilic block copolymers into nanoparticles via nanoprecipitation was followed (section 3.3.2). The model drug was fully dissolved with the BCP in acetonitrile, which is a good solvent for both blocks of the polymer and the model drug. The concentration of the BCP in the final nanoparticle suspension was varied to examine whether a higher concentration of polymer could encapsulate a higher amount of hydrophobic model drug. Then, the homogeneous solution of Nile red-BCP-acetonitrile was nanoprecipitated into the desirable amount of distilled water, under continuous stirring. The solvent exchange process from the

organic good solvent (acetonitrile) to the aqueous block selective solvent (distilled water) was triggered instantly when the two solutions were mixed. In this case, the phase transition of the BCP from a fully dissolved solution to a nanoparticle suspension is accompanied by the model drug. During this process, Nile red is driven by its hydrophobic nature avoiding the molecular interactions with water. In contrast, the hydrophobic block of the polymer and the Nile red interactions are favourable and therefore are driving the self-assembly of the BCP and the encapsulation of the model drug within the nanoparticle structures during the NP formulation process. The rest of the nanoprecipitation conditions and procedure are the same as before.

3.5.2. Encapsulation quantification

The ability of the polymeric nanoparticles to incorporate the model drug within their structure and form an effective drug delivery system was determined through two methods. First, the encapsulation efficiency (EE%) of the polymeric nanoparticles, which determines the amount of drug that was captured and encapsulated within the NP structure compared to the amount of drug that was initially used for the experiment (Pignatello *et al.*, 2001), was determined. The EE% can be calculated using Equation 3.1. Moreover, the drug loading capacity (LC%) of the polymeric nanostructures, which is the weight of the drug encapsulated within the NP compared to the weight of the whole drug loaded system (weight of polymeric NP and encapsulated drug) (Govender *et al.*, 1999), was estimated. The LC% can be determined using Equation 3.2.

Equation 3.1: Encapsulation Efficiency (EE%)

$$EE\% = \frac{Weight\ of\ encapsulated\ drug\ in\ NPs}{Initial\ weight\ of\ drug\ used} \times 100\%$$

Equation 3.2: Drug loading capacity (LC%)

$$LC\% = \frac{Weight\ of\ encapsulated\ drug\ in\ NPs}{Weight\ of\ NPs} \times 100\%$$

The amount of drug that was loaded inside the BCP nanoparticles was measured indirectly by using the amount of drug that was not encapsulated within the nanoparticles. The non-encapsulated Nile red was extracted from the rest of the NP suspension with the help of diethyl

ether (more details in Chapter 7). The amount of model drug extracted was analysed and quantified by UV-visible spectrophotometry. The amount of drug loaded in the nanoparticles was determined by subtracting the non-loaded drug amount from the total amount of drug initially used in the experiment.

3.6. Characterisation techniques

3.6.1. Synthesised polymer product characterisation

The characterisation techniques conducted to analyse all the block copolymers, which were synthesised from the different polymerisation reactions completed throughout this thesis (section 3.2.2), are summarised in this section.

Nuclear magnetic resonance spectroscopy (NMR): NMR is used in a wide range of applications to provide detailed information on the structure of organic compounds and the concentration of molecules in complex mixtures. Also, this method is used for the direct observation of chemical reactions (Pearce *et al.*, 2019; Ruiz-Cantu *et al.*, 2019).

In this instance, the conversion of monomers to polymers, the degree of polymerisation (DP_n) of each reaction and the molecular weight of the final polymer product were determined using ^1H nuclear magnetic resonance spectroscopy (^1H NMR). To achieve this, the ^1H NMR spectra of the initial reaction mixture dissolved in 2-MeTHF before the addition of the catalyst (DBU or lipase), and therefore before the start of the polymerisation reaction, and the ^1H NMR spectra of the final purified polymer product for each case, were compared. $CDCl_3$ (deuterated chloroform) was used as the common deuterated solvent and all samples were analysed using a Bruker DPX 400 MHz spectrometer (Bruker Corporation, Massachusetts, USA) operating at 400 MHz (^1H). Chemical shifts were assigned in parts per million (ppm). MestReNova 6.0.2 copyright 2009 (Mestrelab Research S. L.) was used for analysing the spectra.

The DP_n, conversion and final polymer molecular weight were established from spectra integration. Figure 3.1 shows the integrated ^1H NMR spectra for the final purified HEMA-LA_{25} macromonomer produced in Chapter 4 as an example. The specific macromolecule peaks are annotated on the ^1H NMR spectra (Figure 3.1-B). The desired number of repetitive LA units in the final polymer and target DP_n was 25 (shown in the stoichiometry reaction scheme in Figure 3.1-A). In this case, the number of LA C*H* protons is equal to the number of repetitive LA units

in the final polymer. Although, LA is a symmetric compound and incorporates two C*H* protons in its structure per full unit. Therefore, the total number of LA C*H* protons calculated by the integration of the ^{1}H NMR spectra is divided by two to determine the final DP_n.

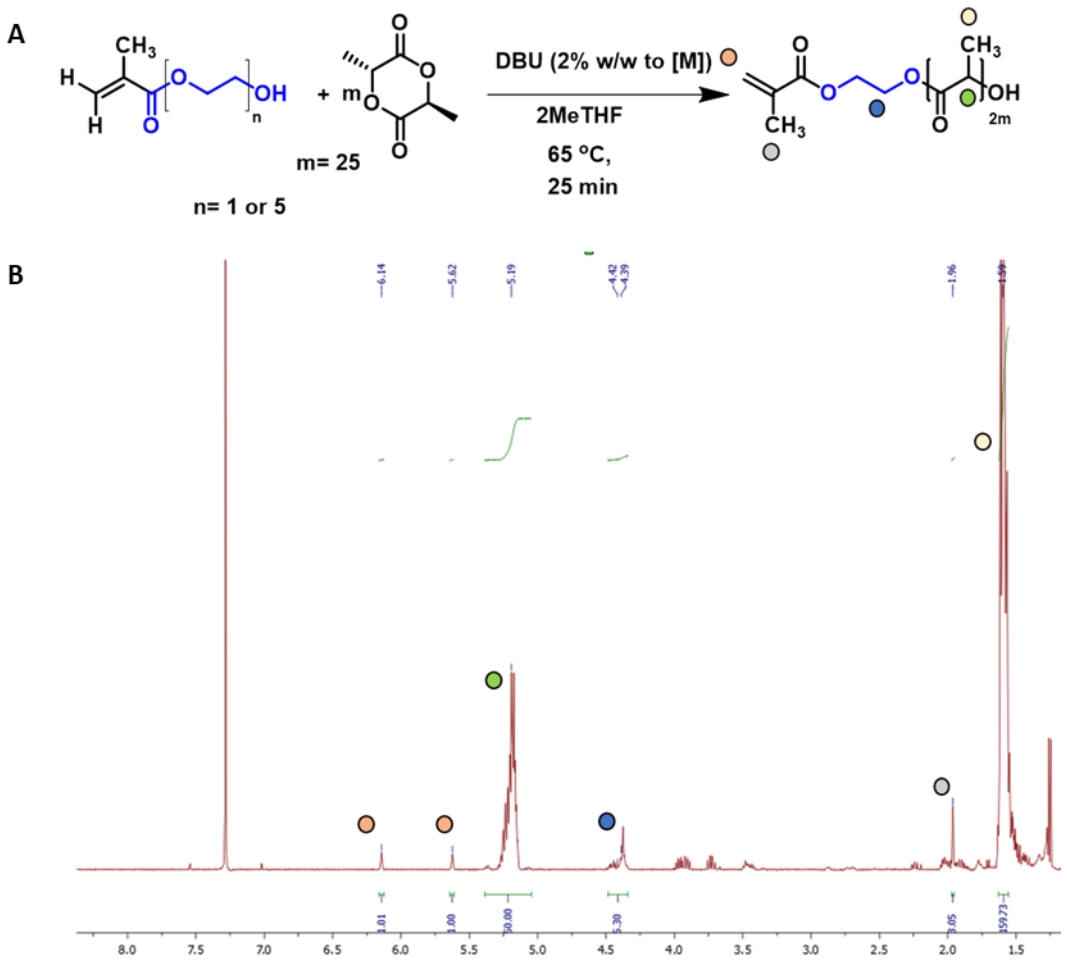

Figure 3.1: **(A)** Reaction scheme for the ROP of lactide initiated by methacrylates to produce methacrylate-LA macromonomers. **(B)** Integrated ^{1}H NMR spectra of the final purified HEMA-LA_{25} macromonomer with all the characteristic peaks assigned.

Size exclusion chromatography (SEC): SEC is also commonly known as Gel permeation chromatography (GPC); the two terms are used interchangeably in the area. It is frequently used in different applications in various areas, such as polymer chemistry, analytical chemistry and biological chemistry. It is a type of liquid chromatography applied for the size separation and analysis of the different molecules present in a sample (Deb *et al.*, 2019; Majeed, Sekhosana and Tuhl, 2020).

The name gel permeation chromatography is given to the process since the porous stationary phase that forms the packing of the column is a gel matrix. The separation of the different sized molecules in a sample is achieved by their filtration through the gel in the column. As seen from Figure 3.2, the working principle of SEC is based on the fact that smaller size molecules can enter and diffuse through the pores of the gel matrix, therefore spending a longer time inside the stationary column. The elution time of smaller molecules is higher. In contrast, the larger molecules, that cannot fit through the pores of the gel matrix, are excluded and have to pass around the gel particles. Thus, taking a shorter pathway and having a lower elution time from the stationary column. This exclusion effect allows the separation of the different size molecules present in a sample and their characterisation based on the detector signal received on the elution times (Hong, Koza and Bouvier, 2012).

In Chapter 4 and 5, the detector signal received for the elution times of the different molecules of the synthesised polymer samples is analysed and used to determine the number average molecular weight (M_n) and the molecular weight dispersity of all the final block copolymer products. More specifically, the GPC was performed with the help of Agilent 1260 Infinity Series HPLC (Agilent Technologies, California, USA). Two Agilent PL-gel mixed-D columns were used in series to form the porous gel matrix. The mobile phase flow rate was 1 ml/min. A differential refractometer (DRI) was used as the sample detector for the elution of molecules from the column. The SEC system was calibrated using poly(methyl methacrylate) (PMMA) standards prior to measurement.

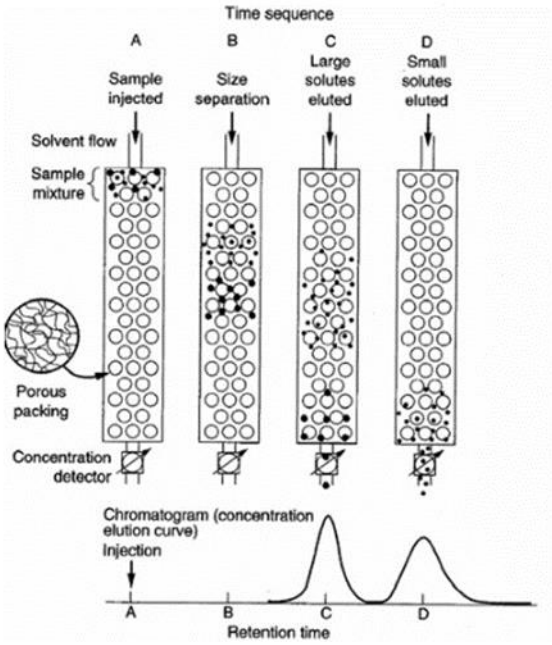

Figure 3.2: Working principle of size exclusion chromatography (SEC) characterisation technique. Figure taken from Striegel *et al*. (2009).

3.6.2. Nanoparticle suspension characterisation

The characterisation techniques employed to analyse the block copolymer nanoparticles, that are produced through the different formulation processes and conditions applied in this thesis, are summarised in this section.

Dynamic light scattering (DLS): DLS measures the Brownian motion of particles in suspension and uses this information to determine their hydrodynamic size. Laser light is scattered by the dispersed particles in solution at different intensities. By analysing the intensity fluctuations, the rate of Brownian motion was determined, which is quantified by the translational diffusion coefficient (D_τ). The Stokes-Einstein equation correlates the translational diffusion coefficient (D_τ) with the hydrodynamic radius (R_H) of the particle as shown in Equation 3.3. Thus, DLS can be used to obtain information on the size of the particles in suspension.

Equation 3.3: The Stokes-Einstein equation

$$R_H = \frac{k_B T}{6\pi\eta D_\tau}$$

R_H Hydrodynamic radius (m)

k_B Boltzmann constant ($m^2 \cdot kg/K \cdot s^2$)

T Temperature (K)

η Dynamic viscosity (Pa·s)

D_τ Translational diffusion coefficient (m^2/s) – rate of Brownian motion

For the experiments performed in this research, DLS was used to establish information about the nanoparticle size distribution and the polydispersity index of the nanoparticle population present in the samples. Nanoparticles were prepared at different concentrations by adopting the formulation techniques discussed in section 3.3.2. The DLS equipment used is the ZetaPALS (2008) model by Brookhaven Instruments Corporation (NY, USA), equipped with a red solid state laser. The measurements were completed at room temperature (25 ºC). The samples were equilibrated at the measurement temperature in the equipment cuvette chamber prior to measurement. Each measurement consisted of 5 runs of the same sample.

In Chapter 4, the particle size analyses were performed by DLS utilizing a Zetasizer Nano spectrometer (Malvern Panalytical Ltd, Worcestershire, UK) equipped with red solid state laser. Nanoparticles were prepared adopting a simple solvent displacement methodology (Phan *et al.*, 2019). Samples were equilibrated at 25 ºC prior to measurements. All experiments were performed in duplicate averaging 15 scans per run of the same sample.

Zeta potential (Z-potential) analysis: Zeta potential (ζ) is a physical property of the material related to the electrostatic potential of the particles that are suspended in solution. For colloidal suspensions, the zeta potential analysis is the direct measurement of their electrokinetic potential. This potential is a major indicator of the colloidal stability of different dispersions, such as suspensions, emulsion and nanoparticles (Gumustas *et al.*, 2017; Gupta and Trivedi, 2018).

Zeta potential is a parameter quantifying the charge developed at a solid-liquid interface. In the case of polymeric nanoparticles, it is the measure of the electrostatic charge developed at the

surface of the nanoparticles surrounding them when present in solutions. A graphic representation of the zeta potential of nanoparticles in suspensions is shown in Figure 3.3.In some cases, researchers refer to this as the surface charge of the particles (Pate and Safier, 2016). The value of this charge is important, especially in nanoparticles aimed for drug delivery systems, since it indicates whether the suspension is physically stable or if it tends towards flocculation or aggregation.

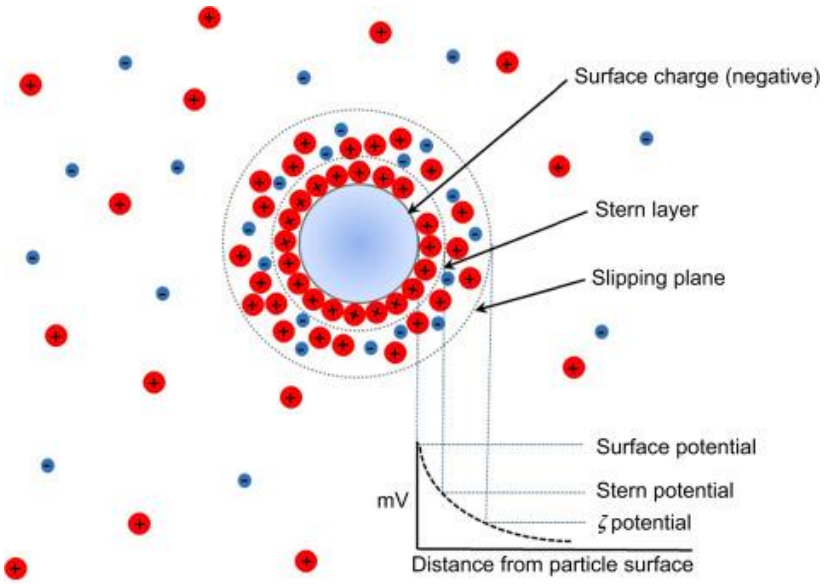

Figure 3.3: Schematic diagram representing the definition of zeta potential in nanoparticle suspensions. Figure taken from Pate and Safier (2016).

It is commonly preferred for the zeta potential of NPs to be negative, since negative zeta potentials are recognized to decrease nonspecific uptake into the liver and spleen. This leads to enhanced electrostatic repulsions between the particles and the cellular surface, consequently promoting the increased blood circulation of the nanoparticles (O'Brien *et al.*, 2020).

In the experiments completed in this thesis, the zeta potential of the colloidal suspensions prepared was measured using the ZetaPALS Zeta Potential Analyser (2008) model by Brookhaven Instruments Corporation (NY, USA), equipped with a red solid state laser. The equipment applies the principle of electrophoresis to measure the velocity of charged particles as they move under the influence of an electric field (electrophoretic mobility – μ). The zeta potential is then calculated based on the Smoluchowski relationship given in Equation 3.4 and the measured electrophoretic mobility (Nita *et al.*, 2011). The measurements were completed at room temperature (25 ºC). The samples were equilibrated at the measurement temperature

in the equipment cuvette chamber prior to measurement. Each measurement consisted of 5 runs of the same sample.

Equation 3.4: The Smoluchowski equation

$$\zeta = {}^{\eta\mu}/_{\varepsilon}$$

ζ Zeta potential of particles (V)

η Dynamic viscosity of the medium (Pa·s)

μ Electrophoretic mobility of particles ($cm^2/V{\cdot}s$)

ε Dielectric constant of the medium ($C^2/N{\cdot}m^2$)

Physical macroscopic investigation: The macroscopic appearance of the samples was investigated throughout all the methodology steps of the experimental work completed for this thesis. This was essential to gather further information about the state and the properties of the different samples prepared throughout the different processes followed. Changes on the appearance of the samples were monitored and noted as observations. To record these macroscopic observations for presentation purposes, a lightbox with LED lighting on the top wall and a blue or white colour backdrop was used to capture images of the samples using a camera.

Transmission electron microscopy (TEM): To examine the self-assembly and the shape in the dry state of the materials produced in the synthesis procedure followed in Chapter 4, a TEM characterisation of RAFT-PEGMA-LA_{25} as an example was performed by Kristoffer Kortsen from the School of Chemistry, at the University of Nottingham. For more details on this measurement see Appendix A.

Biological assays: Since the polymers constructed in Chapter 4 are intended for biomedical applications, the *in vitro* cytotoxicity of mPEG-CL_{50} and mPEG-CL_{50}-LA_{25} was tested on Caco-2 (intestinal), Calu-3 (airway) and THP-1 (macrophage) cells. The *in vitro* cytotoxicity experiments were carried out by Dr. Robert Cavanagh from the School of Pharmacy, at the University of Nottingham. More information on the cytocompatibility tests can be found in Appendix B.

3.6.3. Freeze-dried material characterisation

The freeze-dried material produced in Chapter 6 was characterised for its physical appearance based on the macroscopic investigation method summarised in section 3.6.2 and its surface and structure using SEM imaging. Details of the SEM characterisation technique are presented here.

Scanning electron microscopy (SEM): SEM is a powerful characterisation technique commonly applied for the visualisation of the surface morphology and the structural appearance of materials at very high magnifications (microscale) for a wide range of applications in multiple research areas. During SEM imaging, a focused beam of electrons is scanned across the sample surface as shown in Figure 3.4. The atoms of the sample interact with the electron generating different signals, such as secondary electrons and backscattered electrons. These signals are used to gain information on the sample's topography, composition and morphology (Egerton, 2005). The secondary electrons provide information about the topography and texture of the sample surface. The detection and analysis of these signals is performed by SEM to generate detailed images with depth of field and high resolutions (Goldstein, 2003).

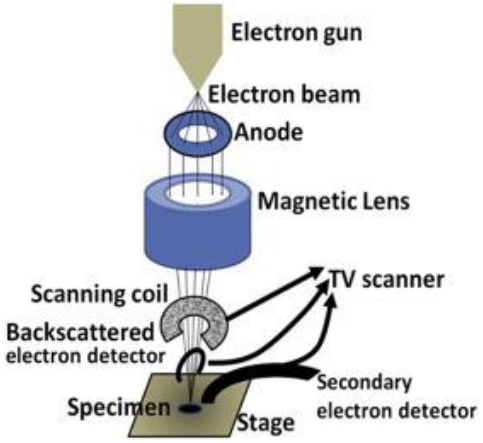

Figure 3.4: Schematic diagram of the SEM components and the focussed electron beam scanning the sample. Figure taken from (Singh, 2016).

The SEM technique was used to gain information about the surface and the structure of the freeze-dried cryoprotectant samples. The procedure followed to characterise the materials incorporated the spreading of the dry sample on a 10 mm diameter SEM stub mounted with the help of a double-sided conductive tape. The top of the stub with the dry sample was deposited with gold by using Agar sputter coater at 0.04 mbar and 40 mA, resulting in a thin Au film.

The prepared SEM samples were then positioned in the JEOL JSM-6010LA SEM instrument (JEOL U.K. Ltd) for microstructure imaging.

3.6.4. Quantification of drug loading

As discussed in section 3.5.2 the amount of the model drug that was encapsulated inside the polymeric nanoparticles was determined indirectly from the amount of the non-loaded Nile red. The quantity of drug encapsulated within the nanoparticles was calculated by deducting the amount of drug not encapsulated from the initial total amount of drug utilised in the experiment. After the amount of loaded drug was determined, the encapsulation efficiency and the drug loading capacity of the produced nanoparticle systems was calculated using Equation 3.1 and Equation 3.2 respectively.

The Nile red that was not encapsulated in the nanoparticles was extracted from the resulting colloidal suspension with the help of diethyl ether. The rationale behind the selection of this solvent for the extraction of Nile red from the NP suspensions is investigated further in Chapter 7. The extracted model drug amount was examined and quantified using UV-visible spectrophotometry using the characterisation methodology explained below.

Ultraviolet-visible (UV-vis) spectroscopy: UV-vis spectroscopy is an analytical characterisation technique employed to analyse the absorption or transmission of ultraviolet and visible electromagnetic radiation by the different materials present in a sample compared to a reference (blank) sample. It is a widely used characterisation method in numerous research areas for a variety of purposes, including the identification of substances present in samples, chemical bonds and reactions monitoring and the concentration quantification of substances in solution.

The general UV-vis spectroscopy system, including its individual components is presented in Figure 3.5. In UV-Vis spectroscopy, a sample is exposed to light covering the range from UV to visible wavelengths of the electromagnetic spectrum. Substances present in the sample can absorb this light when their properties match the energy levels of the incident photons. The sample's absorption spectrum is computed and plotted to determine the absorbance of light as a function of wavelength (Edwards and Alexander, 2010; Passos *et al.*, 2018).

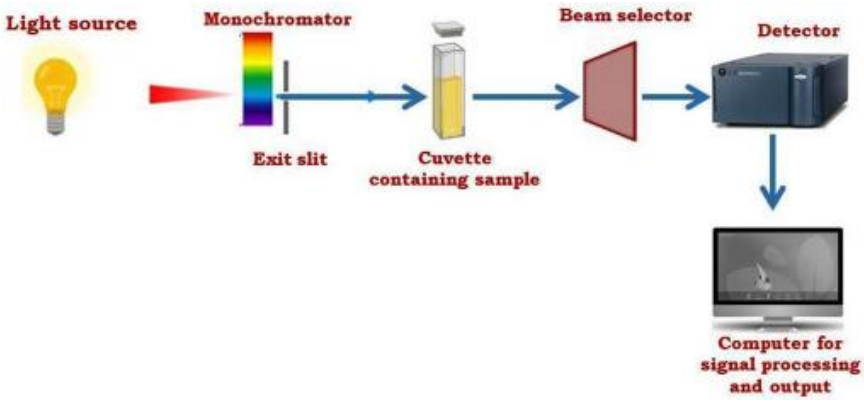

Figure 3.5: Schematic diagram of the UV-vis spectroscopy system with its individual components. Figure taken from Ahmad Mir, Mansoor Shafi and Zargar (2023).

UV-vis spectroscopy was employed in this thesis to determine the concentration of the Nile red model drug that was not loaded into the polymeric nanoparticles. First, the construction of a calibration curve, which plots the absorbance vs the concentration, of the Nile red model drug in the solvent was established. This calibration curve was then utilised to determine the amount of Nile red (non-loaded model drug) in unknown concentration samples. The UV-vis spectra were measured using the Genesys 150 UV-visible spectrophotometer (ThermoScientific, UK) using capped cuvettes. The measurements were completed at 552 nm and at room temperature (25 ºC). The samples were equilibrated at the measurement temperature in the equipment cuvette chamber prior to measurement. Each sample was measured a total of 6 times.

4. Synthesis of block copolymers for biomedical applications using 2-MeTHF as an eco-friendly polymerisation solvent

4.1. Introduction

The following experimental study has been executed in collaboration with Prof Steve Howdle's research group at the University of Nottingham. A paper has been published in the Journal of Polymer Science based on the experimental methodology and the research outcomes (Englezou *et al.*, 2020). Some of the following sections have been extracted from the original source.

The aim of this experimental investigation was to reduce the environmental burden and the health and safety implications associated with the synthesis of polymers designed for pharmaceutical applications based on the monomers of lactide (LA) and ε-caprolactone (ε-CL). To address this, the use of 2-MeTHF, as a biosourced, less-toxic analogue, was implemented to replace conventional petrochemical solvents in the polymerisation process.

The first objective was to examine the suitability of 2-MeTHF as a green multi-polymerisation solvent. To assess this, a range of polymerisation reactions were carried out in 2-MeTHF, as both a single-step process and in tandem. These included metal-free nucleophilic ring opening polymerisation (ROP), enzymatic nucleophilic ring opening polymerisation (eROP), reversible addition-fragmentation chain-transfer (RAFT) and free-radical polymerisation (FRP). The second objective was to produce versatile amphiphilic block copolymers with tunable chemistry and architecture from these reactions. This was achieved by selecting functional hydrophilic initiators to polymerise the hydrophobic monomers of lactide and ε-caprolactone. Subsequently, the amphiphilic polymers were nanoprecipitated in an aqueous environment to test their ability to yield nanoparticles. Finally, the cytocompatibility of the polymer nanoparticles was tested on three model cell lines to assess their ability to perform as drug delivery systems (DDS) in the future.

4.2. Polymer synthesis strategies

4.2.1. Experimental procedure overview

In total, ten amphiphilic block copolymers were synthesised, using the materials described in Chapter 3, with both linear and hyper-branched architectures. Table 4.1 tabulates the synthetic concentrations and architecture targeted for each synthesis.

Table 4.1: Synopsis of the produced amphiphilic block copolymers

Synthesised polymer	**Monomer**	**Initiator**	**Catalyst**	**Monomer/ Initiator ratio**	**Architecture**
mPEG-LA_{25}	lactide	$mPEG_{5000}$	DBU	25	linear
mPEG-LA_{125}	lactide	$mPEG_{5000}$	DBU	125	linear
mPEG-CL_{25}	ε-caprolactone	$mPEG_{5000}$	Novozym 435	25	linear
mPEG-CL_{50}	ε-caprolactone	$mPEG_{5000}$	Novozym 435	50	linear
mPEG-CL_{125}	ε-caprolactone	$mPEG_{5000}$	Novozym 435	125	linear
mPEG-CL_{50}-LA_{40}	lactide	mPEG-CL_{50}	DBU	40	linear
Synthesised polymer	**Monomer**	**Initiator**	**RAFT agent**	**RAFT agent/ Initiator ratio**	**Architecture**
FRP-PEGMA-LA_{25}	PEGMA-LA_{25}	AIBN	N/A	15	grafted brush
RAFT-PEGMA-LA_{25}	PEGMA-LA_{25}	AIBN	CPAB	15	grafted brush
FRP-HEMA-LA_{25}	HEMA-LA_{25}	AIBN	N/A	15	grafted brush
RAFT-HEMA-LA_{25}	HEMA-LA_{25}	AIBN	CPAB	15	grafted brush

Hydrophilic methyl-polyethylene glycol 5000 Da ($mPEG_{5000}$) was used as the macroinitiator for the ROP synthesis of linear diblock copolymers using either lactide (LA) catalysed by DBU or ε-caprolactone (ε-CL) catalysed by Nomozym 435 as the second block. The extension of the mPEG-CL_{50} diblock copolymer could be achieved when used as a macroinitiator to form a linear triblock copolymer via addition of LA catalysed by DBU constructing the third block. If the sequential double catalysis system is successful, the final polymer product will contain both

caprolactone and lactide. This is a material with tunable biodegradability that has the potential construct adaptable polymeric excipients. The linear block copolymers synthetic scheme is shown in Figure 4.1.

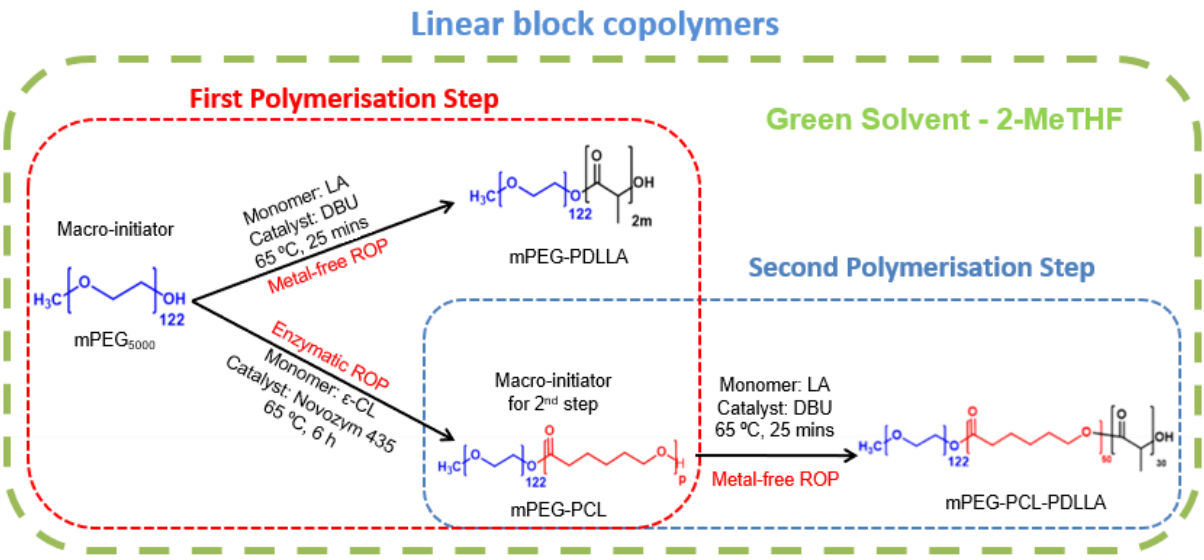

Figure 4.1: Reaction scheme for the synthesis of the linear block copolymers. All reactions were carried out in the green solvent, 2-MeTHF. The first polymerisation step is the formation of the diblock copolymers, and the second step is the formation of the triblock copolymer.

The first step for synthesising the branched block copolymers is the ROP synthesis of linear block copolymers of lactide initiated with polyethylene glycol methacrylate 300 Da (PEGMA-LA) and lactide initiated by hydroxyethyl methacrylate (HEMA-LA). Then, PEGMA-LA and HEMA-LA were initiated by the radical initiator azobisisobutyronitrile (AIBN) to execute the RAFT and FRP reactions. The RAFT reactions were performed in the presence of a RAFT agent, 4-Cyano-4-(phenylcarbonothioylthio) pentanoic acid (CPAB). The radical polymerisations resulted in grafted block copolymers by opening the end-chain double bond of the labile ester initiators (PEGMA or HEMA) to create connections between the individual linear polymers. The synthetic scheme for the hyper-branched block copolymers is shown in Figure 4.2.

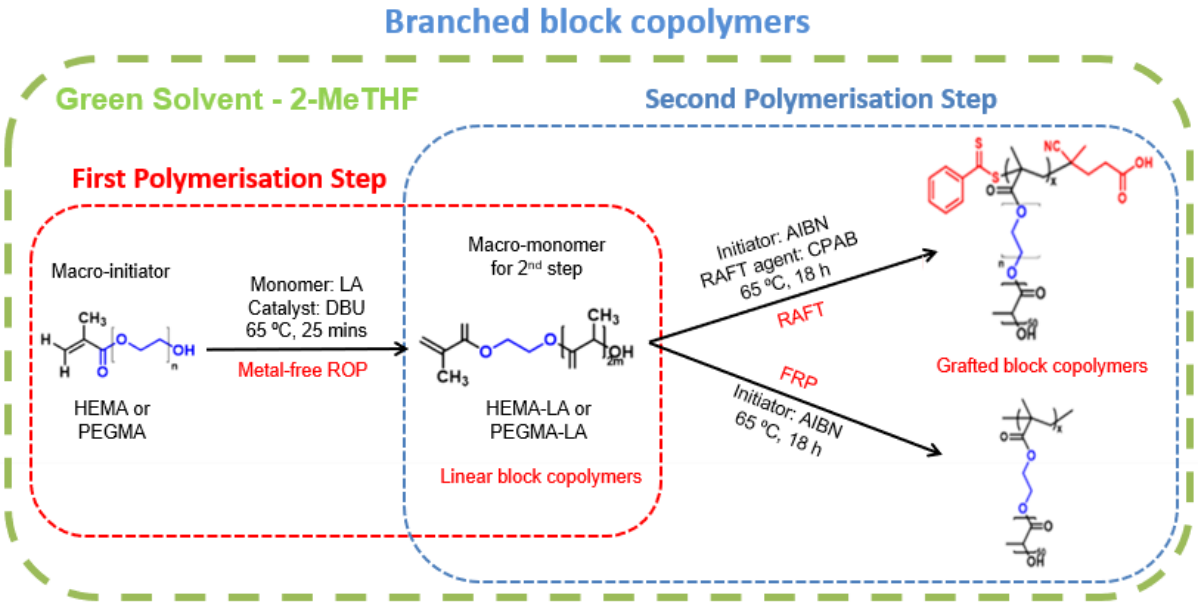

Figure 4.2: Reaction schematic for the synthesis of the grafted block copolymers. All reactions were carried out in the green solvent, 2-MeTHF. The first polymerisation step is the formation of the linear block copolymers via ROP. The second step is the radical polymerisations (FRP and RAFT) of the linear block copolymers to form the final grafted block copolymers.

Both linear and grafted block copolymer architectures enabled the resulting polymers to self-assemble into nanostructures in aqueous environments due to their amphiphilic nature. The final polymers were purified and nanoprecipitated to investigate the resulting self-assembled nanoparticles (NPs). Finally, the formulated nanoparticles were tested for their cytocompatibility in three model cell lines to evaluate their suitability to act as drug delivery carrier-systems in the future.

4.2.2. Detailed description of experiments

DBU-catalysed mPEG-initiated ROP of lactide in 2-MeTHF (M:I ratio of 25)

The desired amount of monomer LA (2000 mg) and $mPEG_{5000}$ initiator were weighed into a glass vial (pre-dried in an oven at 100 °C overnight) containing a magnetic stirrer bar. The [M]:[I] ratios were 25:1 or 125:1. For the synthesis of $mPEG\text{-}LA_{25}$ (25:1 [M]:[I] ratio), 0.55 mmol of $mPEG_{5000}$ and 13.9 mmol of LA were dissolved in 2-MeTHF. The vial was capped with a rubber septum and was stirred at 65 °C. Once the mixture was fully dissolved, the DBU catalyst was added to commence the ROP reaction. After 20 min of reaction time, the process was stopped by precipitating the reaction mixture in cold heptane-diethyl ether solution. The polymer was purified via three precipitation steps in total and finally was dried in a vacuum

oven. The same procedure was applied to produce the mPEG-LA_{125} by altering the monomer/initiator feed-stock ratio to 125:1.

The final dried product was then characterised according to the processes discussed in section 3.6.1. The chemical shifts on the obtained ^{1}H Nuclear magnetic resonance spectroscopy (^{1}H NMR) spectra used to determine the conversion of monomer to polymer and the degree of polymerisation using $mPEG_{5000}$-$(LA)_{25}$ as model (400 MHz, $CDCl_3$, ppm) are: δ 5.19 (broad m, 48H), 3.66 (broad s, 492H), 3.02 (s, 3H), 1.59 (broad m, 144H).

Separately, a mPEG-CL_{50} diblock copolymer was synthesised that served as a macroinitiator, extending the A-B block copolymer to produce an A-B-C triblock copolymer. In this instance, the same procedure to add LA to the mPEG-CL macroinitiator via a single-pot process was used. The only difference was during the multiple precipitation steps, where a solution of cold methanol and diethyl ether was used instead of heptane and diethyl ether solution.

Lipase-catalysed mPEG-initiated ROP of caprolactone in 2-MeTHF (M:I ratio of 50)

The desired amounts of monomer ε-CL (2000 mg) and $mPEG_{5000}$ initiator were weighed into a 20 ml glass vial (pre-dried in an oven at 100 °C overnight) containing a magnetic stirrer bar. The [M]:[I] ratios were 25:1, 50:1 or 125:1. For the synthesis of mPEG-CL_{50} (50:1 M:I ratio), 0.35 mmol of $mPEG_{5000}$ and 17.5 mmol of ε-CL were dissolved in 2-MeTHF. The vial was capped with a rubber septum and then stirred at 65 °C. Once the mixture was fully dissolved, the lipase catalyst (Novozym 435) was added to commence the ROP reaction. After 6 h of reaction time, the process was stopped by precipitating the reaction mixture into cold methanol. The polymer was purified via two further precipitation steps using the same technique with the mPEG-LA materials and finally dried in a vacuum oven. The same procedure was used to produce the mPEG-CL_{25} and mPEG-CL_{125} polymers by altering the monomer to initiator feed-stock ratios to 25:1 and 125:1 respectively. As previously mentioned, the mPEG-CL_{50} polymer was used as an A-B block macroinitiator to be extended with a sequential, one pot DBU catalysed ROP of LA, in a second polymerisation step.

The final dried product was then characterised according to the processes discussed in section 3.6.1. The chemical shifts on ^{1}H NMR spectra used to determine the conversion of monomer to polymer and the degree of polymerisation using $mPEG_{5000}$-$(CL)_{25}$ as model (400 MHz,

$CDCl_3$, ppm) are: δ 4.08 (broad t, 52H), 3.66 (broad s, 492H), 2.32 (broad t, 52H), 1.66 (broad m, 128H), 1.40 (broad m, 52H).

DBU-catalysed PEGMA and HEMA-initiated ROP of lactide in 2-MeTHF (M:I ratio of 25)

For these syntheses, the same procedure was followed with the synthesis of the mPEG-LA materials and the initiator of the polymerisation was altered. The PEGMA and HEMA methacrylate-ester labile initiators were used. The [M]:[I] ratio was kept fixed at 25:1 for both PEGMA and HEMA. The final dried product was characterised according to the processes discussed in section 3.6.1. The chemical shifts on ^{1}H NMR spectra used to determine the conversion of monomer to polymer and the degree of polymerisation using FRP-HEMA-LA_{25} as model (400 MHz, $CDCl_3$, ppm) are: δ 6.14 (s, 1H), 5.62 (s, 1H) 5.18 (broad m, 48H), 4.42 (broad m, 4H), 1.90 (broad s, 3H) 1.59 (broad m, 156H).

The linear polymers synthesised from these reactions were used as macromonomers undergoing RAFT and FRP reactions to form hyper-branched materials, in a second/tandem polymerisation step. This is explained in detail in the following section.

FRP or RAFT polymerisation of PEGMA-LA_{25} and HEMA-LA_{25} in 2-MeTHF

The desired amounts of macromonomer (300 mg) HEMA-LA_{25} (or PEGMA-LA_{25}), AIBN initiator and CPAB RAFT agent (in the case of RAFT reactions) were weighed into a 20 ml glass vial (pre-dried in an oven at 100 °C overnight) containing a magnetic stirrer bar. The monomer to RAFT agent molar ratio was 15:1 and the amount of AIBN initiator was 20% w/w for both HEMA-LA_{25} and PEGMA-LA_{25} RAFT reactions. The macromonomer, initiator and RAFT agent were fully dissolved in 2-MeTHF. The vial was capped with a rubber septum and the reaction mixture was degassed by bubbling Argon (Ar). Subsequently, the vials were placed and stirred in an oil bath at 65 ^{o}C for 18 h. The process was stopped by adding the reaction mixture into cold diethyl ether-THF solution. The polymer was purified via two further precipitation steps using the same technique with the mPEG-LA materials and was dried in a vacuum oven. The same procedure was employed to perform the FRP reactions without the addition of any RAFT agents and using an AIBN percentage of 0.5% w/w.

The final dried product was then characterised according to the processes discussed in section 3.6.1. The chemical shifts on ^{1}H NMR spectra used to determine the conversion of monomer

to polymer and the degree of polymerisation using FRP-HEMA-LA_{25} as model (400 MHz, $CDCl_3$, ppm) are: δ 5.18 (broad m, 48H), 4.30 (broad m, 2H), [2.19 (broad s, 6H) and 1.74 (broad m, 14H); CH_3 and CH_2 of polymer backbone and $CHCH_3$] 1.65 (broad m, 156H).

Nanoparticle formulation

All of the final polymeric products were formulated into NPs. To construct the polymeric nanoparticles, the nanoprecipitation, or solvent displacement, method was applied. The goal was to form NP suspensions through solvent exchange between the organic solvent (acetone) and the aqueous medium (deionized water). More specifically, the polymer was dissolved in acetone in a glass vial. In another clean glass vial containing a magnetic stirrer bar, 10 ml of deionized water was added. This was then placed on top of a magnetic stirrer in a fume cupboard. The polymer-acetone solution was added dropwise by hand to the deionized water glass vial, under constant stirring (Pearce *et al.*, 2019; Phan *et al.*, 2019; O'Brien *et al.*, 2020). The acetone-water solution was left uncapped stirring overnight at room temperature to achieve full removal of the acetone from the solution by evaporation.

4.3. Results and discussion

At 65 °C, 2-MeTHF completely dissolves all the polymers, precursors and catalysts used in this investigation. It has a relatively high boiling point (80 °C) compared to other conventional solvents (Table 2.2). This allows the use of 2-MeTHF at a higher temperature (65 °C) than the polymerisation reactions carried out in different solvents with thermal limitations. The higher temperatures accessed by using 2-MeTHF enable faster polymerisation kinetics, which can enhance manufacturing throughput at the scale-up stage. The temperature for all reactions carried out; including metal-free ROP, enzymatic ROP, FRP and RAFT; was chosen to be 65 °C to overcome limitations on solubility and reaction activation, as well as promoting fast kinetics.

4.3.1. Linear block copolymers

The suitability of 2-MeTHF as a ROP solvent for the formation of simple A-B diblock copolymers (single lactide and single lactone) and for the construction of more versatile A-B-C triblock copolymers (lactide and lactone in a single chain), using a single or double catalyst system (DBU and lipase) respectively, was examined in this study.

The data collected from performing the chemical characterisation techniques (^{1}H NMR, GPC and DLS) detailed in Chapter 3 for all the linear block copolymers (mPEG-PDLLA, mPEG-PCL and mPEG-PCL-PDLLA) synthesised in this work are presented in Table 4.2.

Table 4.2: Chemical characterisation and nanoparticle properties of all the linear block copolymers

Polymer label	**M/I ratio**	**Conversion (%)[a]**	**M_n (^{1}H NMR) (Da)[b]**	**M_n (GPC) (Da)[c]**	**$Đ_M$**	**Size (nm)[d]**	**PDI**
mPEG-LA_{25}	25	96	8456	7000	1.21	40±5[e]	0.250
mPEG-LA_{125}	125	98	22568	11000	1.20	48±2 [e]	0.250
mPEG-CL_{25}	25	100	7850	7600	1.20	60±2 [e]	0.140
mPEG-CL_{50}	50	96	10472	9800	1.30	80±5 [e]	0.125
mPEG-CL_{125}	125	99	19136	12400	1.26	79±2 [e]	0.100
mPEG-CL_{50}-LA_{40}	(CL)50+ (LA)40	96(CL)+ 78(LA)	14792	10200	1.30	72±2 [e]	0.130

[a]Calculated by ^{1}H NMR.
[b]Calculated from CH_2 mPEG-initiator backbone peak and C*H* PDLLA or -O-CH_2 PCL peaks ^{1}H NMR integration.
[c]Compared to PMMA standards.
[d]DLS measurements.
[e]Average values from at least two sample replicates.

For the synthesis of pharmaceutical amphiphilic PEGylated-lactide block copolymers in a single reaction step in 2-MeTHF, a metal-free ROP synthetic strategy catalysed by DBU was performed (Figure 4.3).

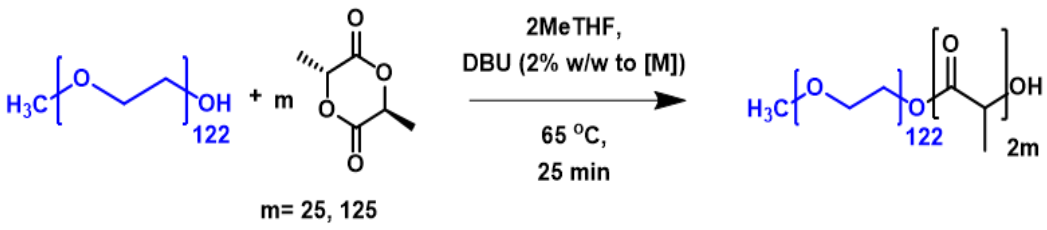

Figure 4.3: Reaction scheme for mPEG-initiated lactide ROP in 2-MeTHF catalysed by DBU.

$mPEG_{5000}$ was used as the macroinitiator and the initiator to monomer ratios were set to produce 25 and 125 LA units. Lactide reached quantitative conversion into polymers within 25 min independent of the monomer/initiator ratio.

^{1}H NMR measurements of the samples were carried out to establish the degree of polymerisation (DP_n) and conversion of the monomers to polymers. The ^{1}H NMR spectra were compared for the initial reaction mixture in 2-MeTHF before the addition of DBU, and therefore before the start of the polymerisation reaction, and for the final purified polymer product. These were used to establish the DP_n, the conversion of monomer lactide to polymer and calculate the molecular weight of the final polymer. Figure 4.4-A shows the ring opening polymerisation reaction of lactide with the characteristic protons marked. The peak shifts of these protons were identified on the ^{1}H NMR spectra collected for the initial reaction solution (at time zero) and the purified polymer (t_0 vs purified) as shown in Figure 4.4-B. The ^{1}H NMR of the purified copolymer shows the characteristic peaks of the polymerised lactide, meaning the polymerisation of the monomer LA was successful in the applied reaction time frame. More specifically, in Figure 4.4-B the clear shift and variations of the lactide-related peaks, methine C*H* group at 5.05 ppm (quadruplet, monomer) to 5.25 ppm (broad multiplet, polymer), and methyl CH_3 group at 1.60 ppm (sharp doublet, monomer) to 1.59 ppm (broad multiplet, polymer) can be observed. By integrating these characteristic peaks, the number of polymerised lactide protons present in the purified polymer product can be obtained. From the results, there was good agreement with the monomer and initiator feed ratios with DP_n of 24 and 122 LA units for the mPEG-LA_{25} and mPEG-LA_{125} respectively. A conversion of the monomer LA to PLA of 96% and 98% and polymer molecular weights of 8,456 Da and 22,568 Da for the mPEG-LA_{25} and mPEG-LA_{125}, respectively, was calculated as shown in Table 4.2.

The Gel permeation chromatography (GPC) trace acquired for the final purified block copolymer of mPEG-LA_{25} is also shown in Figure 4.4-C. The results show a monomodal GPC trace with low molecular weight dispersity ($Đ_M$). Dispersity values of 1.21 and 1.20 were established from the GPC analysis for mPEG-LA_{25} and mPEG-LA_{125} respectively (Table 4.2). These polydispersity values are low for this ROP synthesis and confirm a degree of control over the molecular weight of the final polymer products.

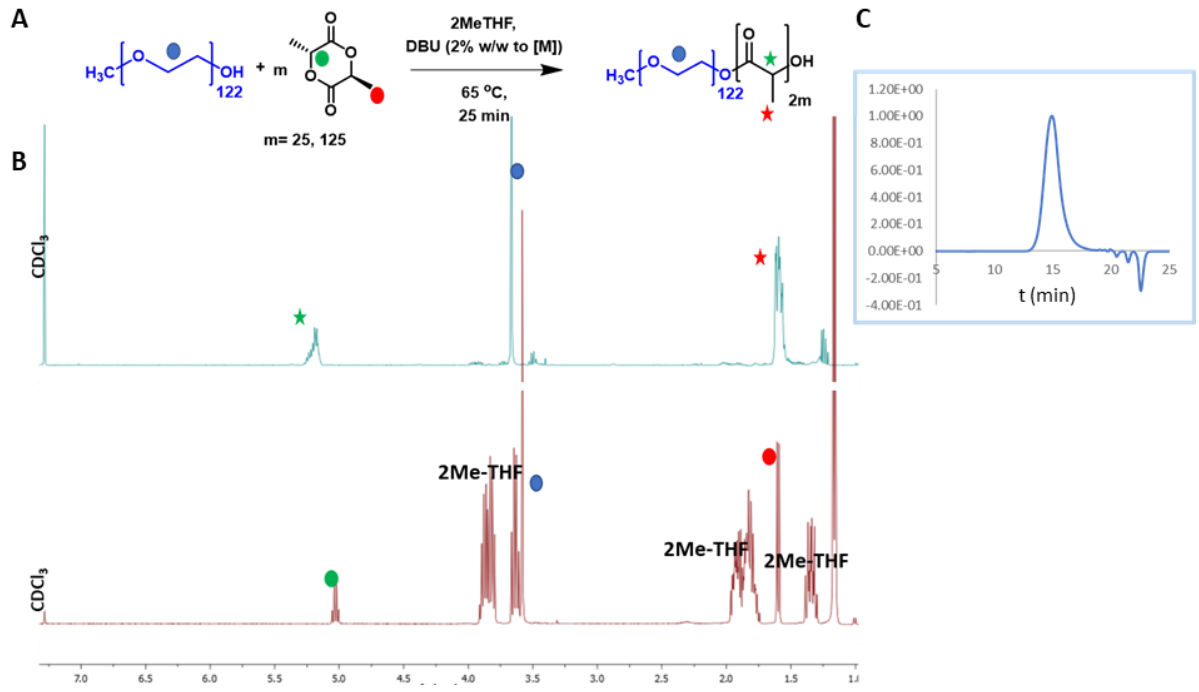

Figure 4.4: (**A**) ROP reaction scheme of A-B block copolymers of mPEG-LA with the characteristic protons marked. (**B**) Stacked ^{1}H NMR spectra of the starting reagents mixture in 2-MeTHF (t = 0, before DBU addition) and purified final polymer. (**C**) Monomodal GPC trace of the final purified polymer.

To alter the nature of the hydrophobic monomer, and with the aim of expanding the library of amphiphilic materials synthesisable in 2-MeTHF, a lipase (Novozym 435) catalysed ROP of ε-caprolactone was performed. $mPEG_{5000}$ was maintained as the macroinitiator and the initiator to monomer ratio was altered to achieve a final polymer chain length of 25, 50 and 125 ε-CL units (Figure 4.5).

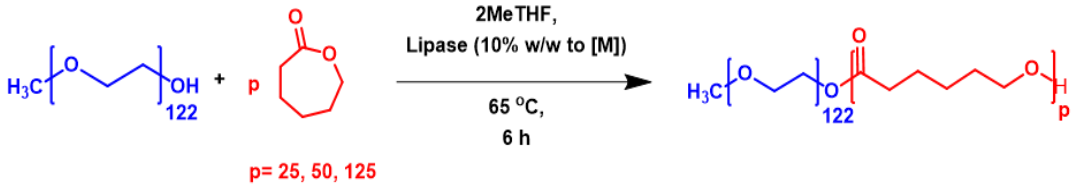

Figure 4.5: Reaction scheme for mPEG-initiated ε-caprolactone eROP catalysed by Novozym 435 (lipase) in 2-MeTHF.

ε-CL was quantitatively converted into polymers within 6 h, with no perceptible reactivity differences between each monomer/initiator feed ratio. This is observed since the reaction time frame was long enough for all polymers to reach their final conversion. As expected, considering the bioprocess being heterogeneous due to the use of immobilised lipase as well

as the different nature of the catalytic step, the reaction time was longer than the DBU-catalysed ROP of lactide.

^{1}H NMR measurements were compared for the initial reaction solution, before addition of lipase (at time zero), and the final purified polymer to obtain the DP_n, the conversion of ε-CL to form PCL and the molecular weight of the final polymer. Figure 4.6-A shows the ring opening polymerisation of ε-CL with the characteristic protons marked. The peak shifts of the ε-CL and PCL characteristic protons were identified on the ^{1}H NMR spectra collected for the reaction mixture at time zero and the purified polymer (t_0 vs purified) as shown in Figure 4.6-B. The ^{1}H NMR of the purified copolymer contains the characteristic peaks for PCL, suggesting that an appropriate time frame was chosen for the successful polymerisation of ε-CL. Specifically, the clear shift and variations of caprolactone-related peaks, the alcohol-methylene -O-CH_2 group at 4.25 ppm (sharp doublet, monomer) to 4.08 ppm (broad triplet, polymer), the methylene CH_2 group at 2.62 ppm (doublet, monomer) to 2.32 ppm (broad triplet, polymer), and the methylene CH_2 groups at 1.88 ppm (doublet, monomer) and 1.75 ppm (doublet, monomer) to 1.66 ppm (broad multiplet, polymer) and 1.40 ppm (broad multiplet, polymer) can be observed in Figure 4.6-B. By integrating these characteristic peaks, degrees of polymerisation (DP_n) of 25, 48 and 124 ε-CL units for the mPEG-CL_{25}, mPEG-CL_{50} and mPEG-CL_{125}, respectively, were found, showing agreement with the monomer/initiator feed ratios. Subsequently, the conversion of ε-CL to PCL was calculated as 100%, 96% and 99% and the estimated polymer molecular weights were 7,850, 10,472 and 19,136 Da for mPEG-CL_{25}, mPEG-CL_{50} and mPEG-CL_{125}, respectively. These values are shown in Table 4.2.

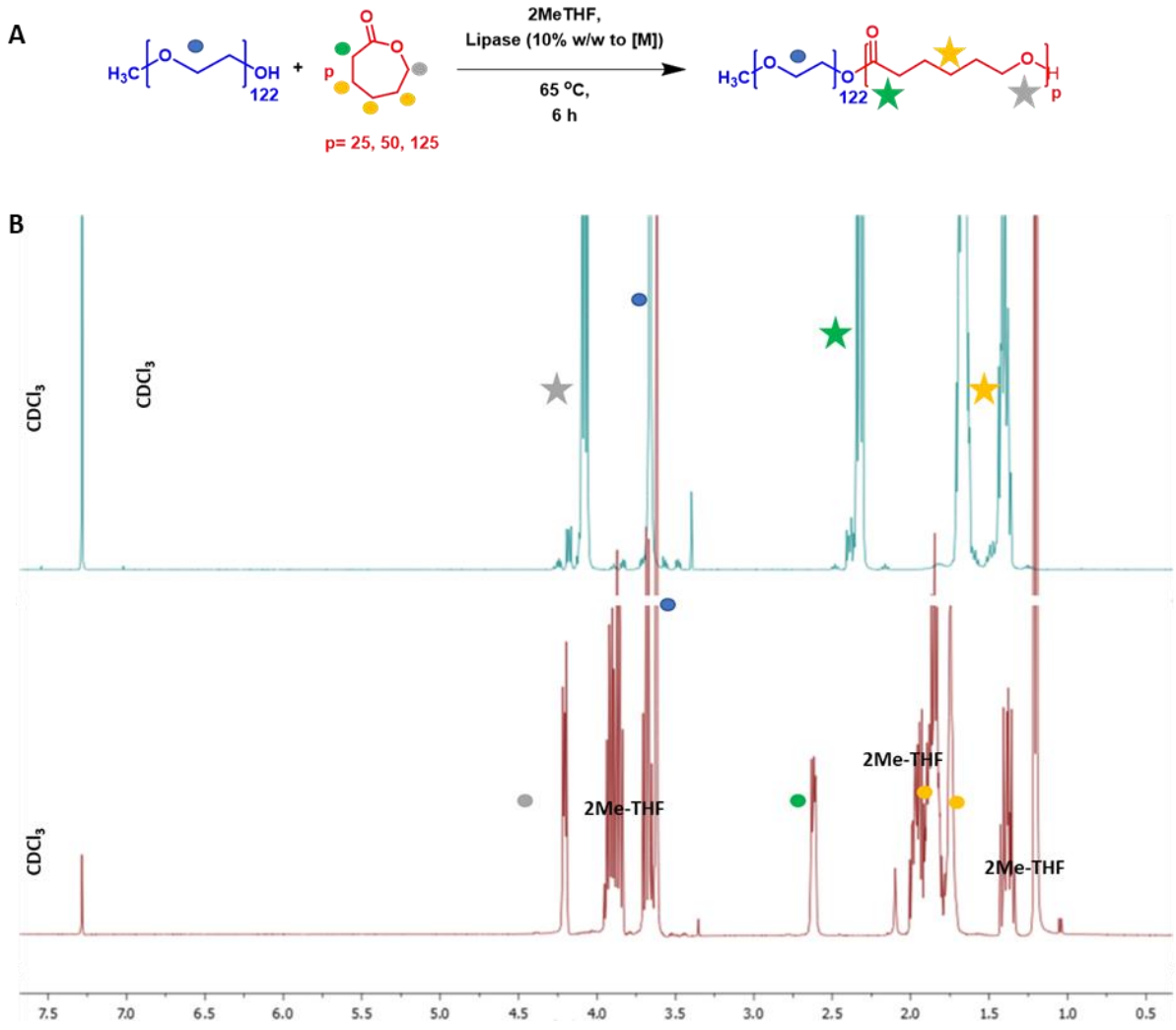

Figure 4.6: (**A**) ROP reaction scheme of A-B block copolymers mPEG-CL with the characteristic protons marked. (**B**) Stacked ^{1}H NMR spectra of the starting reagents mixture in 2-MeTHF (t = 0, before lipase addition) and purified final polymer.

Adequately controlled molecular weight dispersities ($Đ_M$) were observed by GPC analysis, with values of 1.20, 1.30 and 1.26 for mPEG-CL$_{25}$, mPEG-CL$_{50}$ and mPEG-CL$_{125}$, respectively (Table 4.2). A small shoulder in the GPC trace of the mPEG-CL$_{50}$ (Figure 4.7-Cii) can be observed, which is possibly due to some uncontrolled side reactions, such as transesterification.

The stability of the living polymer chain in 2-MeTHF was studied by producing an A-B-C (A=mPEG$_{5000}$, B=ε-CL and C=LA) triblock copolymer (Figure 4.7-A). To explore the feasibility of a sequential ROP, the lipase catalysed ring opening of ε-CL initiated by mPEG$_{5000}$ (M:I ratio of 50) was performed for 6 h, (see Table 4.2 and Figure 4.7). Subsequently, without catalyst removal or any purification steps, lactide and DBU catalyst were added with a M:I (monomer LA:A-B macroinitiator) feed ratio of 40:1. After 25 min (the reaction time

previously established for DBU catalysed ROP of LA) the reaction was terminated with the precipitation in an alcohol and ether solution and the reaction mixture was analysed by ^{1}H NMR, which is shown in Figure 4.7-Bi. The presence of peaks at 5.05 ppm (quadruplet) and at 5.25 ppm (broad multiplet), related to the monomeric LA and the polymeric PDLLA *CH* group respectively, suggested slower reaction kinetics for the growth of the third block. Again, by extracting information on the number of protons from the characteristics peaks on the ^{1}H NMR spectra (Figure 4.7-Bi), the conversion of monomer LA into polymer was estimated to be 78% (Table 4.2). This is much lower (~20% lower) when compared to an almost full conversion for the previously formed diblock mPEG-LA in the same reaction timeframe (see Table 4.2). The slower reaction kinetics might be due to the reduced flexibility and reactivity of the A-B (mPEG-CL_{50}) macroinitiator compared to pure $mPEG_{5000}$, which was used for the synthesis of the mPEG-LA diblock copolymers. Nonetheless, the A-B-C block copolymer showed an asymmetric GPC peak (clear shoulder at lower molecular weight) indicating that the LA chain grew from the macroinitiator, however, products from a series of side reactions and unreacted macroinitiator may be present (Figure 4.7-Ci and -Cii).

The use of 2-MeTHF as a polymerisation solvent enabled the successful synthesis of the mPEG-CL-LA triblock copolymer. The application of this polymer can be further explored in the design of biomedical devices with adjustable physical properties and tunable biodegradability due to the coexistence of different hydrophobic polyesters in a single chain (Stavila *et al.*, 2014).

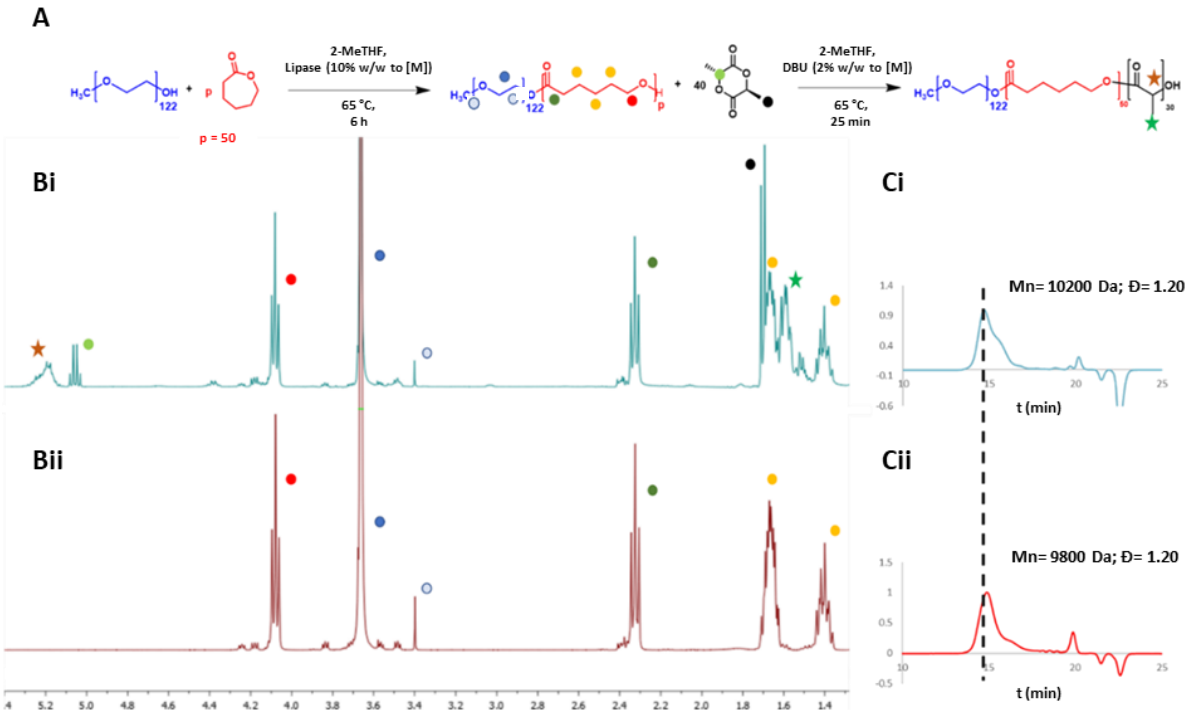

Figure 4.7: (**A**) Sequential ROP reaction scheme of mPEG-CL_{50} and mPEG-CL_{50}-LA_{40}, namely A-B and A-B-C block copolymers, with the characteristic protons marked. (**Bi-Bii**) ^{1}H NMR spectra of mPEG-CL_{50}-LA_{40} and mPEG-CL_{50} respectively with all the main polymeric and monomeric peaks assigned. (**Ci-Cii**) GPC traces of mPEG-CL_{50}-LA_{40} and mPEG-PCL_{50} respectively.

From the results presented in Table 4.2, some incompatibility in terms of the molecular weight values calculated from ^{1}H NMR versus measured via GPC was observed. These discrepancies are possibly due to the significant chemical differences between the amphiphilic block copolymers and the PMMA standards, which were used for calibration of the system for the GPC analysis. This observation is known from literature (Al-Natour *et al.*, 2020) and might be due to the presence of various polymer-column interactions and different solvated volumes. Variation between molecular weights calculated by ^{1}H NMR and GPC is present consistently throughout the different amphiphilic linear and hybrid polymers generated in this investigation.

All the polymers were able to self-assemble in an aqueous environment into well-defined NPs, with diameters ranging from approximately 40 nm up to 80 nm and PDIs equal or below 0.250 (Table 4.2). No additional stabilizers were used during the nanoprecipitation step.

As discussed in the Literature review chapter of this thesis, the chosen formulation technique applied for the construction of nanoparticles can lead to a variety of nanoparticle structures depending on various factors, such as polymer physicochemical properties, composition,

environment conditions, solvents quality, etc. The nanoprecipitation technique is widely reported in the literature as an easy, robust, and fast process for the preparation of polymeric micelles (Salvage *et al.*, 2015; Martínez Rivas *et al.*, 2017). Dynamic light scattering (DLS) is employed here as the characterisation technique for the resultant nanoparticle suspensions. This method is commonly used to provide information on the particle size distribution and the polydispersity index (PDI) of the prepared nano-suspensions. Based on the DLS results gathered, all the linear block copolymers synthesised in this study, were able to form nanoparticles with diameters within the typical size range of polymeric micelles (10-100 nm) (Rapoport, 2007) and exhibited a low PDI. However, this characterisation technique alone cannot confirm whether the nanoparticles formed are indeed polymeric micelles, since it lacks structural characterisation capabilities. Therefore, the exact type of polymeric nanoparticles constructed in this investigation remains unknown. Future work should consider the combination of DLS with other characterisation techniques, such as cryo-TEM or X-ray scattering, to reach a definitive conclusion about the exact type of polymeric nanoparticles formulated.

The tabulated data in Table 4.2 suggest a potential association between polymer molecular weights and nanoparticle diameter size; however, this relationship remains inconclusive, as shown in Figure 4.8. For the mPEG-CL polymers, increasing the molecular weight (and in this case DP_n of CL), increases the diameter size of the nanoparticles formed. This seems reasonable since a polymer chain of higher molecular weight excludes more volume when self-assembled into a nanoparticle, relative to shorter polymer chains. The same possible trend is noted for mPEG-LA, but the trend is not conclusive. Notably, the triblock copolymer appears to behave more like the mPEG-CL precursor than the mPEG-LA.

The diameter of the nanoparticles formed does not appear to scale linearly with molecular weight for the mPEG-CL diblock copolymers. The material may be kinetically trapped during the nanoprecipitation process. In this situation, kinetically trapped refers to the phase transition from the homogeneous phase of solvated polymer in solution to the two-phase mixture of precipitated polymer in a non-solvent blend when it does not occur along an equilibrium trajectory. The nanoparticles formed could be kinetically trapped when introduced rapidly into the non-solvent. At equilibrium, the chains would micellise with the hydrophobic CL and LA group within the core to avoid interactions with the aqueous solvent. In the solvent displacement method, the organic solvent is constantly evaporated until only the aqueous

solvent is left. If the evaporation is slow enough to allow equilibration, the equilibrium size of micelles will be formed. If the evaporation is faster than the time required for the system to equilibrate (after each infinitesimal step), a trapped nanoparticle structure may result. Although, it is not certain that this is the exact phenomenon happening during the nanoprecipitation step nor that this causes the complicated correlation between nanoparticle size and molecular weight observed in this set of data. Further investigation of the nanoprecipitation process and the self-assembling mechanism of nanoparticles is required to achieve a greater understanding of these phenomena. This is the main research emphasis of Chapter 5 of this thesis.

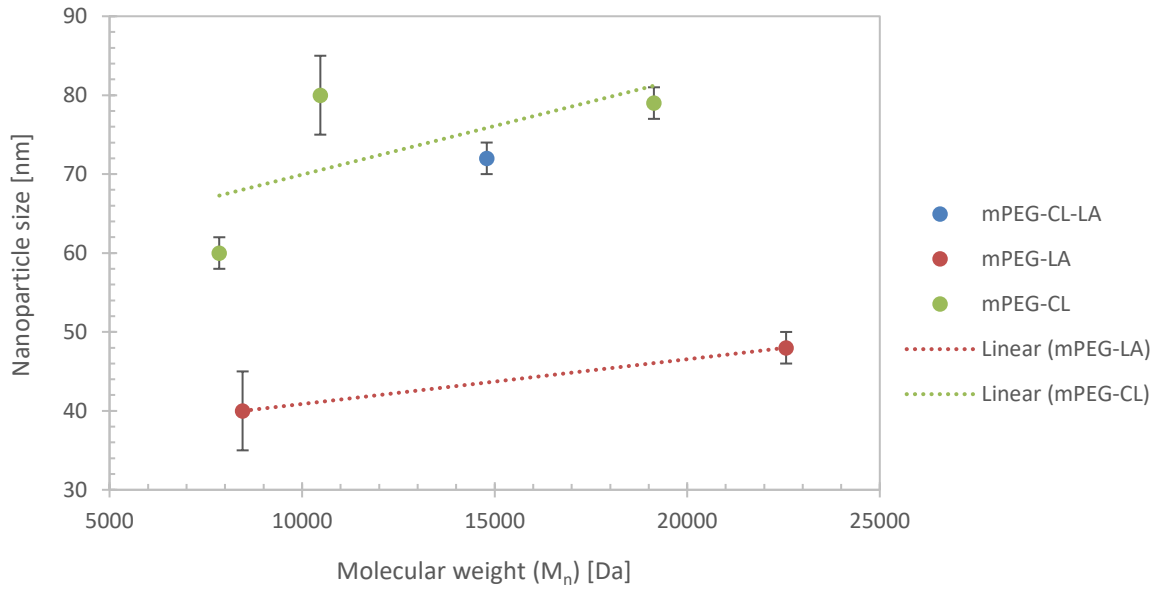

Figure 4.8: Effect of the polymer molecular weight on its nanoparticle size. The graph shows the molecular weights (M_n) calculated from ^{1}H NMR for all the linear block copolymers produced vs their nanoparticle sizes measured through DLS. The data have been separated into three parts (**blue**) the linear triblock with the diblock macroinitiator at ~10K Da, (**red**) the two linear mPEG-LA diblock and (**green**) the three linear mPEG-CL diblock copolymers. For the two latter cases a linear trendline has been included to illustrate the trajectory of the data more clearly, but this is not conclusive of the relationship between the two parameters as there are not enough data points.

Since these materials are intended for biomedical applications, such as drug delivery vehicles, the *in vitro* cytotoxicity of mPEG-CL_{50} and mPEG-CL_{50}-LA_{25} was tested on Caco-2 (intestinal), Calu-3 (airway) and THP-1 (macrophage) cells at a fixed concentration of 500 µg/ml. The *in vitro* cytotoxicity experiments were carried out by Dr. Robert Cavanagh from the School of Pharmacy, at the University of Nottingham.

The nanoparticle cytotoxicity was examined through the evaluation of the cell membrane integrity and cellular metabolic activity with the employment of the lactate dehydrogenase (LDH) release assay and the PrestoBlue cell viability assay, respectively. In both assays, neither of the linear nanoparticles exhibited cytotoxic effects across all three studied model cell types, mirroring the results observed with the cell culture medium HBSS used as a vehicle control (Figure B.1 in Appendix B.2). More information on the cytocompatibility tests and the results collected for the polymer materials produced in this work can be found in Appendix B.

By adopting 2-MeTHF as a solvent it was able to make the synthesis greener for polymeric excipients, which have a high demand in the drug delivery and biomedical fields (Werner *et al.*, 2013; Yin *et al.*, 2014; Yu *et al.*, 2016). The ability of these linear block copolymers to self-assemble into NPs along with testing their cytocompatibility has been confirmed. The use of 2-MeTHF also allowed the sequential one-pot ROP of ε-CL and LA, which leads to a material with tunable biodegradability. This double catalysis process was able to overcome the limitations of DBU and lipase in the ROP of lactones and lactide respectively. Therefore, it was confirmed that the properties of the final materials produced in the ROP process were not compromised using 2-MeTHF as the polymerization solvent.

4.3.2. Grafted block copolymers

Amphiphilic copolymers with hybrid architectures capable of self-assembling into biodegradable NPs for biomedical applications were synthesised using a combination of ROP with radical polymerisations. The strategy employed to construct these hybrid functionalised polymers is the synthesis of radically polymerisable macromonomers via ROP. These could then undergo tandem polymerisations, allowing the production of materials with a wide range of architectures and chemistries. The labile-ester initiators of HEMA and PEGMA were used for the ROP of lactide to introduce an end-chain reactive double bond in the macromonomer, which would then be radically polymerised to yield grafted block copolymers. HEMA- and PEGMA-initiated LA macromonomers were synthesised to confirm the versatility of 2-MeTHF and the ability of DBU to control the polymerisation reactions (and limiting transesterification reactions) at 65 ^{o}C, rather than at room temperature as previously explored in the literature (Pearce *et al.*, 2019). The target degree of polymerisation (DP_n) was 25 LA units. The reaction temperature led to an increased radical flux due to the thermal decomposition of AIBN radical initiator, allowing for tandem radical polymerisation processes

to take place in 2-MeTHF. This happened because the rate of thermal decomposition of AIBN starts at temperatures higher than 30 °C at a very slow rate. As the temperature is increased, the rate of AIBN decomposition increases significantly (Li, Wangb and Koseki, 2008; Guo *et al.*, 2013; Roduit *et al.*, 2015). Therefore, the higher boiling point of 2-MeTHF allowing radical polymerisation to take place at 65 °C enhances the rate of AIBN thermal decomposition and therefore the rate of polymerisation.

For both methacrylate initiators (HEMA and PEGMA) control of the ROP from DBU was observed as no transesterification side reactions occurred in the reaction time frame of 25 min (Figure 4.9 inset). A conversion of monomer to polymer higher than 96% was observed, as estimated from the ^{1}H NMR spectra in Figure 4.9. Moreover, the final DP_n was confirmed via ^{1}H NMR to be equal to 25 LA units as targeted in the M:I feed ratio.

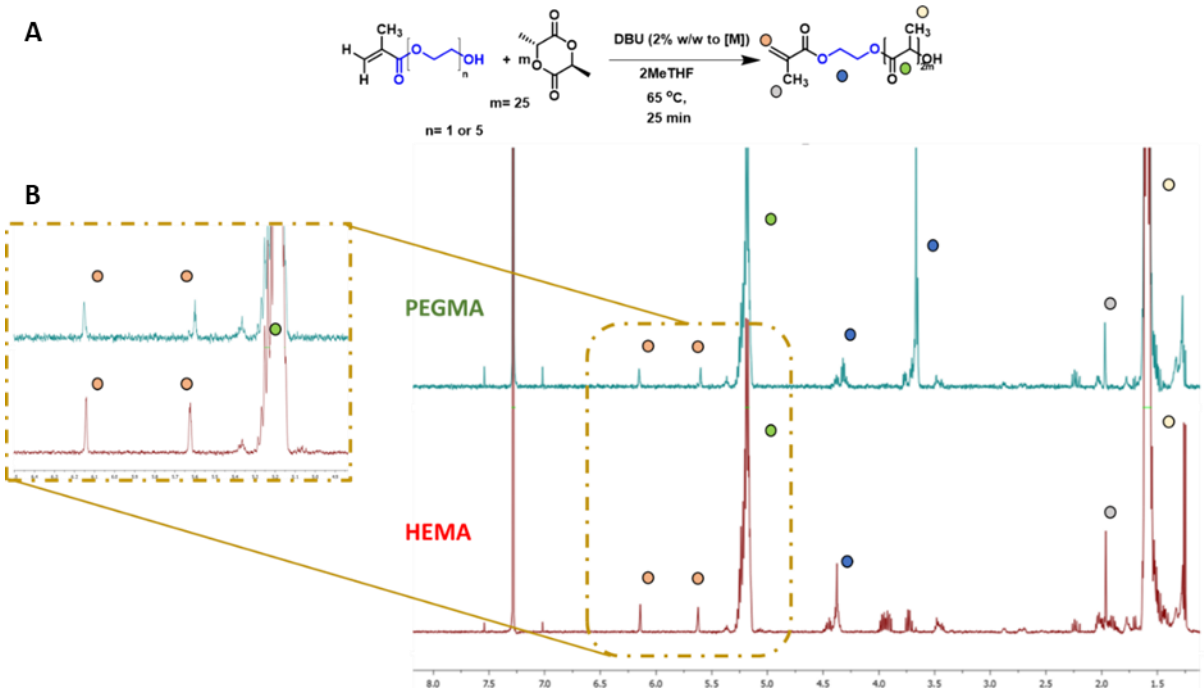

Figure 4.9: (**A**) ROP reaction scheme of methacrylate-lactide hybrid macromonomers in 2-MeTHF with the characteristic protons marked. (**B**) ^{1}H NMR of the final purified macromonomers (PEGMA and HEMA initiated) and main macromolecule peak assignments. The targeted DP_n of the final oligomer was 25 LA units, as reported in the stoichiometry of the reaction scheme. In this case, the number of LA C*H* protons is equal to the number of repetitive units. However, LA bears two C*H* protons per full unit and thus the final DP_n is calculated by halving the total number of LA C*H* protons obtained from integration.

The data collected from performing the chemical characterisation techniques (^{1}H NMR, GPC and DLS) detailed in Chapter 3 for all the grafted block copolymers (FRP-PEGMA-LA, RAFT-

PEGMA-LA, FRP-HEMA-LA and RAFT-PEGMA-LA) synthesised in this work are presented in Table 4.3.

Table 4.3: Chemical characterisation and nanoparticle properties of all the grafted block copolymers

Polymer label	Conversion (%)[a]	M_n (^{1}H NMR) (Da)[b]	M_n (GPC) (Da)[c]	$Đ_M$	Size (nm)[d]	PDI
FRP-PEGMA-LA_{25}	100	-	11000	5.14	117±2[e]	0.120
RAFT-PEGMA-LA_{25}	70	27300	9800	1.40	95±2 [e]	0.140
FRP-HEMA-LA_{25}	100	-	20000	4.30	125±2 [e]	0.080
RAFT-HEMA-LA_{25}	70	26110	9300	1.30	93±2 [e]	0.090

[a]Calculated by ^{1}H NMR.
[b]Calculated from C*H* PEGMA- HEMA-initiator acrylic peak and C*H* PDLLA ^{1}H NMR integration.
[c]Compared to PMMA standards.
[d]DLS measurements.
[e]Average values from at least two sample replicates.

To further extend the ability of 2-MeTHF to serve as a multi-polymerization solvent, FRP and RAFT tandem polymerisations of the produced macromonomers were explored, keeping the reaction temperature at 65 ^oC as for the ROP step. Both FRP and RAFT model reactions yielded grafted amphiphilic biodegradable hybrid-polymers. Figure 4.10-A shows the two reactions (RAFT and FRP) for HEMA-LA and the chemical structure of the two different grafted amphiphilic polymers constructed. For both the final polymeric materials, the end-chain reactive double bond has opened to bond with other similar long HEMA-lactide or PEGMA-lactide side chains and form a grafted brush.

For the FRP reactions full conversion (100%) was observed (Table 4.3) for both PEGMA-LA_{25} and HEMA-LA_{25} macromonomers into grafted-polymer. This is illustrated in Figure 4.10-B by the complete absence of the residual double bond related peaks on the ^{1}H NMR spectra. For the RAFT polymerisations, a conversion of around 70% was estimated for the two polymers with some peaks present related to residual double bonds. The polymer molecular weights of the synthesised grafted block polymers by RAFT polymerisation were estimated as 27,300 Da and 26,110 Da for PEGMA-LA_{25} and HEMA-LA_{25}, respectively, as shown in Table 4.3. For both RAFT and FRP reactions, the target DP_n was 15 units. The same reaction timeframe of 18 h was used for all the reactions. The difference between the conversion of the two radical

polymerisation reactions was expected since the RAFT agent (CPAB) is incorporated in the process to control the radical (RAFT) reaction. The RAFT agent controls the kinetics of the polymerisation and lowers conversion rate. CPAB controls the RAFT reaction mechanism through a coordination process, which happens at a slower rate than FRP. The reaction was stopped after 18 h, at which point the conversion was not 100% yet, but if the reaction were allowed for longer, the conversion would have been higher. RAFT could potentially reach 100% conversion, but would need a significantly longer time than the FRP reaction due to the slower kinetics.

GPC analysis detected a single, although slightly asymmetric, polymeric species for the RAFT synthesised polymers (Figure 4.10-C-top). The asymmetry is possibly indicating some minimal amount of side reactions, although overall the data indicate that the macromonomers were compatible with the tandem ROP controlled radical reaction cycle. The polymer molecular weights were measured as 9,800 Da and 9,300 Da for RAFT-PEGMA-LA_{25} and RAFT-HEMA-LA_{25}, respectively, as shown in Table 4.3. For both the polymers synthesised by FRP, broad bimodal peaks were detected (Figure 4.10-C-bottom). The polymer molecular weights were measured as 11,000 Da and 20,000 Da for FRP-PEGMA-LA_{25} and FRP-HEMA-LA_{25}, respectively, as shown in Table 4.3.

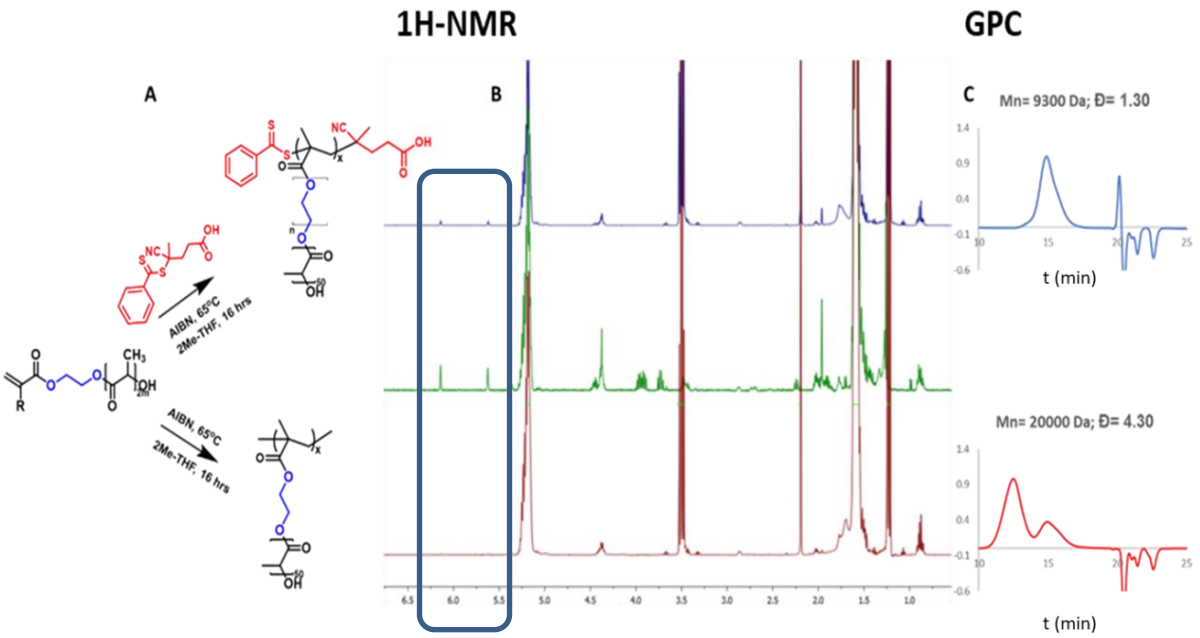

Figure 4.10: **(A)** RAFT and FRP reaction scheme of hybrid HEMA-LA_{25} macromonomer in 2-MeTHF. **(B)** (**bottom**) ^{1}H NMR spectra of FRP-HEMA-LA_{25} (absence of residual double bond-related peaks in the outlined region), (**centre**) macromonomer starting material and (**top**) RAFT-HEMA-LA_{25} (residual double bond-related peaks in the squared region). **(C)** (**top**) GPC monomodal trace of RAFT-HEMA-LA_{25} and (**bottom**) GPC bimodal trace of FRP-HEMA-LA_{25}.

From Table 4.3, a variation between the molecular weights (M_n) estimated from ^{1}H NMR and M_n measured from GPC can be observed for the controlled RAFT synthesised chains. This might be due to the spatial restriction of the long-grafted chains, along the new formed backbone, leading to a more confined solvated volume inside the GPC system. The experimental M_n was lower than the theoretical estimated M_n for RAFT polymerisations. Also, the M_n for the FRP reactions was significantly higher than the M_n for the RAFT polymerisations, which is evidence that the RAFT agent (CPAB) successfully controlled the radical polymerisation reaction, with good control over the final polymer molecular weight for both PEGMA-LA_{25} and HEMA-LA_{25}. Another indication for the successful control of CPAB is the data collected for the molecular weight dispersities, tabulated in Table 4.3. For the FRP reactions, values between 4.30-5.14 have been obtained, which are much higher when compared to the values gathered for the RAFT reactions, ranging from 1.30-1.40. This suggests that good control over the molecular weight dispersities has been achieved with the use of CPAB as the RAFT agent.

Considering the amphiphilic character of the grafted copolymers constructed from tandem polymerisation steps, the ability for these materials to self-assemble into nanoparticles was

investigated. It was envisaged that doing so will lead to medical and pharmaceutical applications. All the hybrid-polymers formulated into well-defined nanoparticles in an aqueous environment when following the same nanoprecipitation method, as used for the linear block copolymers, described previously. Both RAFT-PEGMA-LA_{25} and RAFT-HEMA-LA_{25} showed smaller nanoparticle sizes, 95 and 93 nm respectively, when compared to the two counterparts synthesised via FRP, 117 and 125 nm (Table 4.3). This observation might be suggesting an improved packing of the hydrophobic core when similar chain lengths are in contact during the nanoprecipitation process, as in the RAFT-products case. This could potentially lead to a lower degree of interaction between the grafted chains when compared to materials with a variety of different chain lengths, as in the case of FRP-synthesised polymers (Table 4.3). Furthermore, it is observed that the nanoparticle sizes formed using the grafted materials (ranging from 93-125 nm) were persistently larger than the NPs produced from the linear diblock and triblock copolymers (ranging from 40-80 nm), as shown in Table 4.3 and Table 4.2, respectively. This is usually the case when long side chains (in this case LA) are present in grafted polymer materials, resulting in higher steric hindrance, which causes a less efficient packing arrangement of the hydrophobic blocks.

As discussed previously in this chapter, the selected nano-formulation technique, in this case nanoprecipitation, can yield various nanoparticle structures influenced by several factors. According to the DLS results obtained, the grafted block copolymers synthesised in this study successfully formed nanoparticles with diameters ranging from 93 – 125 nm. These values are at the higher end of the typical range for polymeric micelles (10-100 nm) (Rapoport, 2007), which may indicate that the formulated material has an entirely different nanoparticle structure. DLS characterisation alone cannot verify what type of polymeric nanoparticles are constructed due to its limitations in structural characterisation. Consequently, the precise nature of the polymeric nanoparticles developed in this study remains undetermined. Future work should integrate DLS with additional characterisation methods, such as cryo-TEM or X-ray scattering, to lead to a conclusive identification of the specific type of polymeric nanoparticles formed.

The PDIs obtained for the grafted block copolymers are, in most cases, lower than the ones obtained for the linear block copolymers (BCPs), with values ranging from 0.080-0.140 (Table 4.3). This indicates a greater uniformity of the nanoparticle sizes for the grafted BCPs compared to the linear ones. The investigation of the self-assembly of biodegradable and biocompatible nanoparticles has been incorporated in Chapter 5 of this thesis to assess the

different possibilities and generate a better understanding on how different parameters affect the nanoparticle formulation efficiency and characteristics.

To examine the self-assembly of these types of hyper-branched materials and their shape in the dry state, a TEM characterisation of RAFT-PEGMA-LA_{25}, as an example, was performed by Kristoffer Kortsen from the School of Chemistry, at the University of Nottingham. The results show spherical particles, measuring between 41 and 59 nm (with an average of 50 ± 9 nm), confirming the nanoparticle characteristics (Figure A.1 in Appendix A.2). More details and results of this measurement are given in Appendix A.

Since the materials produced in this investigation are intended for pharmaceutical applications the *in vitro* cytotoxicity of the grafted copolymers was tested using the same procedure that was followed for the linear block copolymers. The initial cytocompatibility assessment of the synthesised branched block copolymers on three model cell lines was carried out by Dr. Robert Cavanagh from the School of Pharmacy, at the University of Nottingham.

The three model cell lines used in this case are Caco-2 (intestinal), Calu-3 (airway) and THP-1 (macrophage) cells. The cytocompatibility of the NPs was evaluated at a consistent and relatively high concentration of 500 μg/ml. Their toxicity effects were examined through monitoring the cell membrane integrity and cellular metabolic activity with the application of the lactate dehydrogenase (LDH) release assay and the PrestoBlue cell viability assay, respectively. All four grafted polymer nanoparticles demonstrated no cytotoxic effects in both assays conducted across all studied cell types, following the same trend observed by the results of the cell culture medium HBSS, used as a vehicle control (Figure B.2 in Appendix B.2). More information on the cytocompatibility tests and the results collected for the polymer materials produced in this work can be found in Appendix B.

4.4. Conclusions

The experimental investigation presented in this work focussed on minimising the health and safety implications related to the synthesis of polymeric excipients intended for biomedical and drug delivery applications. For this reason, the bio-based and non-toxic 2-methyltetrahydrofuran solvent has been employed as a multi-polymerisation solvent replacing the conventional petrochemical polymerisation solvents.

The use of 2-MeTHF as the polymerisation solvent created a greener synthesis pathway for polymeric vehicles based of LA and ε-CL, which are materials with high demand in the pharmaceutical field. It has been proved that 2-MeTHF is an effective reaction solvent for the ROP, eROP, FRP and RAFT polymerisations (separately or in tandem) of LA, ε-CL and their copolymers.

The sequential one-pot ROP of ε-CL and LA was successfully performed in the 2-MeTHF reaction solvent. A double catalyst system was used to overcome the challenges associated with the lipase and DBU catalyst limitations for the lactide and lactone ROP respectively. The chemistry of the final polymeric product of the sequential ROP can be adjusted to achieve adaptable physical properties and biodegradability.

To produce grafted amphiphilic block copolymers, first the hydrophilic HEMA and PEGMA methacrylate-ester ROP initiators were used to initiate the hydrophobic lactide monomer. In the reaction timeframe applied, no transesterification side reactions occurred with quantitative conversion of monomer to polymer for both initiators. The constructed lactide macromonomers were then examined in their ability to undergo FRP and RAFT tandem polymerisations at 65 ^{o}C as for the ROP step. Both radical polymerisations yielded grafted amphiphilic biodegradable block copolymers. Most of radical polymerisations have temperature requirements higher than room temperature to facilitate the radical initiation. The higher boiling point of 2-MeTHF has allowed its use in a wider range of polymerisation processes when compared to solvent-free conditions and the lower boiling point solvents of DCM and THF. 2-MeTHF is therefore suitable for ROP and radical polymerisation reactions due to its higher boiling point and the high solubility of all the starting materials.

All the constructed amphiphilic block copolymers, both linear and grafted, were able to self-assemble into nanoparticles by implementing the solvent displacement method without the use of stabilisers. Also, the cytocompatibility of materials intended for biomedical applications and formed hybrid-grafted materials with promising properties for utilisation as drug nanocarriers has been proved through cytotoxicity experiments on three model cell lines.

Finally, the preliminary trends established from the resulting nanoparticle sizes vs the polymer molecular weights raised great interest over the phenomena that take place during the

nanoprecipitation step. The kinetics and the processing conditions of this technique are further investigated and discussed in Chapter 5 of this thesis leading to a greater understanding of the nanoprecipitation procedure as a method to formulate polymeric nanoparticles for drug delivery applications.

5. Investigation of the self-assembly mechanism of polymeric nanoparticles and the effect of the formulation technique and parameters on the final product characteristics

5.1. Introduction

The desirable characteristics that a drug delivery system (DDS) of chemotherapy drugs should incorporate has been discussed in the literature review. The ideal DDS should prioritize biocompatibility and biodegradability, ensuring safety and compatibility with human tissue while allowing for natural decomposition and elimination within the body (Capasso Palmiero *et al.*, 2018). One of the primary goals of a DDS is to increase the bioavailability of chemotherapy drugs by improving their aqueous solubility and preventing recognition and removal by the reticuloendothelial system (RES), thereby enhancing the drug retention time in the body and particularly in the circulation system (Park *et al.*, 2008). An essential feature of the ideal DDS is high physical and chemical stability, ensuring robust and reliable delivery of chemotherapy drugs by tolerating mild thermal and chemical fluctuations to prevent decomposition before reaching the cancer target site or desired circulation time (Iqbal and Ahmad, 2018). An important aspect of the ideal DDS is cost-effectiveness, where the cost should justify the benefits of delivering anticancer drugs in the body while remaining within a reasonable range to facilitate widespread commercial application in the future.

The nanoparticles prepared from the self-assembly of amphiphilic block copolymers (BCPs) have the ability of addressing all the required characteristics of an effective DDS. Therefore, polymeric nanoparticles represent a highly promising option for serving as a secure and durable DDS for cancer chemotherapy medicines. Polymeric micelles are nano-scale structures formed through the self-assembly of amphiphilic block copolymers when present in aqueous environments. These are nanoparticles with a hydrophobic core and a hydrophilic corona and their size usually ranges from 10-100 nm (Park *et al.*, 2008). Depending on the amphiphilic block copolymer materials and the formulation method used to construct the polymeric nanoparticles, their stability, biocompatibility and biodegradability can be tailored (Ferrari *et al.*, 2013).

Polymeric nanoparticles can be constructed by employing a variety of different formulation techniques. Some of the commonly used methods for formulating BCPs into polymeric

nanoparticles include emulsion polymerisation (Colombo *et al.*, 2014), thin film hydration (Ho *et al.*, 2020) and the most applied technique in literature, the nanoprecipitation (or solvent displacement) method (Kakde *et al.*, 2016; Phan *et al.*, 2019; Englezou *et al.*, 2020). All these techniques are kinetic processes, meaning their procedures are primarily driven by kinetics rather than the thermodynamics of the system. These kinetic formulation techniques could result in the production of polymeric micelles that are kinetically trapped (otherwise known as kinetically frozen) (Almoustafa, Alshawsh and Chik, 2017). This phenomenon was also discussed in Chapter 4 based on the observations emerged from the results obtained when the nanoprecipitation technique was applied. The term kinetically trapped is used when the kinetics and dynamics of the self-assembly processes are so fast that the system does not have enough time to conform into a structure that is under thermodynamic equilibrium. This leads to the formation of a kinetically trapped micellar structure, where there is no distinct interface between the two blocks of the polymer (hydrophilic and hydrophobic blocks) since some of the polymer hydrophilic chains could be kinetically trapped inside the nanoparticle core (hydrophobic region) (Zhu, 2013).

The research investigation followed in this chapter applies the traditional nanoprecipitation process examining its different formulation parameters. The effect of the variation of the processing conditions on the final constructed polymeric nanoparticles is tested. In addition, a slow self-assembly process with a controlled transition from the good solvent for both blocks to the selective solvent for one of the polymer blocks is employed to monitor the nanoparticle formulation process. This is explored both as a stepwise process and as a single-step process. By comparing the final polymeric products prepared by applying the different formulation methodologies, the system that would serve as a more ideal DDS for cancer chemotherapy is determined.

5.1.1. Aim

The main goal of this investigation is to gain a greater understanding of the self-assembly mechanism of amphiphilic block copolymers into polymeric nanoparticles and more specifically the diblock copolymers of methyl-poly(ethylene glycol)-*block*-poly(lactide) (mPEG-PLA), by employing different formulation techniques and varying the formulation parameters to examine their effect on the final product characteristics.

5.1.2. Objectives

The objectives of this research include the synthesis and characterisation of a library of mPEG-PLA diblock copolymers with different mPEG and PLA block lengths, to investigate the effect of the hydrophobic block, the hydrophilic block and the total polymer molecular weight on the nanoparticle suspension. Subsequently, the employment of different formulation techniques, such as the conventional nanoprecipitation method, the stepwise slow self-assembly and the single-step slow self-assembly method is performed. Moreover, the effects of different formulation parameters, namely the rate of addition of the anti-solvent (selective solvent of one block), rate of addition of the good (for both blocks) solvent, the good solvent quality, the concentration of final block copolymer in suspension, the hydrophobic (LA) and hydrophilic (mPEG) block lengths on the final nanoparticle suspension properties are examined. Finally, the experimental results obtained from the different formulation techniques and parameters employed are compared to evaluate which method is more appropriate for the formulation of the ideal nanoparticle DDS required for cancer chemotherapy.

5.2. Nanoparticle formulation methodology

5.2.1. Research investigation overview

An overview of the experimental methodology procedures performed in the research investigation of this chapter is presented in Figure 5.1. The different procedures included in the boxes of Figure 5.1 are in line with the objectives mentioned in section 5.1.2. Detailed descriptions of the different procedures and information on the processing conditions applied and the parameters examined are presented in the following sections. Moreover, details about the characterisation techniques employed in this research investigation to analyse the different materials constructed are included in section 5.2.5.

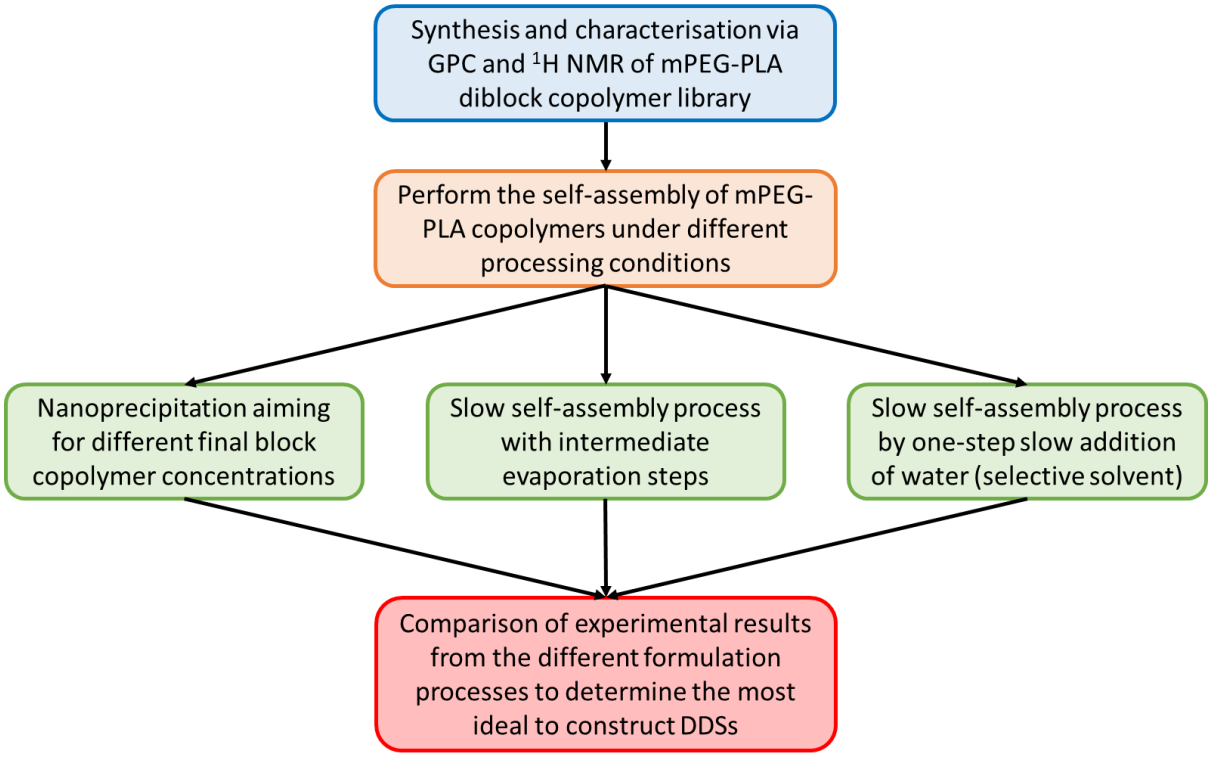

Figure 5.1: Summary of the experimental procedures completed in this research investigation.

5.2.2. Polymer material

For this investigation, six linear amphiphilic diblock copolymers with a PEG hydrophilic block and a PLA hydrophobic block were synthesised in total. Synthesis details of the diblock copolymers produced for this research investigation are summarised in Table 5.1.

Table 5.1: Summary of the six amphiphilic diblock copolymers constructed.

Polymer	**Initiator**	**Monomer**	**Catalyst**	**M/I mass ratio***	**Architecture**
mPEG5k-*b*-PLA5k	$mPEG_{5000}$	lactide	DBU	1	linear
mPEG5k-*b*-PLA10k	$mPEG_{5000}$	lactide	DBU	2	linear
mPEG5k-*b*-PLA20k	$mPEG_{5000}$	lactide	DBU	4	linear
mPEG2k-*b*-PLA2k	$mPEG_{2000}$	lactide	DBU	1	linear
mPEG2k-*b*-PLA4k	$mPEG_{2000}$	lactide	DBU	2	linear
mPEG2k-*b*-PLA8k	$mPEG_{2000}$	lactide	DBU	4	linear

*M/I is the monomer to initiator mass ratio applied for the synthesis of each polymer.

The polymer library of this study consists of six diblock copolymers of a poly(ethylene) glycol methyl ether block and a poly(lactide) block (details of materials used are given in Chapter 3). Hydrophilic methyl-poly(ethylene) glycol of two different molecular weights, 5000 and 2000 Da ($mPEG_{5000}$ and $mPEG_{2000}$), was applied as the macroinitiator of the ring opening polymerisation (ROP) reaction of lactide (LA). For each mPEG macroinitiator, three different monomer-to-initiator mass ratios (1, 2 and 4) were used to produce the final polymers. The use of the two different mPEG molecular weights and the three M/I mass ratios were applied to construct a polymer library with varying hydrophilic and hydrophobic block lengths. This would allow the investigation and comparison of the self-assembly mechanism of polymeric materials with a different hydrophobic/hydrophilic balance and with a range of PEG block, PLA block and total molecular weights. The ROP of all the polymers was performed by using the metal-free organic catalyst of DBU, which is considered to be one of the best catalysts for the ROP of aliphatic polyesters as discussed in the literature review in Chapter 2. All the resulting polymers have a linear molecular structure.

5.2.3. Polymerisation procedure

The reaction scheme of the general polymerisation reaction applied for the synthesis of all the amphiphilic diblock copolymers summarised in Table 5.1 is presented in Figure 5.2.

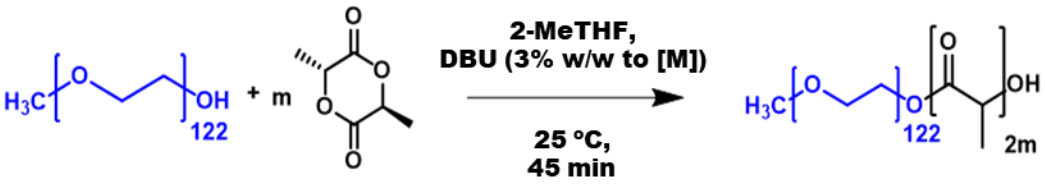

Figure 5.2: Reaction scheme of the general DBU-catalysed ROP applied for the synthesis of the mPEG-initiated lactide diblock copolymers presented in this chapter.

The detailed procedure followed in this investigation for the synthesis of the mPEG-PLA diblock copolymers is described as follows. The specified quantity of lactide monomer (2000 mg) and initiator ($mPEG_{5000}$ or $mPEG_{2000}$) were measured and placed into a 20 ml glass vial containing a magnetic stir bar. This vial had been previously cleaned and dried in an oven at 100 °C overnight. The amounts of LA and mPEG initiator were determined based on the

desired M:I mass ratios. As an example, for the synthesis of mPEG5k-*b*-PLA5k (1:1 M:I mass ratio), 2000 mg of LA and 2000 mg of $mPEG_{5000}$ were weighed and added in a vial with 2-MeTHF. The glass vial was capped with a rubber septum, placed on a magnetic stirring plate and stirred at room temperature (25 ºC) until the monomer and initiator were fully dissolved. Then, the chosen catalyst (DBU) was added to the solution at 3% w/w to start the ROP reaction of lactide at room temperature. The reaction was terminated after 45 min by precipitating the reaction mixture in a hexane and diethyl ether solution. A total of three precipitation steps were followed to purify the final synthesised polymer. The purified polymer was placed in a vacuum oven to fully dry. The same polymerisation procedure was followed to produce all six amphiphilic diblock copolymers of mPEG-PLA studied in this investigation by varying only the initiator used ($mPEG_{5000}$ or $mPEG_{2000}$) and the monomer-to-initiator mass ratio (1:1, 2:1 and 4:1).

All six synthesised diblock copolymers were analysed and characterised according to the characterisation techniques outlined in section 3.6.1. The ^{1}H Nuclear magnetic resonance spectroscopy (^{1}H NMR) spectra of the initial (before polymerisation) reaction mixture and the final dry polymer product were used to determine the conversion of the monomer to polymer, the degree of polymerisation (DP_n) and the final polymer total number average molecular weight (M_n) based on their chemical shifts. Also, the total number average molecular weight (M_n) of the final polymer and the molecular weight dispersity (Đ) were measured with Gel permeation chromatography (GPC).

5.2.4. BCP self-assembly procedures

Three different self-assembly methodologies have been applied in this research investigation. The commonly used nanoprecipitation process, and two slow formulation procedures were performed. The two latter processes include the stepwise and the single-step slow self-assembly of polymeric micelles through the controlled transition between the chosen solvent and anti-solvent.

5.2.4.1. Nanoprecipitation technique

5.2.4.1.1 Detailed procedure

For the nanoprecipitation experiments a similar procedure was followed as in Chapter 4. Here, acetonitrile or acetone were applied to serve as the good solvents (oil phase), while distilled water (Stuart Distinction D4000 water still) acts as the anti-solvent (aqueous phase). The amphiphilic diblock copolymers undergo self-assembly, resulting in the formation of nanoparticle suspension via solvent exchange from the oil to the aqueous phase following a kinetically driven process.

More specifically, the necessary amount of polymer was measured and introduced into the appropriate volume of acetonitrile within a glass vial. During all the nanoprecipitation experiments, the concentration of polymer in acetonitrile (initial concentration) was maintained at 15 mg/ml. This was decided in order to ensure a constant concentration driving force at the start of the nanoprecipitation process across all polymer materials and processing conditions employed. The polymer fully dissolved in acetonitrile to ensure uniformity in solution. The appropriate volume of distilled water for nanoprecipitation was added to a new, clean glass vial containing a magnetic stirrer bar. The amount of distilled water needed was determined by the desired final concentration of polymer in water when formulated into a nanoparticle suspension. The vial containing distilled water was positioned on a stirrer plate (MR Hei-Tec magnetic stirring hotplate, Heidolph Instruments GmbH & CO. KG) within a fume cupboard at room temperature (~25°C). Subsequently, the initial polymer solution in acetonitrile was added dropwise to the distilled water vial either by hand or by a syringe pump (PHD ULTRA™, Harvard Apparatus), while under constant stirring. Following the complete addition of the initial polymer solution to the distilled water, the acetonitrile-water-polymer mixture was left uncovered in the fume cupboard at room temperature overnight. This duration allowed for the full evaporation of acetonitrile from the suspension and ensured the completion of the solvent displacement procedure.

A schematic diagram showing the experimental set up applied in this case for the nanoprecipitation process completed either with a syringe pump or by hand is shown in Figure 5.3.

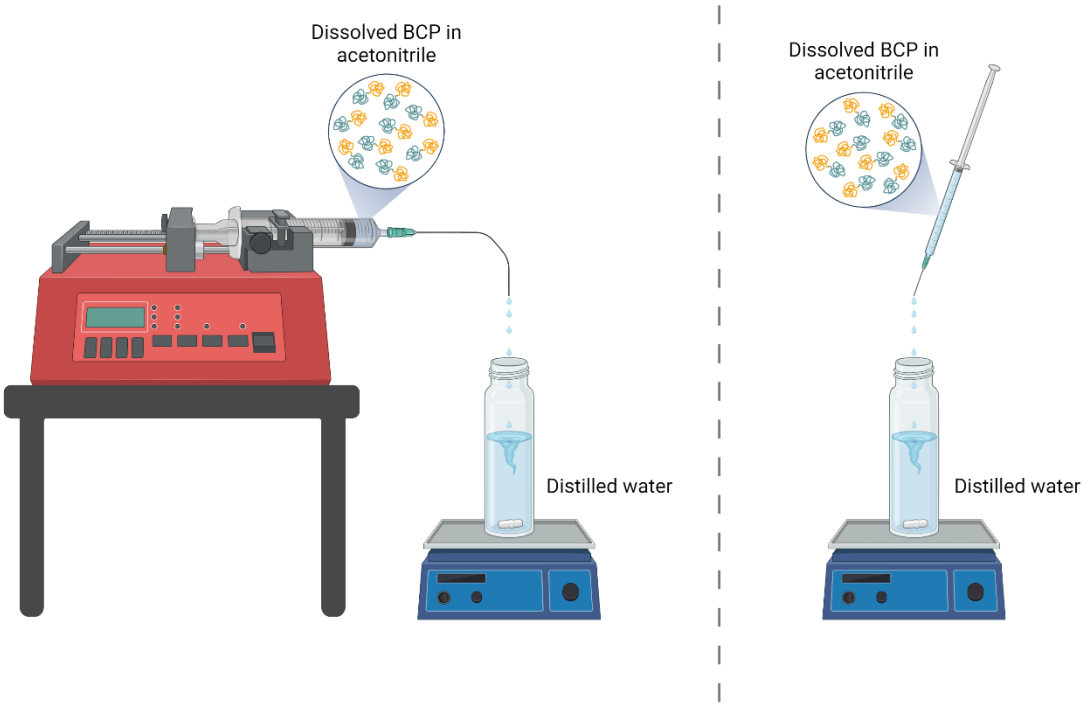

Figure 5.3: Schematic representation of experimental set-up employed for the nanoprecipitation procedure either by syringe pump (**left**) or by hand (**right**).

5.2.4.1.2 Processing parameters

The effect of processing parameters on the final nanoparticle suspension, such as the final BCP concentration in the final nanoparticle suspension formed, the rate of addition of the BCP-acetonitrile solution in the anti-solvent (water) and the solvent quality of the good solvent for both blocks of the BCPs, were examined.

The final BCP concentration in nanoparticle suspension was varied from 0.025-0.25wt%. This wide range of concentrations was employed to examine whether the nanoprecipitation technique is successful in formulating nanoparticle suspensions from very low concentration to relatively high concentration of polymers.

The rate of addition of the BCP-acetonitrile solution into distilled water was varied from 1-6 ml/min using a syringe pump. This was also compared to the estimated rate of approximately 30 ml/min achieved when the solution was nanoprecipitated by hand. The effect of the rate of addition of the BCP solution on the final particle size distribution (PSD) of the nanoparticle suspension was examined.

For the investigation of the good solvent quality both the polar solvent of acetonitrile, which is primarily used in this investigation, and the volatile solvent of acetone, which was used during the nanoprecipitation procedure in Chapter 4, were employed. The effect of the different solvent properties on the nanoparticle suspension was explored.

A summary of the different nanoprecipitation experiments performed for all the six diblock copolymers of mPEG-PLA synthesised in this research investigation (section 5.2.2) and the different processing parameters varied to assess their effect on the formulated nanoparticle suspension are presented in Table 5.2.

Table 5.2: Summary of performed nanoprecipitation experiments and varied processing parameters.

Nanoprecipitation processing parameters		
Good solvent	**Rate of addition (ml/min)**	**Final BCP concentration (wt%)**
Acetonitrile	30	0.025
Acetonitrile	30	0.05
Acetonitrile	30	0.1
Acetonitrile	30	0.15
Acetonitrile	30	0.25
Acetonitrile	6	0.1
Acetonitrile	2	0.1
Acetonitrile	1	0.1
Acetone	30	0.1

5.2.4.2. Stepwise slow self-assembly

For the two designed procedures, the aim was to create a slower self-assembly process when compared to the nanoprecipitation technique. This was performed by reducing the mixing rate of the solvent and anti-solvent during the formulation process, through the reduction of the stirring rate and rate of anti-solvent addition.

In the stepwise slow self-assembly, the slow transition between the good solvent for the two blocks of the BCP and the selective solvent for one of the blocks was performed in a controlled manner. The transition was monitored to gain a better understanding of the self-assembly

procedure. In particular, a very slow dilution process of the BCP-acetonitrile solution with distilled water was performed followed by an evaporation step. In total, 10 of these dilution-evaporation steps were applied to reach different solvent volume percentages of acetonitrile and water (see Table 5.3).

Table 5.3: Volume percentage of water and acetonitrile in each of the dilution-evaporation steps of the stepwise slow self-assembly process.

Dilution-evaporation step	**Volume percentage of material in solvent system (vol%)**	
	Water	**Acetonitrile**
Initial solution	0	100
1	10	90
2	20	80
3	30	70
4	40	60
5	50	50
6	60	40
7	70	30
8	80	20
9	90	10
10	100	0

The distilled water dilution of each of the dilution-evaporation steps was performed by employing a syringe pump at a constant flowrate of 0.04 ml/min. During this process, the BCP solution was under constant stirring at 100 rpm on a magnetic stirring plate placed in a fume cupboard. The dilution process was completed at room temperature (25 ºC). A schematic diagram showing the experimental set up applied in this case for the water dilution step of the stepwise slow self-assembly process is presented in Figure 5.4. The evaporation step was conducted under constant stirring on a magnetic stirring plate in a fume cupboard and at room temperature. The same process was followed for all 10 dilution-evaporation steps. The BCP-acetonitrile-water mixture was monitored in-between all the performed dilution-evaporation steps using Dynamic light scattering (DLS) to investigate when nanoparticles forms and how the PSD varies with increasing water content in the solvent system.

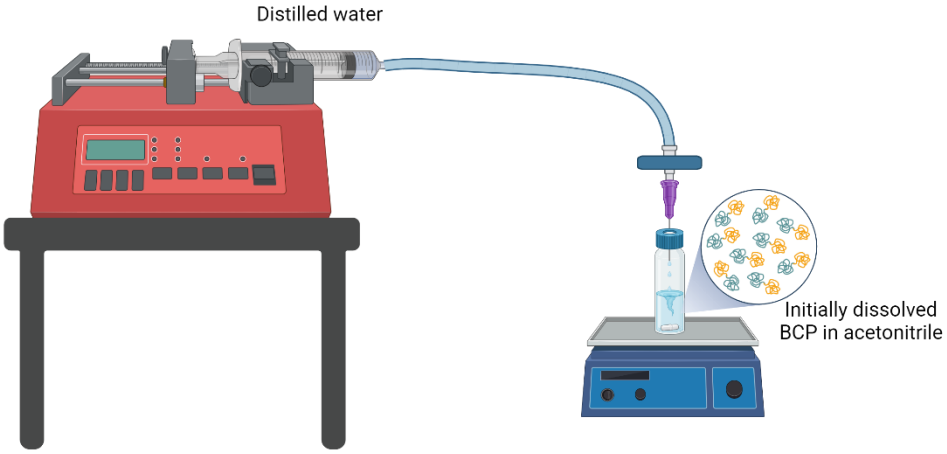

Figure 5.4: Schematic diagram presenting the experimental set up applied for the slow self-assembly procedure of the synthesised diblock copolymers.

The concentration of the BCP in solution was kept constant for the different dilution-evaporation steps to eliminate the effects of varied BCP solution concentration on the procedure. Two BCP concentrations in solution were investigated, 1.25wt% and 0.1wt%. Since this procedure is extremely time consuming, as a proof of concept, only one of the synthesised BCPs (mPEG5k-*b*-PLA5k) was used to perform this formulation technique and assess its feasibility for the production of an ideal DDS.

In the stepwise slow self-assembly process, the rate of mixing of water and acetonitrile, in terms of the rate of anti-solvent addition and the solution stirring speed, is significantly reduced when compared to the conditions used during the nanoprecipitation method.

5.2.4.3. Single-step slow self-assembly

Based on the observations and results gathered from the application of the stepwise slow self-assembly process, the single-step slow self-assembly procedure was developed. This formulation procedure is considered to be in-between the nanoprecipitation and the stepwise slow self-assembly processes. This is based on the processing conditions applied when performing this nanoparticle formulation technique.

As already discussed, the stepwise slow self-assembly process (presented in section 5.2.4.2) was mainly used to gain a greater understanding of the self-assembly process of diblock

copolymers. However, it is an extremely time consuming procedure. Therefore, an alternative process that would reduce the processing time is required. This is the rationale behind the development of the single-step slow self-assembly process.

This nanoparticle formulation procedure is essentially a single-step process of the stepwise slow self-assembly process presented in section 5.2.4.2 with the application of some of the processing conditions used during the nanoprecipitation technique presented in section 5.2.4.1. Here, the distilled water dilution of the BCP-acetonitrile solution was carried out in one single-step followed by one full acetonitrile evaporation step, in contrast to the 10 dilution-evaporation steps performed in the stepwise slow self-assembly process. The initial concentration of the BCP in acetonitrile solution was 15 mg/ml, as in the nanoprecipitation technique. The volume of distilled water used was based on the desired final concentration of polymer in water.

The distilled water dilution was performed by employing a syringe pump at a constant flowrate of 0.04 ml/min; the same as the stepwise slow self-assembly process. During this process the BCP solution was under constant stirring at 250 rpm on a magnetic stirring plate placed in a fume cupboard to ensure good mixing between water and acetonitrile. The dilution process was completed at room temperature (25 ºC). The experimental set up used to perform the single-step water dilution process is the same as the stepwise process, presented in Figure 5.4.

The evaporation single-step was conducted under constant stirring on a magnetic stirring plate in a fume cupboard and at room temperature of 25 ºC, as in the nanoprecipitation process.

In the single-step slow self-assembly process employed, the rate of mixing of water and acetonitrile, in terms of the rate of solvent addition and the solution stirring speed, was reduced when compared to the conditions used during the nanoprecipitation method and increased compared to the conditions used during the stepwise self-assembly process. This nanoparticle preparation technique is regarded as an intermediate approach, in terms of rate of mixing of solvent and anti-solvent, between nanoprecipitation and stepwise slow self-assembly processes, as it combines processing conditions from both methods.

5.2.5. Characterisation analysis techniques

In this section, the characterisation techniques performed to analyse the materials produced during the different self-assembly procedures are summarised. Further details about the characterisation techniques, the equipment utilised to perform these analyses and the measurement procedures can be found in Chapter 3.

Nuclear magnetic resonance spectroscopy (NMR): The conversion of monomers to polymers, the degree of polymerisation (DP_n) of each reaction and the molecular weight of the final polymer product were determined using ^1H nuclear magnetic resonance spectroscopy (^1H NMR). $CDCl_3$ (deuterated chloroform) was used as the common deuterated solvent and all samples were analysed using a Bruker DPX 400 MHz spectrometer operating at 400 MHz (^1H). Chemical shifts were assigned in parts per million (ppm). MestReNova 6.0.2 copyright 2009 was used for analysing the spectra.

Gel permeation chromatography (GPC): The GPC was performed with the help of Agilent 1260 Infinity Series HPLC. Two Agilent PL-gel mixed-D columns were used in series to form the porous gel matrix. The mobile phase flow rate was 1 ml/min. A differential refractometer (DRI) was used as the sample detector for the elution of molecules from the column. The GPC system was calibrated using poly(methyl methacrylate) (PMMA) standards prior to measurement.

Dynamic light scattering (DLS): This characterisation technique was used to establish information about the nanoparticle size distribution and the polydispersity index (PDI) of the nanoparticle population present in the samples. The DLS equipment of Brookhaven ZetaPALS (2008) was used. All the measurements were completed at room temperature (25 ºC). The samples were equilibrated at 25 ºC in the equipment cuvette chamber prior to measurement. Each measurement consisted of 5 runs of the same sample.

Zeta potential (Z-potential) analysis: The zeta potential (ζ) of the colloidal suspensions prepared was measured using a Brookhaven ZetaPALS Zeta Potential Analyser (2008). The measurements were completed at room temperature (25 ºC). The samples were equilibrated at the measurement temperature in the equipment cuvette chamber prior to measurement. Each measurement consisted of 5 runs of the same sample.

5.3. Results and discussion

5.3.1. Synthesised polymer characterisation

The results obtained from the chemical characterisation techniques (^{1}H NMR and GPC) employed for analysing the properties of the synthesised diblock copolymers of mPEG-PLA are summarised in Table 5.4.

Table 5.4: Chemical characterisation results for all the synthesised polymers.

Polymer	Conversion (%)[a]	Total molecular weight (M_n) (^{1}H NMR) [kDa][b]	Total molecular weight (M_n) (GPC) [kDa][c]	$Đ_M$
mPEG5k-*b*-PLA5k	97.8	9.89	12.24	1.14
mPEG5k-*b*-PLA10k	98.0	14.80	14.24	1.18
mPEG5k-*b*-PLA20k	98.1	24.62	16.22	1.32
mPEG2k-*b*-PLA2k	97.9	3.96	6.03	1.21
mPEG2k-*b*-PLA4k	98.5	5.94	7.67	1.20
mPEG2k-*b*-PLA8k	98.5	9.88	10.93	1.30

[a]Calculated by ^{1}H NMR.
[b]Calculated from C*H*$_2$ mPEG-initiator backbone peak and C*H* PDLLA peaks ^{1}H NMR integration.
[c]Compared to PMMA standards.

The M/I mass ratio applied for the synthesis of the mPEG-PLA diblock copolymers also represents the hydrophobic-to-hydrophilic mass ratio of the final polymer material. This is an indication on the hydrophobicity and the hydrophilicity of the amphiphilic diblock copolymers produced. The higher the value of this ratio, the higher is the hydrophobic nature of the polymer material. Another indication of the hydrophobic and hydrophilic nature of the amphiphilic diblock copolymers synthesised is the volume fraction of block A (f_A), which represents the volume fraction of the mPEG block, and therefore the hydrophilic section, of the final polymer material.

The degree of polymerization (DP_n), the conversion of lactide monomers to polymers and the total molecular weight achieved by the diblock copolymers synthesis was determined by performing the ^{1}H NMR analysis. Initially, the ^{1}H NMR spectra of the reaction mixture in 2-MeTHF were examined before adding the DBU catalyst, marking the pre-polymerization phase. This was then compared with the ^{1}H NMR spectra established for the final purified diblock

copolymers to assess the DP_n, the monomer lactide conversion into polymer, and to compute the final polymer molecular weight. The ^{1}H NMR spectra collected before the reaction and for the final purified polymer, were analysed based on the same methodology followed and discussed in Chapter 3 and Chapter 4.

As seen from Table 5.4, high conversions of the lactide monomers into polymers were established with all the diblock copolymers achieving a conversion of 97.8% and higher. The degree of polymerisation (DP_n) was calculated as 34, 68 and 136 LA units for mPEG5k-*b*-PLA5k, mPEG5k-*b*-PLA10k and mPEG5k-*b*-PLA20k, respectively. These were in agreement with the calculated theoretical polymerisation index (35, 69 and 139, respectively) targeted for the synthesised polymers. The DP_n established for mPEG2k-*b*-PLA2k, mPEG2k-*b*-PLA4k and mPEG2k-*b*-PLA8k is 14, 27 and 55 LA repeating monomers. These are also consistent with the desired theoretical polymerisation index of 14, 28 and 56 LA repeating units, respectively. All the calculated total polymer molecular weights from ^{1}H NMR spectra analysis and integration are presented for each of the synthesised polymeric materials in Table 5.4.

Gel permeation chromatography was also performed for the characterisation of the synthesised diblock copolymer of mPEG-PLA to establish information on the total molecular weight of the polymers and the polydispersity of the measured molecular weights for each of the samples. The results obtained from the GPC measurements and analysis presented a monomodal GPC trace for all the produced polymers. The GPC measured total polymer molecular weights are summarised in Table 5.4 for each of the produced polymers. As seen in Table 5.4, all polymer materials synthesised in this research investigation are characterised by a narrow molecular weight dispersity ($Đ_M$). The GPC analysis revealed dispersity values of 1.32 and lower for all the polymers. Such low polydispersity values for this type of ring opening polymerisation (ROP) synthesis performed here demonstrate a controlled molecular weight distribution in the final polymer products.

From the data shown in Table 5.4, some discrepancies can be observed between the molecular weight values measured from GPC and established by the ^{1}H NMR spectra integration. These differences are probably caused from the significant chemical differences between the PMMA standards, which were applied for the calibration of the GPC equipment, and the synthesised amphiphilic diblock copolymers. This finding has been previously reported in the literature (Al-Natour *et al.*, 2020) and is also reflected in the results presented in Chapter 4. As discussed

in Chapter 4, the possible reason behind these discrepancies could be the diverse interaction between the polymers and the chromatography column and the differences in solvated volumes.

5.3.2. Nanoprecipitation technique

All the amphiphilic diblock copolymers of mPEG-PLA synthesised in this research investigation were successfully formulated into nanoparticles by applying the nanoprecipitation (solvent displacement) method described in section 5.2.4.1. The effects that the properties of the six different diblock copolymers have on the final constructed nanoparticle formulation were investigated. Moreover, the variation of nanoprecipitation processing conditions, such as the final BCP concentration in suspension, the rate of addition of the oil phase (polymer-acetonitrile solution) into the aqueous phase (distilled water) and the solvent used for the oil phase, was performed to determine their influence on the final nanoparticle suspension. The varied nanoprecipitation processing conditions are summarised in Table 5.2.

5.3.2.1. Diblock copolymer properties influence

All the synthesised diblock copolymers were able to formulate polymeric nanoparticles using the nanoprecipitation technique, confirming their amphiphilic nature and their ability to self-assemble when present in aqueous environments. The six polymer materials produced in this investigation have very distinct properties (see Table 5.4), which can be used for comparisons and lead to an understanding of their influence in the nanoparticle formulation characteristics. The diblock copolymer properties examined here for their influence on the final nanoparticle size include the total molecular weight of the polymer, the molecular weight of each of the blocks comprising the polymer (mPEG and PLA), the hydrophobic to hydrophilic ratio of each of the polymers, the degree of polymerisation (DP_n) and the volume fraction of each of the two blocks in the final diblock copolymers formed.

The mean diameter (measured by DLS) of the nanoparticle suspension formed by nanoprecipitation of all the produced diblock copolymers are plotted in Figure 5.5 as a function of the GPC measured total polymer molecular weight (Table 5.4).

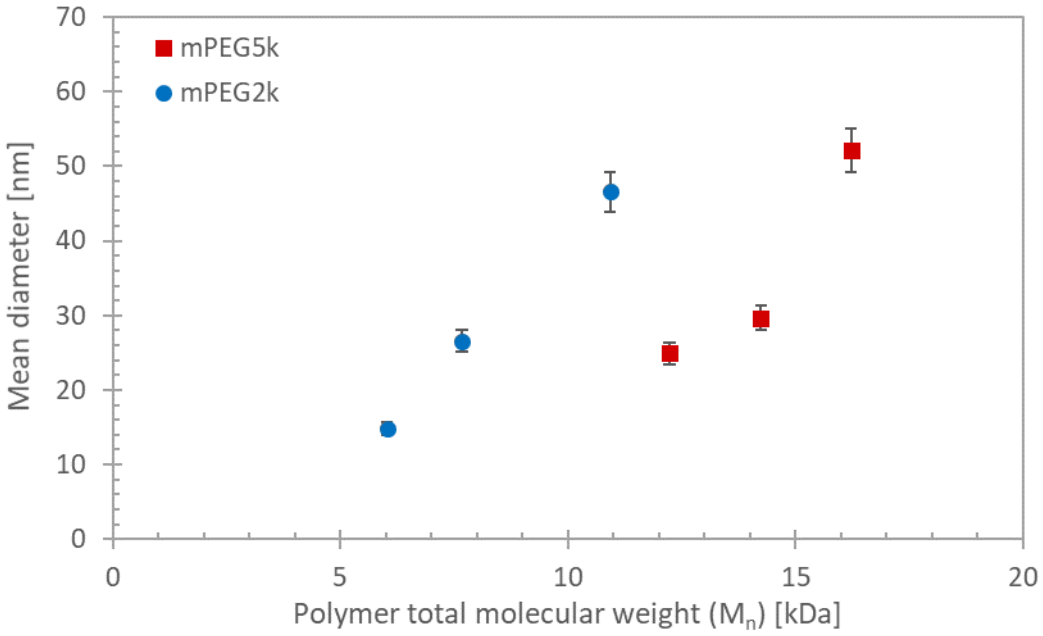

Figure 5.5: Plot of the nanoparticle mean diameter results obtained via DLS for all the synthesised diblock copolymers versus the polymer total M_n measured via GPC. The blue circle data points are for the diblock copolymers having a mPEG2k hydrophilic block and the red square data points are for the polymers with a mPEG5k hydrophilic block. Data presented are the mean values of three independent experiments and the error bars are the standard error.

From the plotted data in Figure 5.5, it is observed that the mean diameter of the nanoparticle suspension formed through nanoprecipitation is increasing with the increasing total molecular weight of polymer. In addition, for the mPEG2k block copolymers it is observed that the increase from the polymer at 7.5 kDa to the polymer at 11 kDa is bigger than the increase observed between the 6 to 7.5 kDa. The same trend is followed for the mPEG5k block copolymers. These trends are easily observed due to the separation of the two datasets (mPEG2k and mPEG5k). If the datasets are combined, then these observations would not be entirely true due to the result obtained for the mPEG2k-*b*-PLA8k polymer, which is significantly higher than the mean diameter measured for the mPEG5k-*b*-PLA5k. Therefore, it is clear from the relationships seen here, that there is a general trend between the total molecular weight of the diblock copolymer and the final nanoparticle size. Although, the trends observed from the results lead also to the assumption that there is influence on the final nanoparticle size from other properties of the amphiphilic block copolymer used for the nanoparticle formulation.

The same results were plotted as function of the molecular weight of the mPEG block of each of the diblock copolymers and are presented in Figure 5.6.

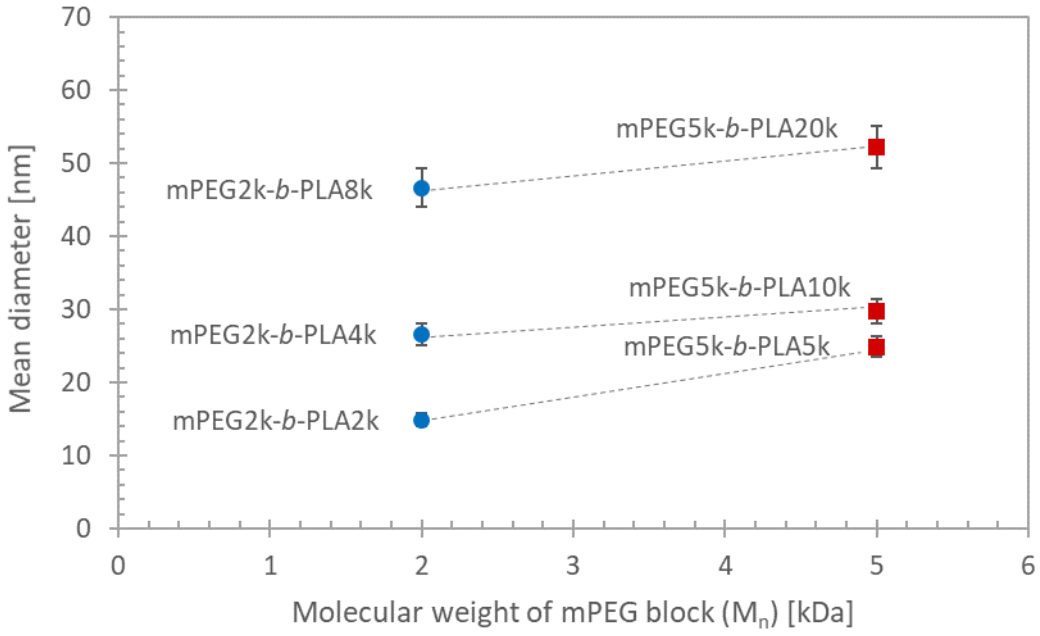

Figure 5.6: Plot of the nanoparticle mean diameter results obtained via DLS for all the synthesised diblock copolymers versus the molecular weight of the mPEG block of the synthesised polymers. The blue circle data points are for the diblock copolymers having a mPEG2k hydrophilic block and the red square data points are for the polymers with a mPEG5k hydrophilic block. Each of the polymer labels is position next to their corresponding data point. Data presented are the mean values of three independent experiments and the error bars are the standard error.

The corresponding diblock copolymers (based on the hydrophobic to hydrophilic block ratio) between the mPEG2k and mPEG5k batch are connected in Figure 5.6 using a dotted line. This is used to illustrate what is the trajectory followed between polymers, when the length of their hydrophilic (mPEG) block is increasing by eliminating the effect of the hydrophobic (PLA) block on the mean nanoparticle size. This is achieved by comparing diblock copolymers that have the same hydrophobic to hydrophilic block ratios.

As it can be seen from the plotted data in Figure 5.6, the mean diameter of the formed nanoparticles increases when the molecular weight of the hydrophilic block (mPEG) of the diblock copolymer is increasing too. This observation is true for all the hydrophobic to hydrophilic ratios established in this study. The other important observation noted from Figure 5.6 is that the mean diameter data established for the same mPEG block lengths are increasing with increasing hydrophobic to hydrophilic ratio and increasing hydrophobic (PLA) block length.

To investigate further the trend between the hydrophobic block molecular weight and the nanoparticle mean size, the mean diameter results shown in Figure 5.6 are plotted as a function of the molecular weight of the PLA block of each of the diblock copolymers and are shown in Figure 5.7.

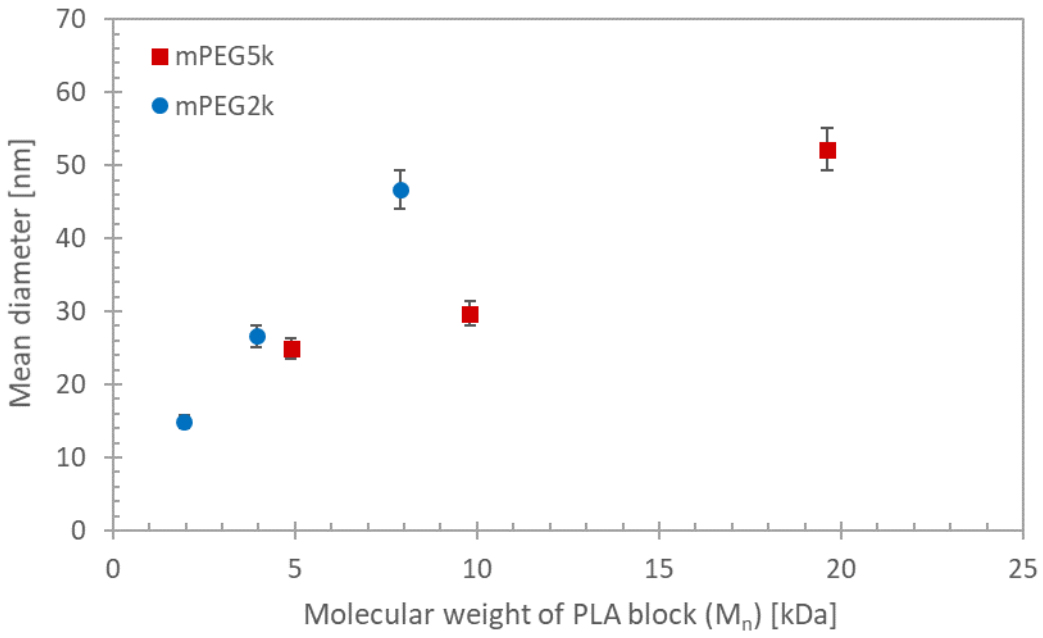

Figure 5.7: Plot of the nanoparticle mean diameter results obtained via DLS for all the synthesised diblock copolymers versus the molecular weight of the PLA block of the synthesised polymers. The blue circle data points are for the diblock copolymers having a mPEG2k hydrophilic block and the red square data points are for the polymers with a mPEG5k hydrophilic block. Data presented are the mean values of three independent experiments and the error bars are the standard error.

The trends followed by the nanoparticle sizes and in general the appearance of the graph when the degree of polymerisation (DP_n) is plotted as a function of the measured mean diameter, looks similar to Figure 5.7. This is because the DP_n is essentially the number of repeating monomer units forming a polymer and in this case that would be the number of lactide repeating units in the final diblock copolymer products. Therefore, DP_n is another way of quantifying the amount of LA in the polymer, as the molecular weight of the PLA block. Thus, DP_n would have an analogous appearance and the data would follow same trends with the PLA molecular weight graphs when plotted with the measured mean diameter of the nanoparticles.

As seen from Figure 5.7, the mean diameter measured by DLS is increasing with increasing molecular weight of the PLA block of the diblock copolymers. The same trend that is observed in Figure 5.5, where the increase between the middle mean diameter points and the highest

diameter data point (for both the mPEG2k and mPEG5k datasets) is bigger when compared to the increase between the low and the middle mean diameter data points, is also detected in Figure 5.7. This is in agreement with the molecular PLA block lengths, where the gaps between the middle and the highest block lengths are larger compared to the molecular weight gaps between the lowest and middle block lengths for both the mPEG2k and mPEG5k datasets. As seen in Figure 5.5, if the two datasets (mPEG2k and mPEG5k) were combined in Figure 5.7 the trends between the molecular weight of the hydrophobic block and the mean diameter would be harder to distinguish based on the data point cross between the mPEG2k-*b*-PLA8k and the mPEG5k-*b*-PLA5k polymers.

The effect of the hydrophobic to hydrophilic ratio of each of the synthesised diblock copolymers on the final nanoparticle size established from DLS was investigated and the results obtained are shown in Figure 5.8.

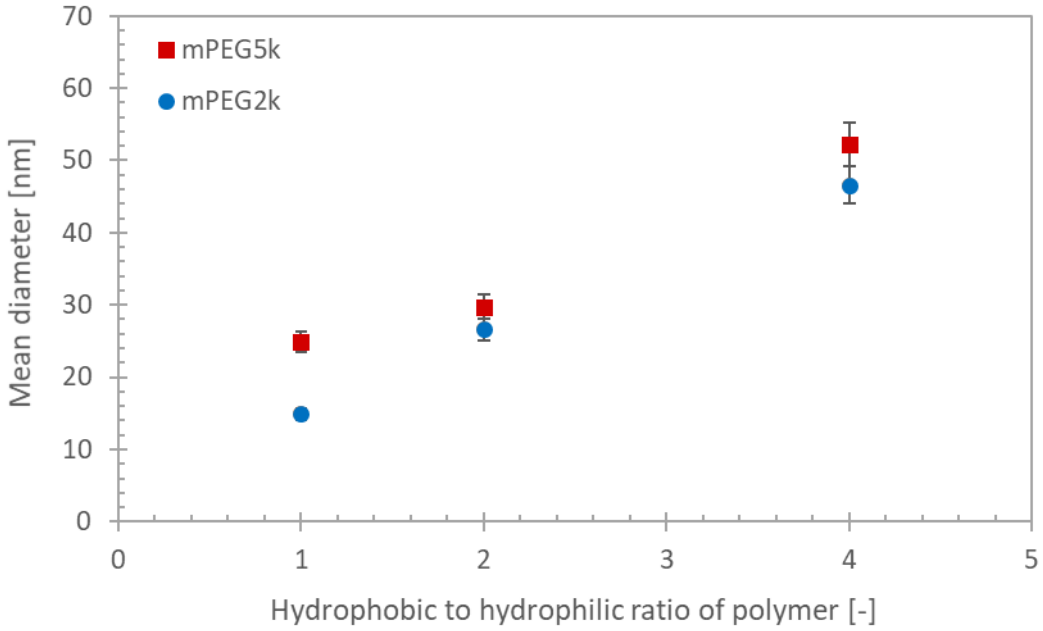

Figure 5.8: Plot of the nanoparticle mean diameter results obtained via DLS for all the synthesised diblock copolymers versus the hydrophobic to hydrophilic ratio of the synthesised polymers. The blue circle data points are for the diblock copolymers having a mPEG2k hydrophilic block and the red square data points are for the polymers with a mPEG5k hydrophilic block. Data presented are the mean values of three independent experiments and the error bars are the standard error.

The hydrophobic to hydrophilic ratio is again another method for quantifying the amount of hydrophobic PLA in the final polymer product. In this case, this quantification is normalised by the amount of hydrophilic mPEG present in the polymer. Therefore, it is expected that the

mean diameter of the nanoparticle suspension measured by DLS is going to be increasing with the increasing hydrophobic to hydrophilic ratio of the diblock copolymers examined, as seen for previous methods of quantification of the hydrophobic PLA block (PLA molecular weight and DP_n). As expected, in Figure 5.8 the mean diameter increases with the increasing hydrophobic to hydrophilic ratio of the polymers. It is also interesting to note that the mPEG5k polymers have consistently higher mean diameters compared to the mPEG2k polymers. This clearly demonstrates the effect of the hydrophilic block on the mean diameter, where higher molecular weights of hydrophilic block increase the nanoparticle size (as observed in Figure 5.6). Figure 5.8 also displays the rise of the nanoparticle dimensions when the overall molecular weight of the polymer is higher.

The influence of the hydrophilic (f_A) and hydrophobic (f_B) volume fractions in the amphiphilic polymer on the mean diameter of the nanoparticle suspension was investigated. In Figure 5.9 the mean diameter measured by DLS is presented as a function of the hydrophilic block (mPEG) volume fraction (f_A).

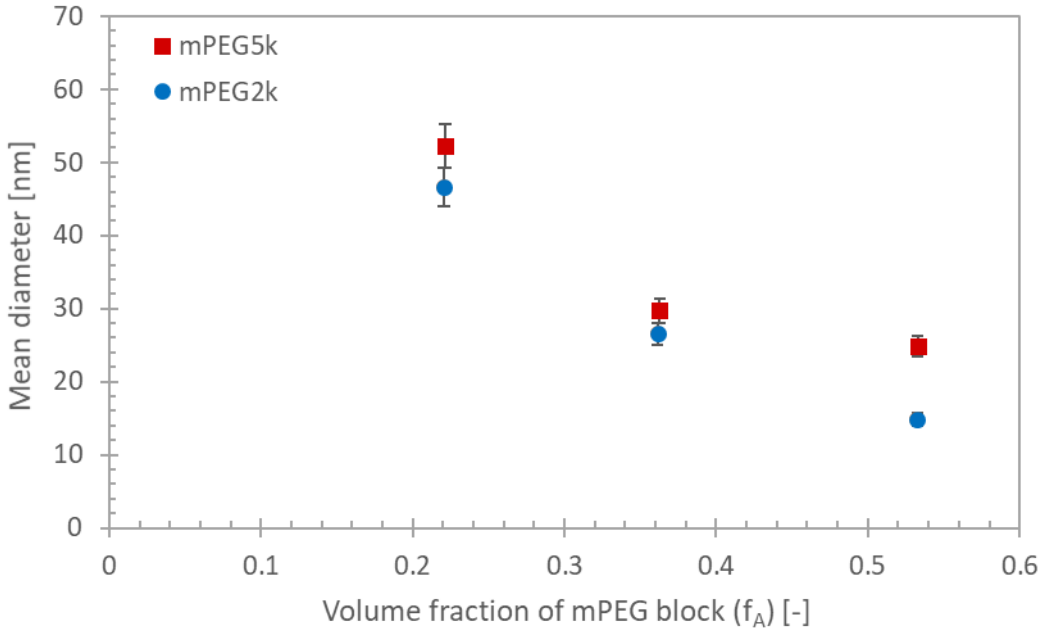

Figure 5.9: Plot of the nanoparticle mean diameter results obtained via DLS for all the synthesised diblock copolymers versus the hydrophilic mPEG volume fraction (f_A) in the synthesised polymers. The blue circle data points are for the diblock copolymers having a mPEG2k hydrophilic block and the red square data points are for the polymers with a mPEG5k hydrophilic block. Data presented are the mean values of three independent experiments and the error bars are the standard error.

The volume fraction of the hydrophobic block (f_B) is a method of determining the proportion of PLA in the final amphiphilic polymer. The volume fraction is a property normalised by the total volume of the system, in this case the diblock copolymer volume. As seen from the previous methods discussed for the quantification of PLA (DP_n, PLA M_n and hydrophobic to hydrophilic ratio), the mean diameter of the nanoparticle grows with higher amounts of PLA. Therefore, the same trend is expected to apply for the volume fraction of PLA. Since the volume fraction of the hydrophilic block (f_A) is equal to 1-(f_B), it is expected that the exact opposite trend will be followed when the results are plotted for the mean diameter versus f_B. As seen from Figure 5.9, the experimental results are in perfect agreement with the expected outcomes. The plot presented in Figure 5.9 is mirroring horizontally the plot established in Figure 5.8. An important observation from the results plotted in Figure 5.9 is that the mean diameter size decreases with increasing volume fractions of mPEG, but grows with increasing volume fraction of PLA. This suggests that even though the mean diameter is depended on both blocks, the hydrophobic block of the amphiphilic polymer has a higher influence on this property.

By observing the results presented in Figure 5.5, Figure 5.6 and Figure 5.7, it is clear that the mean diameter measured by DLS is dependent on the molecular weights of both the hydrophobic and hydrophilic block lengths of the amphiphilic block copolymer. The dependency of nanoparticle size on the total molecular length of the polymer reflects the balance between the respective contributions of each block to the total molecular weight of the diblock copolymers. From the observation of consistently higher nanoparticle sizes established for the longer mPEG chains in Figure 5.8, the findings of increasing diameter with increasing polymer and mPEG molecular weights were confirmed. Finally, the results from Figure 5.9 have proven that out of the two blocks of the synthesised polymers, the PLA hydrophobic block has the highest influence on the average size of the nanoparticle suspension.

5.3.2.2. Final polymer concentration investigation

In this investigation, the final BCP concentration in nanoparticle suspension was varied from 0.025-0.25wt%. A wide range of concentrations were employed to examine the effects of this processing parameter on the final nanoparticle suspension and its properties. To investigate this, the analysis of the final nanoparticle samples produced was performed using DLS to gather information on the nanoparticle size and the PDI. In addition, the broad range explored allows

for the investigation of the ability of the nanoprecipitation technique to be established as a highly successful method for nanoparticle formulation ranging from very low concentrations to relatively high concentrations of polymers in aqueous suspensions.

There is limited literature investigating the effect of the concentration of BCP during the self-assembling procedure and how that influences the final nanoparticle suspension properties. Especially for nanoprecipitation, the most commonly applied BCP concentration in the final nanoparticle suspension is 0.1wt% (Pearce *et al.*, 2019; Phan *et al.*, 2019; O'Brien *et al.*, 2020).

Based on the results obtained from DLS, it is concluded that the nanoprecipitation technique is a successful formulation technique for a vast range of final polymer concentrations. Its ability to form well defined nanoparticles at every concentration employed in this investigation study has been proven. All nanoparticle sizes established are within the acceptable range required for pharmaceutical applications, ranging from 15-55 nm (Capasso Palmiero *et al.*, 2018). Also, the values of the PDIs obtained for all polymers are relatively low, suggesting a low discrepancy in the nanoparticle sizes formed with high levels of suspension uniformity for all materials.

The results of the mean nanoparticle size are plotted against the five different employed polymer final concentrations. The data was separated in the six different mPEG-PLA block copolymers datasets and are presented in Figure 5.10.

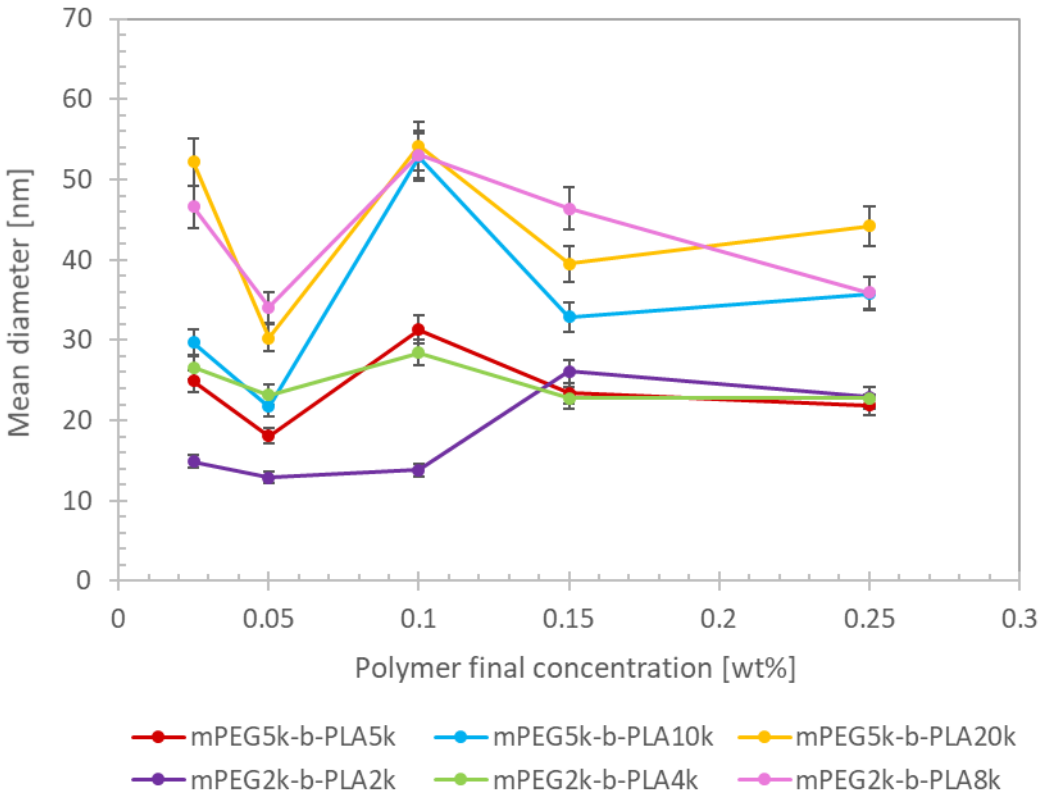

Figure 5.10: Plot of the nanoparticle mean diameter results obtained via DLS for all the synthesised diblock copolymers versus the amphiphilic block copolymer final concentration in nanoparticle suspension.

From the results presented in Figure 5.10, it can be observed that there is not a specific trend between the two plotted parameters that is followed for all the diblock copolymers examined. All six different amphiphilic polymers have a distinct trajectory that is followed between the measured mean diameter and the polymer final concentration.

5.3.2.3. Rate of addition variation

The BCP-acetonitrile solution was added at varying speeds into the selected aqueous phase. The rate of addition was varied from 1-6 ml/min using a syringe pump. The results were also compared to the results obtained for the nanoprecipitation performed by hand, which was estimated to have a rate of addition of approximately 30 ml/min. All other nanoprecipitation processing conditions were kept constant while varying the rate of addition of the oil phase. The influence of the rate of addition on the final mean diameter of the nanoparticle suspension was investigated.

The nanoprecipitation of mPEG5k-*b*-PLA10k was performed at the various rates of addition selected, aiming for a final concentration of 0.1wt%. The polymer material and its final concentration were kept constant for all rates of addition employed.

The resulting nanoparticle suspensions were analysed using DLS to determine the mean nanoparticle size and the PDI. The results of investigating the influence of the addition speed of the BCP-acetonitrile solution in distilled water are summarised in Table 5.5.

Table 5.5: Results for the mean diameter and PDI measured with DLS for the different rates of addition.

Rate of addition [ml/min]	Mean diameter [nm]	Polydispersity index (PDI)
30	52.8	0.106
6	55.4	0.100
2	64.4	0.098
1	65.3	0.089

From the results presented in Table 5.5, it is evident that the rate of addition has a significant influence on the nanoparticle formulation properties. When the rate of addition of the oil phase into distilled water is increased, the nanoparticles average size decreases. This is evident from all the results presented here. The results obtained from the nanoprecipitation experiments performed with the aid of a syringe pump seem to be following their own trajectory. That changes significantly when taking into consideration the results obtained by hand nanoprecipitation.

The observation of a smaller nanoparticle size with increasing rate of addition is in line with the discussions earlier in this chapter (section 5.1), where it was mentioned that nanoprecipitation is a kinetic process and therefore the nanoparticle formulation and properties are based on kinetic factors. This is proven here, where the nanoparticle mean diameter is decreased when the self-assembly process promotes faster formulation conditions.

In addition, the PDI values obtained for all the results of the different rates of addition are very low with values of 0.106 and lower (Table 5.5). This proves that a very narrow particle size distribution is achieved for all the performed experiments. Finally, all nanoprecipitation

processes completed have given rise to a nanoparticle suspension with mean diameters well within the desirable range for biomedical applications (Park *et al.*, 2008).

5.3.2.4. Oil phase effects

The good solvent used to form the oil phase of the initial BCP solution was altered from the polar solvent of acetonitrile (solvent used consistently throughout this chapter) to the volatile solvent of acetone (good solvent employed for nanoprecipitation in Chapter 4). The influence of the solvent quality of the oil phase and its properties on the nanoparticle suspension final characteristics was examined.

The nanoprecipitation of all produced diblock copolymers was performed using the two oil phase solvents chosen. The selected final diblock copolymer concentration in nanoparticle suspension was 0.1wt%. The final concentration and the rest of the processing conditions were kept constant for the two nanoprecipitation experiments to determine the effects caused only by the oil phase solvent quality.

The resultant nanoparticle suspensions from the different experiments were analysed using DLS to determine the mean nanoparticle size and the polydispersity index for the formulated suspensions.

The mean diameters of the nanoparticle suspensions established for both acetone and acetonitrile are plotted for all the diblock copolymers synthesised in this investigation and are presented in Figure 5.11.

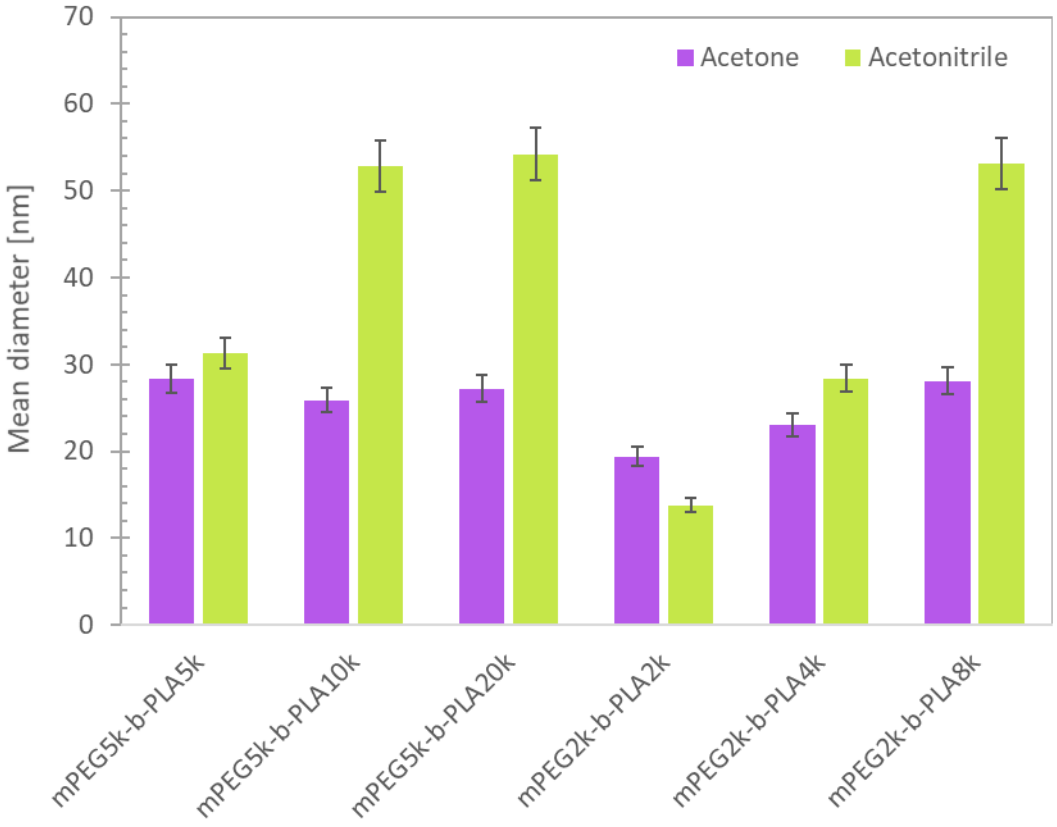

Figure 5.11: Plot of the nanoparticle mean diameter results obtained via DLS for all the synthesised diblock copolymers. A 0.1wt% polymer final concentration in suspension was employed. The purple bars are the data for nanoparticle suspensions formed from the acetone oil phase and the green bars are the data for the nanoparticle suspensions formed from the acetonitrile oil phase.

From the results plotted in Figure 5.11, it can be observed that for almost all diblock copolymers the nanoparticle mean diameter of the suspension formed by using acetone is consistently lower than that established with acetonitrile. This effect can be attributed to the different properties of each solvent. Although, they are both highly polar and miscible with water, acetone has a significantly lower boiling point, which is closer to room temperature compared to the acetonitrile boiling point. Therefore, acetone is more volatile than acetonitrile, which enables acetone to evaporate faster and leave the sample soon after the nanoprecipitation of the polymeric material. When the evaporation of the oil phase is performed at a higher speed, then the process of solvent displacement is significantly faster. As discussed (section 5.3.2.3), when the kinetics of the nanoprecipitation process are faster, the mean diameter of the nanoparticle suspension formed is lower. This is probably the rationale for the smaller nanoparticle sizes for the acetone oil phase compared to the mean diameters measured for the acetonitrile oil phase.

The mean diameters established for all the amphiphilic polymers, for both acetone and acetonitrile (Figure 5.11), are within the acceptable range for nanoparticles intended for medical application. Although, the particle sizes established by acetonitrile could be more beneficial when forming DDS for an increased circulation time and to reduce the risk of fast kidney excretion, that would be observed for nanoparticles that are smaller (~15-25 nm) (Capasso Palmiero *et al.*, 2018).

From the results shown in Figure 5.11, the other important observation is a higher mean diameter measured for polymers with a higher total molecular weight. This observation is more apparent from the acetonitrile oil phase results. Also, the mean diameter appears to increase as the hydrophilic block (mPEG) increases and when the hydrophobic block (PLA) increases for both the acetonitrile and acetone oil phase results. These observations are in line with the observations made in section 5.3.2.1.

The results collected for the PDI of the nanoparticle suspensions presented a relatively narrow nanoparticle size distribution for all materials and experiments performed. However, it was observed that the data shows a consistently lower PDI value for all the diblock copolymers for the nanoprecipitation experiments performed using acetonitrile as the oil phase. This phenomenon could be attributed to the high volatility of acetone, which by evaporating quickly from the sample after nanoprecipitation, does not allow a sufficient time for the amphiphilic polymer chains to organise into a more uniform nanoparticle size distribution.

The results obtained by varying the solvent quality of the oil phase indicate that out of the two solvents tested, acetonitrile is a more effective solvent based on its physical properties. This was concluded by the resulting mean diameter and the PDI of the formulated nanoparticle suspensions. Overall, it was concluded that a controllably volatile solvent performs better as it is required to evaporate out of solution after the nanoprecipitation process is completed, but should also allow for a sufficient time for the amphiphilic diblock copolymers to organise into polymeric nanoparticles with the required characteristics of a DDS intended for pharmaceutical applications.

5.3.3. Stepwise slow self-assembly

For the slow self-assembly procedure results presented here, the aim was to create a slower process, when compared to the solvent displacement method (section 5.3.2), by reducing the rate of mixing of solvent and anti-solvent. The rate of anti-solvent addition and the solution stirring speed is significantly reduced compared to the nanoprecipitation process to achieve a different formulation process.

The slow transition between the selected oil phase (acetonitrile) to the selected aqueous phase (distilled water) was performed in a controlled manner during the stepwise slow self-assembly. The transition process was monitored via DLS measurements to gain a better understanding of the self-assembly procedure of the amphiphilic diblock copolymer of mPEG5k-*b*-PLA5k and assess the feasibility of the process to produce nanoparticle formulations with the desirable characteristics of a DDS. The concentration of the mPEG5k-*b*-PLA5k in solution was kept constant throughout the process to eliminate the influence of the BCP solution concentration on the self-assembly procedure.

For the stepwise slow self-assembly process followed with a concentration of 1.25wt% of mPEG5k-*b*-PLA5k in solution, six steps of slow water dilution and acetonitrile evaporation were completed in total. The process was terminated after six steps (60vol% of water, see Table 5.3) due to polymer material precipitating out of solution and depositing on the bottom of the glass vial forming a sediment layer. Therefore, it was obvious that a nanoparticle suspension was not applicable in this polymer concentration in solution. The DLS measurement of the sample at 60vol% of water was not performed as macroscopic observation of the sample indicated the size of the particles present in solution are much bigger than nanoparticle size.

The mean diameters of the six dilution-evaporation steps were plotted against the volume percentage content of distilled water in the solvent system (distilled water and acetonitrile), as shown in Figure 5.12.

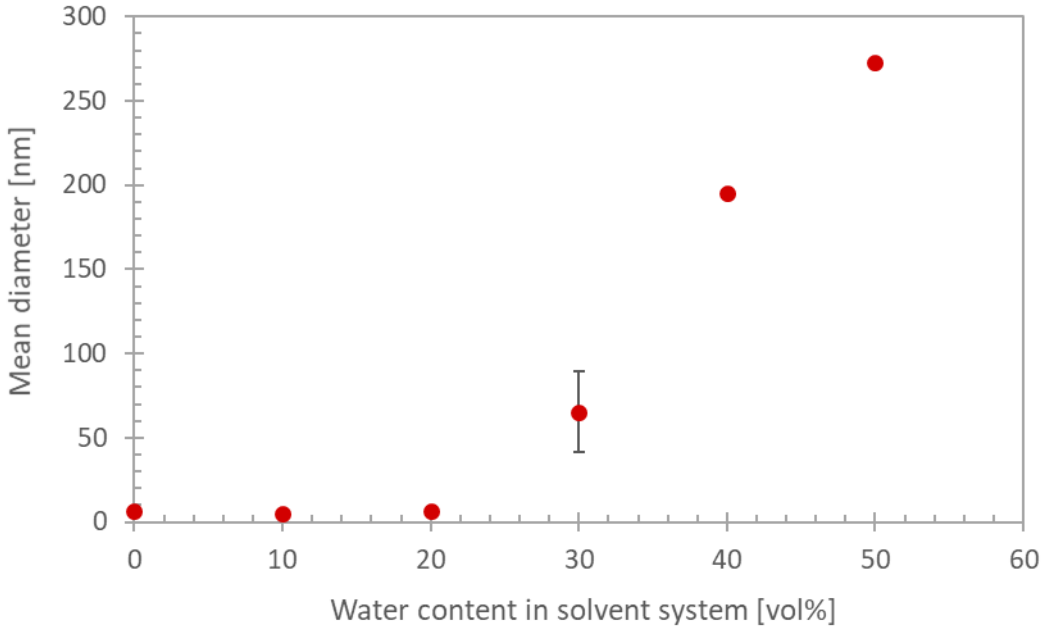

Figure 5.12: Plot of the mean diameter results obtained via DLS for all six dilution-evaporation steps performed for the stepwise slow self-assembly of mPEG5k-*b*-PLA5k at a constant solution concentration of 1.25wt% against the corresponding vol% content of water in the solvent system (acetonitrile and water). Data presented are the mean values of five DLS runs of the sample and the error bars are the standard error of these runs (in most cases hidden behind the data points).

From the results presented in Figure 5.12, it can be noted that with the increasing water content in the solution, the nanoparticle average size increases. At water contents between 0 - 30vol%, this is the expected trend since amphiphilic block copolymers self-assemble in the presence of aqueous solvents. Therefore, the results suggest that when the aqueous solvent concentration in solution increases, more free amphiphilic diblock copolymer chains self-assemble and form nanoparticles.

It is observed that as the water content in solution keeps increasing (from 40vol% and higher), the mean diameter of the polymeric nanostructures formed, keeps increasing. This could indicate the formulation of a more complex structure with this formulation process compared to the different polymeric nanoparticles introduced in section 2.3.2 of the Literature review in Chapter 2. Also, it is possible that polymeric micelles are initially forming at lower water content percentages and as the process progresses the micelles aggregate to form larger particles, which are effectively measured by DLS and give the results observed in Figure 5.12. However, as discussed already for the DLS results in Chapter 4, this characterisation alone cannot provide confirmation on the exact type of polymeric nanostructure formed, since it does not incorporate structure characterisation of the measured material. Therefore, the precise

physical and structural condition of the polymeric nanoparticles formed here remains undefined. More specialised characterisation techniques, that can perform structural analysis, are required in this case to address the physical nature of the formulated polymeric nanoparticles. Cryo-TEM and X-ray scattering characterisation are such processes, that could provide this information.

The results for the initial state of the solution and the first two dilution steps (from 0-20vol% of water) present a very low mean diameter of approximately 6 nm. Such low average diameters are observed when the polymer chains are free in solution and are adopting the random walk configuration (see section 2.6 for random walk in literature review). Therefore, it is expected that at contents of 0-20vol% of water in the solvent system, the diblock copolymer is adopting its random walk configuration. In this cases, the average nanoparticle size measured by DLS represents the radius of gyration of the polymer in solution (see section 2.6).

The most important observation from the results plotted in Figure 5.12 is the increase in mean diameter from ~6 nm to ~65 nm, between the second and the third dilution-evaporation step. The data collected for these two process steps could mean that the initiation of the micelle formation process is taking place between 20-30vol% content of water in the solvent system. Inside this water composition range, the transition from free open polymer coils in solution to self-assembled micellar structures in suspension is likely occurring.

The physical macroscopic appearance of the sample was completely clear and transparent from 0-30vol% of water in the solvent mix. After the fourth dilution-evaporation step the sample transitioned to a hazy and cloudy solution. Finally, it was observed that the polymer material started precipitating out of solution after the sixth dilution-evaporation step and settling at the bottom of the glass vial. The stepwise dilution-evaporation process was terminated after the sixth step was completed since it was obvious that a nanoparticle suspension was not feasible at such high concentrations using this formulation technique.

The exact same methodology was applied with same conditions and material for a stepwise slow self-assembly at a constant polymer concentration of 0.1wt% in solution. This concentration was chosen since it is the most employed concentration for the nanoprecipitation process. The aim was to assess the applicability of this formulation method to prepare

nanoparticle suspensions and form an alternative process to nanoprecipitation for nanoparticle formulation with desirable characteristics.

For the stepwise slow self-assembly process followed with a constant concentration of 0.1wt% of mPEG5k-*b*-PLA5k in solution, eight steps of slow water dilution and acetonitrile evaporation were completed. The first process step incorporated the water addition of a volume equal to the sum of water volumes that would be required to complete the first three dilution steps. During the evaporation of the first process step, the total amount of acetonitrile that was required to evaporate after the first three steps was removed. The combination of the first three dilution-evaporation steps was applied since the results gathered from the 1.25wt% stepwise process indicated that the self-assembly and micelle formation process starts at the third dilution-evaporation step.

The mean diameters of the eight dilution-evaporation steps were plotted against the volume percentage composition of distilled water in the solvent system (distilled water and acetonitrile), as shown in Figure 5.13.

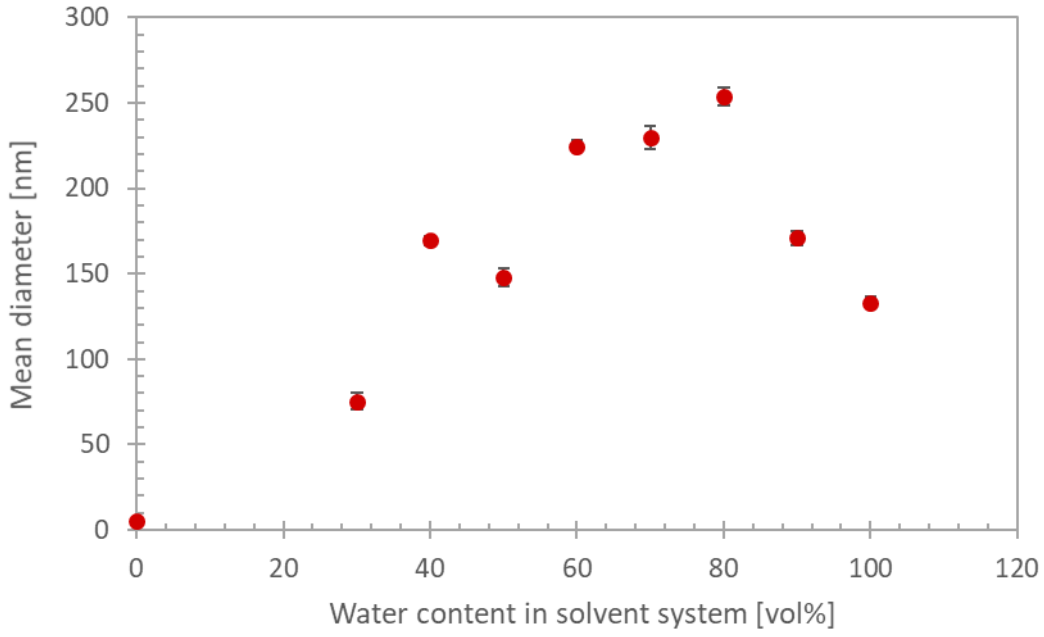

Figure 5.13: Plot of the mean diameter results obtained via DLS for all eight dilution-evaporation steps performed for the stepwise slow self-assembly of mPEG5k-*b*-PLA5k at a constant solution concentration of 0.1wt% against the corresponding vol% content of water in the solvent system (acetonitrile and water). Data presented are the mean values of five DLS runs of the sample and the error bars are the standard error of these runs (in some cases hidden behind the data points).

As seen from Figure 5.13, the results obtained for the 0.1wt% solution concentration follow a similar trend to that seen for the 1.25wt% solution concentration (Figure 5.12). The initial mean diameter of the sample is similar to the values obtained for the 1.25wt% concentration results, with a value of approximately 6 nm. This indicates the initial state of the sample incorporates free polymer chains conformed in random walk configuration in solution. As expected, after the first process step, where the volume percentage of water in the solvent mixture is 30vol%, the self-assembly process was initiated, with the formed polymeric nanoparticles having a mean size of approximately 75 nm.

From 0-80vol% of water in solvent, the average nanoparticle size increases with increasing water content in solution, with a maximum observed at 80vol% water composition (Figure 5.13). As discussed for the 1.25wt% polymer concentration, this relationship could potentially mean aggregation of the initially formed polymeric micelles, leading to an increase in the measured nanoparticle size.

From 80-100vol% water content, the average nanoparticle size decreases with increasing water composition. This is an interesting trend that could suggest a re-organisation process of the polymeric nanoparticles in this range, leading to smaller nanostructure sizes. Although, the exact phenomenon taking place here cannot be verified from these results alone. A more specialised characterisation technique, in combination with DLS, could determine the specific polymer nanoparticle structure formed in solution during the different water content percentages.

5.3.4. Single-step slow self-assembly

The single-step slow self-assembly procedure is employed as an alternative process to the stepwise process (section 5.3.3), that would reduce the process time. This self-assembly process is essentially in-between the nanoprecipitation and the stepwise slow self-assembly processes. A combination of the latter two processing conditions is applied to perform the single-step slow self-assembly.

All six polymer materials synthesised in this investigation were formulated into nanoparticles via the single-step slow self-assembly method. The results obtained by DLS for the nanoparticle mean diameters and PDIs are plotted and presented in Figure 5.14.

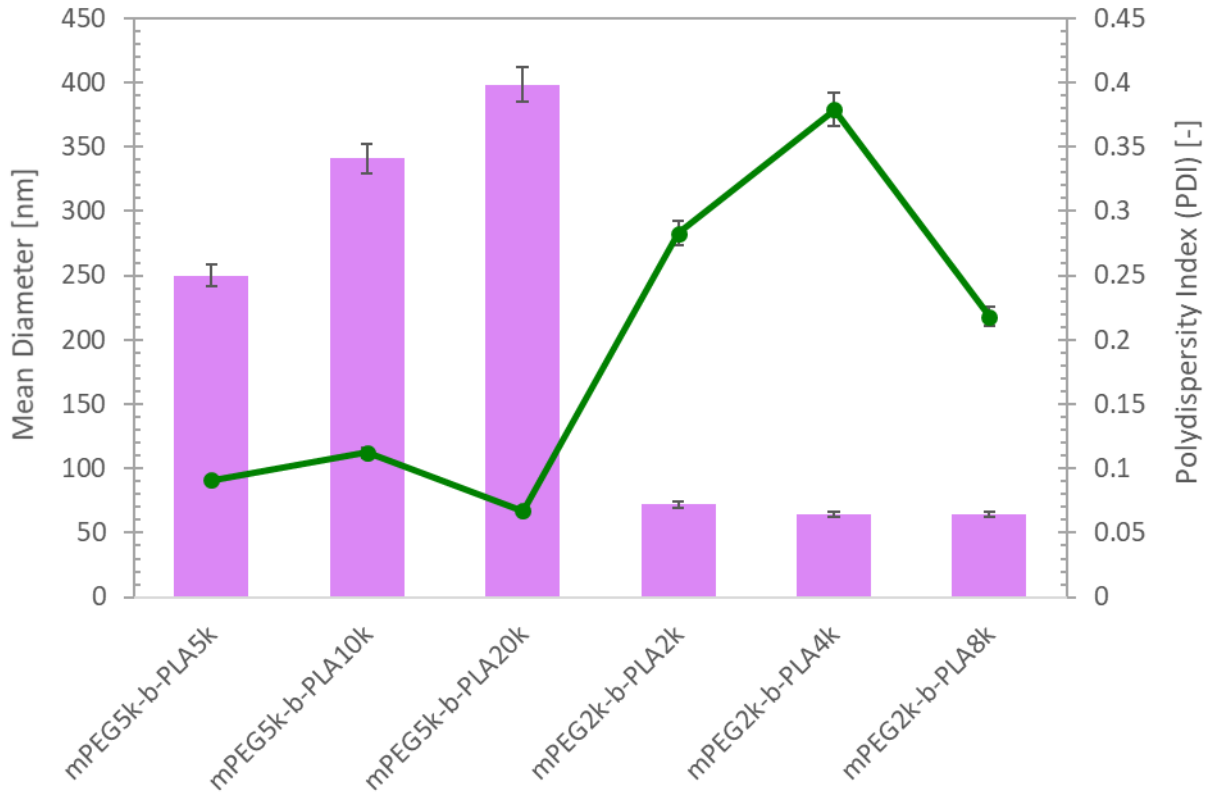

Figure 5.14: Plot of the mean diameter and the PDI results obtained via DLS for the nanoparticle suspensions formed from all six synthesised diblock copolymers prepared through the single-step slow self-assembly process. The pink bars represent the results for the mean diameter and the green circle data points represent the polydispersity index results. Data presented are the mean values of three independent experiments and the error bars are showing the standard error of these experiments.

From Figure 5.14, it is observed that the diblock copolymers containing mPEG5k as the hydrophilic block are consistently forming nanoparticles with larger mean diameters, compared to the diblock copolymers with mPEG2k as the hydrophilic block. Therefore, materials with higher molecular weights form bigger nanoparticles by employing the single-step slow self-assembly method. The results for the mPEG5k diblock copolymers follow an increasing mean diameter for increasing hydrophobic block length trend. This trend is not apparent for the mPEG2k diblock copolymers. An interesting finding in Figure 5.14 is that the PDI value of all the mPEG5k diblock copolymers is very low compared to the mPEG2k diblock copolymers. This contrasts the mean diameter measured for the samples, which is higher for the mPEG5k polymers compared to mPEG2k polymers.

The zeta potential results of all the nanoparticle suspensions formed by the single-step slow self-assembly process are plotted and presented in Figure 5.15.

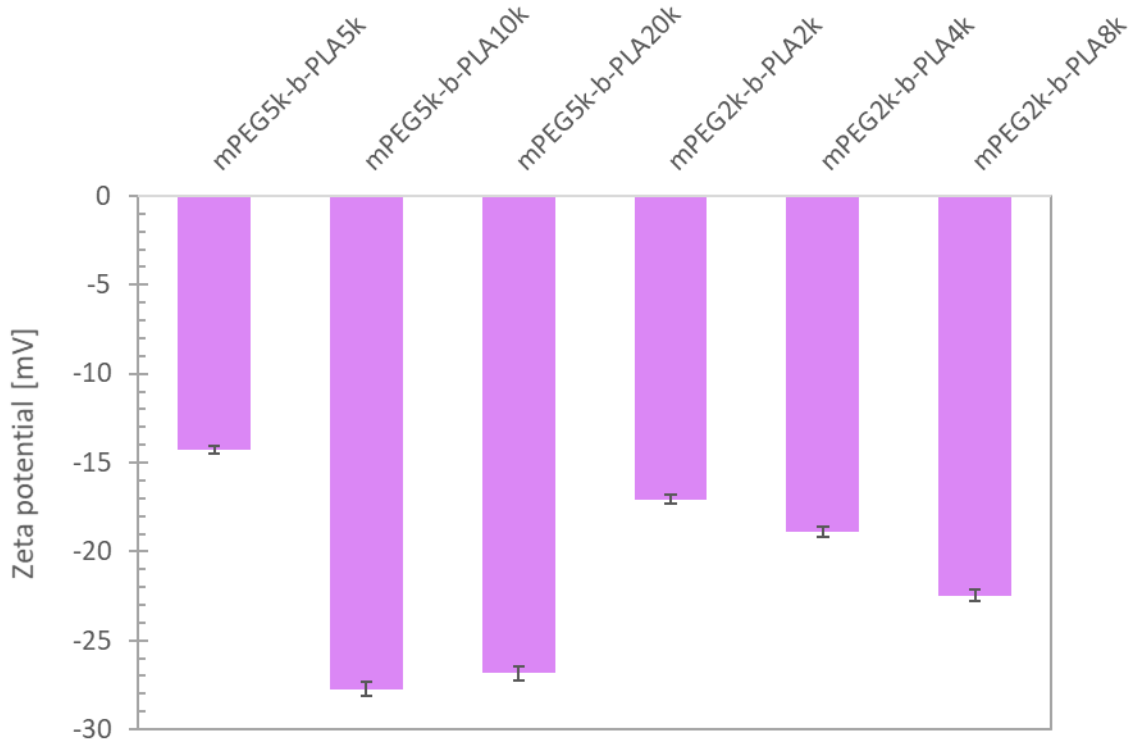

Figure 5.15: Plot of the zeta potential results for the nanoparticle suspensions formed from all six synthesised diblock copolymers prepared through the single-step slow self-assembly process. Data presented are the mean values of three independent experiments and the error bars are showing the standard error of these experiments.

The particle surface charge measured through zeta potential analysis for all the diblock copolymer suspensions formed is between -28 and -17 mV, suggesting a high colloidal stability of the nanoparticle suspensions based on electrostatic repulsion forces (Andreana *et al.*, 2023). The electrostatic repulsion forces emerge from the surface charge of nanoparticles. The higher the surface charge, the higher the repulsion forces between nanoparticles. It is important to have a high surface charge and resultant repulsion forces in nanoparticle suspensions. When the repulsion forces between nanoparticles are strong, they remain apart from each other in solution and therefore experience a higher colloidal stability. In contrast, if the surface charge and accompanying repulsion forces are low, then the nanoparticles in suspension can collide leading to the formation of aggregates since there are no repulsion forces keeping them apart (Dora *et al.*, 2010).

From Figure 5.15, it can be seen that the zeta potential in most cases increases with increasing molecular weight of the diblock copolymers. Also, it seems to be increasing with increasing PLA block length, when considering the results presented for the mPEG2k diblock copolymers. This is in agreement with the literature since this has been documented before (Ghasemi *et al.*, 2018). It has been observed in the literature that the composition of polymer material in solution does not have a big effect on the surface charge measured for the nanoparticle suspensions (Andreana *et al.*, 2023). Therefore, it is expected that the zeta potential measurements established here are representative for all similar nanoparticle suspensions that are formed by the different diblock copolymers in water.

It is known that PEG is an uncharged compound and therefore is expected to be neutral when measured for zeta potential, with values close to zero. The zeta potential analysis performed here has yielded negative values, suggesting that maybe some PLA chains are trapped in the hydrophilic PEG corona and therefore contributing to the values obtained. The zeta potential of PLA is around -50 mV according to the literature (Govender *et al.*, 1999; Luz *et al.*, 2017). This is a lot higher than the values measured in this study, meaning that the PEG block of the diblock copolymers is indeed forming the corona, with the possibility of a few PLA chains being in the corona and getting in contact with water.

To investigate this finding further, the results presented in Figure 5.15 are compared with data available in the literature for the same system of polymeric materials (PEG-PLA). The zeta potential range of -28 to -17 mV measured in this study is comparable with values established from the literature, with results being around -23 mV (Lu, Li and Wang, 2008; Wang and Xu, 2017). In other cases, the zeta potential was found to be lower than the values established in this investigation, with values around -12 mV for PEG-PLA nanoparticles (Dong and Feng, 2004; Zheng *et al.*, 2010). The variation of zeta potential values for PEG-PLA nanoparticles between the different sources is due to the differences in the nanoparticle structures formed. As already discussed, the specific type and structure of polymeric nanoparticles formed in this study is not fully determined. However, on average the zeta potential results established here are generally in agreement with the values reported in the literature.

5.3.5. Different self-assembly methodologies comparison

The three different formulation techniques that were applied in this investigation for the preparation of different nanoparticle suspensions are compared in this section.

The DLS data from section 5.3.2.2 support that nanoprecipitation is an effective formulation method for various polymer concentrations. This technique consistently produced well-defined nanoparticles at all concentrations tested in this study, from very low to relatively high weight fractions (0.025-0.25wt%). In contrary, the two slow self-assembly procedures employed in this investigation were not able to formulate nanoparticles at relatively high concentrations as seen in sections 5.3.3 and 5.3.4. These results suggest that a kinetic process, such as nanoprecipitation, is more effective in this case to perform the formulation of nanoparticles with desirable characteristics at high concentrations of material.

The size of all the nanoparticles produced via solvent displacement method fall within the 15-65 nm range, which is suitable for pharmaceutical uses (Park *et al.*, 2008). From the stepwise slow self-assembly process performed it was observed that in general the nanoparticle average size was significantly higher than the nanoprecipitation sizes. The results show that the nanoparticle structures organise into larger nanoparticles compared to the nanoprecipitation nanoparticles. Specifically, the only nanoparticle measurement that was within the acceptable range was approximately 65 nm obtained for 30vol% of water in solvent. However, the high acetonitrile composition disqualifies it from biomedical applications. The nanoparticle average sizes obtained through the single-step slow self-assembly process for the mPEG5k are not within the acceptable range for DDSs aimed for pharmaceutical applications. The nanoparticle suspension mean diameters measured for mPEG2k diblock copolymers are highly promising, although the PDI values associated with these suspensions are considered to be high.

For the solvent displacement method, the low PDI values recorded for all polymers indicate minimal variation in nanoparticle sizes, ensuring a high degree of uniformity across the suspensions (Table 5.5). On the other hand, the PDI values for the stepwise slow self-assembly and the single step self-assembly, in general, are higher than PDIs achieved using nanoprecipitation for the same diblock copolymer formulation, as seen from the DLS results. These results indicate that the nanoparticle suspensions obtained for the two slow formulation

processes exhibit a higher diversity in their nanoparticle size distributions compared to nanoprecipitation prepared BCP formulations.

All these results and observations lead to the conclusion that nanoprecipitation is a highly qualified, robust and reliable technique for producing polymeric nanoparticles from the self-assembly of amphiphilic diblock copolymers of mPEG-PLA.

5.4. Conclusions

The primary aim of this study was to deepen the understanding on how amphiphilic block copolymers, particularly diblock copolymers of mPEG-PLA, self-assemble into polymeric nanoparticles. This was achieved by using three formulation methods and altering the formulation parameters to assess their impact on the characteristics (mean diameter and PDI) of the final product.

The results obtained for the nanoprecipitation experiments conclude that the mean diameter and the PDI of the nanoparticle suspension is highly depended on the properties of the polymer material used including the total molecular weight of the block copolymer, the lengths of both blocks, the hydrophobic to hydrophilic ratio and the blocks volume fractions in the polymer. Moreover, it was concluded that the solvent displacement method reliably generated well-defined nanoparticles across all tested concentrations in this study, ranging from very low to relatively high weight fractions (0.025-0.25wt%). The results obtained for the rate of addition of the BCP-acetonitrile solution in water validate the dependence of the final product PDI and mean diameter on the kinetic driving forces applied during formulation. By varying the solvent quality of the oil phase, it was demonstrated that acetonitrile is a more effective solvent than acetone based on its physical properties. It was found that solvents with lower volatility, allow sufficient time for amphiphilic diblock copolymers to form polymeric nanoparticles that are optimal for creating DDS suitable for pharmaceutical applications with low PDI values and desirable nanoparticle size.

Even though the slow self-assembly processes were not fully successful in forming a nanoparticle suspension with all the desirable characteristics of a DDS intended for biomedical applications (based on PDI and mean nanoparticle size), they have contributed into the understanding of the self-assembly process of diblock copolymers. Where the process starts

with diblock copolymers fully dissolved in a good solvent for both of their blocks, forming free open polymer chains that have the configuration of the random polymer walk. Following the addition of the selective solvent, they formulate into polymeric nanoparticles driven by their amphiphilic nature, to limit the interactions of the hydrophobic block with the aqueous solvent. By increasing the selective solvent content in solution, polymeric nanoparticles keep increasing in size possibly due to aggregation of the individual nanostructures and formation of larger particles, which are measured by DLS.

The stepwise slow self-assembly process was highly successful in indicating the position where the solvent exchange process triggers the micelle formation process, which was observed in the 20-30vol% composition range of water in the solvent mixture. Between these two compositions, the transition from free open polymer coils shaped into the radius of gyration in solution to self-assembled micellar structures in suspension occurs.

Zeta potential analysis of all diblock copolymer suspensions reveals a particle surface charge ranging from -28 to -17 mV, indicating a high colloidal stability in the nanoparticle suspensions due to electrostatic repulsion effects.

Finally, through the comparison of all the formulation techniques and process parameters investigated in this study, it was concluded that the nanoprecipitation process is the best performing formulation method. This conclusion is supported by the obtained results for the mean diameters and PDIs of the produced nanoparticle suspensions. The nanoprecipitation technique was successfully forming well defined nanoparticles in all processing conditions applied. In all cases, the characteristics required for a DDS intended for pharmaceutical applications were achieved with nanoparticle mean diameters within the desirable size range of 10-100 nm and low PDI values.

6. Systematic study of different cryoprotectants for an improved freeze-drying process and enhanced storage stability of PEG-PLA nanoparticles

6.1. Introduction

Polymeric nanoparticles with a poly(ethylene) glycol (PEG) corona and a poly(lactide) (PLA) core are very promising materials to act as the drug encapsulation device of hydrophobic chemotherapy drugs delivering them to the cancer site. However, the commercial applications of polymeric nanoparticles are very limited at the moment. The constraint behind their limited use in clinical applications is their inadequate long-term stability in an aqueous medium. Pharmaceutical formulations are desired to have a prolonged storage capability to be deemed as a successful and a safe device for their intended applications. For this reason, enhancing the long-term stability of colloidal nanoparticle systems, and therefore increasing their storage time capabilities, is one of the biggest concerns and the focus of recent studies (Lazzari *et al.*, 2012; Morgen *et al.*, 2012; Zielinska *et al.*, 2020).

The poor stability of the polymeric nanoparticles after extended storage in aqueous mediums is caused from their physical instabilities, which are usually associated with particle aggregation and fusion, and their chemical instabilities, which are associated with hydrolysis of the polymers forming the nanostructures, drug chemical reactivity and leakage from nanoparticles (Abdelwahed *et al.*, 2006). Therefore, the chemical and physical instabilities of the nanoformulations can be reduced by the removal of water from the system. The most common methodology used in the pharmaceutical and biological industry to transform suspensions and solutions into a dry solid product with a suitable stability for storage and transportation is freeze-drying (Franks, 1998).

Freeze-drying, alternatively known as lyophilisation, is an industrial unit operation where water in the form of ice crystals is removed by sublimation under low pressures. It consists of three main steps: (i) the freezing step where the aqueous suspension is frozen and pure water ice crystals are formed within the material, (ii) the primary drying step where the ice crystals are removed by sublimation under vacuum and (iii) the secondary drying step where the residual absorbed water is removed (Ciurzyńska and Lenart, 2011; Nowak and Jakubczyk, 2020). Freeze-drying is a very intensive process and it gives rise to considerable stresses in the

suspension during freezing and drying. Polymeric nanoparticles are very fragile suspensions and it has been documented that the freeze-drying of these materials without extra caution could lead to activity disruption (Lemoine *et al.*, 1996; De Jaeghere *et al.*, 1999; Abdelwahed, Degobert and Fessi, 2006; Bejrapha *et al.*, 2010). The nanoparticles could become unstable due to the mechanical stresses and pressures generated by ice crystal formation during the freezing step. This would have unfavourable effects on the nanoparticle robustness and size (Fonte *et al.*, 2014; Mohammady, Mohammadi and Yousefi, 2020).

There are some excipients that can be added into the nanoparticle suspension before freeze-drying to avoid the disturbances to the formulation during the process. These materials are called cryoprotectants and lyoprotectants and they act as stability enhancements during the freeze-drying process and also provide an improved physical stability during storage (Sadikoglu, Ozdemir and Seker, 2006). Cryoprotectants are used to protect the nanoparticles during the freezing step and lyoprotectants shield the formulation from the stresses rising during the drying process. Some materials can act as both cryoprotectants and lyoprotectants (Trenkenschuh and Friess, 2021).

When cryoprotectants and lyoprotectants are employed during the freeze-drying process, they help retain the integrity and structure of sensitive materials from damage that ice crystallisation and dehydration stresses could have caused. Among cryoprotective agents, glycerol and dimethyl sulfoxide (DMSO) typically preserve the material structure during the freezing step by preventing the formation of ice crystals within the structures by reducing the temperature at which freezing occurs (Awan *et al.*, 2020; Murray and Gibson, 2022). Lyoprotective agents, such as sucrose, trehalose and other sugars, protect polymeric nanoparticles by creating a glass matrix which inhibits the molecular mobility, preventing their structural collapse during the drying step (Han *et al.*, 2007; Tonnis *et al.*, 2015). By combining these protective agents, the stability and recovery of the lyophilised products is improved. Their properties and course of action are highly beneficial, making cryoprotectants and lyoprotectants essential during freeze-drying for the preservation of polymeric nanoparticles prepared by diblock copolymers intended for cancer chemotherapy applications.

In this chapter, the investigation focuses on the freezing step of the freeze-drying process and how it affects the colloidal suspensions of PEG-PLA nanoparticles. The aim is to control and minimise the mechanical stresses caused by the ice crystal formation during the freezing step,

with the emphasis on the effects and efficiency that the different cryoprotectants employed have in shielding the PEG-PLA formulations. Cryoprotectants are inert, inactive and non-invasive materials that, when incorporated in nanoparticle suspensions, can act as a barrier of protection of the nanoparticle size and structure from the freezing processes by controlling the ice crystal formation in the sample.

6.2. Freeze-drying investigation methodology

6.2.1. Polymeric nanoparticles

6.2.1.1. Polymer material

The polymer material chosen to carry out this study is the diblock copolymer of mPEG5k-*b*-PLA10k. This polymer was used throughout the investigation for all different parameters to emphasise on the effects of the added excipients on the freeze-drying process and avoid implications that could have been caused by varying the properties of the polymer material, such as the length of the different blocks, molecular weight, hydrophobicities, hydrophilicities, etc. The diblock copolymer was synthesised and characterised based on the methodologies and analysis techniques described in Chapter 5. This specific polymer was selected out of all the polymers synthesised in Chapter 5 due to its total molecular weight. The polymer library prepared in Chapter 5 consisted of a wide range of polymer total molecular weights ranging from 4-25 kDa. Therefore, it was considered more reasonable selecting a polymer for this research that its total molecular weight is in closer proximity to the average total molecular weight of the polymer library formed.

The most important properties of the mPEG5k-*b*-PLA10k polymer are summarised and presented in Table 6.1.

Table 6.1: Important properties of the mPEG5k-*b*-PLA10k polymer.

Polymer	Molecular weight of block A (M_A) [kDa]	Molecular weight of block B (M_B) [kDa]	Volume fraction of block A (f_A)	Volume fraction of block B (f_B)	Total molecular weight (M_n) [kDa][a]	Melting temperature (T_m) [ºC][b]	Glass transition temperature (T_g) [ºC][b]
mPEG5k-*b*-PLA10k	5	9.8	0.36	0.64	14.8	119.3	19.2

[a]Calculated by ^{1}HNMR.
[b]Estimated based on information provided by the material supplier, Sigma Aldrich.

6.2.1.2. Nanoparticle formulation

The mPEG5k-*b*-PLA10k polymeric nanoparticles were formed using the nanoprecipitation method, otherwise known as the solvent displacement method, following a similar procedure as described in Chapters 3-5. In this case, acetonitrile was used as the good solvent (oil phase) and distilled (Stuart Distinction D4000 water still) water (aqueous phase) as the anti-solvent. The amphiphilic diblock copolymer self-assembles giving rise to a nanoparticle suspension through solvent exchange from the oil to the aqueous phase. The amount of polymer required was weighed and added to the corresponding volume of acetonitrile in a glass vial. The concentration of polymer in acetonitrile was kept constant at 5 mg/ml to keep the concentration driving force constant. The polymer was dissolves instantly in acetonitrile. The desired amount of distilled water for nanoprecipitation was added in a new clean glass vial containing a magnetic stirrer bar. The volume of distilled water was estimated to give a 0.1wt% final concentration of polymer in water. The distilled water vial was placed on a stirrer plate (MR Hei-Tec magnetic stirring hotplate, Heidolph Instruments) in a fume cupboard at room temperature (~25 ºC). The initial solution of polymer in acetonitrile was added with a syringe pump (PHD ULTRA™, Harvard Apparatus). The syringe pump was set up to add the polymer-acetonitrile solution in the distilled water in a dropwise manner. After the full addition of the initial polymer solution in the distilled water, the acetrontrile-water-polymer mixture was left uncapped in the fume cupboard at room temperature overnight to achieve the full evaporation of acetonitrile from the suspension and complete the solvent displacement procedure. A schematic diagram representing the experimental set up applied in this case for the nanoprecipitation process using the syringe pump is shown in Figure 6.1.

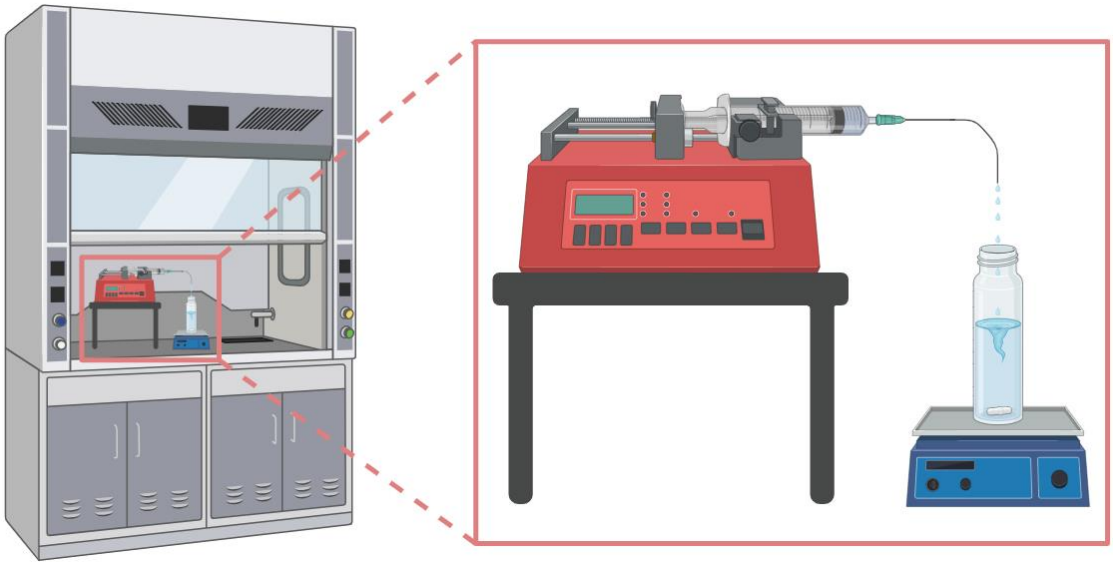

Figure 6.1: Schematic representation of the experimental set up applied for nanoprecipitation with a syringe pump.

6.2.2. Cryoprotectant selection

The cryoprotectants selected to be used in this research investigation are poly(ethylene) glycol (PEG) of different molecular weights, glycerol and DMSO. Further information about these materials and their selection is presented in section 3.4.1.

The most important properties of the cryoprotective agents chosen in this systematic research investigation are summarised in Table 6.2.

Table 6.2: Important properties of the selected cryoprotectants.

Material Properties	Cryoprotectants employed in this study					
	PEG1k	**PEG6k**	**PEG10k**	**PEG35k**	**DMSO**	**Glycerol**
Melting temperature (T_m) [ºC][a]	37-41	60-63	62-65	64-66	16-19	20
Glass transition temperature (T_g) [ºC][b]	-36	-17	-20	-36	-	-
Molecular weight (M_n) [Da][a]	1000	6000	10000	35000	78.13	92.09
Density (ρ) at 25 ºC [g/ml][a]	1.116	1.116	1.116	1.116	1.1	1.25
Molecular volume (υ) [nm^3][c]	1490	8930	14900	52100	1180	1230
Radius of gyration (Rg) [nm][c]	1.7-2.5	3-4	4-6	6-8	0.35	0.3-0.4
Solubility in water at 25 ºC [mg/ml][a]	256 – completely soluble	256 – completely soluble	256 – completely soluble	256 – completely soluble	Completely miscible	1000 - miscible

[a]Provided by the material supplier, Sigma Aldrich.
[b]PEG T_g data taken from (Faucher *et al.*, 1966).
[c]Estimated from information provided by the material supplier, Sigma Aldrich.

6.2.3. Experimental procedure

In total, four different molecular weights of PEG (1000, 6000, 10000 and 35000 Da) and the two common cryoprotectants, DMSO and glycerol, were used in this study to investigate the effects of the PEG chain length on the properties of the mPEG5k-*b*-PLA10k nanoparticle suspension after the freezing step and the final freeze-dried material.

An overview of the experimental methodology steps conducted in this research investigation in order of completion is presented in Figure 6.2.

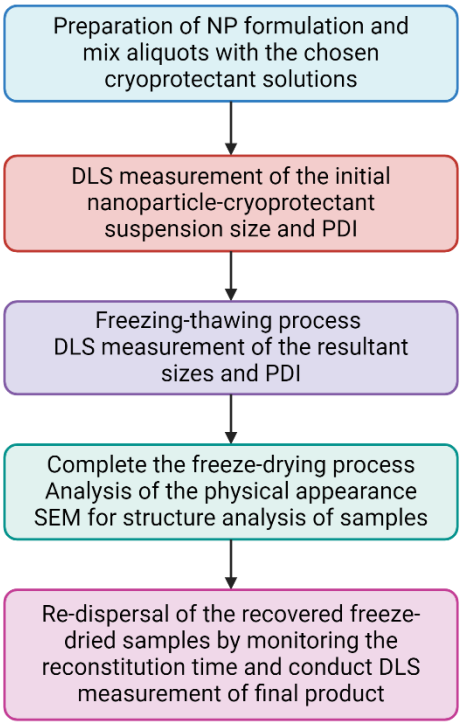

Figure 6.2: Summary of the experimental methodology steps followed in this research investigation.

The experimental procedure starts with the preparation of the PEG-PLA nanoparticle formulation by nanoprecipitation (see section 6.2.1) that will be used to carry out this systematic study of the different cryoprotectants. The cryoprotectant solutions were prepared by accurately weighing the estimated amount of each of the chosen cryoprotectants in a new clean glass vial and dissolving it in the desired volume of distilled water. The volume of water and weight of excipient were pre-calculated, aiming for a 10wt% concentration of cryoprotectant in water. The glass vials were shaken vigorously to fully dissolve the cryoprotectants in water. Even though all cryoprotectants chosen are highly soluble in water (see Table 6.2), the samples were also shaken on a vortex mixer to ensure a homogeneous solution. Aliquots of the nanoparticle suspension were added in six glass vials. Subsequently, aliquots of each of the prepared cryoprotectant-water solutions were added to each of the six glass vials. The final concentration of cryoprotectant in solution was ~5wt%. The cryoprotectant-nanoparticles suspensions were mixed gently.

At this point, the initial nanoparticle sizes and polydispersities, after the addition of the six cryoprotective agents to the suspension, were measured with Dynamic light scattering (DLS). A small volume of the original nanoparticle formulation was also measured with DLS to act as

a control sample for this investigation. Following the DLS initial measurement, all of the seven samples were placed in the lab freezer to perform the initial freezing step. The freezing process was completed overnight at approximately -30 ºC and atmospheric pressure, followed by thawing of the samples the next day until they reached room temperature (25 ºC). Since the aim is to assess the ability of the six different chosen excipients to act as cryoprotective agents for PEG-PLA nanoparticles, the condition of all the nanoparticle-cryoprotectant suspensions after the freezing-thawing process has to be examined and compared with the PEG-PLA control nano-suspension. Therefore, a second DLS measurement of all seven samples was completed to assess the effect of the freeze-thawing process on all the different cryoprotectant samples and the original nanoparticle control sample. In addition, a re-measurement of the DLS sample sizes and polydispersities was completed after a week of equilibration of all the samples at atmospheric conditions. The DLS measurement was repeated to make sure that the nanoparticle sizes determined directly after the freezing-thawing process were representative of the sample and there was no change of the properties after a week of equilibration.

The next step was to complete the freeze-drying process. The freezing step was repeated for all six cryoprotectant samples and the PEG-PLA-NPs control. After the freezing step was completed, the drying step was carried out in a Telstar LyoQuest freeze-drier (Azbil Telstar) with a condenser temperature of approximately -56 ºC and under vacuum at approximately 0.3 mbar. The samples were retrieved and characterised for their physical appearance. Moreover, a structural and surface analysis using SEM imaging was performed for the freeze-dried materials.

Finally, the re-dispersibility properties of the retrieved freeze-dried materials in water were investigated. A modified procedure form (Kulkarni *et al.*, 2018) was followed for the reconstitution experiments. Filtered distilled water at 25 ºC was added to the freeze-dried white fluffy cake and stirred for 1 min followed by a 15 sec observation step. This procedure was repeated until the full re-dispersal of the freeze-dried material was observed. The reconstitution time, which is the time required for the full re-dispersal of the freeze-dried sample, was measured for all the recovered materials. It was estimated by adding up the 1 min stirring steps and including the 15 sec observation steps after each stirring step. The reconstitution experiments were carried out at room temperature and pressure (25 ºC and 1 bar). In addition, the size and polydispersity of the reconstituted samples were measured using DLS, to fully

assess the ability of the chosen cryoprotectants to shield the PEG-PLA nanoparticles during the freeze-drying processes.

6.2.4. Characterisation analysis techniques

In this section, the characterisation techniques performed to analyse the materials constructed in this cryoprotectant systematic study and their properties are summarised. Further details about the equipment utilised to perform these analyses and the measurement conditions and procedures can be found in Chapter 3.

Dynamic light scattering (DLS): This characterisation technique was used to establish information about the nanoparticle size distribution and the polydispersity index (PDI) of the nanoparticle population present in the samples. The DLS equipment used is the ZetaPALS (2008) model by Brookhaven Instruments Corporation, equipped with a red solid state laser. The measurements were completed at room temperature (25 ºC). The samples were equilibrated at 25 ºC in the equipment cuvette chamber prior to measurement. Each measurement consisted of 5 runs of the same sample.

Physical macroscopic investigation: The macroscopic appearance of the samples was investigated throughout the whole methodology procedure of this research work. Changes on the appearance of the samples were monitored and noted as observations. To record these macroscopic observations for presentation purposes, a lightbox with LED lighting on the top wall and a blue colour backdrop was used to capture images of the samples using a camera.

Scanning electron microscopy (SEM): The freeze-dried cryoprotectant samples were characterised using SEM imaging to gain information about the surface and the structure of the material. The dry sample was spread on a 10 mm diameter SEM stub using a double-sided conductive tape. The top of the stub with the dry sample was deposited with gold using an Agar sputter coater. The prepared SEM samples were then positioned in a JEOL JSM-6010LA SEM instrument (JEOL U.K. Ltd) for microstructure imaging.

Statistical analysis: Unless otherwise stated, all results are expressed as the mean value ± standard error (SE). All methodologies were conducted in three independent experimental

procedures. The mean values and the standard errors were estimated from analysis of the three independent experimental procedures.

6.3. Results and discussion

6.3.1. Preliminary experiment

In this section, the data for the preliminary experiment are presented, where the freeze-thawing process of a nanoparticle suspension without any excipients and in the presence of PEG6000 as cryoprotectant was performed. The results from this preliminary experiment formed the motivation behind the systematic study of different molecular weight PEGs as cryoprotectants for the PEG-PLA nanoparticle formulations.

The aim was to convert the aqueous nanoparticle suspensions into dry products to prolong the storage lifetime of the PEG-PLA drug delivery systems (DDSs). Based on information gathered from the literature, it was expected to encounter issues with the process, as discussed earlier (section 6.1), due to the high mechanical stresses and pressures involved in the freeze-drying process. Thus, to better understand the influence of each step on the nanoparticle properties, the freezing step was carried out separately to assess its effects on the nanoparticle characteristics.

The first step was to freeze and thaw the PEG-PLA nanoparticle suspension and monitor the changes of the nanoparticle size and the PDI before and after the process using DLS. The results obtained for the nanoparticle (NP) size and PDI before and after the freeze and thawing process are shown in Table 6.3 and are plotted in Figure 6.3.

Table 6.3: Nanoparticle size and PDI data for preliminary experiment.

Sample	Before freezing-thawing		After freezing-thawing		Percentage increase (%)	
	Mean diameter [nm]	PDI	Mean diameter [nm]	PDI	Mean diameter	PDI
Original	41.1	0.123	165.6	0.411	302.9	234.1
PEG6k	57.1	0.147	101.9	0.365	78.4	148.3

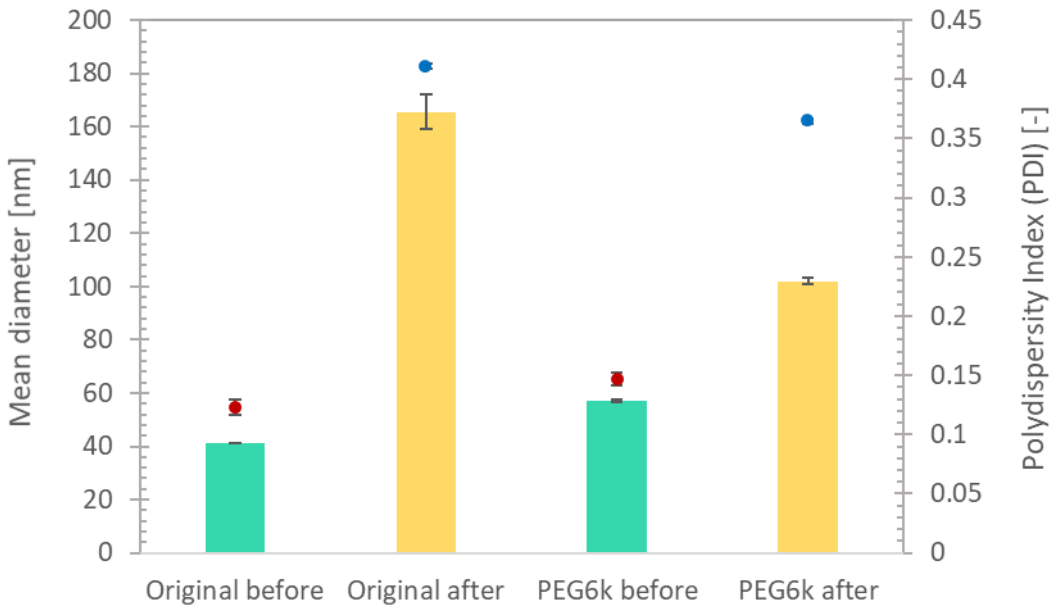

Figure 6.3: Graph with the plotted results from the preliminary experiment. The green bars represent the mean diameter data of the samples before the freeze and thaw process. The yellow bars represent the mean diameter data of the samples after the freeze and thaw process. The red circle points show the polydipersity index data for before the freeze-thawing process and the blue circle points show the polydispersity index data for after the freeze-thawing process. Data are the mean values of 5 independent runs of the same sample and the error bars show their standard error.

As it can be seen from the results, the mean diameter of the PEG-PLA nanoparticles has increased dramatically from 41.1 nm to 165.6 nm after the freeze and thawing process. This was calculated to be an increase of 302.9% of the mean diameter of the nanoparticles. The same was observed for the polydispersity index of the nanoparticles. The PDI has increased from 0.123 to 0.411, with a 234.1% increase after the freeze-thawing process. This means that the nanoparticle population has not only increased significantly after the freezing step, but also the nanoparticle size distribution has broadened significantly, giving a large range of nanoparticle sizes coexisting in the sample.

After these observations were made about the original sample, it was decided to initially use PEG6k to examine whether it can act as a cryoprotectant of the PEG-PLA nanoparticle formulation. The same process was followed, as for the original PEG-PLA nanoparticle sample, for freezing and thawing of the PEG6k nanoparticle suspension. The changes of the sample's particle size and PDI before and after the freeze-thaw process were monitored using DLS. The results obtained are shown in Table 6.3 and are plotted in Figure 6.3, alongside the results obtained for the original PEG-PLA freeze-thaw process.

There is a similar trend with the original sample data. The nanoparticle mean diameter increases from 57.1 nm to 101.9 nm, with a 78.4% increase after the freeze-thaw process. Also, the PDI transitions from 0.147 to 0.365, calculated as an increase of 148.3%. Even though there is still an increase of the two NP properties, the percentage increase of both the PDI and mean nanoparticle diameter of the PEG6k sample are significantly lower than the corresponding percentage increases measured for the original sample. Moreover, the final NP mean diameter of the PEG6k sample (101.9 nm), although increased, is still well within the acceptable size range required for particles intended for drug delivery systems (Capasso Palmiero *et al.*, 2018). Both the values obtained for the PDI and the mean NP diameter of the PEG6k sample are notably lower than those determined for the original sample. This means that PEG6k was able to act as a stabiliser of the NP suspension to some extent.

The effects of PEG6k acting as a cryoprotectant for the PEG-PLA nanoparticle suspension were also examined through physical macroscopic observation of the samples. Both the original NP suspension and the PEG6k-NP suspension were completely clear and transparent before the freeze and thawing process. However, after the freeze-thawing, the original NP sample has transitioned into a hazy and cloudy sample. The PEG6k suspension remained clear and transparent as before the freeze-thawing process, indicating again the ability of the excipient to control the aggregation of the NP suspension during the freezing step. The image captured for the two samples after the freeze-thawing process can be seen in Figure 6.4.

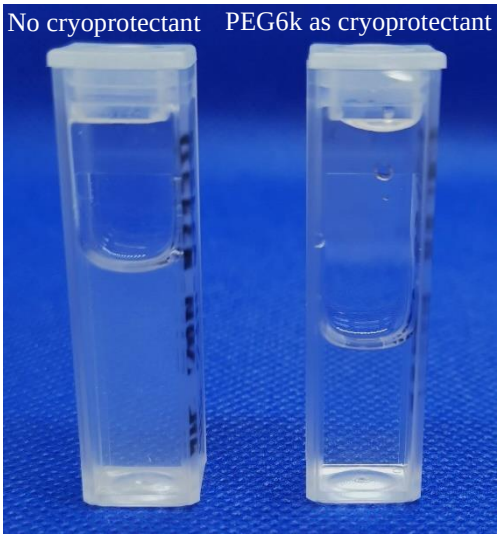

Figure 6.4: Image of the two samples analysed during the preliminary experiment in the lightbox for physical macroscopic observation of their appearance after the freeze-thawing process. On the left is the original PEG-PLA nanoparticle suspension appearing hazy and cloudy after the freezing step. On the right is the PEG6k-nanoparticle suspension sample remaining clear and transparent after the freezing step.

The results obtained from the preliminary experiment raised some interesting questions. Does the stabilisation effect experienced by the use of PEG6k in the nanoparticle suspension vary with the molecular weight of PEG? And if yes, which ones are performing better; the higher molecular weight PEGs or the lower molecular weights? Also, it was observed that the initial (before freezing and thawing) mean diameter of PEG6k-NP suspension was measured as 57.1 nm, which is higher compared to the 41.1 nm of the original NP suspension (Table 6.3). Does this observation mean that the chain length of PEG has an effect on the difference in mean diameters that are measured? All these research questions developed by the preliminary experiment results formed the motivation behind the conduction of a systematic cryoprotectant study focusing on the effect of PEG molecular weight during the freezing step of the freeze-drying process.

6.3.2. Systematic study: Before freezing step

In this section, the results obtained from the systematic cryoprotectant study discussed in section 6.2.3 of this chapter are presented. The data reported here are collected before performing the freeze and thawing process of the chosen cryoprotectant samples.

The mPEG5k-*b*-PLA10k nanoparticle suspension prepared by nanoprecipitation was mixed with six cryoprotectant excipients, namely four different molecular weight PEGs (1000, 6000,

10000 and 35000 Da), glycerol and DMSO. All of the six different cryoprotectants samples, plus a control sample of the original nanoparticle suspension without any additional excipients, were analysed using DLS. The mean diameter and the polydispersity index of the nanoparticle populations of each of the seven samples were measured. The results were compared to understand the effect of the cryoprotectants on the properties of the initial state (before freezing step) of the suspensions.

The results of the initial state of each of the seven suspensions are plotted for comparison and shown in Figure 6.5. The green bars show the results collected for the mean diameter and the red circular points show the data for the polydispersity index.

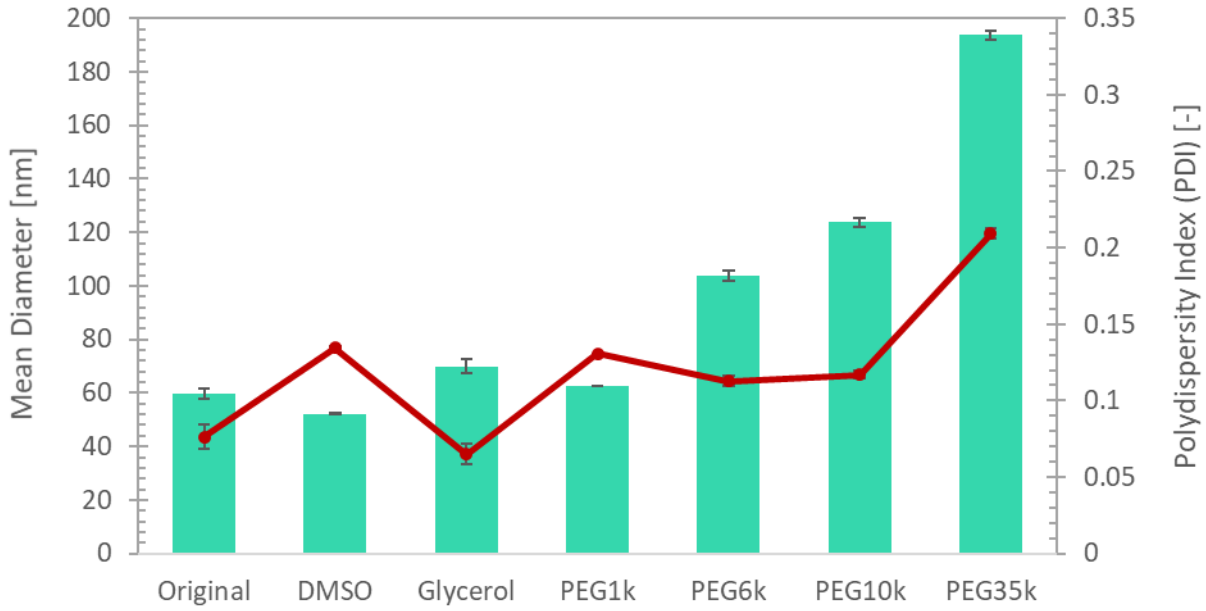

Figure 6.5: Plot of the mean diameter and the PDI results obtained via DLS for all cryoprotectants and the control (original) sample before the freezing and thawing process. The green bars represent the results for the mean diameter and the red circle data points represent the polydispersity index results. Data shown are the mean values of three independent experiments and the error bars show the standard error of these three experiments.

From the results of the mean diameter, it is seen that the cryoprotectant samples that are the closest to the size of the original PEG-PLA nanoparticles sample (59.6 nm) are the DMSO, glycerol and PEG1k NP suspensions with a mean diameter of 52.1, 69.9 and 62.5 nm respectively. The percentage difference from the control (original) sample of the mean diameters of these cryoprotectants was calculated as -12.5, 17.5 and 4.9% respectively. Out of these values, the lowest one is the percentage difference calculated for PEG1k. In the PEG1k sample, the suspension components include PEG-PLA and PEG1k in a water solution.

Therefore, the reason behind the lower discrepancy from the control could be due to PEG being present both in the polymeric NP structure and freely dissolved in water. This means there is a reduced number of components and consequently less complicated and competing component interactions. In this case, the number of competing interaction dynamics taking place in the sample would decrease. Moreover, it is well known that the interactions between water and PEG (both in polymer and free PEG1k) are stronger than the interactions exhibited in the water-glycerol-PEG(polymer) and water-DMSO-PEG(polymer). This is again due to the fact that PEG1k cryoprotectant is more compatible with the PEG corona of the PEG-PLA polymeric nanoparticles, since is the same chemical compound, when compared to PEG-DMSO and PEG-glycerol (Weng, Chen, *et al.*, 2011; Zhao *et al.*, 2015). Also, the water and polyethylene glycol experience stronger intermolecular interactions because of the strong hydrogen bonding between the two compounds. The presence of multiple (-OH) groups along the polymer chain of PEG facilitates a higher number of hydrogen bonds with water when compared to water-DMSO-PEG and water-glycerol-PEG, therefore leading to stronger intermolecular interactions (Kim *et al.*, 2002). Therefore, the differences between the mean diameters of the cryoprotectants with the control (original) sample are probably due to the different component intermolecular interactions experienced in each of the cryoprotectant samples.

The measured mean diameters for the four PEG cryoprotectants are plotted against their corresponding molecular weight and are shown in Figure 6.6.

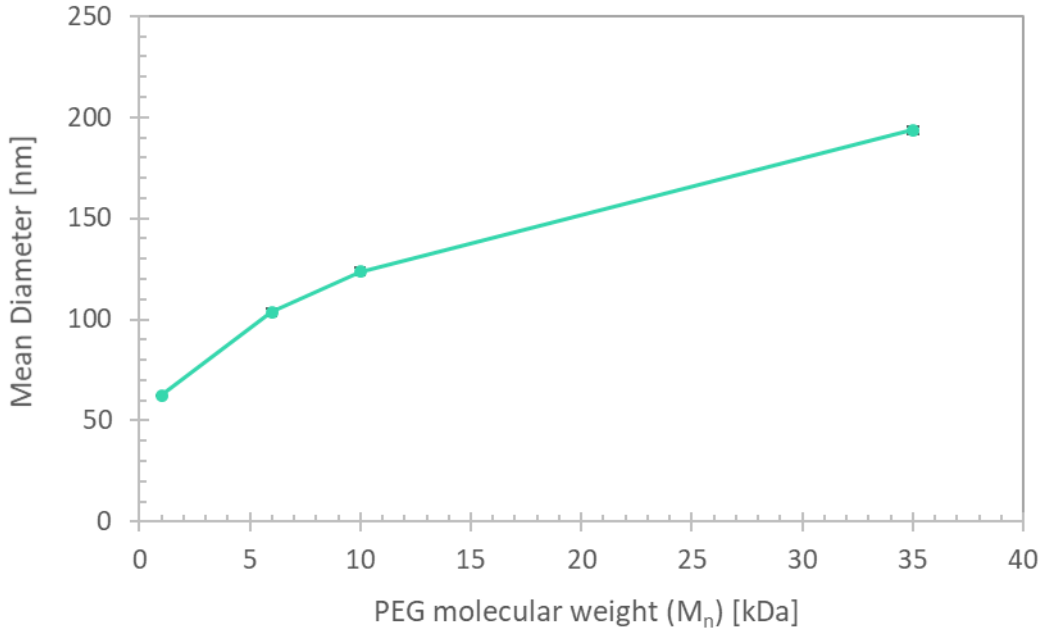

Figure 6.6: Plot presenting the mean diameter measured though DLS vs the molecular weight for the four different PEGs chosen in this systematic study before carrying out the freezing step. Data shown are the mean values of three independent experiments and the error bars (hidden behind the diameter of the points in most cases) show the standard error of the three experiments.

In the results shown in Figure 6.6, it is obvious that as the chain length of the PEG employed as a cryoprotectant increases, the mean diameter measured is also increasing. This is in line with what was observed in the preliminary experiment and raised the question of whether the molecular weight of PEG has an effect on the mean diameter measured by DLS. From the results of this systematic study presented in Figure 6.6, it can be concluded that the chain length of the PEG cryoprotectant employed indeed does have an effect on the measured particle size. The reasoning behind this is probably related to the PEG molecule size when in suspension.

It is believed that when PEG is employed as a cryoprotectant for polymeric nanoparticles it works as a stabiliser for the suspension by forming some kind of coating around the polymer NPs protecting them during the freeze-drying process. Initially before freezing, it acts as a layer around the polymeric NPs, and during the freezing step it limits the ice crystal formation and its disruption on the NPs. During the two drying steps, it acts a replacement of the water interactions with the NPs to stabilise them by substituting the hydrogen bonds between the solvent and nanoparticles that were present in the suspension and no longer exist in the dry form of the nanoparticles (Abdelwahed *et al.*, 2006).

As discussed in the literature review, it is known that the radius of gyration (R_g) of polymers relates to the molecular weight of the polymer and depends on parameters such as the solution temperature and solvent used for the suspension of the polymer (Fixman, 1962). In addition, the other property that is scaling with the molecular weight of the compound is the molecular volume (υ), which is also dependent on the density of the material. Both the molecular volume and the radius of gyration increase with polymer molecular weight (Table 6.2). Therefore, the higher chain length PEGs will have a higher R_g and υ when compared to lower molecular weight PEGs. Consequently, based on the hypothesis that the PEG is acting a coating layer around the polymeric nanoparticles when in suspension before the freezing step, if the PEG molecular size (expressed either as Rg or υ) is higher, then the coating layer would also be thicker leading to a larger particle being effectively measured by the DLS measurement. This is the reason that the DLS measured mean diameter is increasing with the molecular weight of the PEG cryoprotectant used in the NP suspension.

The mean diameter results are all within 10-200 nm. According to the literature, these are within the range that is acceptable for nanoparticles intended for clinical and pharmaceutical use as drug delivery systems (Capasso Palmiero *et al.*, 2018). The PDI values obtained for all the cryoprotectant-NP suspensions are well below 0.25 meaning that the nanoparticle size distributions are relatively narrow and monodisperse. Finally, the macroscopic appearance of all the six cryoprotectant samples and the control (original) sample was observed to be completely clear and transparent before performing the freezing step of freeze-drying.

6.3.3. Systematic study: After freezing step

The results collected after completing the freeze and thawing process discussed in section 6.2.3 for all the chosen cryoprotectant samples are presented in this section.

All the six cryoprotectant samples and the original sample, that were discussed in section 6.3.2, are examined here after the freezing and thawing process was performed. To assess the effectiveness of the selected excipients to act a cryoprotectants of the mPEG5k-*b*-PLA10k nanoparticle suspension, the properties of the cryoprotectant-NP samples had to be determined. For this reason, all the samples were analysed using DLS to establish information on the mean diameter and PDI of each of the cryoprotectant suspensions after the freeze-thawing process. The results obtained were compared with the data obtained for the same samples in their initial

state (before freeze-thaw) and with each other. The results and comparisons are presented and discussed in this section to understand which excipients are more ideal to act as cryoprotectants of the polymeric nano-formulation.

The results of all seven different samples after the freeze-thaw process are plotted for comparison and shown in Figure 6.7. The yellow bars show the results collected for the mean diameter and the blue circular points show the data for the PDI.

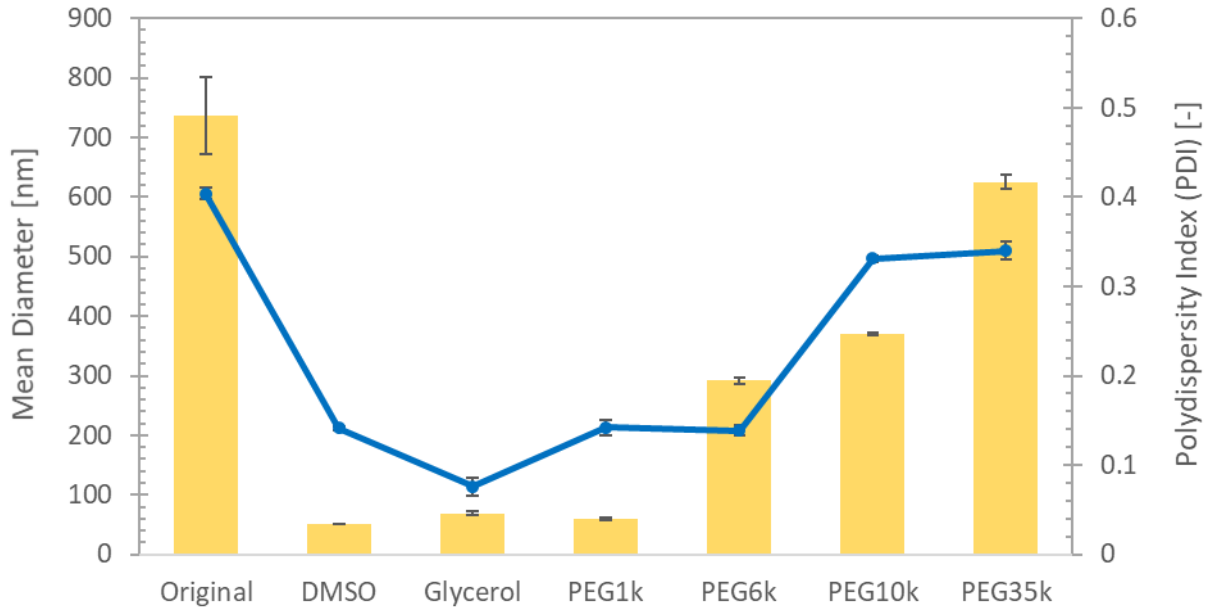

Figure 6.7: Plot of the mean diameter and the PDI results obtained via DLS for all cryoprotectants and the original sample after the freezing and thawing process. The yellow bars represent the results for the mean diameter and the blue circle points represent the polydispersity index results. Data shown are the mean values of three independent experiments and the error bars show the standard error of these three experiments.

The results show that the original, PEG6k, PEG10k and PEG35k nanoparticle populations have increased significantly in size after the freezing-thawing process with a positive percentage difference of 1136.1, 389.8, 522.5 and 949.6% respectively compared to the control sample (original sample mean diameter before freeze-thawing). The suspension with the highest percentage difference is, as expected, the original PEG-PLA nanoparticle suspension. This was expected to have the most dramatic increase in size since it is the polymeric NP formulation without any excipients acting as stabilisers of the nanoparticles structures. Therefore, the results from the original NP suspension after the freeze-thaw process confirm the requirement of excipients to act as cryoprotectants to protect the NP formulation and its properties for a safe and reliable final pharmaceutical product with a robust stability for prolonged storage.

Moreover, from Figure 6.7, the values that are the closest to the control sample results are obtained for the DMSO, glycerol and PEG1k NP suspensions. This is the same as with the results gathered in this systematic study before the freeze-thaw process. These were measured to have a mean diameter of 50.5, 68.7 and 60.6 nm respectively after the freeze-thaw process, with a percentage difference of -15.2, 15.4 and 1.8% respectively when compared to the control sample. Out of the three, the cryoprotectant-NP suspension size that is closest to the original sample mean diameter is, again, the PEG1k sample. The rationale behind this is probably the same as for the results collected for the samples before carrying out the freeze-thawing process. The differences of the mean diameters between the cryoprotectant samples with the control sample is related to the various intermolecular interactions encountered by the components of each of the cryoprotectant systems.

The PDI values obtained for the DMSO, glycerol, PEG1k and PEG6k cryoprotectant-NP suspensions after the freeze-thaw process are well below 0.25 meaning that the nanoparticle size distributions remain relatively narrow and monodisperse. However, the PDI results for the original, PEG10k and PEG35k samples after freezing and thawing have increased above the value of 0.25, which means that for those samples the size population has a broader size distribution. The higher the PDI, the wider the range of the particle size distribution and in this case the highest PDI is the one from the original sample with a value of 0.404. This is expected since there is no cryoprotectant in the sample to stabilise the nanoparticle population and protect it from the ice crystal formation and the extensive mechanical stresses taking place during the freezing step of freeze-drying leading to aggregation of the nanoparticles and bigger variation in their particle size distribution.

All the results established for the nanoparticle size and PDI, both before and after the freezing and thawing process, are combined and are plotted for comparison. The mean diameter results collected for both before and after the freeze-thaw process are shown in Figure 6.8. The PDI data gathered for both before and after the freeze-thaw process are presented in Figure 6.9. The green bars represent the data from the measurements carried out before the freezing step and the yellow bars represent the data from the measurements completed after the freezing step for both the nanoparticle size and polydispersity plots.

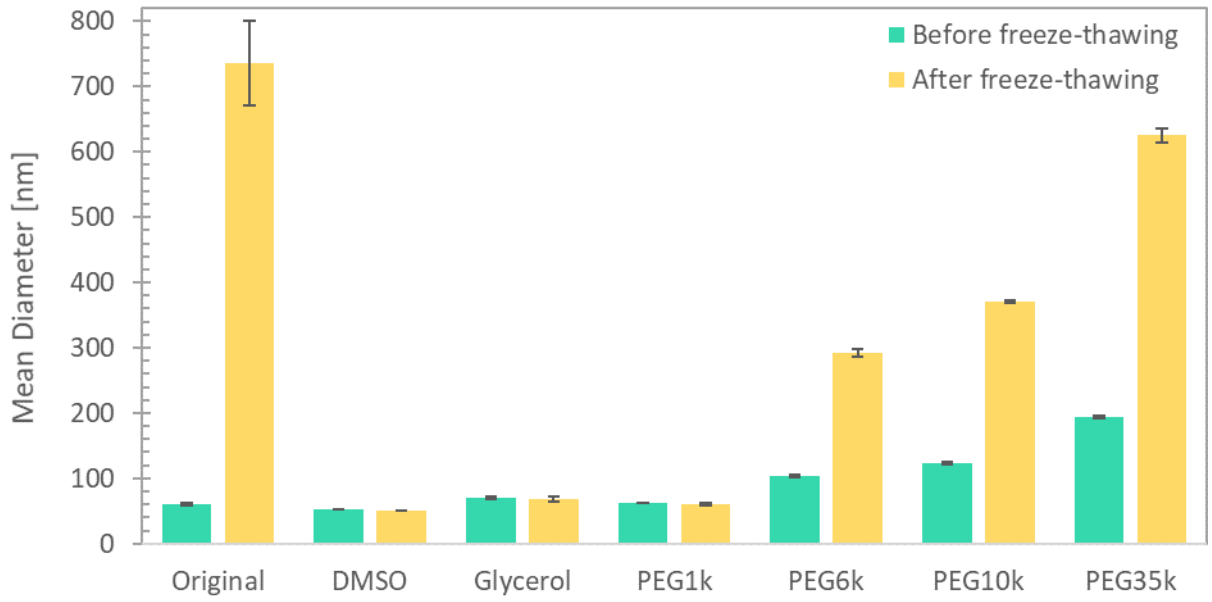

Figure 6.8: Graph showing the mean diameter DLS results for all the cryoprotectants including the original sample for both before and after the freeze-thawing process. The green bars represent the mean diameter data before the freeze-thaw process and the yellow bars represent the mean diameter data after the freeze-thaw process. Data shown are the mean values of three independent experiments and the error bars show the standard error of these three experiments.

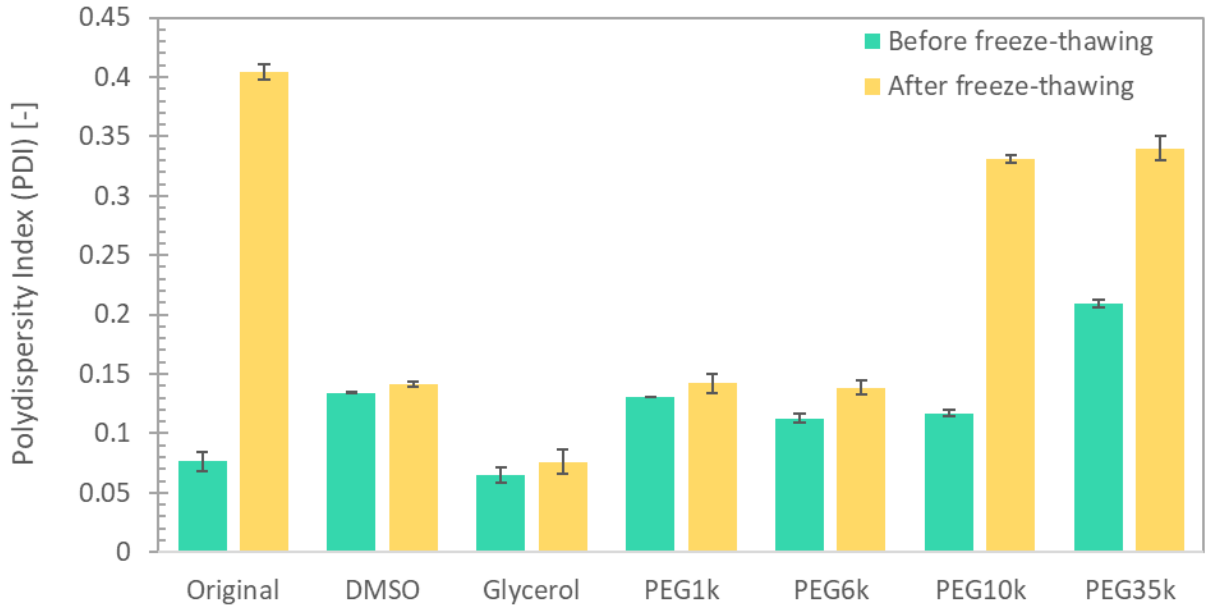

Figure 6.9: Graph showing the polydispersity index (PDI) data gathered through DLS for all cryoprotectants including the original sample for both before and after the freeze-thawing process. The green bars represent the PDI data before the freeze-thaw process and the yellow bars represent the PDI data after the freeze-thaw process. Data shown are the mean values of three independent experiments and the error bars show the standard error of these three experiments.

From the results plotted in Figure 6.9, all the PDI values for all cryoprotectants and the original sample have increased after the freeze-thawing process. This means that the cryoprotectant nanoparticle suspensions size distributions increase and are broader after the freeze-thawing process. The bigger the effect of the freeze-thawing process on the PDI, the lower the effectiveness of the cryoprotectant used to stabilise the nanoparticle suspension. The results show that the highest increase in PDI is observed for the original NP suspension, which is expected since no cryoprotectant was used to stabilise the nanoparticles, followed by the PEG10k and the PEG35k samples. This signifies that these two excipients are maybe not very effective in protecting the properties of the NP suspension. On the other hand, the results suggest that the best performing cryoprotectants so far are DMSO and PEG1k, since they have the lowest PDI increase during the freezing step, with 5.2 and 8.7% respectively.

Looking at the data plotted in Figure 6.8, the first thing to observe is the dramatic mean diameter increase of the original NP formulation, having a percentage difference of 1136.1% from the initial NP size. This verifies the necessity for a cryoprotective agent when the nanoparticle formulation undergoes a freeze-drying procedure to form a more durable and stable state for storage and transportation. Another point of interest is the fact that the mean diameter measured for DMSO, PEG1k and glycerol is relatively unaffected by the freeze-thawing process. All three of these cryoprotectants exhibit a percentage difference of less than 3.5% compared to their initial particle size. This suggests that DMSO, PEG1k and glycerol are the most promising cryoprotective agents so far in this investigation.

To facilitate the comparison and discussion about the effectiveness of the four PEG cryoprotectants explored in this investigation and how that relates to their chain length, their measured particle size is plotted, both for before and after the freeze-thaw process, against their molecular weight. The plot can be seen in Figure 6.10.

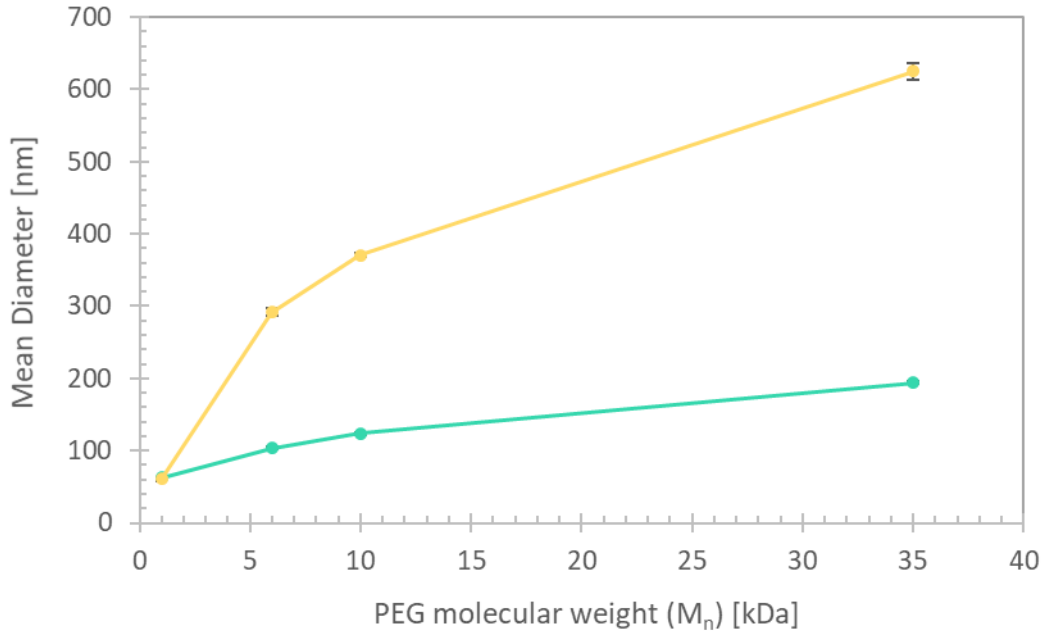

Figure 6.10: Graph of the mean diameter results obtained by DLS against the molecular weight of the corresponding PEG cryoprotectant. The green data points are for the results before the freeze-thaw process and the yellow data points are for after freeze-thaw process. Data shown are the mean values of three independent experiments and the error bars (hidden behind the diameter of the points in most cases) show the standard error of the three experiments.

As observed before, the mean diameter measured by DLS is increasing with increasing molecular weight of the PEG cryoprotectant (Figure 6.10). The mean diameters of all the PEG cryoprotectants are significantly higher after the freeze-thaw process compared to their initial state, except for the PEG1k which remains almost the same. Based on the results, the higher molecular weight PEGs not only experience higher mean diameters, they also encounter a higher degree of percentage increase of their mean diameter after the freezing step.

The rationale behind this finding is likely based on the freezing and glass transition temperatures of PEGs. The freezer temperature of -30 ºC used in this experimental investigation is remarkably lower than the freezing temperature of PEGs (Table 6.2). Although, it is very close or even higher in some cases than the glass transition temperature of PEGs (Table 6.2). When substances are above their glass transition temperature they are more viscous and rubbery compared to the glassy, rigid and brittle phase that they experience below the T_g. In this case, since the PEGs are above their glass transition temperature, the PEG molecules can still move freely in the suspension matrix, even though the sample is frozen. If the PEG molecules can move freely in the suspension, then it means that they could get into close proximity with other PEG chains in the sample and their interaction can lead to entanglements

of multiple PEG molecular chains. The higher the chain length of the PEG molecule, the more probable it is to come across other PEG molecular chains in the sample. Consequently, for higher number average molecular weight (M_n) PEGs, the likelihood of this entanglement phenomena being present increases, forming bigger lumps of entangled PEG molecules. Based on the theory discussed in section 6.3.2, PEG is acting as a coating layer around the nanoparticles when used as a cryoprotectant and a larger PEG molecular size (either in terms of R_g or υ) would result in a larger mean diameter being effectively measured by DLS. Therefore, the lumps of entangled PEG molecules would create a much thicker coating for the NP suspension when compared to lower M_n PEGs, where chain entanglement is less prominent. This thicker coating then leads to a drastically increased mean diameter measured by DLS. As a consequence, a higher percentage increase of the mean diameter for higher molecular weight PEGs after the freezing step is noticed. This is possibly the reason that some researchers claim that PEGs above 10 kDa are not as efficient cryoprotectants, since instead of reducing, they are promoting the NP aggregation (Almalik *et al.*, 2017; Umerska *et al.*, 2018; Patel, Park and Jeong, 2023).

The physical macroscopic appearance of the samples before and after the freezing and thawing process was also monitored to better understand the visible effects of the different cryoprotectants on the NP suspension. All six cryoprotectant samples and the original sample (used as the control) before the freezing step were completely clear and transparent. The picture captured in the lightbox to assess the physical appearance of all the samples after the freeze-thaw process is presented in Figure 6.11. From the image, it is noticed that the PEG35k and the PEG10k samples appear to be the haziest and cloudiest out of all seven samples. The original NP suspension appears to be hazier and cloudier compared to its initial transparent state before the freezing step. The DMSO, glycerol, PEG1k and PEG6k samples seem to remain completely clear and transparent even after the freeze-thawing process. This is another indication that these excipients are successful in preserving the properties and controlling the aggregation of the NP suspension during the freezing step of the freeze-drying process. These physical macroscopic observations are in line with the results obtained from the DLS measurements, where the larger particle sizes where obtained from the samples appearing as hazy and cloudy in Figure 6.11.

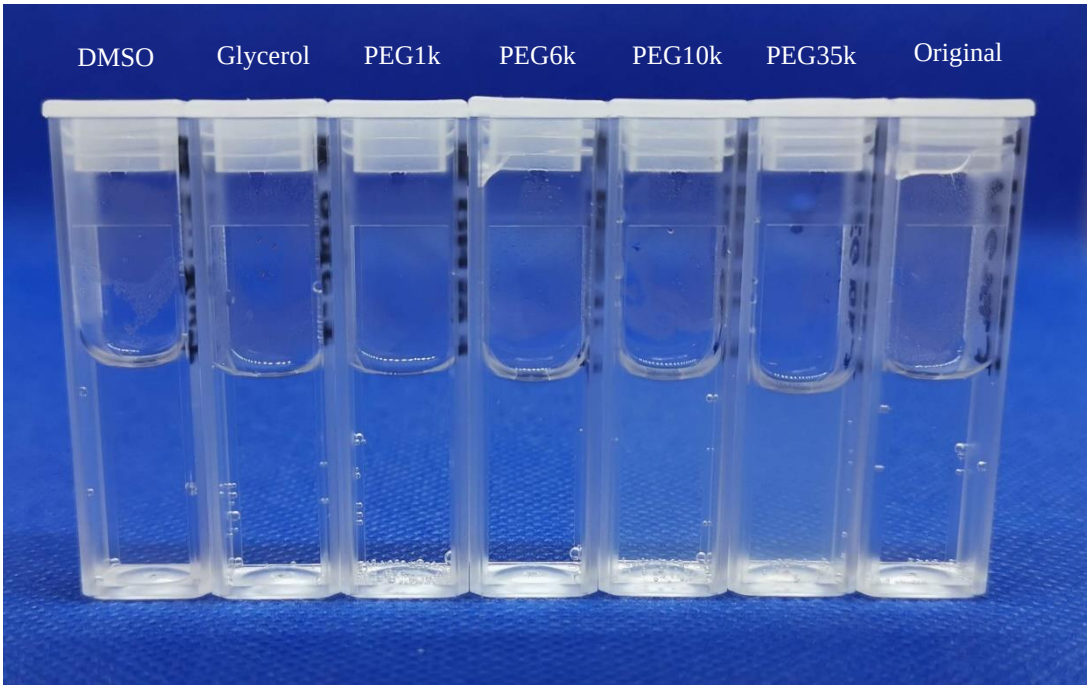

Figure 6.11: Image of all the cryoprotectant samples and the original nanoparticle suspension in the lightbox after the freezing and thawing process for physical macroscopic observation of their appearance. From left to right the samples are DMSO, Glycerol, PEG1k, PEG6k, PEG10k, PEG35k and the original (cryoprotectant-free) sample.

6.3.4. Equilibration after freezing step

The experimental results presented in section 6.3.3 for after the freezing and thawing process, were performed the same day after defrosting the samples and waiting for them to reach room temperature. The equilibration of samples at room temperature for a few days in some cases could lead to physical change, either further aggregation of the NP suspensions or either relaxation and decrease of their sizes. Therefore, to ensure that the acquired measurement results for after the freeze-thaw process are reliable and no physical change occurred, the DLS measurements of all the seven samples were repeated after a week of equilibration. The repeated DLS measurements were completed for only one batch (out of three batches) of the samples. The results obtained for particle size and PDI of the samples after equilibration are presented in Table 6.4. The results obtained for the same batch directly after the freeze-thawing process and the percentage difference between these and the equilibration results are also summarised in Table 6.4 to facilitate comparisons.

Table 6.4: Particle size and PDI data for all samples after freeze-thaw process and after equilibration.

Sample	After freeze-thaw		After equilibration		Percentage difference (%)	
	Mean diameter [nm]	**PDI**	**Mean diameter [nm]**	**PDI**	**Mean diameter [nm]**	**PDI**
Original	777.3	0.428	802.3	0.358	+3.2	-16.3
DMSO	49.7	0.145	49.6	0.151	-0.2	+4.1
Glycerol	67.6	0.079	58.9	0.108	-12.9	+36.7
PEG1k	52.3	0.174	55.6	0.172	+6.3	-1.1
PEG6k	239.3	0.142	259	0.149	+11.7	+4.9
PEG10k	368.7	0.318	379.2	0.341	+2.8	+7.2
PEG35k	651.7	0.343	652.7	0.411	+0.1	+19.7

When comparing the results of this batch for after the freeze-thaw process and after equilibration it is seen that the differences between their values are very low for all the samples examined in this study. As seen in Table 6.4, all the percentage differences calculated for the mean diameters of this batch are considerably lower than 15% meaning that there is no significant change in the mean diameters of the samples after a week of equilibration at room temperature. The PDI values percentage differences are also very low, except for the original and PEG35k samples because they are the most aggregated samples. Also, the glycerol PDI discrepancy could be related to the material's very high viscosity. However, it is not concerning since even with an increase in PDI, the value is still very low (0.108) denoting a very narrow and monodisperse particle distribution. Therefore, with this investigation the reliability of the results established for all the samples directly after the freeze-thawing process is confirmed. Also, it was verified that after a week of equilibration at room temperature, there are no physical changes occurring in the samples.

6.3.5. Freeze-dried material

The freeze-drying of all the liquid cryoprotectant-nanoparticle suspensions and the original PEG-PLA nanoparticles was performed to receive a dry material capable of prolonged storage provided that the cryopreservation of the material was successful. After following the freeze-drying procedure mentioned in section 6.2.3, the dry materials were retrieved and the physical appearance of their dry form was inspected.

It was observed that the DMSO and glycerol cryoprotectant-NP suspensions were very difficult to recover in a dry state by using freeze-drying processes. For both excipients, the complete

loss of sample during their freeze-drying was experienced multiple times. This finding was compared with information available in the literature and it was revealed that difficulties and issues in recovering materials into a dry format in the presence of DMSO have been reported multiple times (Almoustafa, Alshawsh and Chik, 2017). The reason behind the problems rising in the freeze-drying of samples containing DMSO and glycerol is based on their physical and chemical properties when in solutions with water. Both pure DMSO and glycerol have a higher freezing temperature than the temperatures used in this investigation for the freezing and the drying steps (Table 6.2). It has been reported in the literature that the intermolecular interaction of these two chemical compounds with water leads to the formation of eutectic mixtures, which means the freezing temperature of their mixture is considerably lower than the freezing temperature of the pure components that are comprising the solution (Zainal-Abidin *et al.*, 2017; Azougagh *et al.*, 2023). The eutectic mixtures formed by DMSO and glycerol with water cause an extensive depression to the freezing point of the solution (Weng, Li, *et al.*, 2011; Lomba *et al.*, 2023). The mixtures of water-glycerol and water-DMSO will solidify forming a single phase when cooled at conditions following the eutectic line of the mixture, otherwise above this line the mixture remains liquid and below this line the mixture solidifies into separate phases (Pena-Pereira and de la Calle, 2019). To achieve the sufficient freezing of the eutectic mixture, a considerably lower temperature or a longer duration of the freezing step of the freeze-drying process is required. Therefore, the loss of the product integrity of the DMSO and glycerol NP suspensions in this work is probably attributed to the phase separation of these two cryoprotectants during freeze-drying from the rest of the sample. This leads to the collapse of the NPs and the formation of aggregates adhering to the walls of the vial at the end of the freeze-drying process. Future work could focus on the optimisation of the conditions used during the freezing and the drying steps to achieve a successful recovery of the NP suspensions in a freeze-dried state when using DMSO and glycerol as cryoprotectants.

The other four PEG cryoprotectants used in this investigation have successfully produced freeze-dried materials in the applied conditions. Images of the freeze-dried materials obtained from the rest of the cryoprotectant samples (PEG1k, PEG6k, PEG10k and PEG35k) taken in the lightbox for physical macroscopic observation are shown in Figure 6.12.

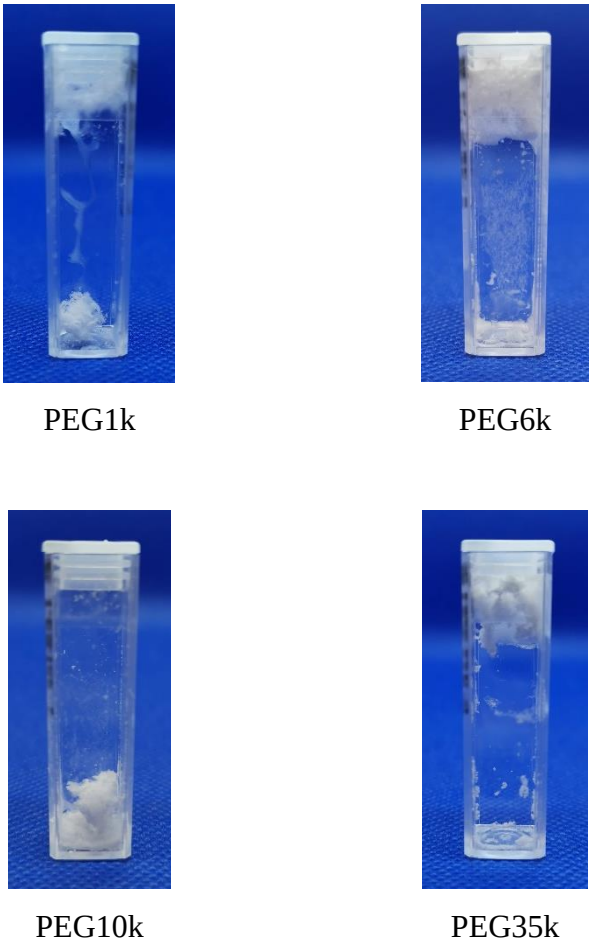

Figure 6.12: Images of the freeze-dried materials of the four PEG cryoprotectants employed in this study in the lightbox for physical macroscopic observation of their appearance.

As seen from Figure 6.12, all of the four PEG cryoprotectants used in this study have successfully freeze-dried following the procedure described in section 6.2.3. All the freeze-dried materials appear to have formed a stable white fluffy, sponge-like cake with high porosity and permeability; properties that have been proven desirable for the wettability, reconstitution solvent penetration into the cake and re-dispersibility of the freeze-dried material (Fonte *et al.*, 2014; Kulkarni *et al.*, 2018).

The freeze-dried materials obtained from the four PEG cryoprotectant NP suspensions were also analysed for their surface and structural morphology by performing their SEM characterisation. The visualisation of individual nanoparticles and their surfaces is extremely challenging in SEM. The surfaces of the NPs are expected to look comparable and indistinguishable in SEM. However, information about the NP formulation morphology and surface can be obtained by observing the larger particles and structures that are visible with

SEM. Images of the freeze-dried PEG1k, PEG6k, PEG10k and PEG35k microscopic structures obtained with SEM are presented in Figure 6.13.

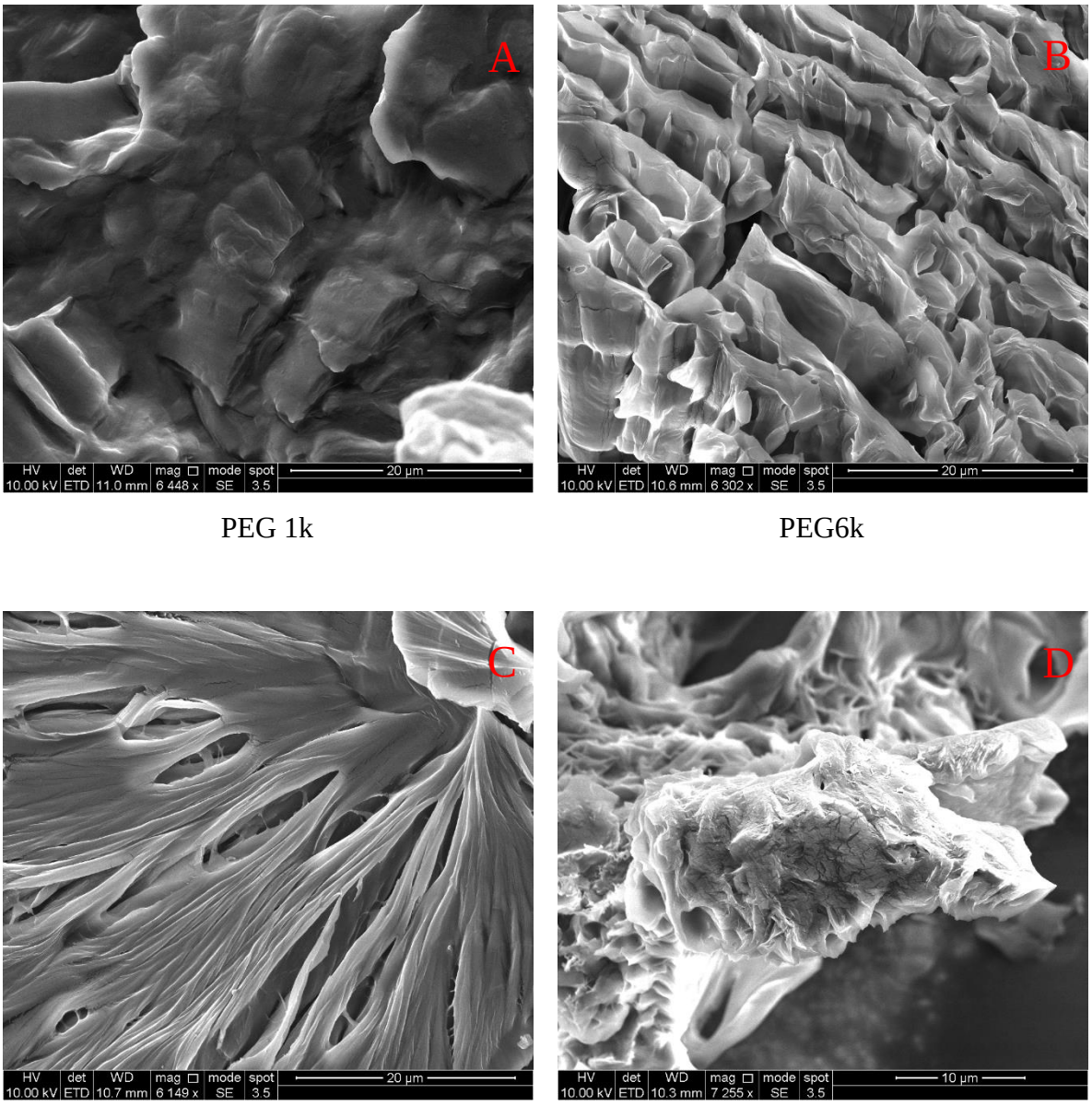

PEG 1k PEG6k

PEG10k PEG35k

Figure 6.13: SEM images of the freeze-dried materials produced from the four PEG cryoprotectants employed in this study. (A) Freeze-dried PEG1k nanoparticle suspension, (B) Freeze-dried PEG6k nanoparticle suspension, (C) Freeze-dried PEG10k nanoparticle suspension and (D) Freeze-dried PEG35k nanoparticle suspension. Scale bars: 20 µm (A, B, C) and 10 µm (D).

All freeze-dried PEG nanosuspensions form a compact sample as seen from their SEM images (Figure 6.13). This is a beneficial structure since the nanoparticles are coated and positioned inside the compact structure. Therefore, the polymeric nanoparticles are shielded away from the surface avoiding contact with surrounding conditions that could lead to sample degradation.

All PEG freeze-dried nanoparticle suspensions display some smaller microstructures under the surface of the compact structure, which could be shape dependent on the enclosed particles of the suspension. The only sample that did not display clear microstructures was the PEG10k freeze-dried nanoparticle suspension. Finally, it can clearly be observed from the SEM images of all the PEG samples that the freeze-dried materials are highly porous. This confirms the discussions from the physical macroscopic observations (Figure 6.12), where the porosity and, therefore, the permeability of the materials was noted. These structural characteristics would enhance the penetration of the reconstitution solvent leading to faster and easier re-dispersal of the freeze-dried nanosuspensions.

It is important to note that PEG is employed in this study primarily as a cryoprotectant of the nanoparticle formulation, to perform the protection of the material during the freezing step of the freeze-drying process. Its effectiveness as a lyoprotectant, controlling and reducing the disruption effects of the drying step on the polymeric nanoparticles, is probably limited compared to other highly employed lyoprotective agents found in literature.

The most commonly used lyoprotectants in the literature are different types of sugars, such as trehalose, sucrose, glucose and others (Li *et al.*, 1996; Chang *et al.*, 2005; Mensink *et al.*, 2017). The reasoning behind their wide application is their high efficiency in replacing water in the suspensions during the drying step of the freeze-drying process. The nanoparticle structure is preserved through stabilisation of the polar groups on the nanoparticle surface when they form hydrogen bonds with the lyoprotectant molecules. A process that is driven by the removal of water during the drying step (Abdelwahed *et al.*, 2006). Sugars have high glass transition temperatures, making them great cryoprotectants, since the freezing step can be carried out at a temperature below T_g leading to the formation of a glassy matrix in their presence, which increases colloidal stability (Trenkenschuh and Friess, 2021).

The successful use of PEG as a lyoprotectant was documented before in literature, meaning it is capable of acting as the replacement of water during drying, stabilising the material though hydrogen bond formation. The combination of PEG and trehalose was also performed, achieving a successful lyophilisation process with promising results (Umerska *et al.*, 2018; Mohammady, Mohammadi and Yousefi, 2020). Here, the capability of PEG to perform as a successful cryoprotectant was examined. However, its application as a functional lyoprotectant, or its combination and comparison with other lyoprotective materials was not the focus of this

research investigation and therefore was out of the scope of this experimental study. Future work could include the comparison of different molecular weight PEGs with common lyoprotectants in preserving polymeric nanoparticle structures during the drying step.

6.3.6. Reconstitution experiments

The final step of this research study was to investigate the ability of the recovered freeze-dried materials to re-disperse back in distilled water. The reconstitution time of the white fluffy cakes recovered (Figure 6.12) in water was estimated based on the procedure described in section 6.2.3. The results for the measured reconstitution times of the four PEG cryoprotectants employed in this study are presented in Figure 6.14.

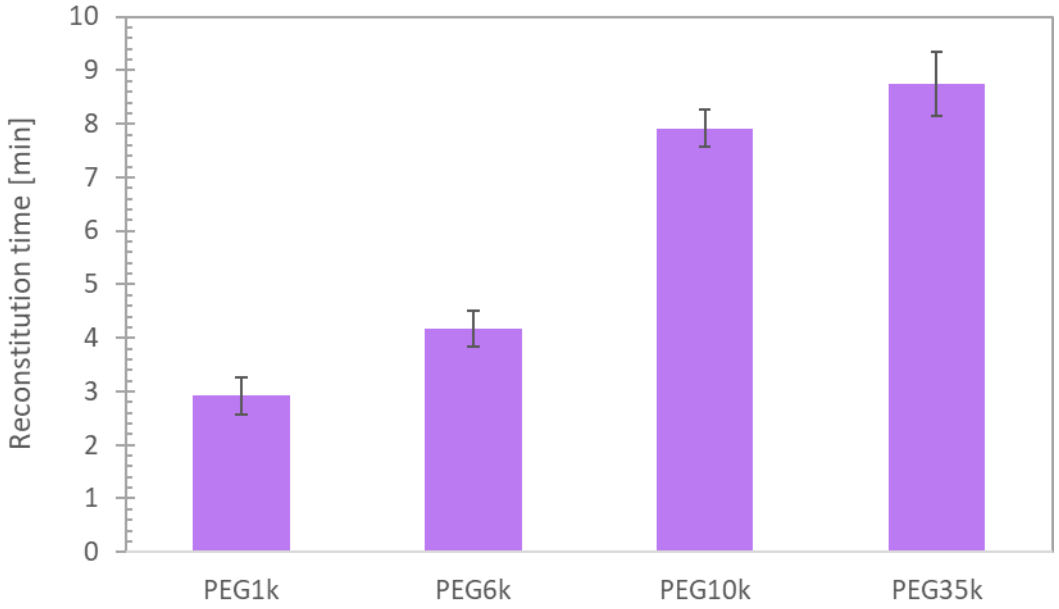

Figure 6.14: The measured reconstitution time for the re-dispersal of the four freeze-dried PEG cryoprotectant samples employed in this investigation in distilled water.

The reconstitution time of all the PEG cryoprotectant freeze-dried samples was estimated to be less than 10 mins. It is desirable to have a low reconstitution time for freeze-dried formulations to ensure a faster preparation when the drug delivery system is required. Also, the lower the reconstitution time, the safer and more reliable the administration of the pharmaceutical materials will be, with limited risks of un-suspended and aggregated particles. The reconstitution times measured in Figure 6.14 are in line with reconstitution times reported by experimental research found in the literature for cryopreserved nanoparticles (Kulkarni *et al.*,

2018; Luo *et al.*, 2021). Therefore, all the recovered freeze-dried PEG-nanoparticle suspensions have a reconstitution time within the desirable range for pharmaceutical applications.

Finally, the mean particle size and polydispersity index of the re-dispersed PEG samples was determined through DLS measurements. These results are important to assess whether the cryoprotectants employed in this investigation were able to protect the PEG-PLA nanoparticle properties from the highly strenuous freeze-drying process. The results of the mean particle size and the PDI for the reconstituted formulations are shown in Figure 6.15.

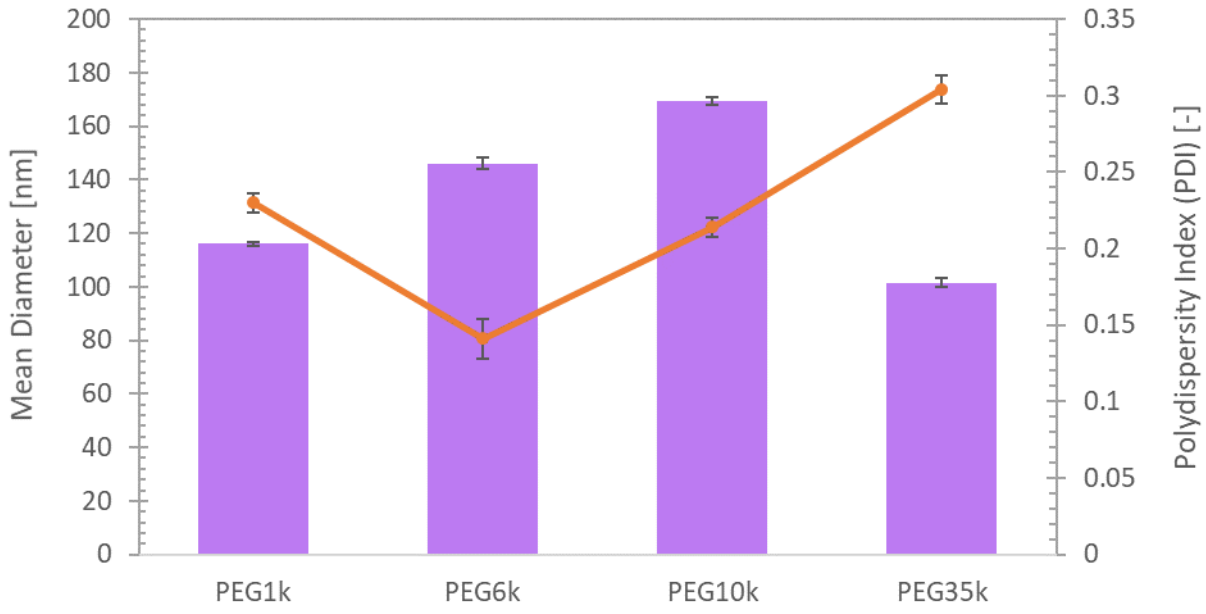

Figure 6.15: Plot of the mean diameter and the PDI results obtained via DLS for all the recovered and reconstituted freeze-dried cryoprotectants. The purple bars represent the results for the mean diameter and the orange circle data points represent the polydispersity index results. Data shown are the mean values of 5 sample runs and the error bars show their standard error.

The mean diameters of all the reconstituted cryoprotectant-NP formulations range from approximately 100-170 nm. These values are within the acceptable range that DDSs should have when aimed for pharmaceutical and clinical uses (Capasso Palmiero *et al.*, 2018). The mean diameter appears to increase with increasing molecular weight of PEG employed as cryoprotectant, with the exception of PEG35k. Also, the fact that the sizes have now returned in the acceptable NP size range, when compared to the slightly aggregated NP formulations that were measured after the freezing step (Figure 6.8), could be attributed to the re-dissolving

of the PEG free chains of the cryoprotectants after the freeze-dried material was reconstituted back in water.

The PDI values are below 0.25 for all PEG cryoprotectants, with PEG35k being only slightly higher at approximately 0.3, which means that the nanoparticle size distributions of the reconstituted formulations are relatively narrow and monodisperse. Finally, the macroscopic appearance of all four PEG cryoprotectant samples was observed to be completely clear and transparent after the re-dispersal and reconstitution of the freeze-dried materials.

Therefore, it can be concluded that the re-dispersibility of the four recovered freeze-dried PEG-nanoparticle suspensions was confirmed to be highly successful with all the PEG cryoprotectant suspensions having beneficially low reconstitution time, sensible and controlled nanoparticle size and desirably low polydispersity index after their reconstitution in water.

6.4. Conclusions

The experimental investigation presented in this work focussed on enhancing the freeze-drying process of PEG-PLA polymeric nanoparticles for an improved stability and prolonged storage capability. This is the first systematic study conducted to test the effect and performance of different molecular weight PEGs on the cryopreservation of polymeric nanoparticles. Six different cryoprotectants, DMSO, glycerol, PEG1k, PEG6k, PEG10k and PEG35k were employed to examine their ability to shield the polymeric nanoparticles during the extremely strenuous process of freeze-drying and the preservation of the formulations properties.

From the results before carrying out the freezing step, it was observed from all the PEG cryoprotectants that the mean diameter increases with increasing PEG molecular weight. This phenomenon was attributed to the free PEG chains forming a coating layer around the polymeric nanoparticles, making their effective diameter larger than the actual nanoparticle diameter. The larger the molecular PEG size, the larger the mean diameter measured by DLS.

After the completion of the freezing step, the mean diameter of the original nanoparticle suspension increased dramatically. This observation confirmed the necessity for the addition of a cryoprotective agent in the nanoformulation to protect polymeric nanoparticles from the mechanical stresses involved in the freezing step and ice crystal formation, which cause

disruptions to the nanostructures. The use of a cryoprotectant acts as a shield for the nanoparticle properties, which is required for a safe and reliable final pharmaceutical product with a robust stability for prolonged storage.

The results obtained for both before and after the freezing step suggest that the best performing excipients for cryopreservation are DMSO, glycerol and PEG1k, which are perfect representatives of the original nanoparticle suspension sizes and preserve a low PDI.

Looking at the results for the four different PEG cryoprotectants after the freeze-thawing process it is observed that not only does the mean diameter of the suspension increase with increasing molecular weight, but also the percentage difference between the before and after measurements increases. This is believed to be related to the glass transition temperature of PEG, which is very close or even lower than the temperature applied during the freezing step. Thus, PEG chains are moving freely in the frozen sample potentially interacting with other PEG chains forming aggregates. These results indicate that higher M_n PEGs are not as effective cryoprotectants of polymeric suspensions during the freezing step.

The reliability of the results of all the samples after the freeze-thawing process was confirmed and it was verified that after a week of equilibration at room temperature that there was no physical change occurring in the samples. Moreover, the physical macroscopic observations were always in agreement with the results obtained from DLS measurements.

When conducting the freeze-drying of all the samples, it was discovered from literature that DMSO and glycerol form eutectic mixtures with water, which cause an extensive depression to the freezing point of the solution leading to material recovery difficulties. To achieve the sufficient freezing of the eutectic mixture, a considerably lower temperature or a longer freezing step duration in the freeze-drying process is required. The four PEG cryoprotectants have successfully formed freeze-dried materials with the desirable physical characteristics as detected from the physical macroscopic observation and SEM imaging of the samples.

Finally, it was concluded that the re-dispersibility of the four PEG NP suspensions was verified to be very efficient, since all of them have a favourably low reconstitution time, a practical and controlled mean diameter and a desirably low polydispersity index after their full reconstitution in water.

7. Experimental evaluation of the encapsulation capacity of PEG-PLA block copolymers using a model chemotherapy drug

7.1. Introduction

The investigation of amphiphilic block copolymers with the aim of forming an effective drug delivery system (DDS) for cancer chemotherapy treatments has been the focus of this thesis. The synthesis of a library of methyl-poly(ethylene glycol)-*block*-poly(lactide) (mPEG-PLA) diblock copolymers with varying polymer properties was performed in Chapter 4 and Chapter 5. The investigation of the self-assembly of these materials into polymeric nanoparticles and micelles using different formulation methodologies and varying key processing conditions was studied in depth. Their prolonged stability and storage was successfully enhanced with the implementation of different cryoprotective agents during the systematic study performed in Chapter 6. Here, the chapter emphasis lies on the examination of the effectiveness of these diblock copolymers in encapsulating a hydrophobic drug inside the polymeric nanoparticle structure.

Since the synthesised mPEG-PLA diblock copolymers are intended for DDS of antineoplastic drugs and their delivery to the cancerous tissue, their encapsulation efficiency and drug loading capacity evaluation is required (Dora *et al.*, 2010). The effectiveness of the produced polymeric nanoparticles as nanocarriers for anticancer drugs will be evaluated based on two main criteria. First, their ability to incorporate a highly hydrophobic drug within the hydrophilic corona of the nanoparticle. Second, the successful creation of a nanoparticle suspension with controllable average size and particle size distribution. These two criteria will indicate the success of the final polymeric nanoparticle product.

The encapsulation of the hydrophobic drug within the structure of polymeric nanoparticles is driven by physical and chemical interactions occurring during the formulation procedure. As encountered before in this thesis (Chapter 5), the amphiphilic block copolymers self-assemble into polymeric nanoparticles when present in aqueous environments. The association of the polymer chains is caused by the repelling interactions of the hydrophobic block of the copolymer with the aqueous selective solvent. The self-organisation of the copolymer chains into polymeric nanostructures is based on the effort of the hydrophobic parts of the polymer to minimise the interfacial free energy of the system (Park *et al.*, 2008). When a hydrophobic

molecule is incorporated into the polymer self-assembly process, the repelling interactions between the hydrophobic drug and water and the favourable interactions between the polymer chains and the free drug molecules would lead to drug encapsulation. The formed suspension is composed from nanoparticles with drug molecules packed inside their hydrophobic core, surrounded by a hydrophilic corona protecting the drug from aqueous interactions. The encapsulation of hydrophobic substances within polymeric nanoparticles, specifically micelles in this case, is presented schematically in Figure 7.1.

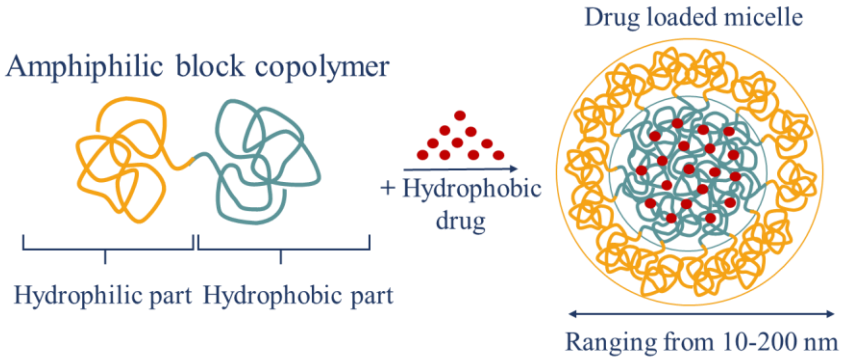

Figure 7.1: Schematic diagram presenting the encapsulation procedure of a hydrophobic drug inside the hydrophilic corona of a polymeric nanoparticle, through the self-assembly of amphiphilic block copolymers.

7.1.1. Aim

The main focus of the research presented in this chapter was the evaluation of the effectiveness of the mPEG-PLA diblock copolymer library synthesised in performing as a successful DDS for cancer chemotherapy by encapsulating a hydrophobic model drug within the constructed polymeric nanoparticles.

7.1.2. Objectives

The objective is to perform the encapsulation of the chosen model drug (Nile red) by employing all six diblock copolymers of mPEG-PLA produced in Chapter 5. The encapsulation experiments of Nile red are completed via the nanoprecipitation procedure. The block copolymer final concentration in suspension is varied to assess its influence on Nile red encapsulation. The challenging separation of the nonencapsulated Nile red from the rest of the drug loaded nanoparticle suspension is addressed with the employment, testing and comparison of three different solvents performing the extraction of Nile red. The construction of a

concentration vs absorbance plot is conducted to calibrate the UV-visible (UV-vis) equipment used for the determination of the Nile red non-loaded amount. Finally, the encapsulation of the model drug is quantified through the measurement of the encapsulation efficiency (EE%) and the drug loading capacity (LC%) of each of the drug loaded nanoparticle suspensions constructed.

7.2. Encapsulation methodology

7.2.1. Material information

The polymer materials investigated for their encapsulation capabilities in this work, are the diblock copolymers synthesised and characterised in Chapter 5. As seen in section 5.3.1, the produced polymers are varying in structural parameters, such as total molecular weight, the two block lengths, block volume fractions and the hydrophilic-to-hydrophobic ratio. Therefore, the study of this polymer library would enable the exploration of the effect that all these key polymer parameters have on the drug loading effectiveness of the constructed polymeric nanoparticles. The main properties of the six employed diblock copolymers of mPEG-PLA in this investigation are summarised in Table 7.1.

Table 7.1: Key properties of the investigated mPEG-PLA diblock copolymer library.

Polymer	**Hydrophobic to hydrophilic ratio**	**Volume fraction of block A (f_A)[a]**	**Molecular weight of block A (M_A) [kDa]**	**Molecular weight of block B (M_B) [kDa]**	**Total molecular weight (M_n) (GPC) [kDa][b]**
mPEG5k-*b*-PLA5k	1	0.53	5	7.24	12.24
mPEG5k-*b*-PLA10k	2	0.36	5	9.24	14.24
mPEG5k-*b*-PLA20k	4	0.22	5	11.22	16.22
mPEG2k-*b*-PLA2k	1	0.53	2	4.03	6.03
mPEG2k-*b*-PLA4k	2	0.36	2	5.67	7.67
mPEG2k-*b*-PLA8k	4	0.22	2	8.93	10.93

[a]Block A is the mPEG block and block B is the PLA of the diblock copolymer.
[b]Measured by GPC, compared to PMMA standards.

Nile red is the hydrophobic model drug employed in this study to mimic the properties, interactions and distribution that chemotherapy drugs would experience in the polymeric nanoparticle suspension. Nile red is a fluorescent chemical substance regularly used in biological and pharmaceutical research areas as a dye to promote faster detection and

quantification of the product (Halim and Webley, 2015; Rumin *et al.*, 2015; Teo *et al.*, 2021). By staining the area of research focus, the characterisation of the final product becomes significantly easier. This is an extensively applied procedure in the literature for rapid identification and evaluation of samples for numerous applications (Maes *et al.*, 2017; Kang *et al.*, 2020; Nalbone *et al.*, 2021). Therefore, the use of a compound that fluoresce brightly was identified as extremely valuable for the characterisation of the encapsulation properties of the diblock copolymers.

Nile red has unique fluorescence properties, which vary depending on the polarity of the solvent that is dissolved in. Upon excitation, typically in the blue-to-green range (~488–540 nm), Nile red emits in the yellow-to-red range (~570–650 nm) in non-polar environments, with intensity and emission wavelength shifting based on the solvent polarity. In polar solvents, such as water, Nile red fluorescence is significantly quenched, resulting in weak or negligible emission (Greenspan, Mayer and Fowler, 1985). These properties and its solvatochromic behaviour allow for highly sensitive detection in hydrophobic environments, making Nile red highly valuable for visualising and quantifying the encapsulation of hydrophobic materials within polymeric nanoparticles in drug delivery research. In addition, Nile red is a highly hydrophobic material with low aqueous solubility making it an ideal model drug to mimic the effects that the anticancer drugs would have in the nanoparticle formulations produced in this work.

UV-vis spectroscopy is an effective method commonly used for determining the content of Nile red in samples due to the simplicity and accessibility of the process. Nile red has a strong absorbance in the visible region, with a characteristic peak typically around 550–570 nm depending on the solvent environment, which allows for fast and easy detection (Erlebach et al., 2016; Ho et al., 2020). In this study, DMSO is used as the solvent containing Nile red for the UV-vis measurements, with an absorbance peak at around 552 nm. By measuring the absorbance at this wavelength, a calibration curve can be developed using a series of known Nile red concentrations. This calibration curve allows for accurate determination of unknown concentrations by correlating the measured absorbance values with concentration (Ho et al., 2018). This method is particularly useful for analysing Nile red in homogeneous solutions, typically obtained in hydrophobic solvents, where the absorbance properties are stable and consistent. Based on these characteristics, UV-vis spectroscopy is chosen as the

characterisation technique to act as an effective and rapid method for quantifying Nile red in solutions.

7.2.2. Encapsulation experiments

The encapsulation of Nile red was performed through the self-assembly of the amphiphilic diblock copolymers into polymeric nanoparticles by applying the nanoprecipitation process. Further details of the exact procedure followed to formulate the nanoparticles with loaded drug within their structure is presented in Chapter 3, section 3.5.1. Briefly, the Nile red was dissolved in the oil phase (acetonitrile) with the amphiphilic polymer and the solution was nanoprecipitated in the aqueous solvent (water) following the same procedure and applying the same conditions as in previous chapters. The final concentration of the diblock copolymers was varied from 0.1-0.2wt% to examine if this could lead to higher encapsulation of the model drug.

7.2.3. Encapsulation process evaluation

As discussed in section 3.5.2 of Chapter 3, the effectiveness of the polymeric nanoparticles as a DDS, in terms of incorporating a model drug, was assessed using two key metrics commonly used in the literature. Firstly, the encapsulation efficiency (EE%), which measures the proportion of the drug successfully captured and contained within the nanoparticle structure relative to the initial drug quantity used in the experiment (Pignatello *et al.*, 2001), was calculated using Equation 3.1. Secondly, the drug loading capacity (LC%), reflecting the weight of the drug encapsulated relative to the total weight of the drug-loaded system, including the weight of both the polymeric nanoparticles and the encapsulated drug (Govender et al., 1999), was estimated with Equation 3.2.

The quantity of drug encapsulated within the polymeric nanoparticles was indirectly determined by measuring the amount of drug that remained unencapsulated. The unencapsulated Nile red was separated from the nanoparticle suspension using the methodology described in section 7.2.4. The extracted model drug was then quantified using UV-visible spectrophotometry using the methodology presented in section 7.2.5. The drug loaded within the nanoparticles was calculated by deducting the quantity of drug that was not encapsulated from the total drug amount initially used in the experiment.

7.2.4. Drug-loaded nanoparticles separation

Once the encapsulation procedure is completed the final sample produced is a mixture of drug loaded polymeric nanoparticles in suspension and Nile red aggregates either in suspension or on the vial walls. The direct characterisation of this sample using UV-visible spectroscopy is not possible since this would lead to unreliable and fluctuating results based on the presence of bigger aggregates (microscale) inside the nanoparticle suspension. Therefore, an indirect characterisation method has to be employed, where the unencapsulated Nile red is separated and characterised to gather information on the amount of Nile red loaded within the polymeric nanoparticles.

The separation of Nile red from the rest of the product also leads to challenges since the separation method applied could result in detrimental effects on the nanoparticle suspension. Filtration of the sample was tested and proven to be ineffective since all the Nile red aggregates deposit on the filter, making it impossible to recover, re-dissolve, characterise and quantify. The application of a dialysis method is extremely time consuming since it is driven by diffusion, requiring the dialysis experiment to run for days in order to reach a high efficiency separation process (de Castro, Capote and Ávila, 2008; Luo *et al.*, 2011). On the other hand, the use of centrifugation as a method of separation, based on the size differences of the Nile red aggregates and the drug-loaded nanoparticles, is a fast process and seems appealing in theory. Although, the nanoparticle suspensions prepared are considered highly fragile structures and since they are intended for biomedical applications their integrity is required to remain intact. Therefore, an intense process such as centrifugation with the high speeds, significant shear forces and heat accumulation could lead to physical damage and aggregation of the drug-loaded nanoparticles (Vauthier, Cabane and Labarre, 2008; Ciria *et al.*, 2021).

In this experimental investigation, the use of three different solvents for the separation of Nile red from the rest of the nanoparticle suspension was performed. During the search for solvents that would be more ideal for the extraction of the nonencapsulated Nile red, a number of conditions were identified to guide the selection. The requirements that should be satisfied by the chosen extraction solvent are the following:

- Good solvent for Nile red, offering a high solubility for the aggregated particles
- Immiscible with water (nanoparticle suspension medium), to form two separate liquid layers

- Non solvent for the mPEG-PLA copolymers, to avoid interactions between extraction solvent and polymeric nanoparticles, ensuring the latter's integrity
- Either miscible with the solvent used for UV-vis characterisation (dimethyl sulfoxide - DMSO), to form a homogeneous solution, or highly volatile, to remove before DMSO is added to re-dissolve and analyse the non-loaded Nile red

In the search of solvents that would be effective as extraction mediums of the unloaded Nile red, four solvents that satisfy the requirement listed above were discovered. These are ethyl acetate, diethyl ether, heptane and hexane. Hexane is expected to have a very similar solvency ability with heptane based on similar chemical and physical properties between the two solvents and since it is highly hazardous and toxic compared to the rest of the materials identified, it was eliminated from the experimental investigation. The rest of the three solvents were tested for their ability to perform the extraction of Nile red aggregates from pure water. The extraction solvent that performed the best in this trial was employed as the solvent used for the separation of the unencapsulated Nile red in the produced nanoparticle suspensions.

7.2.5. Unloaded drug quantification

To determine the amount of non-encapsulated model drug, UV-vis spectroscopy was used for the characterisation of the extracted Nile red from the nanoparticle suspensions in a pre-determined volume of DMSO. The concentration of the model drug in DMSO solution was established based on a calibration curve developed from the absorbance measurements of Nile red-DMSO solutions of known concentrations.

DMSO was used as the UV-vis characterisation solvent out of all the solvents that were tested for solubilising Nile red (DCM, ethanol, heptane, ethyl acetate, diethyl ether, acetonitrile). This solvent was chosen because the fluorescent dye experiences a very high solubility in DMSO, producing a strong and bright fuchsia sample, which would facilitate the quantification of Nile red even at very low concentrations.

For the construction of the calibration curve a total of nine different of concentrations of Nile red in DMSO solution were characterised and analysed through UV-vis spectroscopy. The concentrations were ranging from 0.0001-0.005wt% of Nile red in DMSO. The process of

preparing the Nile red-DMSO solutions of nine different concentrations and analysing them by UV-vis spectroscopy was performed in triplicate to ensure the reliability of the calibration curve developed. This calibration curve was then used to establish the amount of non-loaded and successfully extracted Nile red in the unknown concentration samples at a fixed DMSO volume. Then, through the subtraction of the established value from the initial Nile red amount used for the encapsulation experiment, the total amount of encapsulated model drug within the polymeric nanoparticles was determined.

7.2.6. Characterisation analysis techniques

In this section, the characterisation techniques performed to analyse the materials constructed from the encapsulation experiments and their properties are summarised. Further details about the characterisation techniques, the equipment utilised to perform these analyses and the measurement procedures can be found in Chapter 3.

Dynamic light scattering (DLS): This characterisation technique was used to establish information about the nanoparticle size distribution and the polydispersity index (PDI) of the nanoparticle population present in the samples. The DLS equipment used is the Brookhaven ZetaPALS (2008). The measurements were completed at room temperature (25 ºC). The samples were equilibrated at 25 ºC in the equipment cuvette chamber prior to measurement. Each measurement consisted of 5 runs of the same sample.

Zeta potential (Z-potential) analysis: The zeta potential (ζ) of the Nile red loaded nanoparticle suspensions prepared was measured using the Brookhaven ZetaPALS Zeta Potential Analyser (2008). The measurements were completed at room temperature (25 ºC). The samples were equilibrated at the measurement temperature in the equipment cuvette chamber prior to measurement. Each measurement consisted of 5 runs of the same sample.

Ultraviolet-visible (UV-vis) spectroscopy: This analysis technique was used in this work to the determine the concentration of the Nile red model drug that was not loaded into the polymeric nanoparticles. Initially, the construction of a calibration curve, which plots the absorbance vs the concentration, of the Nile red model drug in the solvent of DMSO was performed. The UV-vis spectra were measured using the Genesys 150 UV-visible spectrophotometer (ThermoScientific, UK) using plastic disposable cuvettes. The

measurements were completed at 552 nm and at room temperature (25 ºC). The samples were equilibrated at the measurement temperature in the equipment cuvette chamber for 60 secs prior to measurement. Each sample was measured a total of 6 times.

Statistical analysis: Unless otherwise stated, all results are expressed as the mean value ± standard error (SE). All methodologies were conducted in three independent experimental procedures. The mean values and the standard errors were estimated from analysis of the three independent experimental procedures.

7.3. Results and discussion

7.3.1. Nile red calibration curve

For determining the weight of Nile red present in unknown concentration samples at fixed volumes of DMSO, the development of a concentration vs absorbance calibration curve is required. In total, nine samples of varying concentrations in the range of 0.0001-0.005wt% were measured for their absorbance through UV-vis spectroscopy.

In the literature, the wavelength used for measuring the absorbance of Nile red in DMSO was 550 nm (Ho *et al.*, 2018). To determine where in the wavelength spectrum the prepared samples of known concentrations experience the maximum absorbance, a scan measurement at a wavelength range of 400-700 nm was performed. The results obtained for the 5 highest concentrations of Nile red in DMSO prepared can be seen in Figure 7.2.

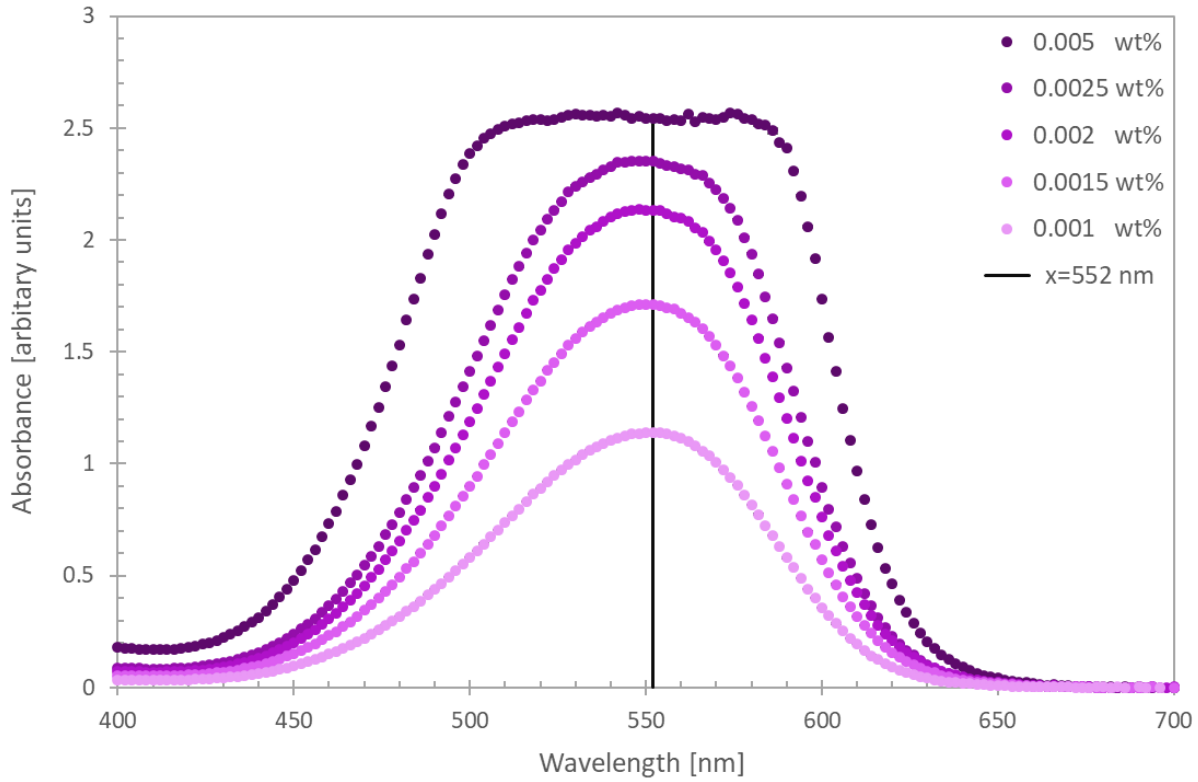

Figure 7.2: Absorbance vs wavelength results for the 5 highest concentration samples of Nile red in DMSO prepared for the calibration curve development. The x = 552 nm line, which is the highest absorbance experienced by all samples, is incorporated in the plot.

From the presented data in Figure 7.2, it can be observed that the highest absorbance of the samples is experienced at 552 nm, which is in agreement with the wavelengths used usually in the literature for the Nile red in DMSO absorbance (Ho *et al.*, 2018). In addition, from Figure 7.2, it is very clear that the highest concentration of Nile red-DMSO sample prepared (0.005wt%) has saturated the UV-vis detector. Therefore, it is expected that these absorbance results are not reliable and do not represent the real concentration of Nile red present in the sample, and they are eliminated from the construction of the calibration curve.

Based on the results gathered from Figure 7.2, the construction of the Nile red calibration curve in DMSO was performed by measuring the absorbance of the known concentration samples at a wavelength of 552 nm. The results collected from the UV-vis analysis of the prepared concentrations are presented in Figure 7.3. The axis origin point (0,0) is also included in the plot since the concentration vs absorbance plot established should be a line passing through the axis origin. This represents the absorbance of a sample of pure DMSO (blank sample used as reference), which is equal to zero since no Nile red is present in the sample.

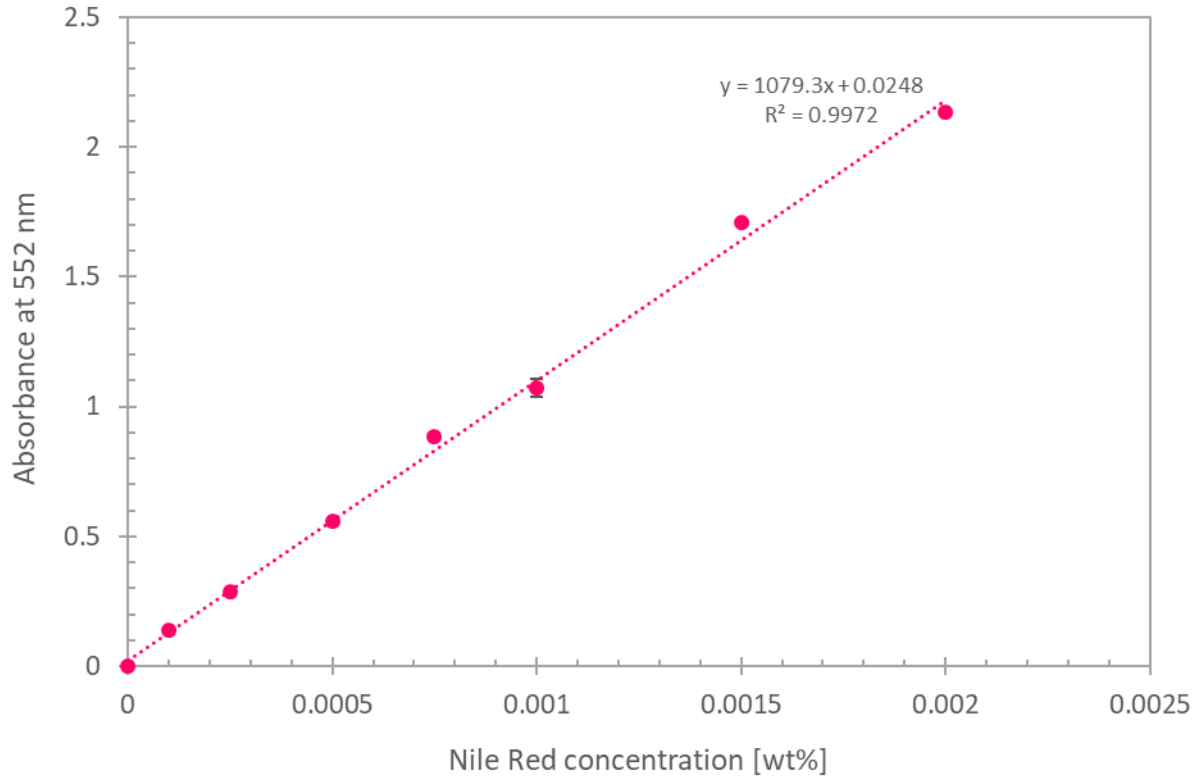

Figure 7.3: Plot of the absorbance at 552 nm vs the Nile red known concentration in DMSO, forming the calibration curve used for the determination of the unloaded drug amount of encapsulation experiments. Data shown are the mean values of three independent experiments and the error bars show the standard error of these three experiments.

The calibration curve presented in Figure 7.3 was employed for the quantification of the non-loaded drug from the encapsulation studies. A linear trendline fitting the measured data is presented, including the linear function equation and the R^2 of the line. The linear function equation is used to determine the unencapsulated drug quantity. The R^2 is considerably close to 1, meaning the linear fitting of the trendline has a high accuracy for the plotted data points.

7.3.2. Nile red extraction

Three different solvents were tested for their ability to extract Nile red from the drug-loaded nanoparticle suspensions as discussed in section 7.2.4. To test their ability as extraction solvents, samples containing Nile red aggregates were employed. The addition of each of the extraction solvents in corresponding Nile red-water sample vials and the mixing of the mixtures was performed. After this, the top layer of the mixture, organic solvent with dissolved Nile red, was extracted. The extracted solution was diluted with DMSO and analysed via UV-vis

spectroscopy and the developed calibration curve, to establish the amount of Nile red extracted for each of the investigated extraction solvents. Finally, their retrieval efficiency was calculated based on the amount of Nile red extracted and the initial amount that was aggregated into water.

The results obtained for the retrieval efficiencies of the three extraction solvent employed in this investigation are presented in Table 7.2.

Table 7.2: Retrieval efficiency of the three employed extraction solvents

Extraction solvent	Nile red retrieval efficiency (%)
Ethyl acetate	94
Diethyl ether	95
Heptane	83

From Table 7.2, it can be seen that ethyl acetate and diethyl ether are better performing extraction solvents compared to Heptane. Out of the two solvents, the one that was selected as the extraction solvent for the encapsulation experiments performed in this investigation, was the diethyl ether. The rationale behind this selection is based on the fact that it is very well known from the synthesis experiments performed in Chapter 4 and Chapter 5 that diethyl ether is a strong non solvent for both PEG and PLA blocks of the copolymer. This property would ensure that the interaction of the mPEG-PLA diblock copolymers would be avoided entirely, leading to the sustained integrity of the polymeric nanoparticles during and after the completion of the extraction process.

The extraction of the Nile red not encapsulated was performed for all the samples prepared from the encapsulation experiments using diethyl ether. The resultant extracted Nile red-DMSO sample was characterised through UV-vis measurement at 552 nm, which is the maximum absorbance across the wavelength spectrum. As an example, the scan measurement of the extracted Nile red from all block copolymer nanoparticle suspensions, prepared with a final concentration of 0.1wt%, in the wavelength range of 400-700 nm is presented in Figure 7.4. From these results, the effectiveness of diethyl ether to separate and extract the aggregates of unencapsulated Nile red from the drug-loaded nanoparticle suspensions has been proven.

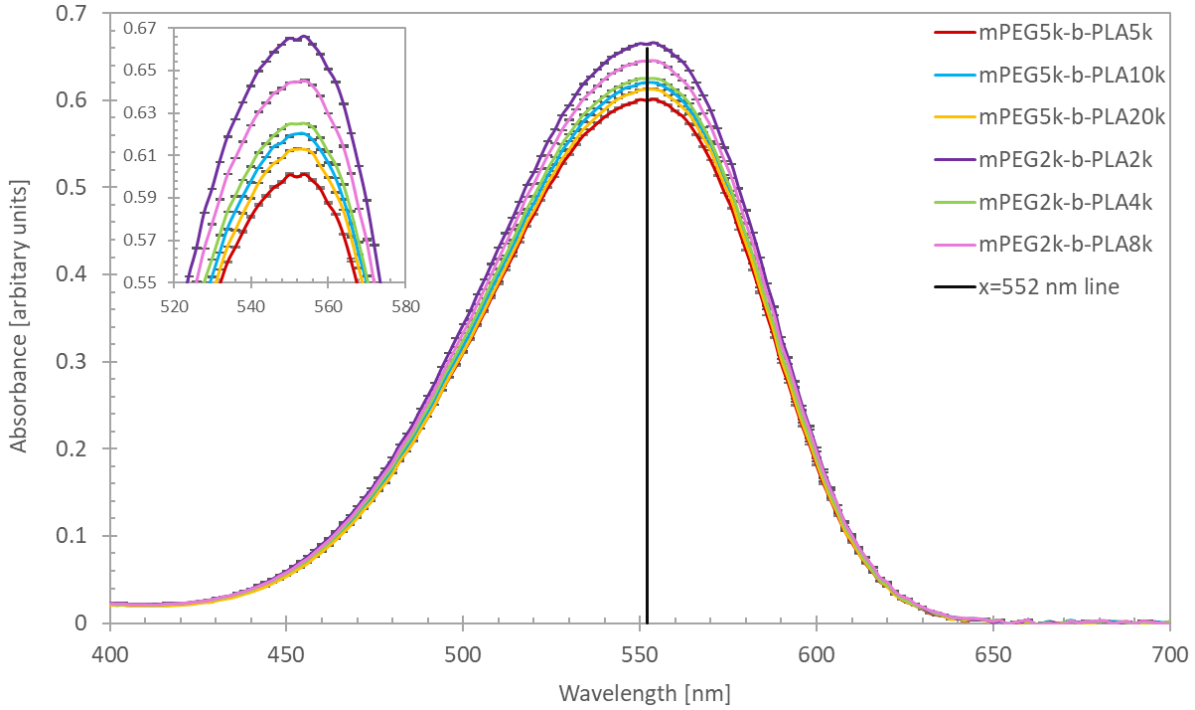

Figure 7.4: Absorbance vs wavelength results for the extracted non-loaded Nile red from all the mPEG-PLA diblock copolymer drug-loaded nanoparticle suspensions prepared at a 0.1wt% final concentration. Nile red is dissolved in a fixed volume of DMSO. The x = 552 nm line, which is the highest absorbance experienced by all samples, is incorporated in the plot.

7.3.3. Encapsulation efficiency

The encapsulation experiments were performed by employing the nanoprecipitation technique as the self-assembly procedure of the diblock copolymers investigated in this work. The nanoprecipitation was performed with the aim of forming drug-loaded nanoparticle suspensions with varying final concentrations of the diblock copolymer in the final formulation. The goal was to determine whether the presence of more polymeric material self-assembling into nanoparticles can also enhance the encapsulation efficiency and drug loading capacity of the formulated drug-loaded nanoparticle suspensions.

The encapsulation efficiency of all the nanoprecipitation-encapsulation experiments completed was determined by applying the calculation method described in section 7.2.3. The results obtained from all the diblock copolymer materials and the three different final concentrations employed are presented in Figure 7.5.

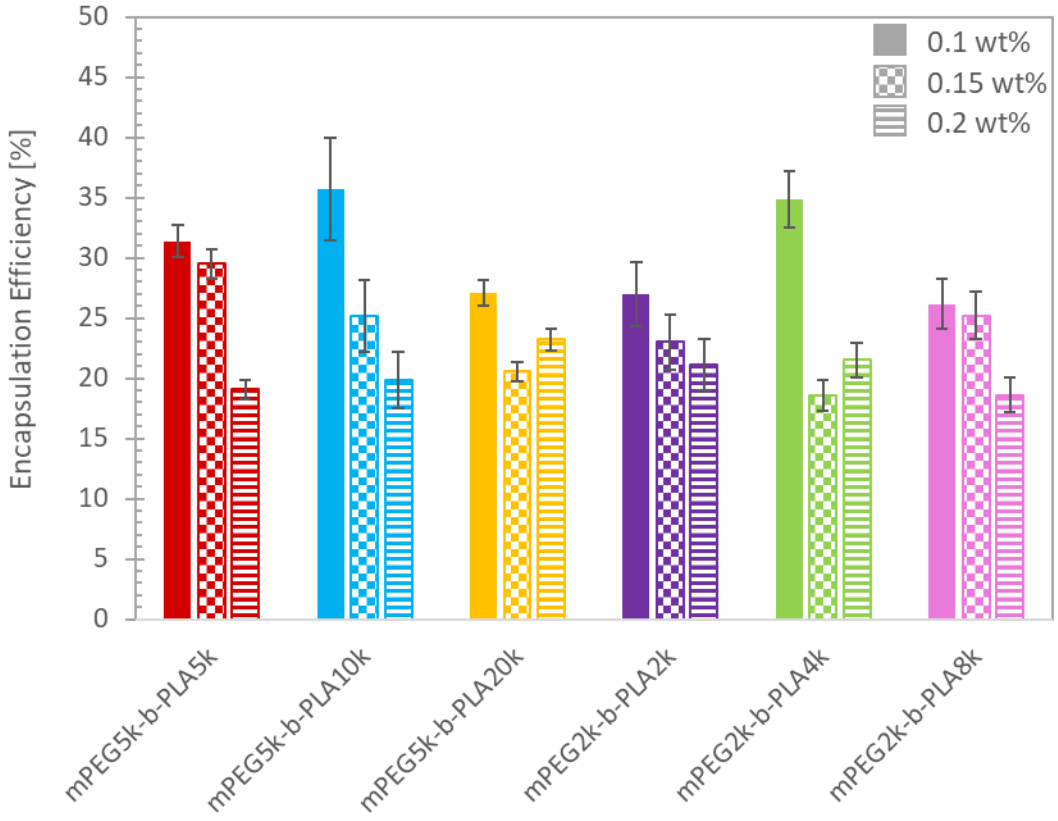

Figure 7.5: Plot of the calculated encapsulation efficiency percentage with respect to the six different diblock copolymers of mPEG-PLA studied in this work at three different final polymer concentrations. Data shown are the mean values of three independent experiments and the error bars show the standard error of these three experiments.

From the results presented in Figure 7.5, it can be observed that the encapsulation efficiency, in general, it decreases with increasing final concentration of diblock copolymer in the nanoparticle formulation. This finding is related probably to the increased polymer-polymer interactions when the concentration of the diblock copolymer is increased and the amount of the model drug remains fixed. Moreover, at higher concentrations of diblock copolymer, the entanglement of polymer chains occurs more frequently since the polymer coils are closer in proximity. Polymer chain entanglement can physically hinder the encapsulation of a drug within the enclosed structure of a polymeric nanoparticle during the self-assembly procedure.

There is no significant correlation between the different diblock copolymers employed in this study and the calculated encapsulation efficiency as seen from Figure 7.5. This suggests that the encapsulation efficiency does not have a strong dependency on the properties of the diblock copolymer employed. Therefore, the Nile red model drug interacts in a similar way with all six different mPEG-PLA block copolymers.

The encapsulation efficiencies established for the encapsulation experiments performed in this work are ranging from 20-36% for all the materials and conditions applied. These results were compared with values of encapsulation efficiencies obtained in the literature for similar nanoparticles and materials. In Van Gheluwe *et al.* (2023) for mPEG-PLA nanosystems they were able to obtain Nile red encapsulation efficiencies of 25% on average at a polymer concentration of 0.4wt%. This is comparable with the results obtained here, with the encapsulation efficiencies acquired in this research reaching slightly higher values in some cases. Compared to Prasad *et al.* (2017), the encapsulation efficiencies established here are approximately 20% higher, on average, from the results they obtained for Nile red encapsulation. The same was observed for the results collected from Erlebach *et al.* (2016), where they have received an encapsulation efficiency of approximately 3% for PEG-PLA nanoparticles compared to the 20-36% that was established in this research investigation. Therefore, the encapsulation procedures followed in this work have achieved higher encapsulation efficiencies of Nile red model drug compared to multiple studies in the literature with the use of same materials.

7.3.4. Drug loading capacity

The drug loading capacity of all the nanoprecipitation-encapsulation experiments completed were determined by applying the methodology described in section 7.2.3. The results obtained from all the diblock copolymer materials and the three different final concentrations employed are presented in Figure 7.6.

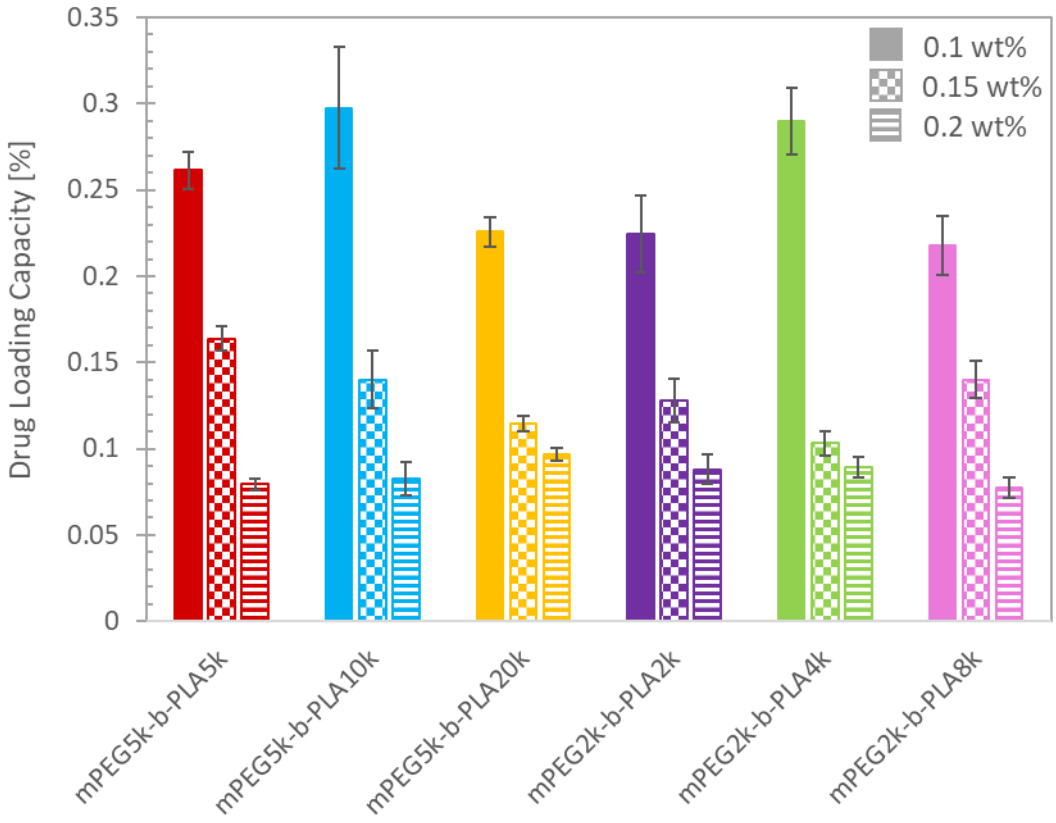

Figure 7.6: Plot of the calculated drug loading capacity percentage with respect to the six different diblock copolymers of mPEG-PLA studied in this work at three different final polymer concentrations. Data shown are the mean values of three independent experiments and the error bars show the standard error of these three experiments.

As observed in Figure 7.6, the drug loading capacity percentage decreases with increasing concentration for all the diblock copolymers. This is expected based on the equation used to determine the drug loading capacity (Equation 3.2), where the weight of the encapsulated Nile red is divided by the total weight of the polymeric nanoparticle. Therefore, the weight of the polymeric nanoparticles in solution increases with the increasing concentration and the calculated drug loading capacity decreases.

As with the encapsulation efficiency, there is no clear correlation between the different diblock copolymers employed in this study and the calculated drug loading capacities as presented in Figure 7.6. This indicates that the values obtained for the drug loading capacity of the polymeric nanoparticles do not follow a specific trajectory with the properties of the diblock copolymer employed. Thus, the Nile red dye interacts in a similar way with all six different mPEG-PLA block copolymers at the conditions and processing parameters employed during the encapsulation process.

The drug loading percentages range from approximately 0.1-0.3% for all the diblock copolymers and all the concentrations employed. These values may seem low, but this is caused by the weights of the block copolymers used in the experiments, which are higher when compared to the amounts of the model drug used in the encapsulation experiments. Also, based on the calculation method for the determination of this parameter is more probable to have a low drug loading capacity. Significantly low percentages of drug loading capacities are observed throughout the literature due to these reasons (Chu *et al.*, 2016; Ho *et al.*, 2020).

7.3.5. Drug loaded nanoparticles mean diameter

The mean diameter of the drug-loaded nanoparticles produced during the encapsulation experiment performed via the self-assembly of the different diblock copolymers through nanoprecipitation, was determined from the characterisation of the final product with DLS measurements. The results obtained for the average drug-loaded nanoparticle size from all the diblock copolymer materials and the three different final concentrations employed are presented in Figure 7.7.

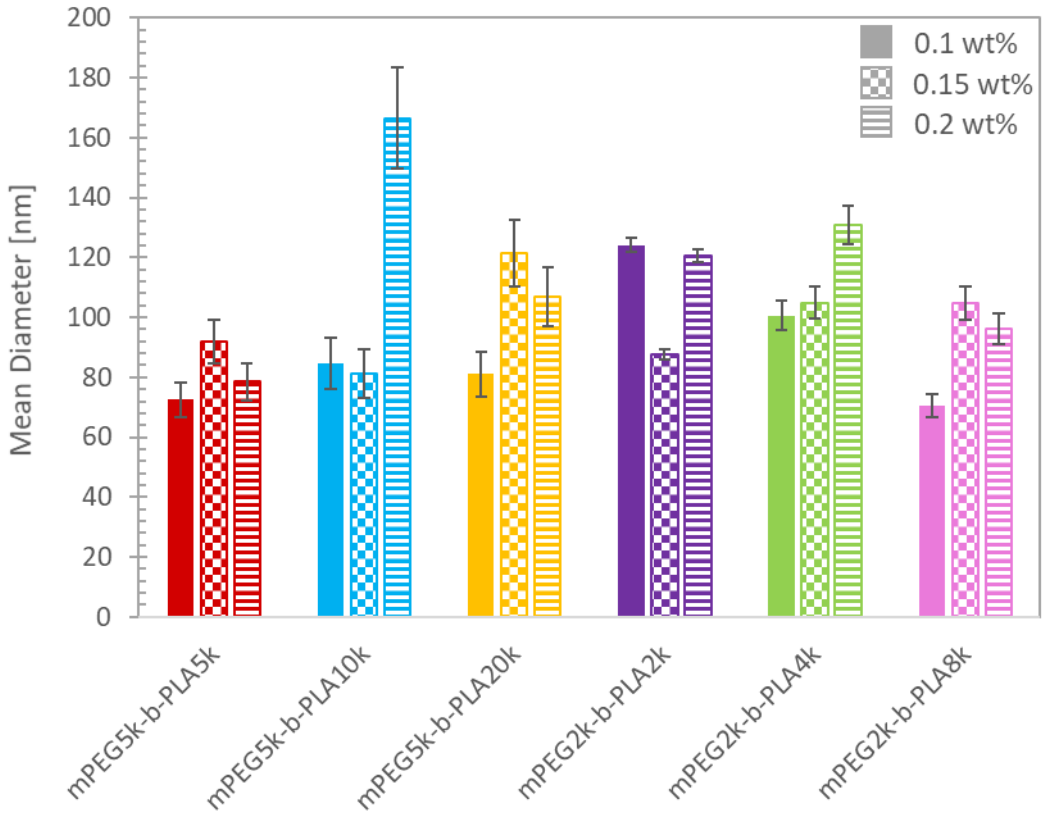

Figure 7.7: Plot of the measured mean diameter of the drug-loaded nanoparticles with respect to the six different diblock copolymers of mPEG-PLA studied in this work at three different final polymer concentrations. Data shown are the mean values of three independent experiments and the error bars show the standard error of these three experiments.

The results plotted in Figure 7.7, on average, show a slight increase in the drug-loaded nanoparticle mean size with increasing PLA molecular weight and total polymer molecular weight for the mPEG5k polymers. The opposite trend seems to be followed by the mPEG2k diblock copolymers, were the mean nanoparticle size is decreasing, on average, with the increasing PLA and total polymer molecular weight. The mean diameter obtained for the mPEG2k drug-loaded nanoparticles seems to be higher than the corresponding, in terms of hydrophobic to hydrophilic ratio, mPEG5k materials. An exception to this, is the results obtained for the polymers of mPEG5k-*b*-PLA20k and mPEG2k-*b*-PLA8k (hydrophobic to hydrophilic ratio of 4), where the mean diameter decreases with decreasing mPEG chain length.

The average nanoparticle size results range from 70-165 nm as seen from Figure 7.7 for all the diblock copolymers and processing conditions employed in this study. Therefore, the final drug-loaded nanoparticles prepared through the nanoprecipitation encapsulation technique presented here have formulated into materials with highly desirable mean diameters for DDS

applications in cancer chemotherapy (Park *et al.*, 2008). This is a very important outcome of this work, since in the literature achieving an acceptable average size of the drug-loaded nanoparticles has proven to be challenging, with researchers achieving either too small or too large mean diameters of the encapsulated material aimed for drug delivery applications (Dora *et al.*, 2010; Chu *et al.*, 2016; Ho *et al.*, 2018).

7.3.6. Polydispersity index of drug-loaded suspensions

The PDI values of the drug-loaded nanoparticles produced during the encapsulation experiment performed via the self-assembly of the different diblock copolymers through nanoprecipitation, were established from the characterisation of the final product with DLS measurements. The results obtained for the PDI of all the diblock copolymer nanoparticle suspensions prepared in all three different final concentrations employed are presented in Figure 7.8.

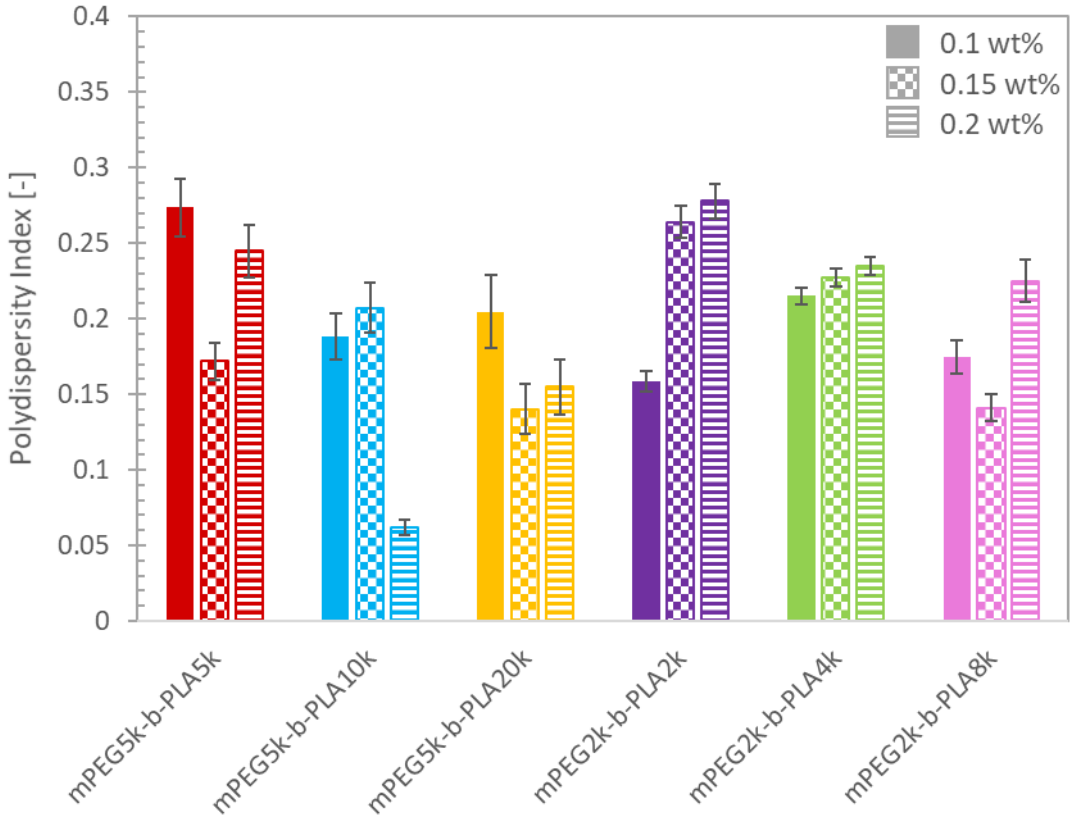

Figure 7.8: Plot of the polydispersity index (PDI) results obtained for the drug-loaded nanoparticles with respect to the six different diblock copolymers of mPEG-PLA studied in this work at the three different final polymer concentrations employed. Data shown are the mean values of three independent experiments and the error bars show the standard error of these three experiments.

As seen from the results plotted in Figure 7.8, the PDI of the final formulated nanoparticle suspensions with encapsulated model drug experiences values of 0.27 and lower for all the diblock copolymer material and final polymer concentrations employed in this study. This is another important finding from the current investigation since the formation of a uniform drug-loaded nanoparticle suspension has been observed based of the PDI results. This was not always the case for similar studies in the literature (Dora *et al.*, 2010; Prasad *et al.*, 2017).

7.3.7. Zeta potential measurements

Zeta potential measurements were completed for the drug-loaded nanoparticle suspensions produced via the encapsulation-nanoprecipitation experiments of the different diblock copolymers. These measurements were an indication of the particle surface charge and the stability of the final drug-loaded suspensions formed. The values collected from the zeta potential analysis of all the diblock copolymer suspensions and the three final concentrations applied are presented in Figure 7.9.

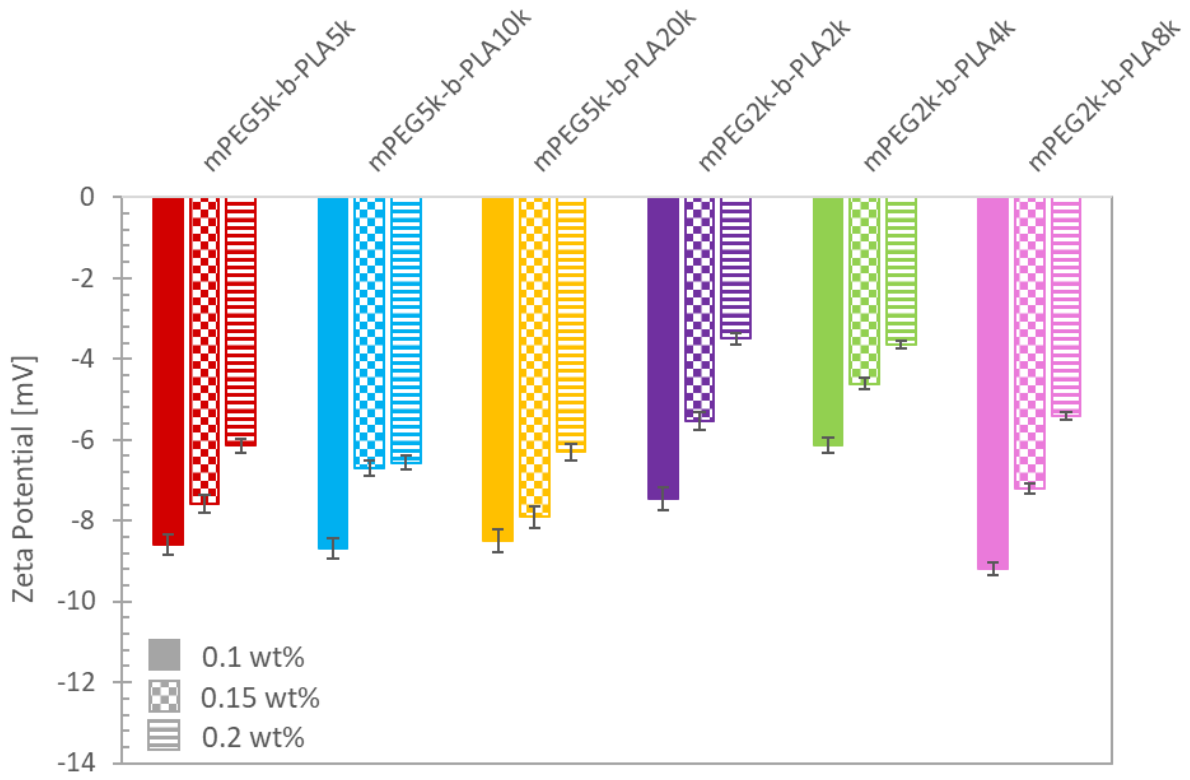

Figure 7.9: Plot showing the results obtained from the zeta potential analysis of all the drug-loaded nanoparticle suspensions with respect to the six different diblock copolymers of mPEG-PLA studied in this work at the three different final polymer concentrations employed. Data shown are the mean values of three independent experiments and the error bars show the standard error of these three experiments.

The results plotted in Figure 7.9 from the zeta potential measurements of the different drug-loaded nanoparticle suspensions prepared in this work, show that the surface charge of the nanoparticles is decreasing consistently with increasing polymer concentration in the final suspension. This observation can be justified based on the fact that when the concentration of polymer is higher in the final product, the polymer proximity and interactions are also higher in the formulated suspension. Therefore, the nanoparticle concentration, which is also higher at higher polymer concentrations, leads to more interactions between the polymeric nanostructures since they are also closer in proximity. Consequently, the collision and aggregation phenomena of neighbouring nanoparticles in a more concentrated suspension are more frequent, leading to the measurement of a lower zeta potential and surface charge for higher polymer concentration suspensions.

The resultant zeta potential values are ranging between -10 to -4 mV for all the diblock copolymer materials. These values are negative a characteristic required for DDS since the

negative charge reduces non-specific absorption of the material by the liver and spleen. This results in increased electrostatic repulsions between the nanoparticles and the cellular surfaces, thereby extending the blood circulation time of the nanoparticles (O'Brien *et al.*, 2020). Also, the values of surface charge obtained in this work are higher than the zeta potential results established for similar systems in the literature, suggesting a higher colloidal stability of the constructed drug-loaded nanoparticles presented here (Chu *et al.*, 2016).

7.4. Conclusions

The effectiveness of the synthesised library of mPEG-PLA diblock copolymers in functioning as a DDS for chemotherapy, was assessed using a hydrophobic model drug in the research presented in this chapter. The goal was to encapsulate the selected model drug (Nile red) using all six mPEG-PLA diblock copolymers produced in Chapter 5, by employing the nanoprecipitation method for the encapsulation experiments.

To address the challenge of separating the non-encapsulated Nile red from the drug-loaded nanoparticle suspension a list of requirements, that should be met by an ideal solvent for the aggregated unloaded Nile red extraction, was created. Based on this list, three different solvents were identified with promising properties; ethyl acetate, diethyl ether and heptane. The evaluation of the three solvents was performed in extracting a pre-determined amount of Nile red aggregated in water. The results were compared for the three solvents suggesting that diethyl ether is the most appropriate Nile red extraction solvent based on the Nile red retrieval efficiency achieved and the inherent properties of the solvent.

A concentration vs absorbance calibration curve was developed by characterising nine known Nile red concentrations in DMSO, ranging from 0.0001 to 0.005wt%, through UV-vis spectroscopy. This curve was then employed to quantify the amount of Nile red not encapsulated in nanoparticle suspensions based on its absorbance measured via UV-vis spectroscopy. The amount of Nile red loaded within the polymeric nanoparticles was then determined through the subtraction of the non-loaded drug from the initial amount of Nile red used for the encapsulation experiment. The Nile red encapsulation amount obtained was then analysed further to establish the encapsulation efficiency and the drug loading capacity for all the encapsulation experiments performed.

The final concentration of the block copolymer in the suspension was varied to determine its effect on the encapsulation of Nile red. There is limited information in the literature about the polymer concentration effect on the final drug loading capabilities of the materials. The results gathered in this research show that the encapsulation efficiency generally decreases as the concentration of diblock copolymer increases, likely due to enhanced polymer-polymer interactions and chain entanglements that interfere with drug encapsulation. The encapsulation efficiencies achieved in the Nile red loading experiments conducted in this study range from 20-36% across all materials and conditions used. The encapsulation techniques employed in this research achieved higher efficiencies than those reported in multiple other studies in the literature using similar materials.

The drug loading capacity of all diblock copolymers used in this study decreases as their concentration increases. This trend is anticipated based on the method used to determine its value. The formula used divides the weight of the encapsulated Nile red by the total weight of the polymeric nanoparticle. As the concentration of the polymeric nanoparticle increases, its weight increases, therefore leading to a reduction in the calculated drug loading capacity. The values obtained from this investigation are comparable to the drug loading capacities established in the literature for similar materials.

The mean diameter size of the drug-loaded nanoparticles was determined via DLS measurement. The measured sizes range from 70-165 nm, proving that the materials produced have a suitable nanoparticle size for DDS applications in cancer chemotherapy. Moreover, a uniform nanoparticle size distribution was observed for the drug-loaded nanoparticle suspensions produced, with PDIs equal or lower than 0.27.

Finally, the zeta potential values gathered from the final products range from -10 to -4 mV, thus exhibiting a beneficial negative charge that minimises non-specific organ absorption and enhances circulation time. These values are indicating a higher colloidal stability compared to similar systems in existing literature.

8. Conclusions and future work

8.1. Conclusions

The goal of the experimental research conducted in this thesis was to complete and investigate thoroughly the necessary steps leading to the development of an improved drug delivery system (DDS) for cancer chemotherapy. These steps include synthesising biodegradable and biocompatible block copolymers, achieving their self-assembly into polymeric nanoparticles, enhancing their stability for prolonged storage and stability, and ensuring high encapsulation efficiency of a hydrophobic drug within the structure of the formulated polymeric nanoparticles.

The experimental work completed in Chapter 4 was focussing on minimising health and safety concerns in the synthesis of polymeric excipients for biomedical and drug delivery applications by using the bio-based, non-toxic solvent 2-methyltetrahydrofuran (2-MeTHF) instead of traditional petrochemical solvents. 2-MeTHF proved effective for various polymerisation methods including ROP, eROP, FRP, and RAFT, specifically with LA and ε-CL, which are materials that have high demand for applications in the pharmaceutical industry. In this research chapter, the sequential one-pot ROP of ε-CL and LA was successfully conducted, using a double catalyst system to address catalyst limitations. Grafted amphiphilic block copolymers were synthesised using methacrylate-ester ROP initiators for the hydrophobic LA monomer, achieving complete conversion without transesterification side reactions. The higher boiling point of 2-MeTHF facilitated various polymerisation processes at elevated temperatures, which are typically necessary for radical initiation. Furthermore, the resulting amphiphilic block copolymers self-assembled into nanoparticles using the solvent displacement method, demonstrated cytocompatibility through tests on three model cell lines, and showed potential as drug nanocarriers.

The limitations of the research investigation performed in Chapter 4 include the use of toxic and harmful solvents for the purification of the final polymeric material produced. Also, the lack of clarity on the type and structure of the polymeric nanoparticles formed limits the understanding and reasoning behind the trends observed through Dynamic light scattering (DLS) characterisation.

Chapter 5 investigated how diblock copolymers, specifically methyl-poly(ethylene glycol)-*block*-poly(lactide) (mPEG-PLA), self-assemble into polymeric nanoparticles and micelles

using various formulation methods. Formulation process parameters were adjusted to see their effects on the product characteristics. The findings highlighted that nanoparticle size and polydispersity index (PDI) are significantly influenced by the polymer properties, such as molecular weight, both block lengths, and the hydrophobic to hydrophilic ratio. Notably, the solvent displacement method using acetonitrile proved superior to acetone, producing well-defined nanoparticles across a range of concentrations. Although slow self-assembly processes did not always yield the desired nanoparticle characteristics for biomedical applications, they provided insights into the diblock copolymer self-assembly dynamics, starting with open polymer coils in a good solvent and transitioning into micelles upon adding a selective solvent. The slow self-assembly was particularly effective in mapping micelle formation, which was triggered in the 20-30vol% water composition in solvent. Additionally, zeta potential analysis confirmed the high colloidal stability of the nanoparticles with particle surface charge ranging from -17 to -28 mV for all diblock copolymers. Out of all the employed formulation process, nanoprecipitation was proven to be the most effective, consistently achieving desirable PDIs and mean diameters for nanoparticles for pharmaceutical use.

The limitations of the experimental procedures followed in Chapter 5 include the inability of all three different nanoparticle formulation techniques to monitor accurately the self-assembly procedure into polymeric nanoparticles. The tracking of the nanoparticle formation process requires a specialised characterisation technique. DLS, in this case, is insufficient to provide all the important properties and information required to fully characterise and understand the self-assembly process. Moreover, the synthesis of a larger diblock copolymer library would probably be more beneficial to expand on the general trends observed in the results. The use of more polymeric material can lead to a greater understanding of the diblock copolymer properties influence on the nanoparticle suspension. Similarly to Chapter 4, the other limitation of this investigation is not knowing the exact type and structure that the diblock copolymers conform to construct polymeric nanoparticles in all three formulation techniques applied in Chapter 5. This limits the understanding of the procedures performed, the discussion of the obtained results and the justification of the observed phenomena.

The research presented in Chapter 6 focused on enhancing the stability and prolong the storage of mPEG-PLA polymeric nanoparticles by optimising the freeze-drying process. It represents the first systematic study examining the effect of different molecular weight PEGs as cryoprotectants for polymeric nanoparticles of mPEG-PLA. The use of six different

cryoprotectants, including DMSO, glycerol, and PEGs ranging from 1k to 35k, was employed. Results for the suspensions before freezing showed that as PEG molecular weight increased, so did the mean diameter of nanoparticles due to the formation of a protective PEG coating. However, the study also found that higher molecular weight PEGs were less effective as cryoprotectants due to their glass transition temperatures being close to or below the freezing temperatures used, leading to potential aggregation during the freezing step. DMSO, glycerol, and PEG1k were identified as the most effective cryoprotectants, maintaining the original nanoparticle suspension sizes and exhibiting low PDIs. Challenges with eutectic mixtures formed by DMSO and glycerol with water complicated the freeze-drying process. The four PEGs of different molecular weights produced stable freeze-dried materials. All materials had favourable characteristics, verified by SEM imaging, and supported by their efficient re-dispersion qualities post-freeze-drying, with controlled PDI, mean diameter and reconstitution times less than 10 min for all four PEG samples.

The limitations of the research methodology completed in Chapter 6 includes the operating temperature and pressure applied for the freezing and drying step, which are pre-determined by the freeze-drier apparatus used in this investigation. Future work could study the effect that the different processing conditions (temperature of freezing step, pressure of freezing step, temperature of drying step and pressure of drying step) have on the final freeze-dried material and its properties. Same as in previous chapters, the undetermined structure and type of the produced materials is an issue. This leads to limitations on the complete understanding of the measured results and the discussions about reasoning and underlying principles followed by the developed products. Also, another restriction in this work was the inability to freeze-dry the polymeric nanoparticle samples combined with DMSO and glycerol as cryoprotectants. This is caused by the eutectic solution formed by DMSO with water and glycerol with water. Special care on the conditions selected and applied during the freeze-drying process is required to avoid this issue.

In Chapter 7, the effectiveness of a synthesized library of mPEG-PLA diblock copolymers as a DDS for chemotherapy was evaluated using a hydrophobic model drug, Nile red, encapsulated via the nanoprecipitation method. Challenges in separating non-encapsulated Nile red led to testing three solvents, ethyl acetate, diethyl ether, and heptane, with diethyl ether proving most effective based on extraction efficiency and its properties. A calibration curve for Nile red in DMSO, developed through UV-visible spectroscopy, facilitated the quantification

of non-encapsulated Nile red, thereby determining the loaded drug amount in the polymeric nanoparticles. Based on this value, the encapsulation efficiency and the drug loading capacity were calculated for the produced materials. Variations in copolymer concentration influenced Nile red encapsulation, showing decreased efficiency with increased concentration, likely due to heightened polymer-polymer interactions and chain entanglements. Despite these challenges, encapsulation efficiencies ranged from 20-36%, surpassing results from other studies using similar materials. Drug loading capacity also decreased with increasing polymer concentration, due to the measuring correlation of weight ratio of encapsulated drug to total nanoparticle mass. The drug-loaded nanoparticles exhibited sizes between 70-165 nm and low PDI values, making them ideal for DDS in cancer chemotherapy. Finally, they showed high colloidal stability with zeta potential values between -4 and -10 mV, indicating reduced non-specific organ absorption and extended circulation times.

The main limitations of the study performed in Chapter 7 are associated with the separation process of the un-loaded Nile red from the rest of the formulated nanoparticle suspension. The use of toxic solvents for the extraction of un-encapsulated Nile red is not ideal since the material is intended for health applications. Moreover, the evaluation of the retrieval efficiency of the three different employed extraction solvents is completed in the absence of any nanoparticles in the system, affecting the retrieval efficiencies values measured. Another, limitation of this process is the probability of Nile red depositing on the surface of the corona forming the nanoparticle, instead of being encapsulated within the nanoparticle core. This limits the accuracy of the method used to assess the encapsulation efficiency, but also increases the problems with the already challenging separation process of un-loaded Nile red from the prepared nanoparticle suspension. In addition, the important properties of the chosen model drug, Nile red, were compared with real drugs applied for chemotherapy to lead to its selection as the studied material. Although, its performance would not be able to mimic 100% the one from a chemotherapy drug. For a more accurate evaluation of the encapsulation efficiency of the constructed polymeric material, the use of chemotherapy drugs in clinical applications is required.

In conclusion, the use of the bio-based and environmentally friendly polymerisation solvent, 2-MeTHF, was successful in performing the synthesis of a variety of polymeric products through different polymerisation reactions. The investigation of the self-assembly of different polymeric materials, by employing a variety of formulation methods and processing conditions,

was successfully completed, indicating nanoprecipitation as a robust, easy and scalable process. The performance of different cryoprotectants, through their systematic study, was tested during the freeze-drying process, with an emphasis on the freezing step, of polymeric nanoparticles, suggesting that PEGs with lower molecular weights are more successful for their cryopreservation. Finally, the encapsulation of Nile red as a model chemotherapy drug with the polymeric nanoparticle core was performed successfully, achieving higher encapsulation efficiencies than values reported in literature and developing polymeric nanoparticles with mean diameters and PDI within the required range for DDS in cancer chemotherapy.

8.2. Future work

In this section some recommendations, directions and plans for the future work and where the research focus of this work could be emphasised, are presented in the context of the general research area:

- Investigation of the properties of triblock copolymers based on methyl-poly(ethylene glycol)-*block*-poly(caprolactone)-*block*-poly(lactide) (mPEG-PCL-PLA) in-depth. Determining how different important properties of the final material produced, such as biodegradability, solution behaviour, physical and structural properties, are fluctuating by varying the three block lengths comprising the polymeric material. A material with such characteristics is considered highly desirable in the literature for designing biomedical applications due to the ability of tuning the physical and chemical performance of the synthesised material. The coexistence of different hydrophobic polyesters with different degradability timescales has been proven a very powerful tool in controlling and adapting the final material features (Stavila *et al.*, 2014). Moreover, the extensive examination of the self-assembly behaviour of this type of triblock copolymers would be essential in understanding the way this adjusts to the variations of the three block lengths and properties. This information could lead to the ability of tailoring and adapting the final polymeric nanoparticles structures based on the design of different triblock copolymers with the beneficial physical and chemical properties.

- Perform a thorough study in the self-assembly behaviour of methyl-poly(ethylene glycol)-*block*-poly(caprolactone) (mPEG-PCL) diblock copolymers. The formulation of this diblock copolymers into polymeric nanoparticles could be investigation by

varying the different key processing parameters, such as temperature, nature and quality of solvent, copolymer block lengths, molecular weight and others, and testing their influence on the final nanoparticle formulations constructed. The comparisons of the results established from such a study, with the outcomes obtained from the experimental investigation of the formulation of mPEG-PLA diblock copolymers performed in this thesis, could be performed. Gathering the findings of similar studies could lead to the comprehension of a general formulation mechanism followed by the different amphiphilic diblock copolymers for self-assembling into polymeric nanoparticles.

- Complete the investigation of the amphiphilic block copolymers self-assembly by employing more specialised characterisation techniques, such as cryo-TEM and X-ray scattering, and combining them with the information gathered by DLS measurements. This experimental study could lead to the definitive determination of the exact type and structure of polymeric nanoparticle the applied self-assembly procedure yields. The self-assembly process could be successfully monitored by employing one or more of these characterisation techniques leading to the greater understanding of the nanoparticle formulation mechanism followed by amphiphilic block copolymers when they come in contact with aqueous environments.

- Development of a new thorough self-assembly procedure allowing the control and variation of key formulation parameters to alter the rate and kinetics of the association process of the amphiphilic block copolymer material. The application of a such process could lead to the ability of using a formulation technique driven by the thermodynamic association of polymer chains, procedures that are extremely limited in the literature. Formulation processes like these could lead to a better understanding of the self-assembly mechanism of amphiphilic block sopolymers and enhanced DDSs. Moreover, a self-assembly procedure characterised by these factors can allow for the extensive study of the thermodynamics and kinetics associated with the formulation of biodegradable and biocompatible nanoparticles from block copolymers. It is considered that a polymeric structure at thermodynamic equilibrium could offer significant benefits for system stability and improved retention of encapsulated drugs within the bloodstream (Almoustafa, Alshawsh and Chik, 2017). Despite this potential, such equilibrium-based polymeric structures and the methodology that could lead to their production are very scarce in the literature.

- Improving upon the freeze-drying procedures presented in this thesis with the employment of a freeze-drying apparatus that allows for precise control of the different conditions applied during the progression of the freeze-drying process. The processing conditions include the freezing step temperature, the freezing step pressure, the drying step temperature and the drying step pressure. Having control over these processing conditions would be extremely beneficial for achieving an enhanced freeze-drying process for polymeric nanoparticles based on amphiphilic block copolymers. This can be accomplished by the in-depth experimental investigation of the effects that each of those conditions has on the final freeze-dried material and its reconstitution characteristics. Moreover, the improved freeze-drying procedure could allow for addressing the issues that were encountered with the freeze-drying of the DMSO and glycerol cryoprotectants by performing the optimisation of the freeze-drying process accounting for the formation of eutectic mixtures with water.

- Completing the systematic study of different PEG molecular weights employed as both cryoprotectants and lyoprotectants for polymeric nanoparticles prepared by the self-assembly of PEG-PLA diblock copolymers. The effectiveness of PEG as both a cryoprotectant and lyoprotectant in this type of nanoparticle suspensions can be evaluated and compared with the different types of sugars, such as glucose, sucrose, trehalose and others, that are commonly used in the literature as lyoprotectants owing to their desirable physical and chemical properties. Moreover, the combination of PEG with other lyoprotectants could be investigated experimentally, since the integration of desirable properties found in PEG and the selected lyoprotectant could lead to an improved system for cryopreservation with enhanced abilities for the protection of the polymeric nanoparticles integrity and structure during freeze-drying applications.

- Developing upon the encapsulation procedures performed in this thesis, the application and investigation of numerous model chemotherapy drugs could be studied in the future. The different model drugs selected should vary key properties, such as aqueous solubility, pKa, hydrophobicity and others, to assess their effect on the EE% and LC% of the final polymeric nanoparticles. Moreover, the application of real drugs applied in clinical trials for chemotherapy should be used to perform their encapsulation in polymeric nanoparticles prepared by the self-assembly of PEG-PLA diblock

copolymers. This would form a more realistic DDS intended for cancer chemotherapy, since the differences between the Nile red properties and the usually applied chemotherapy drugs, possibly lead to limitations to its mimicking behaviour. Employing chemotherapy drugs in the experimental study would result in a more accurate evaluation of the encapsulation efficiency of the constructed polymeric material.

Since the research and application of self-assembled block copolymers into polymeric nanoparticles in pharmaceutical industry is a relatively new area emerging in recent years, there are multiple research avenues that could be followed for future research and development. In particular, the in depth study of the self-assembly mechanism for a range of block copolymers with varying materials and properties could lead to a mechanistic understanding and the engineering of a formulation process that will produce superior polymeric nanoparticles for biomedical and pharmaceutical applications.

References

Abdelwahed, W. *et al.* (2006) ‘Freeze-drying of nanoparticles: Formulation, process and storage considerations’, *Advanced Drug Delivery Reviews*, 58(15), pp. 1688–1713. doi: 10.1016/J.ADDR.2006.09.017.

Abdelwahed, W., Degobert, G. and Fessi, H. (2006) ‘Investigation of nanocapsules stabilization by amorphous excipients during freeze-drying and storage’, *European Journal of Pharmaceutics and Biopharmaceutics*, 63(2), pp. 87–94. doi: 10.1016/j.ejpb.2006.01.015.

Agostini, A. *et al.* (2017) ‘Synthesis and Degradation Study of Cationic Polycaprolactone-Based Nanoparticles for Biomedical and Industrial Applications’, *Industrial and Engineering Chemistry Research*, 56(20), pp. 5872–5880. doi: 10.1021/acs.iecr.7b00426.

Agostini, A. *et al.* (2018) ‘Synthesis and characterization of pH-sensitive drinkable nanoparticles for oral delivery of ibuprofen’, *Nanotechnology*, 29(22). doi: 10.1088/1361-6528/aab536.

Ahmad Mir, R., Mansoor Shafi, S. and Zargar, S. M. (2023) ‘Analysis of proteomes—II’, in *Principles of Genomics and Proteomics*. Elsevier, pp. 139–163. doi: 10.1016/B978-0-323-99045-5.00010-0.

Al-Natour, M. A. *et al.* (2020) ‘Facile Dye-Initiated Polymerization of Lactide–Glycolide Generates Highly Fluorescent Poly(lactic-co-glycolic Acid) for Enhanced Characterization of Cellular Delivery’, *ACS Macro Letters*, pp. 431–437. doi: 10.1021/acsmacrolett.9b01014.

Albertsson, A. C. and Varma, I. K. (2003) ‘Recent developments in ring opening polymerization of lactones for biomedical applications’, *Biomacromolecules*, 4(6), pp. 1466–1486. doi: 10.1021/bm034247a.

Almalik, A. *et al.* (2017) ‘Effect of cryoprotection on particle size stability and preservation of chitosan nanoparticles with and without hyaluronate or alginate coating’, *Saudi Pharmaceutical Journal*, 25(6), pp. 861–867. doi: 10.1016/j.jsps.2016.12.008.

Almoustafa, H. A., Alshawsh, M. A. and Chik, Z. (2017) ‘Technical aspects of preparing PEG-PLGA nanoparticles as carrier for chemotherapeutic agents by nanoprecipitation method’, *International Journal of Pharmaceutics*, 533(1), pp. 275–284. doi: 10.1016/J.IJPHARM.2017.09.054.

Ambekar, R. S., Choudhary, M. and Kandasubramanian, B. (2020) ‘Recent advances in dendrimer-based nanoplatform for cancer treatment: A review’, *European Polymer Journal*, 126, p. 109546. doi: 10.1016/J.EURPOLYMJ.2020.109546.

American Cancer Society (2020) *Chemotherapy Side Effects*. Available at: https://www.cancer.org/content/dam/CRC/PDF/Public/8419.00. (Accessed: 18 February 2022).

Andreana, I. *et al.* (2023) ‘Freeze Drying of Polymer Nanoparticles and Liposomes Exploiting Different Saccharide-Based Approaches’, *Materials*, 16(3), p. 1212. doi: 10.3390/MA16031212/S1.

Antonucci, V. *et al.* (2011) ‘Toxicological assessment of 2-methyltetrahydrofuran and cyclopentyl methyl ether in support of their use in pharmaceutical chemical process development’, *Organic Process Research and Development*, 15(4), pp. 939–941. doi: 10.1021/op100303c.

Awan, M. *et al.* (2020) ‘Dimethyl Sulfoxide: A Central Player Since the Dawn of Cryobiology, is Efficacy Balanced by Toxicity?’, *Regenerative Medicine*, 15(3), pp. 1463–1491. doi: 10.2217/RME-2019-0145.

Aycock, D. F. (2007) ‘Solvent applications of 2-methyltetrahydrofuran in organometallic and biphasic reactions’, *Organic Process Research and Development*, 11(1), pp. 156–159. doi: 10.1021/op060155c.

Azarova, A. M. *et al.* (2007) ‘Roles of DNA topoisomerase II isozymes in chemotherapy and secondary malignancies’, *Proceedings of the National Academy of Sciences of the United States of America*, 104(26), pp. 11014–11019. doi: 10.1073/pnas.0704002104.

Azougagh, O. *et al.* (2023) ‘Dissolution mechanism of cellulose in a benzyltriethylammonium/urea deep eutectic solvent (DES): DFT-quantum modeling, molecular dynamics and experimental investigation’, *Physical Chemistry Chemical Physics*, 25(34), pp. 22870–22888. doi: 10.1039/D3CP02335D.

Baccile, N. and Poirier, A. (2023) ‘Microbial bio-based amphiphiles (biosurfactants): General aspects on critical micelle concentration, surface tension, and phase behavior’, in Soberon-Chavez, G. (ed.) *Biosurfactants: Research and Development*. Elsevier, pp. 3–31. doi: 10.1016/B978-0-323-91697-4.00001-6.

Bailey, W. J. *et al.* (1984) ‘Free-Radical Ring-Opening Polymerization’, *Journal of Macromolecular Science—Chemistry*, 21(13–14), pp. 1611–1639. doi: 10.1080/00222338408082081.

Balla, E. *et al.* (2021) ‘Poly(lactic Acid): A Versatile Biobased Polymer for the Future with Multifunctional Properties—From Monomer Synthesis, Polymerization Techniques and Molecular Weight Increase to PLA Applications’, *Polymers 2021, Vol. 13, Page 1822*, 13(11), p. 1822. doi: 10.3390/POLYM13111822.

Bansal, K. K. *et al.* (2015) ‘New biomaterials from renewable resources-amphiphilic block copolymers from δ-decalactone’, *Polymer Chemistry*, 6(40), pp. 7196–7210. doi: 10.1039/c5py01203a.

Bao, C. *et al.* (2020) ‘Synthesis of biodegradable protein-poly(ϵ-caprolactone) conjugates via enzymatic ring opening polymerization’, *Polymer Chemistry*, 11(3), pp. 682–686. doi: 10.1039/c9py01464k.

Barner-Kowollik, C. (2008) *Handbook of RAFT Polymerization*, *Handbook of RAFT Polymerization*. John Wiley and Sons. doi: 10.1002/9783527622757.

Beer, V. *et al.* (2015) ‘Polylactide-Based Nanoparticles with Tailor-Made Functionalization’, *Macromolecular Chemistry and Physics*, 216, pp. 1774–1781. doi: 10.1002/macp.201500153.

Beija, M., Charreyre, M. and Martinho, J. M. G. (2011) ‘Dye-labelled polymer chains at specific sites: Synthesis by living/controlled polymerization’, *Progress in Polymer Science*, 36(4), pp. 568–602. doi: 10.1016/j.progpolymsci.2010.06.004.

Bejrapha, P. *et al.* (2010) ‘Physicothermal Properties of Freeze-Dried Fish Oil Nanocapsules Frozen under Different Conditions’, *Drying Technology*, 28(4), pp. 481–489. doi: 10.1080/07373931003613684.

Bhardwaj, H. and Jangde, R. K. (2023) ‘Current updated review on preparation of polymeric nanoparticles for drug delivery and biomedical applications’, *Next Nanotechnology*, 2, p. 100013. doi: 10.1016/J.NXNANO.2023.100013.

Bhattacharya, S. (2018) ‘Cryopretectants and Their Usage in Cryopreservation Process’, in Bozkurt, Y. (ed.) *Cryopreservation Biotechnology in Biomedical and Biological Sciences*. IntechOpen. doi: 10.5772/intechopen.80477.

Bossion, A. *et al.* (2019) 'Opportunities for organocatalysis in polymer synthesis via step-growth methods', *Progress in Polymer Science*, 90, pp. 164–210. doi: 10.1016/J.PROGPOLYMSCI.2018.11.003.

Brannigan, R. P. and Dove, A. P. (2017) 'Synthesis, properties and biomedical applications of hydrolytically degradable materials based on aliphatic polyesters and polycarbonates', *Biomaterials Science*, 5(1), pp. 9–21. doi: 10.1039/C6BM00584E.

Brigger, I., Dubernet, C. and Couvreur, P. (2002) 'Nanoparticles in cancer therapy and diagnosis', *Advanced Drug Delivery Reviews*, 54, pp. 631–651. Available at: www.elsevier.com/locate/drugdeliv.

Byrne, F. P. *et al.* (2016) 'Tools and techniques for solvent selection: green solvent selection guides', *Sustainable Chemical Processes*, 4(1), pp. 1–24. doi: 10.1186/s40508-016-0051-z.

Cancer Research UK (2020) *Cancer incidence statistics | Cancer Research UK*. Available at: https://www.cancerresearchuk.org/health-professional/cancer-statistics/incidence#heading-Four (Accessed: 18 February 2022).

Cao, Y., Dong, X. and Chen, X. (2022) 'Polymer-Modified Liposomes for Drug Delivery: From Fundamentals to Applications', *Pharmaceutics*, 14(4), p. 778. doi: 10.3390/PHARMACEUTICS14040778.

Capasso Palmiero, U. *et al.* (2018) 'Strategies to combine ROP with ATRP or RAFT polymerization for the synthesis of biodegradable polymeric nanoparticles for biomedical applications', *Polymer Chemistry*, 9(30), pp. 4084–4099. doi: 10.1039/c8py00649k.

Capretto, L. *et al.* (2011) 'Continuous-flow production of polymeric micelles in microreactors: Experimental and computational analysis', *Journal of Colloid and Interface Science*, 357(1), pp. 243–251. doi: 10.1016/J.JCIS.2011.01.085.

Castano, M. *et al.* (2014) 'Enzyme-catalyzed ring-opening polymerization of ε-caprolactone using alkyne functionalized initiators', *Polymer Chemistry*, 5(6), pp. 1891–1896. doi: 10.1039/c3py01536j.

de Castro, M. D. L., Capote, F. P. and Ávila, N. S. (2008) 'Is dialysis alive as a membrane-based separation technique?', *TrAC Trends in Analytical Chemistry*, 27(4), pp. 315–326. doi: 10.1016/J.TRAC.2008.01.015.

Chang, L. *et al.* (2005) ‘Mechanism of protein stabilization by sugars during freeze-drying and storage: Native structure preservation, specific interaction, and/or immobilization in a glassy matrix?’, *Journal of Pharmaceutical Sciences*, 94(7), pp. 1427–1444. doi: 10.1002/jps.20364.

Chen, M., Zhong, M. and Johnson, J. A. (2016) ‘Light-Controlled Radical Polymerization: Mechanisms, Methods, and Applications’, *Chemical Reviews*, 116(17), pp. 10167–10211.

Chu, B. *et al.* (2016) ‘Synthesis, characterization and drug loading property of Monomethoxy-Poly(ethylene glycol)-Poly(ε-caprolactone)-Poly(D,L-lactide) (MPEG-PCLA) copolymers’, *Scientific Reports*, 6(1), pp. 1–15. doi: 10.1038/srep34069.

Chu, H. H. and Lin, C. S. (2003) ‘The Effect of Initiators on the Emulsion Polymerization of 2-hydroxyethyl Methacrylate’, *Journal of Polymer Research*, 10(4), pp. 283–287. doi: 10.1023/B:JPOL.0000004631.64826.3c.

Ciria, J. C. *et al.* (2021) ‘Rational description and modelling of the separation of nanotubes from solid nanoparticles in centrifugation processes’, *Carbon Trends*, 5, p. 100084. doi: 10.1016/J.CARTRE.2021.100084.

Ciurzyńska, A. and Lenart, A. (2011) ‘Freeze-Drying - Application in Food Processing and Biotechnology - a Review’, *Polish Journal of Food and Nutrition Sciences*, 61(3), pp. 165–171. doi: 10.2478/V10222-011-0017-5.

Colombo, C. *et al.* (2014) ‘Tunable degradation behavior of PEGylated polyester-based nanoparticles obtained through emulsion free radical polymerization’, *Industrial and Engineering Chemistry Research*, 53(22), pp. 9128–9135. doi: 10.1021/ie4036077.

Corma Canos, A., Iborra, S. and Velty, A. (2007) ‘Chemical routes for the transformation of biomass into chemicals’, *Chemical Reviews*, 107(6), pp. 2411–2502. doi: 10.1021/cr050989d.

Crintea, A. *et al.* (2023) ‘Dendrimers: Advancements and Potential Applications in Cancer Diagnosis and Treatment—An Overview’, *Pharmaceutics*, 15(5), p. 1406. doi: 10.3390/PHARMACEUTICS15051406.

d’Almeida Gameiro, M. *et al.* (2020) ‘Enzymatic one-pot synthesis of renewable and biodegradable surfactants in supercritical carbon dioxide (scCO2)’, *Green Chem.*, 22(4), pp. 1308–1318. doi: 10.1039/C9GC04011K.

Deb, P. K. *et al.* (2019) ‘Pharmaceutical and Biomedical Applications of Polymers’, *Basic Fundamentals of Drug Delivery*, pp. 203–267. doi: 10.1016/B978-0-12-817909-3.00006-6.

Deng, S. *et al.* (2020) ‘Polymeric Nanocapsules as Nanotechnological Alternative for Drug Delivery System: Current Status, Challenges and Opportunities’, *Nanomaterials 2020, Vol. 10, Page 847*, 10(5), p. 847. doi: 10.3390/NANO10050847.

Dong, Y. and Feng, S. S. (2004) ‘Methoxy poly(ethylene glycol)-poly(lactide) (MPEG-PLA) nanoparticles for controlled delivery of anticancer drugs’, *Biomaterials*, 25(14), pp. 2843–2849. doi: 10.1016/J.BIOMATERIALS.2003.09.055.

Dora, C. P. *et al.* (2010) ‘Development and characterization of nanoparticles of glibenclamide by solvent displacement method’, *Acta Poloniae Pharmaceutica - Drug Research*, 67(3), pp. 283–290.

Edward, K. H. and Li, D. (2008) *Drug-like properties: Concepts, Structure Design and Methods: from ADME to toxicity optimization*. 1st edn. Academic Press. Available at: https://www.elsevier.com/books/drug-like-properties-concepts-structure-design-and-methods/di/978-0-12-369520-8.

Edwards, A. A. and Alexander, B. D. (2010) ‘Organic Applications of UV-Visible Absorption Spectroscopy’, in Lindon, J. C. (ed.) *Encyclopedia of Spectroscopy and Spectrometry*. 2nd Edition. Academic Press, pp. 2030–2039. doi: 10.1016/B978-0-12-374413-5.00013-0.

Egerton, R. F. (2005) *Physical Principles of Electron Microscopy*. Boston, MA: Springer US. doi: 10.1007/b136495.

Egorova, K. S. and Ananikov, V. P. (2017) ‘Toxicity of Metal Compounds: Knowledge and Myths’, *Organometallics*, 36(21), pp. 4071–4090. doi: 10.1021/acs.organomet.7b00605.

Elumalai, K., Srinivasan, S. and Shanmugam, A. (2024) ‘Review of the efficacy of nanoparticle-based drug delivery systems for cancer treatment’, *Biomedical Technology*, 5, pp. 109–122. doi: 10.1016/J.BMT.2023.09.001.

Englezou, G. *et al.* (2020) ‘2-Methyltetrahydrofuran (2-MeTHF) as a versatile green solvent for the synthesis of amphiphilic copolymers via ROP, FRP, and RAFT tandem polymerizations’, *Journal of Polymer Science*, 58(11), pp. 1571–1581. doi: 10.1002/pol.20200183.

Engwa, G. A. *et al.* (2019) 'Mechanism and Health Effects of Heavy Metal Toxicity in Humans', in Karcioglu, O. and Arslan, B. (eds) *Poisoning in the Modern World - New Tricks for an Old Dog?* IntechOpen, p. 23. doi: 10.5772/intechopen.73906.

Erlebach, A. *et al.* (2016) 'Thermodynamic compatibility of actives encapsulated into PEG-PLA nanoparticles: In Silico predictions and experimental verification', *Journal of Computational Chemistry*, 37(24), pp. 2220–2227. doi: 10.1002/JCC.24449.

European Commission *et al.* (2017) *Study for the strategy for a non-toxic environment of the 7th Environment Action Programme: final report*. doi: 10.2779/025.

Faucher, J. A. *et al.* (1966) 'Glass Transitions of Ethylene Oxide Polymers', *Journal of Applied Physics*, 37(11), pp. 3962–3964. doi: 10.1063/1.1707961.

Ferrari, R. *et al.* (2013) 'Tunable PLGA-based nanoparticles synthesized through free-radical polymerization', *Macromolecular Materials and Engineering*, 298(7), pp. 730–739. doi: 10.1002/mame.201200069.

Fixman, M. (1962) 'Radius of Gyration of Polymer Chains', *The Journal of Chemical Physics*, 36(2), pp. 306–310. doi: 10.1063/1.1732501.

Fonte, P. *et al.* (2014) 'Stability study perspective of the effect of freeze-drying using cryoprotectants on the structure of insulin loaded into PLGA nanoparticles', *Biomacromolecules*, 15(10), pp. 3753–3765. doi: 10.1021/BM5010383/SUPPL_FILE/BM5010383_SI_001.

Franks, F. (1998) 'Freeze-drying of bioproducts: putting principles into practice', *European Journal of Pharmaceutics and Biopharmaceutics*, 45(3), pp. 221–229. doi: 10.1016/S0939-6411(98)00004-6.

Fu, D. (2013) 'Where is it and how does it get there - Intracellular localization and traffic of P-glycoprotein', *Frontiers in Oncology*, p. 321. doi: 10.3389/FONC.2013.00321/BIBTEX.

Gatti, S. *et al.* (2018) 'Hydrazone linked doxorubicin-PLA prodrug nanoparticles with high drug loading', *Nanotechnology*, 29(30), p. 305602. doi: 10.1088/1361-6528/aac0d3.

Gerrits, L., Hammink, R. and Kouwer, P. H. J. (2021) 'Semiflexible polymer scaffolds: an overview of conjugation strategies', *Polymer Chemistry*, 12(10), pp. 1362–1392. doi: 10.1039/D0PY01662D.

Ghasemi, R. *et al.* (2018) ‘mPEG-PLA and PLA-PEG-PLA nanoparticles as new carriers for delivery of recombinant human Growth Hormone (rhGH)’, *Scientific Reports 2018 8:1*, 8(1), pp. 1–13. doi: 10.1038/s41598-018-28092-8.

Van Gheluwe, L. *et al.* (2023) ‘Smart PEG-Block-PLA/PLA Nanosystems: Impact of the Characteristics of the Polymer Blend on the Redox Responsiveness’, *Materials*, 16(2). doi: 10.3390/MA16020539/S1.

Globocan 2020 (2020) *All cancers statistics*. Available at: https://gco.iarc.fr/today (Accessed: 17 February 2022).

Goldstein, J. (2003) *Scanning Electron Microscopy and X-Ray Microanalysis*. New York: Kluwer Academic/Plenum Publishers. doi: 10.1017/S1431927603030617.

Govender, T. *et al.* (1999) ‘PLGA nanoparticles prepared by nanoprecipitation: drug loading and release studies of a water soluble drug’, *Journal of Controlled Release*, 57, pp. 171–185. Available at: https://pubmed.ncbi.nlm.nih.gov/9971898/.

Greenspan, P., Mayer, E. P. and Fowler, S. D. (1985) ‘Nile red: a selective fluorescent stain for intracellular lipid droplets’, *The Journal of Cell Biology*, 100(3), p. 965. doi: 10.1083/JCB.100.3.965.

Guan, L., Rizzello, L. and Battaglia, G. (2015) ‘Polymersomes and their Applications in Cancer Delivery and Therapy’, *Nanomedicine*, 10(17), pp. 2757–2780. doi: 10.2217/NNM.15.110.

Gumfekar, S. P. *et al.* (2017) ‘Dewatering Oil Sands Tailings with Degradable Polymer Flocculants’, *ACS Applied Materials and Interfaces*, 9(41), pp. 36290–36300. doi: 10.1021/acsami.7b10302.

Gumustas, M. *et al.* (2017) ‘Effect of Polymer-Based Nanoparticles on the Assay of Antimicrobial Drug Delivery Systems’, in *Multifunctional Systems for Combined Delivery, Biosensing and Diagnostics*. Elsevier, pp. 67–108. doi: 10.1016/B978-0-323-52725-5.00005-8.

Guo, S. *et al.* (2013) ‘Thermal decomposition kinetic evaluation and its thermal hazards prediction of AIBN’, *Journal of Thermal Analysis and Calorimetry*, 113(3), pp. 1169–1176. doi: 10.1007/s10973-013-2993-7.

Guo, X. *et al.* (2018) ‘Polymer Synthesis with More Than One Form of Living Polymerization Method’, *Macromolecular Rapid Communications*, 39(20), pp. 1–20. doi: 10.1002/marc.201800479.

Gupta, V. and Trivedi, P. (2018) ‘In vitro and in vivo characterization of pharmaceutical topical nanocarriers containing anticancer drugs for skin cancer treatment’, in Grumezescu, A. M. (ed.) *Lipid Nanocarriers for Drug Targeting*. William Andrew Publishing, pp. 563–627. doi: 10.1016/B978-0-12-813687-4.00015-3.

Haber, C., Ruiz, S. A. and Wirtz, D. (2000) ‘Shape anisotropy of a single random-walk polymer’, *Proceedings of the National Academy of Sciences of the United States of America*, 97(20), pp. 10792–10795. doi: 10.1073/PNAS.190320097.

Halim, R. and Webley, P. A. (2015) ‘Nile Red Staining for Oil Determination in Microalgal Cells: A New Insight through Statistical Modelling’, *International Journal of Chemical Engineering*, 2015(1), p. 695061. doi: 10.1155/2015/695061.

Han, S. *et al.* (2014) ‘Contribution of hydrophobic/hydrophilic modification on cationic chains of poly(ε-caprolactone)-graft-poly(dimethylamino ethylmethacrylate) amphiphilic co-polymer in gene delivery’, *Acta Biomaterialia*, 10(2), pp. 670–679. doi: 10.1016/j.actbio.2021.01.037.

Han, Y. *et al.* (2007) ‘Effects of sugar additives on protein stability of recombinant human serum albumin during lyophilization and storage’, *Archives of Pharmacal Research*, 30(9), pp. 1124–1131. doi: 10.1007/BF02980247/METRICS.

Hege, C. S. and Schiller, S. M. (2014) ‘Non-toxic catalysts for ring-opening polymerizations of biodegradable polymers at room temperature for biohybrid materials’, *Green Chemistry*, 16(3), pp. 1410–1416. doi: 10.1039/c3gc42044b.

Helfand, E. and Tagami, Y. (1971) ‘Theory of the interface between immiscible polymers’, *Journal of Polymer Science Part B: Polymer Letters*, 9(10), pp. 741–746. doi: 10.1002/POL.1971.110091006.

Le Hellaye, M. *et al.* (2008) ‘Simultaneous reversible addition fragmentation chain transfer and ring-opening polymerization’, *Journal of Polymer Science Part A: Polymer Chemistry*, 46(9), pp. 3058–3067. doi: 10.1002/POLA.22647.

Ho, D. K. *et al.* (2018) 'Farnesylated Glycol Chitosan as a Platform for Drug Delivery: Synthesis, Characterization, and Investigation of Mucus-Particle Interactions', *Biomacromolecules*, 19(8), pp. 3489–3501.

Ho, D. K. *et al.* (2020) 'Synthesis and Biopharmaceutical Characterization of Amphiphilic Squalenyl Derivative Based Versatile Drug Delivery Platform', *Frontiers in Chemistry*, 8, p. 937. doi: 10.3389/FCHEM.2020.584242/BIBTEX.

Hong, P., Koza, S. and Bouvier, E. S. P. (2012) 'Size-Exclusion Chromatography for the Analysis of Protein Biotherapeutics and their Aggregates', *Journal of Liquid Chromatography & Related Technologies*, 35(20), p. 2923. doi: 10.1080/10826076.2012.743724.

Huang, W. *et al.* (2019) 'A novel microfluidic enzyme-organocatalysis combination strategy for ring-opening copolymerizations of lactone, lactide and cyclic carbonate', *Chemical Engineering Journal*, 356, pp. 592–597. doi: https://doi.org/10.1016/j.cej.2018.09.033.

Huber, G. W., Iborra, S. and Corma, A. (2006) 'Synthesis of transportation fuels from biomass: Chemistry, catalysts, and engineering', *Chemical Reviews*, 106(9), pp. 4044–4098. doi: 10.1021/cr068360d.

Iaccarino, G. *et al.* (2019) 'Matrix metalloproteinase-cleavable nanocapsules for tumor-activated drug release', *Acta Biomaterialia*, 89, pp. 265–278. doi: 10.1016/J.ACTBIO.2019.02.043.

IARC Monographs (2016) *Some Chemicals Used as Solvents and in Polymer Manufacture*. World Health Organization. Available at: https://publications.iarc.fr/547 (Accessed: 17 February 2022).

IARC Monographs (2019) *Some Chemicals That Cause Tumours of the Urinary Tract in Rodents*. World Health Organisation. Available at: https://publications.iarc.fr/575 (Accessed: 17 February 2022).

Iqbal, S. and Ahmad, S. (2018) 'Recent development in hybrid conducting polymers: Synthesis, applications and future prospects', *Journal of Industrial and Engineering Chemistry*, 60, pp. 53–84. doi: 10.1016/J.JIEC.2017.09.038.

De Jaeghere, F. *et al.* (1999) 'Formulation and lyoprotection of poly(lactic acid-co-ethylene oxide) nanoparticles: influence on physical stability and in vitro cell uptake', *Pharmaceutical research*, 16(6), pp. 859–866. doi: 10.1023/A:1018826103261.

Jain, S. *et al.* (2012) 'Polyelectrolyte stabilized multilayered liposomes for oral delivery of paclitaxel', *Biomaterials*, 33(28), pp. 6758–6768. doi: 10.1016/J.BIOMATERIALS.2012.05.026.

Jaishankar, M. *et al.* (2014) 'Toxicity, mechanism and health effects of some heavy metals', *Interdisciplinary Toxicology*, 7(2), pp. 60–72. doi: 10.2478/intox-2014-0009.

Jang, K. *et al.* (2022) 'A Short Review on Cryoprotectants for 3D Protein Structure Analysis', *Crystals*, 12(2), p. 138. doi: 10.3390/CRYST12020138/S1.

Kakde, D. *et al.* (2016) 'Amphiphilic block copolymers from a renewable ϵ-decalactone monomer: Prediction and characterization of micellar core effects on drug encapsulation and release', *Journal of Materials Chemistry B*, 4(44), pp. 7119–7129. doi: 10.1039/c6tb01839d.

Kamber, N. E. *et al.* (2007) 'Organocatalytic ring-opening polymerization', *Chemical Reviews*, 107(12), pp. 5813–5840.

Kang, H. *et al.* (2020) 'Modification of a Nile Red Staining Method for Microplastics Analysis: A Nile Red Plate Method', *Water 2020, Vol. 12, Page 3251*, 12(11), p. 3251. doi: 10.3390/W12113251.

Katayama, Y., Sonoda, T. and Maeda, M. (2001) 'A polymer micelle responding to the protein kinase a signal', *Macromolecules*, 34(24), pp. 8569–8573.

Keros, V. *et al.* (2005) 'Optimizing cryopreservation of human testicular tissue: comparison of protocols with glycerol, propanediol and dimethylsulphoxide as cryoprotectants', *Human Reproduction*, 20(6), pp. 1676–1687. doi: 10.1093/HUMREP/DEH797.

Kesharwani, P. and Iyer, A. K. (2014) 'Recent advances in dendrimer-based nanovectors for tumor-targeted drug and gene delivery', *Drug discovery today*, 20(5), p. 536. doi: 10.1016/J.DRUDIS.2014.12.012.

Kim, I. W. *et al.* (2002) 'Dipolarity, hydrogen-bond basicity and hydrogen-bond acidity of aqueous poly(ethylene glycol) solutions', *Analytical Sciences*, 18(12), pp. 1357–1360. doi: 10.2116/ANALSCI.18.1357/METRICS.

Kozlov, M. Y. *et al.* (2000) 'Relationship between Pluronic Block Copolymer Structure, Critical Micellization Concentration and Partitioning Coefficients of Low Molecular Mass Solutes', *Macromolecules*, 33(9), pp. 3305–3313. doi: 10.1021/ma991634x.

Kratky, O. and Laggner, P. (2003) 'X-Ray Small-Angle Scattering', *Encyclopedia of Physical Science and Technology*, pp. 939–988. doi: 10.1016/B0-12-227410-5/00832-2.

Krstina, J. *et al.* (1993) 'Further studies on the thermal decomposition of AIBN—implications concerning the mechanism of termination in methacrylonitrile polymerization', *European Polymer Journal*, 29(2), pp. 379–388. doi: 10.1016/0014-3057(93)90108-R.

Kuhn, H. (1950) 'Viscosity, sedimentation, and diffusion of long-chain molecules in solution as determined by experiments on large-scale models', *Journal of Colloid Science*, 5(4), pp. 331–348. doi: 10.1016/0095-8522(50)90058-4.

Kuhn, H., Försterling, H.-D. and Waldeck, D. H. (2009) *Principles of Physical Chemistry*. 2nd Editio. Hoboken: Wiley.

Kulkarni, S. S. *et al.* (2018) 'Mechanisms by which crystalline mannitol improves the reconstitution time of high concentration lyophilized protein formulations', *European Journal of Pharmaceutics and Biopharmaceutics*, 131, pp. 70–81. doi: 10.1016/J.EJPB.2018.07.022.

Kumar, A. *et al.* (2000) 'Efficient ring-opening polymerization and copolymerization of ε-caprolactone and ω-pentadecalactone catalyzed by Candida antartica lipase B', *Macromolecules*, 33(17), pp. 6303–6309. doi: 10.1021/ma000344+.

Kumar, A. and Gross, R. A. (2000) 'Candida antartica Lipase B Catalyzed Polycaprolactone Synthesis: Effects of Organic Media and Temperature', *Biomacromolecules*, 1(1), pp. 133–138. doi: 10.1021/bm990510p.

Kuperkar, K. *et al.* (2022) 'Amphiphilic Block Copolymers: Their Structures, and Self-Assembly to Polymeric Micelles and Polymersomes as Drug Delivery Vehicles', *Polymers*, 14(21), p. 4702. doi: 10.3390/POLYM14214702.

Lazzari, S. *et al.* (2012) 'Colloidal stability of polymeric nanoparticles in biological fluids', *Journal of Nanoparticle Research*, 14(6), pp. 1–10. doi: 10.1007/S11051-012-0920-7/FIGURES/3.

Lee, C. S., Robinson, J. and Chong, M. F. (2014) ‘A review on application of flocculants in wastewater treatment’, *Process Safety and Environmental Protection*, 92(6), pp. 489–508. doi: 10.1016/J.PSEP.2014.04.010.

Lee, E. S., Na, K. and Bae, Y. H. (2003) ‘Polymeric micelle for tumor pH and folate-mediated targeting’, *Journal of Controlled Release*, 91(1–2), pp. 103–113. doi: 10.1016/S0168-3659(03)00239-6.

Leibler, L., Orland, H. and Wheeler, J. C. (1983) ‘Theory of critical micelle concentration for solutions of block copolymers’, *The Journal of chemical physics*, 79(7), pp. 3550–3557. doi: 10.1063/1.446209.

Lemoine, D. *et al.* (1996) ‘Stability study of nanoparticles of poly(ε-caprolactone), poly(d,l-lactide) and poly(d,l-lactide-co-glycolide)’, *Biomaterials*, 17(22), pp. 2191–2197. doi: 10.1016/0142-9612(96)00049-X.

Lepeltier, E., Bourgaux, C. and Couvreur, P. (2014) ‘Nanoprecipitation and the “Ouzo effect”: Application to drug delivery devices’, *Advanced Drug Delivery Reviews*, 71, pp. 86–97. doi: 10.1016/J.ADDR.2013.12.009.

Letchford, K. and Burt, H. (2007) ‘A review of the formation and classification of amphiphilic block copolymer nanoparticulate structures: micelles, nanospheres, nanocapsules and polymersomes’, *European Journal of Pharmaceutics and Biopharmaceutics*, 65(3), pp. 259–269. doi: 10.1016/J.EJPB.2006.11.009.

Li, C. *et al.* (2020) ‘Self-assembly of block copolymers towards mesoporous materials for energy storage and conversion systems’, *Chemical Society Reviews*, 49(14), pp. 4681–4736. doi: 10.1039/D0CS00021C.

Li, S. *et al.* (1996) ‘Effects of Reducing Sugars on the Chemical Stability of Human Relaxin in the Lyophilized State’, *Journal of Pharmaceutical Sciences*, 85(8), pp. 873–877. doi: 10.1021/JS950456S.

Li, X.-R., Wangb, X.-L. and Koseki, H. (2008) ‘Study on thermal decomposition characteristics of AIBN’, *Journal of hazardous materials*, 159(1), pp. 13–18. doi: 10.1016/J.JHAZMAT.2008.01.062.

Lindvig, T., Michelsen, M. L. and Kontogeorgis, G. M. (2002) ‘A Flory-Huggins model based on the Hansen solubility parameters’, *Fluid Phase Equilibria*, 203, pp. 247–260.

Lipinski, C. A. (2000) ‘Drug-like properties and the causes of poor solubility and poor permeability’, *Journal of Pharmacological and Toxicological Methods*, 44(1), pp. 235–249. doi: 10.1016/S1056-8719(00)00107-6.

Lipinski, C. A. *et al.* (2001) ‘Experimental and computational approaches to estimate solubility and permeability in drug discovery and development q settings’, *Advanced Drug Delivery Reviews*, 46, pp. 3–26.

Liu, T., Liu, L.-Z. and Chu, B. (2000) ‘Formation of Amphiphilic Block Copolymer Micelles in Nonaqueous Solution’, in *Amphiphilic Block Copolymers*. Elsevier, pp. 115–149. doi: 10.1016/B978-044482441-7/50007-4.

Lohmeijer, B. G. G. *et al.* (2006) ‘Guanidine and amidine organocatalysts for ring-opening polymerization of cyclic esters’, *Macromolecules*, 39(25), pp. 8574–8583. doi: 10.1021/ma0619381.

Lomba, L. *et al.* (2023) ‘Deep Eutectic Solvents Formed by Glycerol and Xylitol, Fructose and Sorbitol: Effect of the Different Sugars in Their Physicochemical Properties’, *Molecules*, 28(16), p. 6023. doi: 10.3390/MOLECULES28166023/S1.

Lu, Y., Li, J. and Wang, G. (2008) ‘In vitro and in vivo evaluation of mPEG-PLA modified liposomes loaded glycyrrhetinic acid’, *International Journal of Pharmaceutics*, 356(1–2), pp. 274–281. doi: 10.1016/J.IJPHARM.2007.12.047.

Luo, J. *et al.* (2011) ‘Diffusion dialysis-concept, principle and applications’, *Journal of Membrane Science*, 366(1–2), pp. 1–16. doi: 10.1016/J.MEMSCI.2010.10.028.

Luo, W. C. *et al.* (2021) ‘Impact of formulation on the quality and stability of freeze-dried nanoparticles’, *European Journal of Pharmaceutics and Biopharmaceutics*, 169, pp. 256–267. doi: 10.1016/J.EJPB.2021.10.014.

Luz, C. M. *et al.* (2017) ‘Poly-lactic acid nanoparticles (PLA-NP) promote physiological modifications in lung epithelial cells and are internalized by clathrin-coated pits and lipid rafts’, *Journal of Nanobiotechnology*, 15(1), pp. 1–18. doi: 10.1186/S12951-016-0238-1/FIGURES/7.

Machado, C. F. R. *et al.* (2018) 'Carbon dioxide and ethanol from sugarcane biorefinery as renewable feedstocks to environment-oriented integrated chemical plants.', *Journal of Cleaner Production*, 172, pp. 1232–1242. doi: https://doi.org/10.1016/j.jclepro.2017.10.234.

Macmillan Cancer Support (2018) *How is chemotherapy administered? Day units, hospital, home - Macmillan Cancer Support*, *Macmillan Cancer Support*. Available at: https://www.macmillan.org.uk/cancer-information-and-support/treatment/types-of-treatment/chemotherapy/how-chemotherapy-is-given (Accessed: 18 February 2022).

Maes, T. *et al.* (2017) 'A rapid-screening approach to detect and quantify microplastics based on fluorescent tagging with Nile Red', *Scientific Reports 2017 7:1*, 7(1), pp. 1–10. doi: 10.1038/srep44501.

Majeed, S. A., Sekhosana, K. E. and Tuhl, A. (2020) 'Progress on phthalocyanine-conjugated Ag and Au nanoparticles: Synthesis, characterization, and photo-physicochemical properties', *Arabian Journal of Chemistry*, 13(12), pp. 8848–8887. doi: 10.1016/J.ARABJC.2020.10.014.

Mark, J. E. (2007) *Physical Properties of Polymers Handbook*. Second, *Physical Properties of Polymers Handbook*. Second. Edited by J. E. Mark. Springer New York. doi: 10.1007/978-0-387-69002-5.

Martínez Rivas, C. J. *et al.* (2017) 'Nanoprecipitation process: From encapsulation to drug delivery', *International Journal of Pharmaceutics*, 532(1), pp. 66–81. doi: 10.1016/J.IJPHARM.2017.08.064.

Matyjaszewski, K. (1998) 'Overview: Fundamentals of Controlled/Living Radical Polymerization', in *ACS Symposium Series*. Washington: American Chemical Society, pp. 2–30. doi: 10.1021/bk-1998-0685.ch001.

Matyjaszewski, K. and Spanswick, J. (2005) 'Controlled/living radical polymerization', *Materials Today*, 8(3), pp. 26–33. doi: 10.1016/S1369-7021(05)00745-5.

Mensink, M. A. *et al.* (2017) 'How sugars protect proteins in the solid state and during drying (review): Mechanisms of stabilization in relation to stress conditions', *European Journal of Pharmaceutics and Biopharmaceutics*, 114, pp. 288–295. doi: 10.1016/J.EJPB.2017.01.024.

Mi, Y., Wood, G. and Thoma, L. (2004) ‘Cryoprotection mechanisms of polyethylene glycols on lactate dehydrogenase during freeze-thawing’, *The AAPS Journal*, 6(3), p. 45. doi: 10.1208/AAPSJ060322.

Miller, K. D. *et al.* (2016) ‘Cancer treatment and survivorship statistics, 2016’, *CA: A Cancer Journal for Clinicians*, 66(4), pp. 271–289. doi: 10.3322/CAAC.21349.

Moad, G., Rizzardo, E. and Thang, S. H. (2012) ‘Living radical polymerization by the RAFT process a third update’, *Australian Journal of Chemistry*, 65(8), pp. 985–1076. doi: 10.1071/CH12295.

Mohammady, M., Mohammadi, Y. and Yousefi, G. (2020) ‘Freeze-Drying of Pharmaceutical and Nutraceutical Nanoparticles: The Effects of Formulation and Technique Parameters on Nanoparticles Characteristics’, *Journal of Pharmaceutical Sciences*, 109(11), pp. 3235–3247. doi: 10.1016/J.XPHS.2020.07.015.

Morgen, M. *et al.* (2012) ‘Polymeric nanoparticles for increased oral bioavailability and rapid absorption using celecoxib as a model of a low-solubility, high-permeability drug’, *Pharmaceutical Research*, 29(2), pp. 427–440. doi: 10.1007/S11095-011-0558-7/FIGURES/10.

Munch, M. R. and Gast, A. P. (1988) ‘Block Copolymers at Interfaces. 1. Micelle Formation’, *Macromolecules*, 21(5), pp. 1360–1366. doi: 10.1021/ma00183a030.

Murray, K. A. and Gibson, M. I. (2022) ‘Chemical approaches to cryopreservation’, *Nature Reviews Chemistry 2022 6:8*, 6(8), pp. 579–593. doi: 10.1038/s41570-022-00407-4.

Nagarajan, R. (2002) ‘Molecular Packing Parameter and Surfactant Self-Assembly: The Neglected Role of the Surfactant Tail†’, *Langmuir*, 18(1), pp. 31–38. doi: 10.1021/LA010831Y.

Nagarajan, R. and Ganesh, K. (1989) ‘Block copolymer self-assembly in selective solvents: Spherical micelles with segregated cores’, *The Journal of Chemical Physics*, 90(10), pp. 5843–5856. doi: 10.1063/1.456390.

Nalbone, L. *et al.* (2021) ‘Nile Red staining for detecting microplastics in biota: Preliminary evidence’, *Marine Pollution Bulletin*, 172, p. 112888. doi: 10.1016/J.MARPOLBUL.2021.112888.

NCRAS and CRUK (2017) *Chemotherapy, Radiotherapy and Tumour Resections in England 2013-2014*. London. Available at: https://www.cancerresearchuk.org/health-professional/cancer-statistics/treatment#heading-Four (Accessed: 17 February 2022).

NHS (2016) *NHS England - Chemo drug optimisation to improve patient experience of cancer treatment*. Available at: https://www.england.nhs.uk/2016/05/chemo-drug-optimisation/ (Accessed: 18 February 2022).

NHS (2020a) *Chemotherapy - NHS*. Available at: https://www.nhs.uk/conditions/chemotherapy/ (Accessed: 17 February 2022).

NHS (2020b) *Chemotherapy - Side effects - NHS, National Health Service*. Available at: https://www.nhs.uk/conditions/chemotherapy/side-effects/ (Accessed: 18 February 2022).

Nicolas, J. *et al.* (2013) 'Nitroxide-mediated polymerization', *Progress in Polymer Science*, 38(1), pp. 63–235. doi: 10.1016/j.progpolymsci.2012.06.002.

Nistane, J. *et al.* (2022) 'Estimation of the Flory-Huggins interaction parameter of polymer-solvent mixtures using machine learning', *MRS Communications*, 12(6), pp. 1096–1102. doi: 10.1557/S43579-022-00237-X/FIGURES/7.

Nita, L. E. *et al.* (2011) 'Biomaterials based on 2-hydroxyethyl methacrylate: The influence of the initiator type', *Revue Roumaine de Chimie*, 56(5), pp. 537–543.

Nowak, D. and Jakubczyk, E. (2020) 'The Freeze-Drying of Foods—The Characteristic of the Process Course and the Effect of Its Parameters on the Physical Properties of Food Materials', *Foods*, 9(10). doi: 10.3390/FOODS9101488.

O'Brien, D. M. *et al.* (2020) 'A "greener" one-pot synthesis of monoterpene-functionalised lactide oligomers', *European Polymer Journal*, 125(November 2019). doi: 10.1016/j.eurpolymj.2020.109516.

Ochbaum, G. and Bitton, R. (2018) 'Using small-angle X-ray scattering (SAXS) to study the structure of self-assembling biomaterials', *Self-Assembling Biomaterials: Molecular Design, Characterization and Application in Biology and Medicine*, pp. 291–304. doi: 10.1016/B978-0-08-102015-9.00015-0.

Odian, G. (2004) *Principles of Polymerization*. Fourth Edi, *Principles of Polymerization*. Fourth Edi. New Jersey: John Wiley & Sons, Inc. doi: 10.1002/047147875X.

Oerlemans, C. *et al.* (2010) 'Polymeric Micelles in Anticancer Therapy: Targeting, Imaging and Triggered Release', *Pharmaceutical Research 2010 27:12*, 27(12), pp. 2569–2589. doi: 10.1007/S11095-010-0233-4.

Oh, J. K. (2011) 'Polylactide (PLA)-based amphiphilic block copolymers: Synthesis, self-assembly, and biomedical applications', *Soft Matter*, 7(11), pp. 5096–5108. doi: 10.1039/c0sm01539c.

Pace, V. *et al.* (2012) '2-Methyltetrahydrofuran (2-MeTHF): A biomass-derived solvent with broad application in organic chemistry', *ChemSusChem*, 5(8), pp. 1369–1379. doi: 10.1002/cssc.201100780.

Pacheco, Ana A.C. *et al.* (2021) 'Influence of structure and solubility of chain transfer agents on the RAFT control of dispersion polymerisation in scCO2', *Chemical Science*, 12(3), pp. 1016–1030. doi: 10.1039/D0SC05281G.

Pacheco, Ana A. C. *et al.* (2021) 'Influence of structure and solubility of chain transfer agents on the RAFT control of dispersion polymerisation in scCO2', *Chemical Science*, 12, pp. 1016–1030. doi: 10.1039/d0sc05281g.

Park, J. H. *et al.* (2008) 'Polymeric nanomedicine for cancer therapy', *Progress in Polymer Science (Oxford)*, 33(1), pp. 113–137. doi: 10.1016/j.progpolymsci.2007.09.003.

Parkatzidis, K. *et al.* (2020) 'Recent Developments and Future Challenges in Controlled Radical Polymerization: A 2020 Update', *Chem*, 6(7), pp. 1575–1588. doi: 10.1016/J.CHEMPR.2020.06.014.

Passos, M. L. C. *et al.* (2018) 'Organic Compounds', in *Reference Module in Chemistry, Molecular Sciences and Chemical Engineering*. Elsevier. doi: 10.1016/B978-0-12-409547-2.14465-8.

Pate, K. and Safier, P. (2016) 'Chemical metrology methods for CMP quality', in Babu, S. (ed.) *Advances in Chemical Mechanical Planarization (CMP)*. Woodhead Publishing, pp. 299–325. doi: 10.1016/B978-0-08-100165-3.00012-7.

Patel, M., Park, J. K. and Jeong, B. (2023) 'Rediscovery of poly(ethylene glycol)s as a cryoprotectant for mesenchymal stem cells', *Biomaterials Research*, 27(1), pp. 1–11. doi: 10.1186/S40824-023-00356-Z/FIGURES/7.

Paul J. Flory (1953) *Principles of Polymer Chemistry, Macromolecular Science*. Cornell University Press.

Pearce, A. K. *et al.* (2019) 'Versatile, Highly Controlled Synthesis of Hybrid (Meth)acrylate–Polyester–Carbonates and their Exploitation in Tandem Post-Polymerization–Functionalization', *Macromolecular Chemistry and Physics*, 220(21), pp. 1–9. doi: 10.1002/macp.201900270.

Peeters, J. W. *et al.* (2005) 'Lipase-catalyzed ring-opening polymerizations of 4-substituted ε-caprolactones: Mechanistic considerations', *Macromolecules*, 38(13), pp. 5587–5592. doi: 10.1021/ma050510j.

Pellis, A. *et al.* (2019) 'Safer bio-based solvents to replace toluene and tetrahydrofuran for the biocatalyzed synthesis of polyesters', *Green Chemistry*, 21(7), pp. 1686–1694. doi: 10.1039/c8gc03567a.

Pena-Pereira, F. and de la Calle, I. (2019) 'Solvents and Eutectic Solvents', in *Reference Module in Chemistry, Molecular Sciences and Chemical Engineering*. Elsevier. doi: 10.1016/B978-0-12-409547-2.14020-X.

Phan, H. *et al.* (2019) 'Role of self-assembly conditions and amphiphilic balance on nanoparticle formation of PEG-PDLLA copolymers in aqueous environments', *Journal of Polymer Science, Part A: Polymer Chemistry*, 57(17), pp. 1801–1810. doi: 10.1002/pola.29451.

Pignatello, R. *et al.* (2001) 'Preparation and Analgesic Activity of Eudragit RS100® Microparticles Containing Diflunisal', *Drug Delivery*, 8(1), pp. 35–45. doi: 10.1080/107175401300002748.

Prasad, S. *et al.* (2017) 'Fabrication of nanostructures through self-assembly of non-ionic amphiphiles for biomedical applications', *RSC Advances*, 7(36), pp. 22121–22132. doi: 10.1039/C6RA28654B.

Pratt, R. C. *et al.* (2006) 'Triazabicyclodecene: A simple bifunctional organocatalyst for acyl transfer and ring-opening polymerization of cyclic esters', *Journal of the American Chemical Society*, 128(14), pp. 4556–4557. doi: 10.1021/ja060662+.

Ramamoorth, M. and Narvekar, A. (2015) 'Non Viral Vectors in Gene Therapy- An Overview', *Journal of Clinical and Diagnostic Research : JCDR*, 9(1), p. GE06. doi: 10.7860/JCDR/2015/10443.5394.

Ramanathan, M. *et al.* (2013) 'Amphiphile nanoarchitectonics: from basic physical chemistry to advanced applications', *Physical Chemistry Chemical Physics*, 15(26), pp. 10580–10611. doi: 10.1039/C3CP50620G.

Rapoport, N. (2007) 'Physical stimuli-responsive polymeric micelles for anti-cancer drug delivery', *Progress in Polymer Science*, 32(8–9), pp. 962–990. doi: 10.1016/J.PROGPOLYMSCI.2007.05.009.

Roduit, B. *et al.* (2015) 'Thermal decomposition of AIBN, Part B: Simulation of SADT value based on DSC results and large scale tests according to conventional and new kinetic merging approach', *Thermochimica Acta*, 621, pp. 6–24. doi: 10.1016/j.tca.2015.06.014.

Rubin, R. J. (1965) 'Random-Walk Model of Chain-Polymer Adsorption at a Surface', *The Journal of Chemical Physics*, 43(7), pp. 2392–2407. doi: 10.1063/1.1697138.

Ruiz-Cantu, L. A. *et al.* (2019) 'Synthesis of Methacrylate-Terminated Block Copolymers with Reduced Transesterification by Controlled Ring-Opening Polymerization', *Macromolecular Chemistry and Physics*, 220(2), pp. 1800459 (1–11). doi: 10.1002/macp.201800459.

Rumin, J. *et al.* (2015) 'The use of fluorescent Nile red and BODIPY for lipid measurement in microalgae', *Biotechnology for Biofuels*, 8(1), pp. 1–16. doi: 10.1186/S13068-015-0220-4/FIGURES/1.

Sadikoglu, H., Ozdemir, M. and Seker, M. (2006) 'Freeze-Drying of Pharmaceutical Products: Research and Development Needs', *Drying Technology*, 24(7), pp. 849–861. doi: 10.1080/07373930600734018.

Salvage, J. P. *et al.* (2015) 'Nanoprecipitation of polymeric nanoparticle micelles based on 2-methacryloyloxyethyl phosphorylcholine (MPC) with 2-(diisopropylamino)ethyl methacrylate (DPA), for intracellular delivery applications', *Journal of Materials Science. Materials in Medicine*, 26(3), p. 150. doi: 10.1007/S10856-015-5480-9.

Savjani, K. T., Gajjar, A. K. and Savjani, J. K. (2012) 'Drug Solubility: Importance and Enhancement Techniques', *ISRN Pharmaceutics*, 2012, pp. 1–10. doi: 10.5402/2012/195727.

Scheerstra, J. F. *et al.* (2022) 'Polymersomes as a potential platform for cancer immunotherapy', *Materials Today Advances*, 13, p. 100203. doi: 10.1016/J.MTADV.2021.100203.

Schulz, J. D., Gauthier, M. A. and Leroux, J. C. (2015) 'Improving oral drug bioavailability with polycations?', *European Journal of Pharmaceutics and Biopharmaceutics*, 97, pp. 427–437. doi: 10.1016/J.EJPB.2015.04.025.

Seyednejad, H. *et al.* (2011) 'Functional aliphatic polyesters for biomedical and pharmaceutical applications', *Journal of Controlled Release*, 152(1), pp. 168–176. doi: 10.1016/J.JCONREL.2010.12.016.

Shoda, S. *et al.* (2016) 'Enzymes as Green Catalysts for Precision Macromolecular Synthesis', *Chemical Reviews*, 116(4), pp. 2307–2413. doi: 10.1021/acs.chemrev.5b00472.

Siegwart, D. J., Oh, J. K. and Matyjaszewski, K. (2012) 'ATRP in the design of functional materials for biomedical applications', *Progress in Polymer Science*, 37(1), pp. 18–37. doi: 10.1016/j.progpolymsci.2011.08.001.ATRP.

Singh, A. K. (2016) 'Experimental Methodologies for the Characterization of Nanoparticles', in *Engineered Nanoparticles*. Academic Press, pp. 125–170. doi: 10.1016/B978-0-12-801406-6.00004-2.

Sriwidodo *et al.* (2022) 'Liposome-polymer complex for drug delivery system and vaccine stabilization', *Heliyon*, 8(2), p. e08934. doi: 10.1016/J.HELIYON.2022.E08934.

Stavila, E. *et al.* (2014) 'Lipase-Catalyzed Ring-Opening Copolymerization of ε-Caprolactone and β-Lactam', *Biomacromolecules*, 15(1), pp. 234–241. doi: 10.1021/bm401514k.

Storey, K. B. and Storey, J. M. (1991) 'Biochemistry of Cryoprotectants', in Lee, R. E. and Denlinger, D. L. (eds) *Insects at Low Temperature*. Boston, MA: Springer US, pp. 64–93. doi: 10.1007/978-1-4757-0190-6_4.

Striegel, A. M. *et al.* (2009) *Modern size-exclusion liquid chromatography : practice of gel permeation and gel filtration chromatography*. 2nd Edition. New York: Wiley.

Subramanian, M. N. (2015) *Basics of Polymers: Fabrication and Processing Technology*. New York: Momentum Press Engineering. doi: 10.5643/9781606505830.

Takwa, M. *et al.* (2008) ‘Lipase catalyzed HEMA initiated ring-opening polymerization: In situ formation of mixed polyester methacrylates by transesterification’, *Biomacromolecules*, 9(2), pp. 704–710. doi: 10.1021/bm7010449.

Tambasco, M., Lipson, J. E. G. and Higgins, J. S. (2006) ‘Blend miscibility and the Flory-Huggins interaction parameter: A critical examination’, *Macromolecules*, 39(14), pp. 4860–4868. doi: 10.1021/MA060304R.

Tang, Z. *et al.* (2016) ‘Polymeric nanostructured materials for biomedical applications’, *Progress in Polymer Science*, 60, pp. 86–128. doi: 10.1016/J.PROGPOLYMSCI.2016.05.005.

Teo, W. *et al.* (2021) ‘Nile Red fluorescence spectroscopy reports early physicochemical changes in myelin with high sensitivity’, *Proceedings of the National Academy of Sciences of the United States of America*, 118(8), p. e2016897118. doi: 10.1073/PNAS.2016897118/-/DCSUPPLEMENTAL.

Thambi, T., Park, J. H. and Lee, D. S. (2015) ‘Stimuli-responsive polymersomes for cancer therapy’, *Biomaterials Science*, 4(1), pp. 55–69. doi: 10.1039/C5BM00268K.

Tong, R. and Cheng, J. (2008) ‘Paclitaxel-initiated, controlled polymerization of lactide for the formulation of polymeric nanoparticulate delivery vehicles’, *Angewandte Chemie - International Edition*, 47(26), pp. 4830–4834. doi: 10.1002/anie.200800491.

Tonnis, W. F. *et al.* (2015) ‘Size and molecular flexibility of sugars determine the storage stability of freeze-dried proteins’, *Molecular Pharmaceutics*, 12(3), pp. 684–694.

Topel, Ö. *et al.* (2013) ‘Determination of critical micelle concentration of polybutadiene-block-poly(ethyleneoxide) diblock copolymer by fluorescence spectroscopy and dynamic light scattering’, *Journal of Molecular Liquids*, 177, pp. 40–43. doi: 10.1016/J.MOLLIQ.2012.10.013.

Trenkenschuh, E. and Friess, W. (2021) ‘Freeze-drying of nanoparticles: How to overcome colloidal instability by formulation and process optimization’, *European Journal of Pharmaceutics and Biopharmaceutics*, 165, pp. 345–360. doi: 10.1016/J.EJPB.2021.05.024.

Umerska, A. *et al.* (2018) ‘Freeze drying of polyelectrolyte complex nanoparticles: Effect of nanoparticle composition and cryoprotectant selection’, *International Journal of Pharmaceutics*, 552(1–2), pp. 27–38. doi: 10.1016/j.ijpharm.2018.09.035.

Vasey, C. E. *et al.* (2019) ‘Amphiphilic tri- and tetra-block co-polymers combining versatile functionality with facile assembly into cytocompatible nanoparticles’, *Biomaterials Science*, 7(9), pp. 3832–3845. doi: 10.1039/c9bm00667b.

Vauthier, C., Cabane, B. and Labarre, D. (2008) ‘How to concentrate nanoparticles and avoid aggregation?’, *European Journal of Pharmaceutics and Biopharmaceutics*, 69(2), pp. 466–475. doi: 10.1016/J.EJPB.2008.01.025.

Vemula, V. R., Lagishetty, V. and Lingala, S. (2010) ‘Solubility enhancement techniques’, *International Journal of Pharmaceutical Sciences Review and Research*, 5(1), pp. 41–51.

Vergaelen, M. *et al.* (2020) ‘Ethyl acetate as solvent for the synthesis of poly(2-ethyl-2-oxazoline)’, *Green Chemistry*. doi: 10.1039/c9gc03872h.

Wang, R. and Xu, Y. (2017) ‘Development and evaluation of nanoparticles based on mPEG-PLA for controlled delivery of vinpocetine: in vitro and in vivo studies’, *Artificial Cells, Nanomedicine, and Biotechnology*, 45(1), pp. 157–162. doi: 10.3109/21691401.2016.1138492.

Weng, L., Chen, C., *et al.* (2011) ‘Molecular dynamics study of effects of temperature and concentration on hydrogen-bond abilities of ethylene glycol and glycerol: Implications for cryopreservation’, *Journal of Physical Chemistry A*, 115(18), pp. 4729–4737.

Weng, L., Li, W., *et al.* (2011) ‘Osmolality and unfrozen water content of aqueous solution of dimethyl sulfoxide’, *Journal of Chemical and Engineering Data*, 56(7), pp. 3175–3182.

Werner, M. E. *et al.* (2013) ‘Preclinical evaluation of genexol-pm, a nanoparticle formulation of paclitaxel, as a novel radiosensitizer for the treatment of non-small cell lung cancer’, *International Journal of Radiation Oncology Biology Physics*, 86(3), pp. 463–468. doi: 10.1016/j.ijrobp.2013.02.009.

Whaley, D. *et al.* (2021) ‘Cryopreservation: An Overview of Principles and Cell-Specific Considerations’, *Cell Transplantation*, 30. doi: 10.1177/0963689721999617.

Xiao, X. *et al.* (2022a) ‘Polymeric nanoparticles—Promising carriers for cancer therapy’, *Frontiers in Bioengineering and Biotechnology*, 10, p. 1024143. doi: 10.3389/FBIOE.2022.1024143/BIBTEX.

Xiao, X. *et al.* (2022b) ‘Polymeric nanoparticles—Promising carriers for cancer therapy’, *Frontiers in Bioengineering and Biotechnology*, 10, p. 1024143. doi: 10.3389/FBIOE.2022.1024143.

Xiao, Y. *et al.* (2009) ‘Systematic Comparison of HEA and HEMA as Initiators in Enzymatic Ring-Opening Polymerizations’, *Macromolecular Bioscience*, 9(7), pp. 713–720. doi: 10.1002/mabi.200800290.

Xie, Z. *et al.* (2009) ‘Synthesis, self-assembly in water, and cytotoxicity of MPEG-block-PLLA/DX conjugates’, *Journal of Biomedical Materials Research - Part A*, 88(1), pp. 238–245. doi: 10.1002/jbm.a.31861.

Xu, C. *et al.* (2023) ‘Precise control of conjugated polymer synthesis from step-growth polymerization to iterative synthesis’, *Giant*, 14, p. 100154. doi: 10.1016/J.GIANT.2023.100154.

Xu, X. *et al.* (2009) ‘Ultrafine PEG-PLA fibers loaded with both paclitaxel and doxorubicin hydrochloride and their in vitro cytotoxicity’, *European Journal of Pharmaceutics and Biopharmaceutics*, 72(1), pp. 18–25. doi: 10.1016/j.ejpb.2008.10.015.

Yadav, H. K. S. *et al.* (2019) ‘Polymer-Based Nanomaterials for Drug-Delivery Carriers’, in *Nanocarriers for Drug Delivery*. Elsevier, pp. 531–556. doi: 10.1016/B978-0-12-814033-8.00017-5.

Yamada, S. (2014) ‘Surfactant Assemblies (Micelles, Vesicles, Emulsions, Films, etc.), an Overview’, in *Encyclopedia of Polymeric Nanomaterials*. Berlin, Heidelberg: Springer Berlin Heidelberg, pp. 1–6. doi: 10.1007/978-3-642-36199-9_158-1.

Yin, Q. *et al.* (2014) ‘Anticancer camptothecin-N-poly(lactic acid) nanoconjugates with facile hydrolysable linker’, *Polymer Chemistry*, 5(5), pp. 1581–1585. doi: 10.1039/c3py01245j.

Young, R. J. and Lovell, P. A. (2011) *Introduction to polymers*. 3rd Edition. CRC Press.

Yousefi Rizi, H. A., Shin, D. H. and Rizi, S. Y. (2022) ‘Polymeric Nanoparticles in Cancer Chemotherapy: A Narrative Review’, *Iranian Journal of Public Health*, 51(2), pp. 226–239. doi: 10.18502/IJPH.V51I2.8677.

Yu, K. *et al.* (2016) 'Comparison of three different conjugation strategies in the construction of herceptin-bearing paclitaxel-loaded nanoparticles', *Biomaterials Science*, 4(8), pp. 1219–1232. doi: 10.1039/c6bm00308g.

Zainal-Abidin, M. H. *et al.* (2017) 'New horizons in the extraction of bioactive compounds using deep eutectic solvents: A review', *Analytica Chimica Acta*, 979, pp. 1–23. doi: 10.1016/J.ACA.2017.05.012.

Zambrano-Zaragoza, M. L. *et al.* (2011) 'Optimization of nanocapsules preparation by the emulsion–diffusion method for food applications', *LWT - Food Science and Technology*, 44(6), pp. 1362–1368. doi: 10.1016/J.LWT.2010.10.004.

Zhang, J.-Z. *et al.* (2019) 'The Persistence Length of Semiflexible Polymers in Lattice Monte Carlo Simulations', *Polymers*, 11(2), p. 295. doi: 10.3390/polym11020295.

Zhang, P. Q. *et al.* (2022) 'The effect of glycerol as a cryoprotective agent in the cryopreservation of adipose tissue', *Stem Cell Research and Therapy*, 13(1), pp. 1–13. doi: 10.1186/S13287-022-02817-Z/FIGURES/7.

Zhao, T. *et al.* (2015) 'Excess Properties and Spectroscopic Studies for Binary System of Polyethylene Glycol 200 (1) + Dimethyl Sulfoxide (2) at T = (298.15 to 318.15) K', *Journal of Chemical and Engineering Data*, 60(7), pp. 2135–2145.

Zheng, X. L. *et al.* (2010) 'Preparation of MPEG–PLA nanoparticle for honokiol delivery in vitro', *International Journal of Pharmaceutics*, 386(1–2), pp. 262–267. doi: 10.1016/J.IJPHARM.2009.11.014.

Zhong, F. *et al.* (2017) 'Allylthioketone mediated free radical polymerization of methacrylates', *Polymers*, 9(11), pp. 1–17. doi: 10.3390/polym9110608.

Zhou, X., He, J. and Zhou, C. (2019) 'Strategies from nature: Polycaprolactone-based mimetic antimicrobial peptide block copolymers with low cytotoxicity and excellent antibacterial efficiency', *Polymer Chemistry*, 10(8), pp. 945–953. doi: 10.1039/c8py01394b.

Zhou, Y. *et al.* (2023) 'Further Improvement Based on Traditional Nanocapsule Preparation Methods: A Review', *Nanomaterials 2023, Vol. 13, Page 3125*, 13(24), p. 3125. doi: 10.3390/NANO13243125.

Zhu, M. M. *et al.* (2016) 'A facile chemoenzymatic synthesis of amphiphilic miktoarm star copolymers from a sugar core and their potential for anticancer drug delivery', *Polymer*, 93, pp. 159–166. doi: 10.1016/j.polymer.2016.04.035.

Zhu, Z. (2013) 'Effects of amphiphilic diblock copolymer on drug nanoparticle formation and stability', *Biomaterials*, 34(38), pp. 10238–10248. doi: 10.1016/J.BIOMATERIALS.2013.09.015.

Zielinska, A. *et al.* (2020) 'Polymeric Nanoparticles: Production, Characterization, Toxicology and Ecotoxicology', *Molecules*, 25(16). doi: 10.3390/MOLECULES25163731.

Figure acknowledgements

The following figures and tables have been used with permission from the copyright holders:

Figure 2.1 - Tang, Z. et al. (2016) 'Polymeric nanostructured materials for biomedical applications', *Progress in Polymer Science*, 60, pp. 86–128. doi: 10.1016/J.PROGPOLYMSCI.2016.05.005.

Figure 2.2 - Sriwidodo et al. (2022) 'Liposome-polymer complex for drug delivery system and vaccine stabilization', *Heliyon*, 8(2), p. e08934. doi: 10.1016/J.HELIYON.2022.E08934.

Figure 2.5 - Bossion, A. *et al.* (2019) 'Opportunities for organocatalysis in polymer synthesis via step-growth methods', *Progress in Polymer Science*, 90, pp. 164–210. doi: 10.1016/J.PROGPOLYMSCI.2018.11.003.

Table 2.2, Figure 3.1, Chapter 4 Figures - Englezou, G. *et al.* (2020) '2-Methyltetrahydrofuran (2-MeTHF) as a versatile green solvent for the synthesis of amphiphilic copolymers via ROP, FRP, and RAFT tandem polymerizations', *Journal of Polymer Science*, 58(11), pp. 1571–1581. doi: 10.1002/pol.20200183.

Figure 2.6 - Ferrari, R. *et al.* (2013) 'Tunable PLGA-based nanoparticles synthesized through free-radical polymerization', *Macromolecular Materials and Engineering*, 298(7), pp. 730–739. doi: 10.1002/mame.201200069.

Figure 2.9 - Ramanathan, M. *et al.* (2013) 'Amphiphile nanoarchitectonics: from basic physical chemistry to advanced applications', *Physical Chemistry Chemical Physics*, 15(26), pp. 10580–10611. doi: 10.1039/C3CP50620G.

Figure 2.10 - Leibler, L., Orland, H. and Wheeler, J. C. (1983) 'Theory of critical micelle concentration for solutions of block copolymers', *The Journal of chemical physics*, 79(7), pp. 3550–3557. doi: 10.1063/1.446209.

Figure 2.11 and 2.12 - Munch, M. R. and Gast, A. P. (1988) 'Block Copolymers at Interfaces. 1. Micelle Formation', *Macromolecules*, 21(5), pp. 1360–1366. doi: 10.1021/ma00183a030.

Figure 2.13 - Nagarajan, R. and Ganesh, K. (1989) ‘Block copolymer self-assembly in selective solvents: Spherical micelles with segregated cores’, *The Journal of Chemical Physics*, 90(10), pp. 5843–5856. doi: 10.1063/1.456390.

Figure 3.2 - Striegel, A. M. *et al.* (2009) *Modern size-exclusion liquid chromatography : practice of gel permeation and gel filtration chromatography*. 2nd Edition. New York: Wiley.

Figure 3.3 - Pate, K. and Safier, P. (2016) ‘Chemical metrology methods for CMP quality’, in Babu, S. (ed.) *Advances in Chemical Mechanical Planarization (CMP)*. Woodhead Publishing, pp. 299–325. doi: 10.1016/B978-0-08-100165-3.00012-7.

Figure 3.4 - Singh, A. K. (2016) ‘Experimental Methodologies for the Characterization of Nanoparticles’, in *Engineered Nanoparticles*. Academic Press, pp. 125–170. doi: 10.1016/B978-0-12-801406-6.00004-2.

Figure 3.5 - Ahmad Mir, R., Mansoor Shafi, S. and Zargar, S. M. (2023) ‘Analysis of proteomes—II’, in *Principles of Genomics and Proteomics*. Elsevier, pp. 139–163. doi: 10.1016/B978-0-323-99045-5.00010-0.

Appendix

A. TEM measurements

To inspect the self-assembly of the materials synthesised with hyper-branched architectures in Chapter 4 and their shape in the dry state, a TEM characterisation of RAFT-PEGMA-LA_{25} was conducted by Kristoffer Kortsen from the School of Chemistry, at the University of Nottingham. Here, the experimental details and the results collected from the TEM measurement are included as presented in the Englezou *et al.* (2020) journal paper.

A.1 Experimental procedure

To carry out the Transmission Electron Microscopy (TEM) the nanoparticle sample prepared by nanoprecipitation was diluted to a concentration of 0.1 mg/ml. A volume of 13 μL of this aqueous suspension was deposited onto a copper grid (Formvar/carbon film 200 mesh copper [100]). The grid with the nanoparticle aqueous suspension was left to settle. After 10 min, a paper was used to remove the excess material. The grid was placed in a fume cupboard to dry for at least 30 min prior to the analysis. FEI Tecnai BioTwin-12 TEM equipped with a digital camera, located at the Nanoscale and Microscale Research Centre of the University of Nottingham, was utilised to record the TEM images.

A.2 Results

To verify the self-assembly of these novel hyper-branched polymeric material and their form when in the dry state, RAFT-PEGMA-LA_{25} was examined via TEM as an illustration (Figure A.1). Spherical particles, measuring between 41 and 59 nm (with an average of 50 ± 9 nm), were observed, confirming the nanoparticle characteristics.

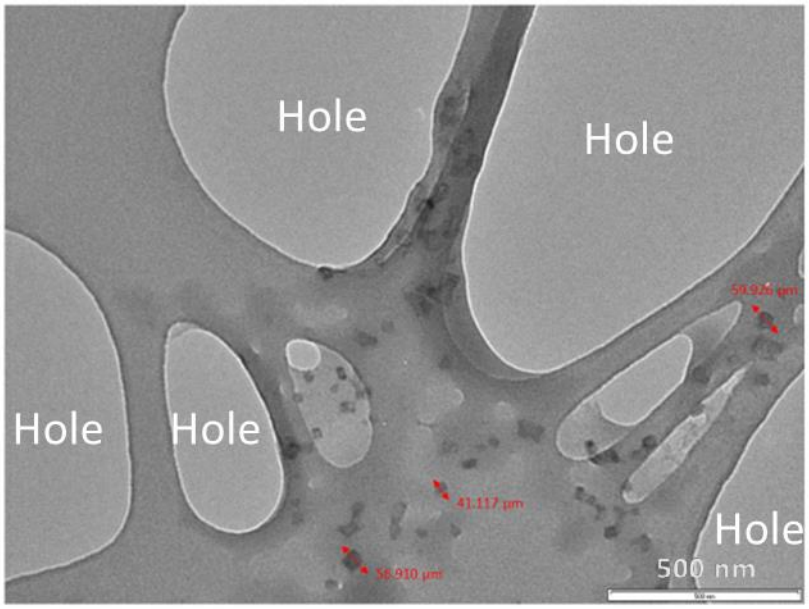

Figure A.1: TEM picture of the RAFT-PEGMA-LA25.

B. Cytotoxicity tests

Following the production of amphiphilic block copolymers in Chapter 4 and their conversion into nanoparticles, their cytocompatibility was evaluated in three model cell lines. This assessment aimed to determine their suitability as potential polymeric components for nanomedicines. The experimental details and the results collected from the biological assays and the cytotoxicity tests are included here as presented in the Englezou *et al.* (2020) journal paper.

B.1 Biological assays experimental methodology

Cell culture conditions

American Type Culture Collection (ATCC; Manassas, VA, USA) was the provider of Caco-2 human epithelial colorectal cells, Calu-3 human epithelial lung cells and THP-1 human monocytes used in this investigation. All these were used within a passage window of 5. Cells were regularly cultivated in a growth medium at 37 °C with 5% CO_2 in 75 cm^2 culture flasks. Dulbecco's Modified Eagle Medium (DMEM) supplied with 10% (v/v) Fetal Bovine Serum (FBS) and 2 mM L-glutamine was used as the growth medium for the Calu-3 and Caco-2 cells. The THP-1 cell growth medium consisted of Roswell Park Memorial Institute (RPMI) 1640 medium supplemented with 10% (v/v) FBS and 2 mM L-glutamine.

Cytotoxicity experiments

The nanoparticle cytotoxicity was examined through the evaluation of the cell membrane integrity and cellular metabolic activity with the employment of the lactate dehydrogenase (LDH) release assay (Sigma-Aldrich, TOX7 kit) and the PrestoBlue cell viability assay (Thermo Fisher Scientific), respectively. In a 96 well plates, all the cells were seeded at $1x10^4$ cells/well. The differentiation into macrophages of the THP-1 monocytic cells was stimulated with the addition of 100 ng/ml phorbol 12-myristate 13-acetate (PMA) when seeded into plates. Cells were incubated in plates for 24 h before performing the assays. Nanoparticle formulations were administered to cells in Hanks Balanced Salt Solution (HBSS) at concentrations of 0.5 mg/ml for a duration of 24 h. A 1% (v/v) concentration of Triton X-100 (TX) was utilized as a positive control for inducing cell death, while a vehicle control consisting of HBSS without nanoparticles was employed as a negative control. Following exposure, 50 µl of the supernatant was collected from each well for the analysis of the LDH content. The cells were subsequently

washed twice with phosphate-buffered saline (PBS), followed by the addition of 100 µl of 10% (v/v) PrestoBlue reagent diluted in phenol red-free medium per well for 60 min. Fluorescence was measured at 560/600 nm ($\lambda_{ex}/\lambda_{em}$) using a Tecan Spark M10 multimode plate reader. Relative metabolic activity was determined by assigning values from the negative control as 100% and those from the positive control as 0% metabolic activity. LDH release detection followed the manufacturer's guidelines, which entailed adding 100 µl of LDH reagent to the collected supernatant samples and then incubating them at room temperature, shielded from light, for 25 min. Absorbance at 492 nm was subsequently recorded. Relative LDH release was calculated with the absorbance of the negative control at 492 nm considered as 0%, and the absorbance of the positive control, presumed to cause complete cell lysis, as 100%.

B.2 Results

Linear block copolymers

Since these materials are intended for biomedical applications, such as drug delivery vehicles, the *in vitro* cytotoxicity of the mPEG-CL_{50} and mPEG-CL_{50}-LA_{25} nanoparticles (NPs) was tested on Caco-2 (intestinal), Calu-3 (airway) and THP-1 (macrophage) cells at a fixed concentration of 500 µg/ml. In both assays, neither particle exhibited cytotoxic effects across all studied cell types, mirroring the results observed with the cell culture medium HBSS used as a vehicle control (Figure B.1).

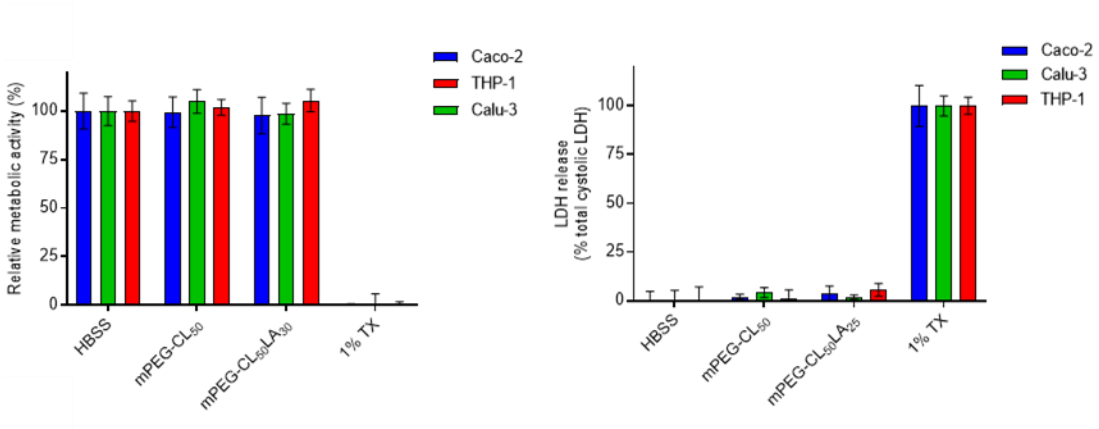

Figure B.1: Cytocompatibility of NPs on Caco-2 (intestinal), Calu-3 (airway) and THP-1 (macrophage) cells. Cytotoxicity was determined by **(Left)** PrestoBlue metabolic activity and **(Right)** LDH release as an indicator of membrane damage. Particles (0.5 mg/ml) were applied to cells in HBSS and exposed for 24 hours to cells. HBSS treatment represents the vehicle control and Triton X-100 (TX) applied at 1% (v/v) was used as the cell death control. Data are presented as mean ± S.D (n=3).

Grafted block copolymers

The same procedure was carried out for the initial assessment of the *in vitro* toxicity on model cell lines for the branched block copolymers (Figure B.2). To simulate administration via oral and inhalation routes, intestinal epithelial (Caco-2 cells) and lung epithelial (Calu-3 cells) were chosen, respectively. Additionally, a macrophage cell line (activated THP-1 cells) was selected as a model for toxicity assessment, given the defensive function of these cells in the innate immune system. The cytocompatibility of the NPs was evaluated at a consistent and relatively high concentration of 500 µg/ml (Vasey et al., 2019). All four particles demonstrated no cytotoxic effects in both assays conducted across all studied cell types (Figure B.2). This encompassed the absence of any reduction in cellular metabolic activity over a 24-hour period (Figure B.2-A) and the absence of membrane disruption, as evidenced by the lack of LDH release (Figure B.2-B).

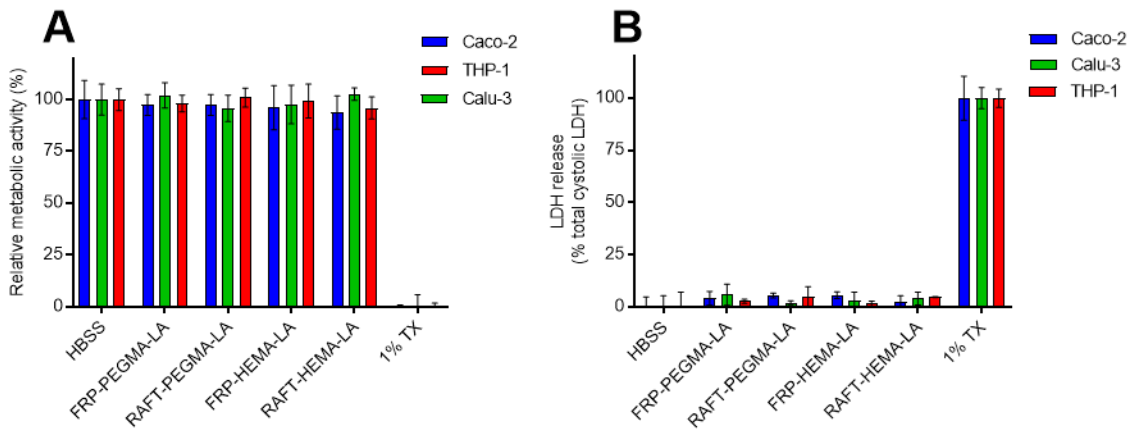

Figure B.2: Cytocompatibility of NPs on Caco-2 (intestinal), Calu-3 (airway) and THP-1 (macrophage) cells. Cytotoxicity was determined by **(A)** PrestoBlue metabolic activity and **(B)** LDH release as an indicator of membrane damage. Particles (0.5 mg/ml) were applied to cells in HBSS and exposed for 24 h to cells. HBSS treatment represents the vehicle control and Triton X-100 (TX) applied at 1% (v/v) was used as the cell death control. Data are presented as mean ± S.D (n=3).